VYSOKÉ UČENÍ TECHNICKÉ V BRNĚ
BRNO UNIVERSITY OF TECHNOLOGY

FAKULTA STROJNÍHO INŽENÝRSTVÍ
ÚSTAV MECHANIKY TĚLES, MECHATRONIKY A BIOMECHANIKY

FACULTY OF MECHANICAL ENGINEERING
INSTITUTE OF SOLID MECHANICS, MECHATRONICS AND BIOMECHANICS

DEFORMAČNĚ NAPĚŤOVÁ ANALÝZA AORTÁLNÍCH ANEURYSMAT

STRESS-STRAIN ANALYSIS OF AORTIC ANEURYSMS

DOKTORSKÁ PRÁCE
DOCTORAL THESIS

AUTOR PRÁCE — *ING. STANISLAV POLZER*
AUTHOR

VEDOUCÍ PRÁCE — *PROF. ING. JIŘÍ BURŠA, PH.D.*
SUPERVISOR

BRNO 2012

Abstrakt

Tato práce se zabývá problematikou aneurysmat břišní aorty a možností využít konečnoprvkovou deformačně-napěťovou analýzu těchto aneurysmat ke stanovení rizika ruptury.

První část práce je věnována úvodu do problematiky, popisu kardiovaskulární soustavy člověka s důrazem na abdominální aortu, anatomii, fyziologii a patologii stěny tepny s důrazem na procesy vedoucí ke vzniku aneurysmatu. Dále se práce věnuje rizikovým faktorům přispívajících ke vzniku aneurysmat spolu s analýzou současných klinických postupů ke stanovení rizika ruptury spolu se srovnáním navrhovaného kritéria maximálního napětí.

Dominantní část této disertace je věnována identifikaci faktorů ovlivňujících napjatost a deformaci stěny aneurysmatu spolu s návrhem nových postupů, prezentací vlastních poznatků vedoucích ke zpřesnění určení rizika ruptury pomocí deformačně- napěťové analýzy a metody konečných prvků.
Nejprve je analyzován vliv geometrie, vedoucí k závěru, že je nezbytné používání individuálních geometrií pacienta. Dále je pozornost zaměřena na odbočující tepny, které ve stěně působí jako koncentrátor napětí a mohou tedy ovlivňovat napjatost v ní. Jako další podstatný faktor byl identifikován vliv nezatížené geometrie a bylo napsáno makro pro její nalezení, které bylo opět zahrnuto jako standardní součást do výpočtového modelu.
Mechanické vlastnosti jak stěny aneurysmatu, tak intraluminálního trombu jsou experimentálně testovány pomocí dvouosých zkoušek. Také je zde analyzován vliv modelu materiálu, kde je ukázáno, že srovnávání maximálních napětí u jednotlivých modelů materiálu není vhodné díky zcela rozdílným gradientům napětí ve stěně aneurysmatu. Dále je zdůrazněna potřeba znalosti distribuce kolagenních vláken ve stěně a navržen program k jejímu získání.
Intraluminální trombus je analyzován ve dvou souvislostech. Jednak je ukázán vliv jeho ruptury na napětí ve stěně a jednak je analyzován vliv jeho poroelastické struktury na totéž.
Posledním identifikovaným podstatným faktorem je zbytková napjatost ve stěně. Její významnost je demonstrována na několika aneurysmatech a i tato je zahrnuta jako integrální součást do našeho výpočtového modelu. Na závěr jsou pak navrženy další možné směry výzkumu.

Klíčová slova: Aneurysma abdominální aorty, metoda konečných prvků, riziko ruptury, napětí ve stěně aneurysmatu.

Abstract

This thesis deals with abdominal aortic aneurysms and the possibility of using finite element method in assessment of their rupture risk.

First part of the thesis is dedicated to an introduction into the problem, description of human cardiovascular system where the abdominal aorta, its anatomy, physiology and pathology is emphasized. There Processes leading to formationing of abdominal aortic aneurysms are also discussed. Risk factors contributing to creation of aneurysms are discussed next. Finally, an analysis of current clinical criteria which determine rupture risk of an abdominal aortic aneurysm is presented and compared with the new maximum stress criterion being currently in development.

Main part of the thesis deals with the identification of relevant factors which affect stress and deformation of aneurysmal wall. This is connected with proposals of new approaches leading to predicting the rupture risk more accurately by using finite element stress-strain analysis.
The impact of geometry is analyzed first with the conclusion that patient-specific geometry is a crucial input in the computational model. Therefore its routine reconstruction has been managed. Attention is then paid to the branching arteries which were neglected so far although they cause a stress concentration in arterial wall. The necessity of knowing the unloaded geometry of aneurysm is then emphasized. Therefore a macro has been written in order to be able to find the unloaded geometry for any patient-specific geometry of aneurysm.
Mechanical properties of both aneurysmal wall and intraluminal thrombus were also experimentally tested and their results were fitted by an isotropic material model. The effect of the material model itself has been also investigated by comparing whole stress fields of several aneurysms. It has been shown that different models predict completely different stresses due to different stress gradients in the aneurysmal wall. The necessity of known collagen fiber distribution in arterial wall is also emphasized. A special program is then presented enabling us to obtain this information.
Effect of intraluminal thrombus on the computed wall stress is analyzed in two perspectives. First the effect of its failure on wall stress is shown and also the impact of its poroelastic structure is analyzed.
Finally the residual stresses were identified as an important factor influencing the computed wall stress in aneurysmal wall and they were included into patient-specific finite element analysis of aneurysms.
Further possible regions of investigation are mentioned as the last part of the thesis.

Key words: Abdominal aortic aneurysm, finite element method, rupture risk assessment, aneurysm wall stress.

Prohlašuji, že tuto disertační práci jsem vypracoval samostatně s použitím odborné literatury a dalších informačních zdrojů, které jsou všechny citovány. V disertační práci jsem také použil texty a informace z článků, kterých jsem autor nebo spoluautor.

Práce je psána v anglickém jazyce

I herewith declare that I have personally penned the doctoral thesis. I have only used the mentioned sources and utilities and have marked parts copied from elsewhere, either literally or by content as such. I have also used texts and information from my own co-authored publications.

The doctoral thesis is written in English language.

Ing. Stanislav Polzer

Acknowledgement

I wish to express my deep gratitude to my supervisor prof. Ing. Jiri Bursa, Ph.D. for all his guidance and support throughout my research. I also want to thank to Ing. Pavel Skacel, Ph.D. who helped me with an immense number of problem in both experimental and computational fields.

I am also very thankful to T.Christian Gasser, Ph.D. from Royal Institute of Technology, Stockholm who helped with many of my researches and provided much appreciated feedback enabling me to improve my work constantly.

I want to express many thanks to prof. MUDr. Robert Staffa, Ph.D., MUDr. Robert Vlachovsky, Ph.D., prof. MUDr. Marketa Hermanova, Ph.D. and MUDr. Michal Tichy who helped me to improve this research greatly by providing priceless advice and consultations and, who also provided samples of aortic tissue and histological analysis.

Last but not least I am thankful to my family and my girlfriend Šárka who supported me for the whole time of my Ph.D. study.

This thesis would not exist without any of these people.

Table of Content

1 Introduction

Abdominal aortic aneurysm (AAA) is a life threatening disease. Its prevalence is 3-7% in population above 65 years[19]. Patient usually does not have any symptoms until the AAA ruptures. Then a massive internal bleeding follows and in $50 \div 70\%$.patients die before help can be provided

From this point of view one could say that any diagnosed AAA should be operated. However not everyone is suitable for surgery. People above 65 can have many contraindications and it may be risky even to put them into a sleep. Although less invasive endovascular repair (using a stentgraft) can be applied in some cases, opened surgery remains the most frequent method in AAA treatment, and operating mortality is here between 3-5%. Also it is important to point out that by far not every AAA ruptures. Therefore a lot of work has been done in order to determine which AAA can be expected to rupture. Several criteria have been developed over the time for this purpose. Determination of potentially dangerous AAAs by finite element analysis gives the best results so far. However there are still many issues which must be solved to improve the predictive capability of this method.

1.1 Goals of the thesis

- Perform a literature review about anatomy, histology and pathology of human aorta
- Perform a literature review about known entities which influence wall stress and wall strength in AAA.
- Investigate the influence of intraluminal thrombus on wall stress.
- Manage to create patient specific geometry of AAA routinely.
- Investigate the influence of residual stresses and prestresing on wall stress of AAA.
- Investigate the structure of the aneurysmal wall in order to decide on necessarity of using anisotropic material models.

2 Definition of aneurysm

There are several definitions of what is aneurysm[31]. One of them suggests defining aneurysm as a local dilatation of artery with the diameter of dilatation being at least 50% greater than the diameter of the original artery. There is a problem with such definition when the diameter of artery does not change rapidly and therefore there is no obvious beginning and end of aneurysm. Another definition suggests to denote as aneurysm a dilatation of artery when the diameter of dilatation is 50% greater than the mean population diameter (based on statistics and including sex, age,…) of the original artery. Because this thesis is focused on AAA, the author will use another definition of AAA which says: AAA is 50% dilatation of infrarenal abdominal aorta compared to the diameter of suprarenal abdominal aorta. This definition is sufficient for this thesis and according to experience of the author it covers all AAAs with respect to individual variations in diameter of abdominal aorta.

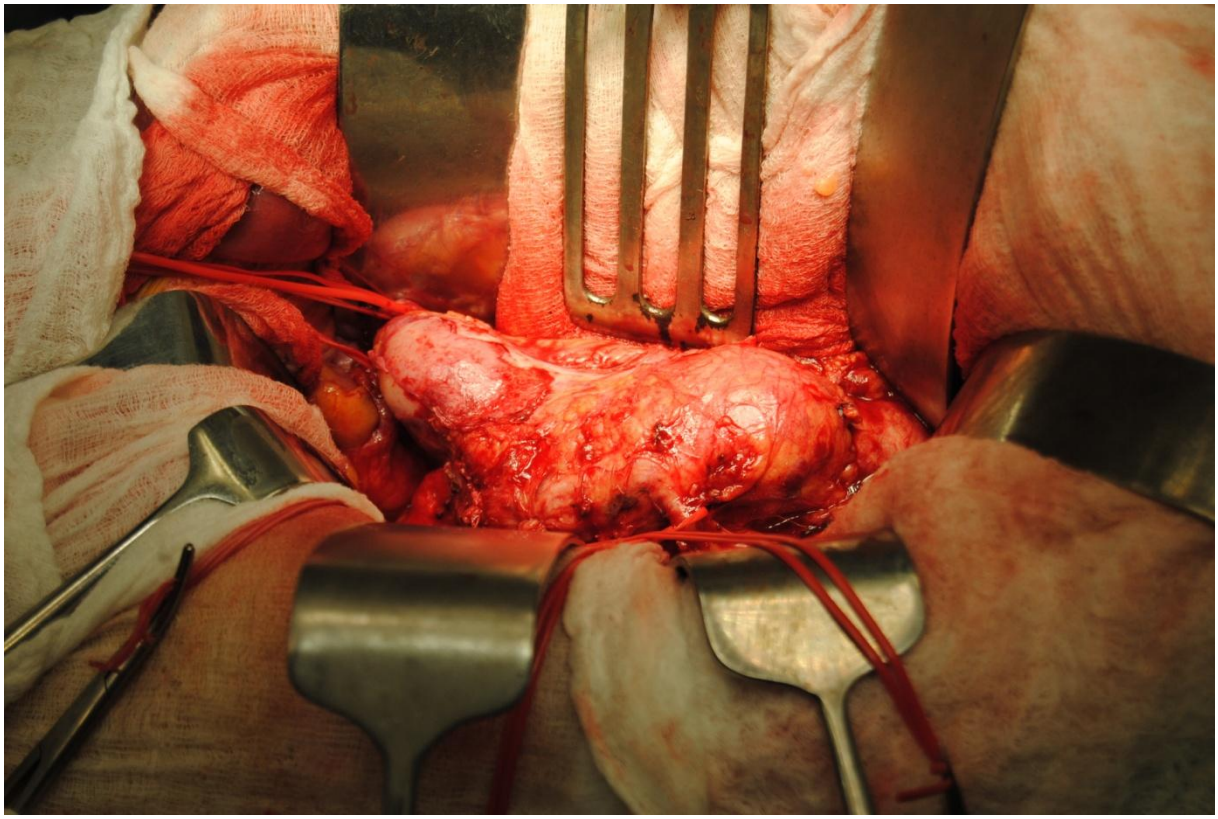

Figure 1. AAA during elective repair surgery. This AAA includes aortic bifurcation and iliac arteries as well. Patient¨s orientation is proximal **(**towards the heart) to the right, distal to the left.

3 Introduction to human cardio-vascular system

This chapter includes basic information about the human cardio-vascular system and its structure with focus on entities important in AAA formation or rupture risk evaluation.

Human vascular system can be divided into several parts. Heart serves as a pump and pushes blood into arteries. Blood flows back to the heart via veins. These main structural parts will be

briefly described in this chapter with focus on entities substantial to abdominal aorta and AAA formation.

3.1 Heart

For our purposes the anatomy of heart is not substantial. The only information relevant to us is that heart activity is cyclic and it pumps the blood under the pressure during a cycle phase called systole. This phase lasts for some 0,2s for 1Hz beat rate. For the rest of the cycle, the heart sucks blood from veins. This phase is called diastole. Human heart can work in the range of frequencies between 0,5Hz up to 4Hz. Phases of cardiac cycle remain roughly proportional to its length.

Blood pressure changes in time(see Figure 2 in Appendix B) just as the heart works[11]. Peak systolic pressure can vary between $16 \div 26\ kPa$ and the lowest diastolic pressure can be as low as $8 \div 16\ kPa$. Normally, the pressure oscillates between $10 \div 16\ kPa$ during the cardiac cycle[70]. It increases during an exercise[81] or psychic stress and its permanent increase is known as hypertension which is a significant risk factor for AAA formation as described in the chapter 4.1.

However, the blood pressure does not change only in time but in space as well. Pressure wave is propagating from the heart through the aorta with a finite speed given by the elasticity and dimensions of arterial wall. For a linear elastic material this speed of propagation depends on fluid density ρ, Young modulus of the wall E, diameter of the tube d and its wall thickness h according to the following (Moens-Korteweg) formula:

$$v = \sqrt{\frac{E \cdot h}{d \cdot \rho}} \tag{1}$$

Although arterial wall does not behave linearly, this formula is still valid at least qualitatively. The wave is propagating faster when the wall is stiffer. And because the arterial wall increases its stiffness during lifetime substantially, the speed of propagation increases with aging as well. It rises from $2\ m \cdot s^{-1}$ for infants up to $4.7 \div 16\ m \cdot s^{-1}$ in people above 55 years[80]. The lower limit is achieved by healthy sporting people while the upper value fits more for obese smokers.

When a pressure wave reaches any bifurcation or other stepwise change along its path it reflects and interferes with the following forward pressure wave. The reflection is most significant at iliac bifurcation[81] and consequently in abdominal aorta the resulting pressure wave can reach an even higher peak pressure than originally created by the heart. Therefore the region of aorta near the iliac bifurcation is loaded by the highest pressure from the whole vascular system; this fact represents another risk factor for AAA formation.

Knowledge of the pressure wave speed and long term values of blood pressure are important inputs into evaluation of risk of rupture of individual AAAs.

3.2 Blood

Blood is a liquid pumped by heart through arteries, which differs significantly from most liquids like water. Water behaves as a Newtonian liquid which means that its viscosity (ratio of shear stress and velocity gradient) is constant and does not depend onthe velocity and diameter of the tube. If one wants to model blood as a Newtonian liquid, the value of its dynamic viscosity of approx. $0{,}004 \mathrm{Pa\ s}$ is used generally. Such assumption can serve as a good approximation when modeling behavior of the blood in large blood vessels. However it does not reflect some important properties of a blood.

First of all blood is not a pure liquid but rather a suspension of blood cells (erythrocytes, leukocytes, blood platelets) and a liquid. The influence of these cells on viscous properties of blood increase when diameter of the artery decreases. At lower velocities individual blood cells tend to stick to each other and therefore an increase of the viscosity occurs, while at higher velocities the forces dragging the blood cells are too high and they tear blood cells away from each other so that the viscosity decreases. Low velocities occur in small arteries and at boundary layer while higher velocities are generally in the middle of large arteries. This type of liquids (in which the viscosity decreases with increasing velocity) is called Bingham fluids.

Regarding the velocities of blood in arteries, it is important to emphasize the difference between the blood flow velocity and the pressure wave propagation speed. In contrast to the pressure wave propagation speed mentioned in chapter 3.1, the velocity of the blood flow changes in the range $-0{,}1 \div 1 m \cdot s^{-1}$. The upper limit is for peak systole in the ascending aorta while negative velocity occurs also herebut during the diastolic phase at the boundary layer, where the blood flows in proximal direction[70]. Of note that flow in arteries is dominantly laminar. Turbulent flow occurs only in ascending aorta right behind the heart or behind extensive atherosclerotic plaques or other stepwise changes in arterial geometry.

Knowledge of blood properties is important because it has been suggested that turbulence in AAA can trigger the thrombus formation[70].

3.3 Arteries

Arteries distribute the blood from the heart through the body. For the purpose of this Thesis only anatomy of thoracic and abdominal aorta with their branches is relevant. Abdominal aorta starts below the renal arteries and ends by iliac bifurcation (see Figure 2). At its anterior side mesenterica inferior and spermatic arteries are located while 3 pairs of lumbal arteries can be found on its posterior side.

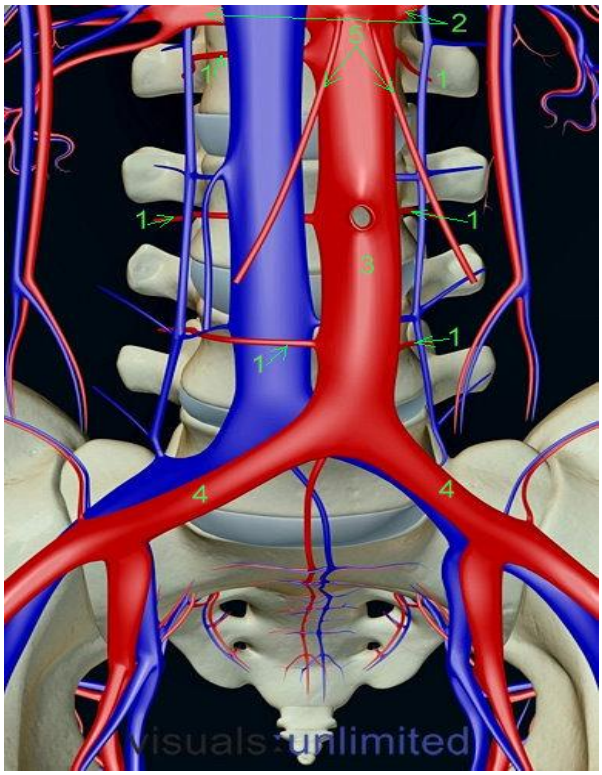

Figure 2 anatomy of healthy male abdominal aorta. 1-lumbar arteries, 2-renal arteries,3-mesenterica inferior, 4-iliac arteries, 5-internal spermatic arteries. Reprint from 83

3.3.1 Structure of arterial wall

First it is important to note that arteries can be divided into several groups by their wall structure: elastic (large) arteries, muscle arteries of medium and small size and arterioles. Elastic arteries include the biggest arteries in a body, therefore we will focus mainly on them. Structure of a healthy artery is shown in Figure 3.

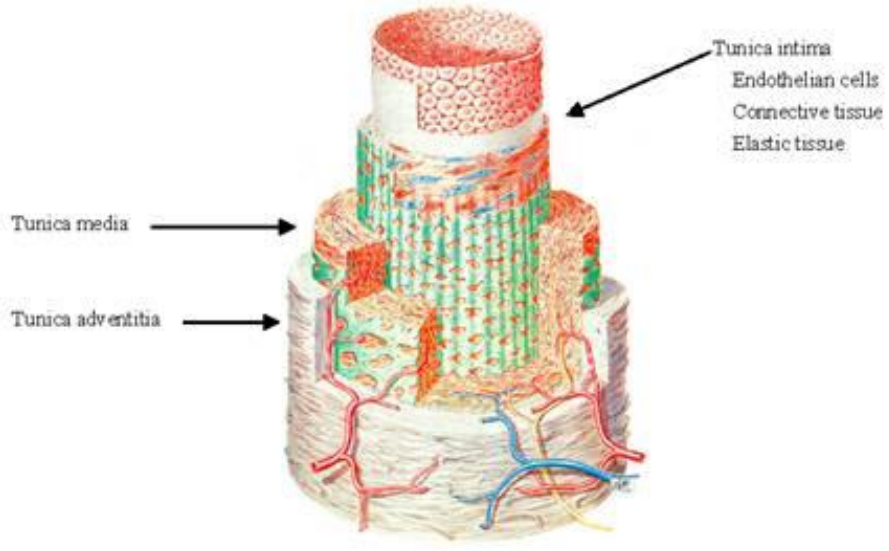

Figure 3 Structure of a healthy artery. Reprint from 84.

INTIMA:

Intimal layer (tunica intima) is located at the inner side of the artery. It consists of a layer of endothelial cells which creates a smooth surface ensuring an easy blood flow. It is very thin in young healthy arteries, but its thickness increases with age[9]. It has been shown that its thickness can grow up to 27% of the total wall thickness for aged arteries[10]. Aging is also connected with increase of extracellular matrix in the intimal layer, of collagen type I, of dispersed SMCs, and of degradation of 3D network of elastin[9]. This structure is similar to that of media. Membrana elastica interna is an elastin layer which separates intimal and medial part of the wall.

MEDIA:

(Tunica) Media creates most of the bulk of artery. Microstructure of media can be seen in Figure 4. It consists of 40 to 80 layers (in aorta) of smooth muscle cells (SMC's), extracellular matrix (ECM) and elastin membranes. This layer is responsible for carrying the substantial part of the blood pressure load during normal state. Elastin absorbs the shock waves while SMC's are capable of active remodeling based on actual pressure conditions. Outwards the media ends by external elastic membrane. Elastin constitutes approximately 30% of the dry weight of major arteries. It is composed of otherwise-soluble tropoelastin monomers that are cross-linked by lysine residues. Under normal circumstances, more than 99% of total elastin in arteries is found in this insoluble cross-linked form. This has been viewed as a network of packed coils. Elastin production occurs during early ontogenesis and is complete by maturity, when tropoelastin synthesis by smooth muscle cells ceases. Elastin remains then relatively stable with an estimated half life of 40 to 70 years. It is found to be resistant to most enzymatic degradation with the exception of elastase[27].

Media also contains some collagen fibers which are dominantly circumferentially oriented and remain slack mostly. Only 6-7% of medial collagen is reported to carry the load under physiological pressure[2]. Some early studies[3] reported meshwork of a helically woven fibers but more recent study[2] showed that collagen fibers in media are parallel with circumferential direction with strictly layered structure and no radial dispersion.

In aorta and major arteries, Media contains also about 23% of SMCs which are oriented circumferentially and also stretched, which suggests that SMCs carry the load as well[2].

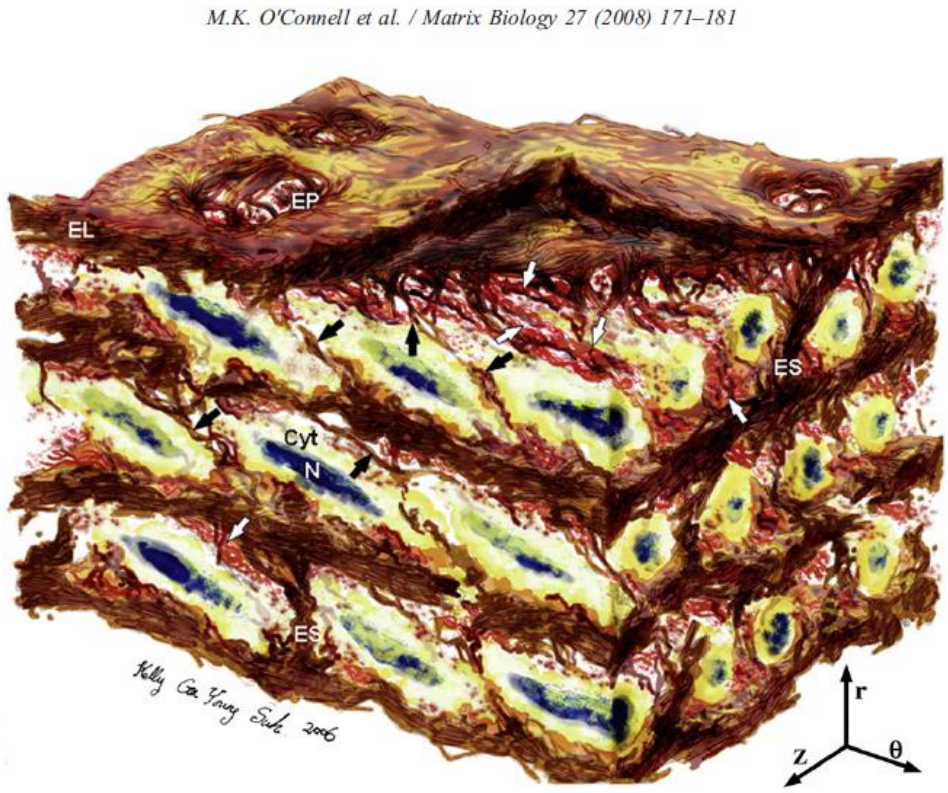

Figure 4 Artistic rendering of rat aortic medial microstructure. Aortic media shows complex, interconnected structure. Elastin features include elastic lamellae (EL), dense network of interlamellar elastin fibers (IEFs shown with black arrows), elastin struts (ES), and reinforced elastin pores (EP). Smooth Muscle Cell (SMC) features include staggered elliptical nuclei (N) oriented circumferentially with radial tilt, and cytoplasm (Cyt) abuts IEFs and overlaps adjacent SMCs. Collagen features include large and small fiber bundles (white arrows) adjacent to lamellar surfaces, arranged in layers of parallel bundles oriented predominantly circumferentially. Image dimensions (θ×Z×r where r indicates radial, Z axial, and θ circumferential directions) are 80 μm×60 μm×45 μm, with lumen surface at the top.. Reprint from 3

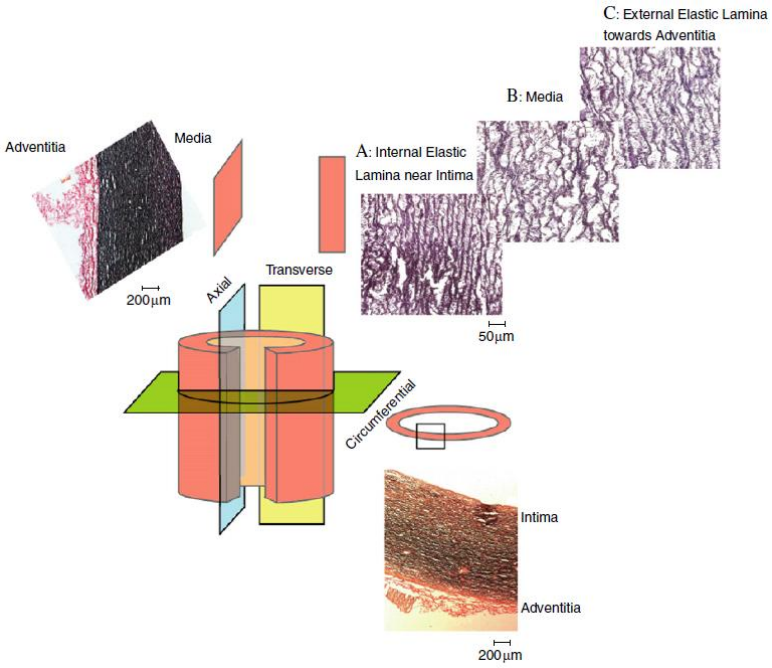

Figure 5 histology of elastin obtained from porcine aorta. Reprint from 1

ADVENTITIA:

Tunica adventitia is a layer consisting mainly of loose fibers of randomly oriented type I and III Collagen. Collagen provides tensile strength and stiffness to the arterial wall[9]. Type I fibrillar collagen, accounting for 65% of the collagen content, defines the load bearing properties of the arterial wall. Type III collagen provides some extensile stretch. Under normal circumstances, most collagen remains slack[27] (see Figure 15 left). In large arteries adventitia contains also vasa vasorum which are responsible for delivery of nutrients into arterial wall. Adventitia also fixes the artery to other structures in a body.

3.3.2 Mechanical behavior of major arterial wall constituents

Elastin:

From mechanical point of view elastin is very compliant and can be stretched over 70% as shown in Figure 6. Globally the elastin network behaves isotropically and can be described[1] by the following neo-Hookean strain energy function Ψ:

$$\Psi = c_{01}(I_1 - 3) \tag{2}$$

where I_1 denotes the first invariant of right Cauchy-Green deformation tensor and c_{01} is a stress-like material parameter

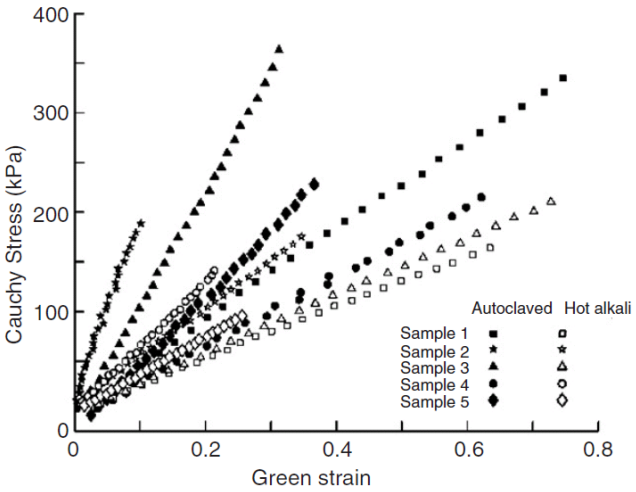

Figure 6 tests of elastin network acquired from porcine aortas by two different approaches. Reprint from 1

Values of parameter c_{01} vary between $77 \div 163\ kPa$ [1]. Global isotropic orientation of elastin is confirmed by histology as shown in Figure 5.

Collagen:

In this chapter the type I collagen will be discussed because it is the dominant collagen type present in the aortic wall[9].

Structure of a collagen fiber is shown in Figure 7. Polypeptidic chains form a triple helix macromolecule of collagen. These molecules overlap each other by a certain length. Collagen fibrils with diameter from tens to hundreds of nm are packed into thick collagen bundles with diameter of tens of μm which can be seen in histological images as shown in Figure 23.

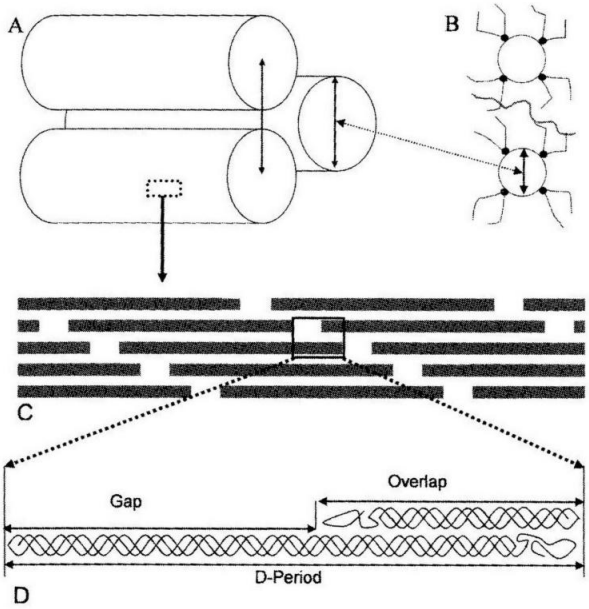

Figure 7. Structure of collagen fibril. Scheme of fibril lateral(A) packing. Collagen fibrils (circles) with associated proteoglycans (B). Scheme of collagen macromolecules which form an individual fibril (C). Triple helix of polypeptidic chains and its formation within collagen macromolecule (D). Reprint from 9

Mechanical properties of collagen are mainly given by cross-links of polypeptidic chains and by cross-links between individual fibrils[9]. These cross-links evolve in time after collagen fibril has been created as shown in Figure 8. It can take up to two years for collagen fiber to reach its maximal stiffness and strength. This phenomenon explains why AAA growth rate is considered as one of the important criteria for elective (planned) surgical repair.

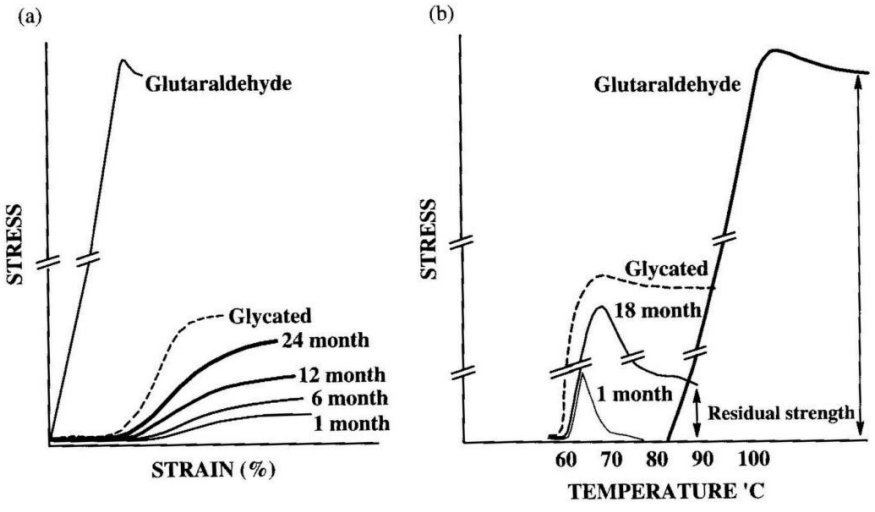

Figure 8 Stiffness and strength of collagen as a function of time and temperature. Reprint from 9

Matured collagen is the stiffest structural part of arterial wall. Its tangential modulus is on the order of GPa[4]. Unlike elastin, collagen can only be stretched elastically by 2–4% from its uncoiled form; rupture in bending, however, occurs under strains of 30% or so as shown in Figure **9**. Because of its fibrous structureit can be bended substantially.

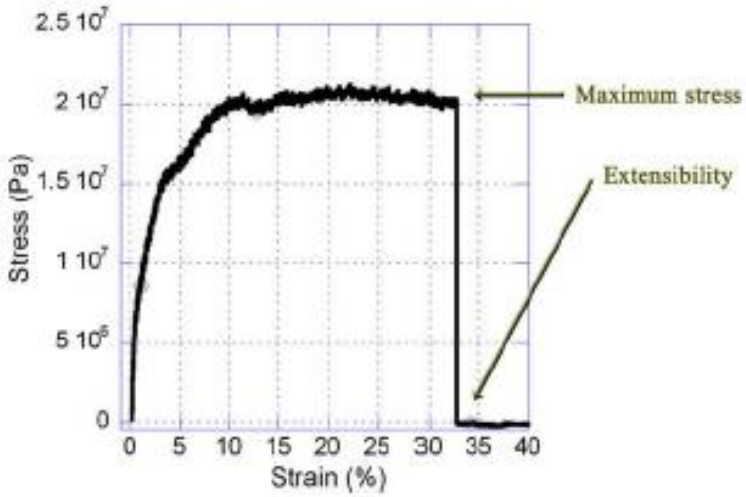

Figure 9 Single type I collagen fiber stress-strain response for bending test. Reprint from 4

In contradiction to a single collagen fiber, three-dimensional collagen fiber network exhibits a quite different behavior as shown in Figure 10. Of note that Figure 10 was taken for low concentration gel which explains low values of tangential modulus as well as other mechanical properties but it shows nicely the general behavior of the collagen mesh. The stress-strain curve consists of three regions. Under low strains fibers are gradually straightened from its naturally occurring tortuous configuration. It is called the “Toe” region. Then they carry the load and stretch themselves in the “linear” region. After the cross links between fibers and fibers themselves reach their strength, a gradual failure of the specimen will occur.

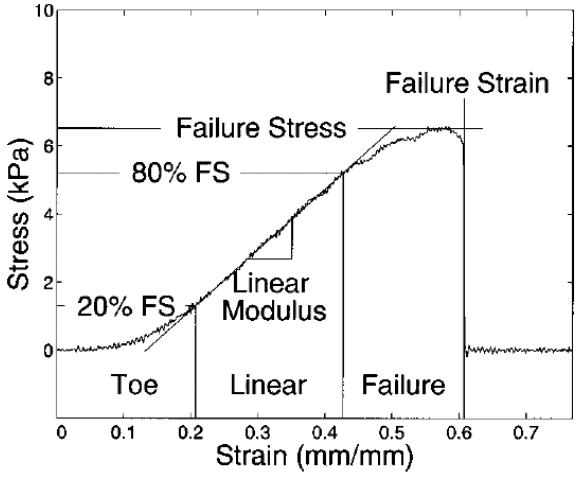

Figure 10 Representative stress-strain curve of a collagen matrix (2 mg/mL, pH 7.4). Reprint from 5

SMCs:

Although being relatively compliant in their relaxed state, SMCs contribute substantially to the mechanical properties of the arterial wall. When contracted they can increase the stiffness by some 30% for strains below 10% and by 10% for 25% strain[6] (similar results have been observed by other investigators[11]). Mechanism of the stiffening is very complex because SMCs are connected with other structural parts of the arterial wall so that they stretch also the collagen fibers when contracting. Then the observed stiffening of the wall is combination of both effects.

SMCs are also dominantly responsible for viscoelastic behavior of arterial wall (although the collagen matrix exhibits also some viscous behavior[9]). SMCs contract or relax as a short time response to the load in order to keep the homeostatic conditions around themselves. For the same purpose they produce substances to make their surround stiffer or more compliant in a longer time period. From the mechanical point of view it can be stated that the wall appears stiffer[7] with an increasing speed of loading.

3.3.3 Intraluminal Thrombus

Although an Intraluminal thrombus (ILT) is not present in a healthy artery it is present in almost any AAA[122]. Therefore it is important to mention some of its main properties. This Chapter is focused on ILT in AAA.

Structure of ILT depends highly on the distance from lumen as well as on the age of the ILT. Generally, ILT has an onion-like structure, due to the fact that the first layer of ILT is formed when the diameter of the aorta reaches some 25mm. As the AAA is growing, new layers of ILT are formed to keep the lumen smooth. The first layer sticks firmly to the aneurysmal wall. However, as the AAA grows, this layer is subjected to excessive strains; it cannot hold, so it ruptures. Rupture causes a stress relaxation of both parts of the ruptured ILT tissue. This relaxation is however not complete because the ruptured layer is still connected to the aneurysmal wall and other ILT layers as well. The actual mechanism of this failure has been neither described nor included into numerical models.

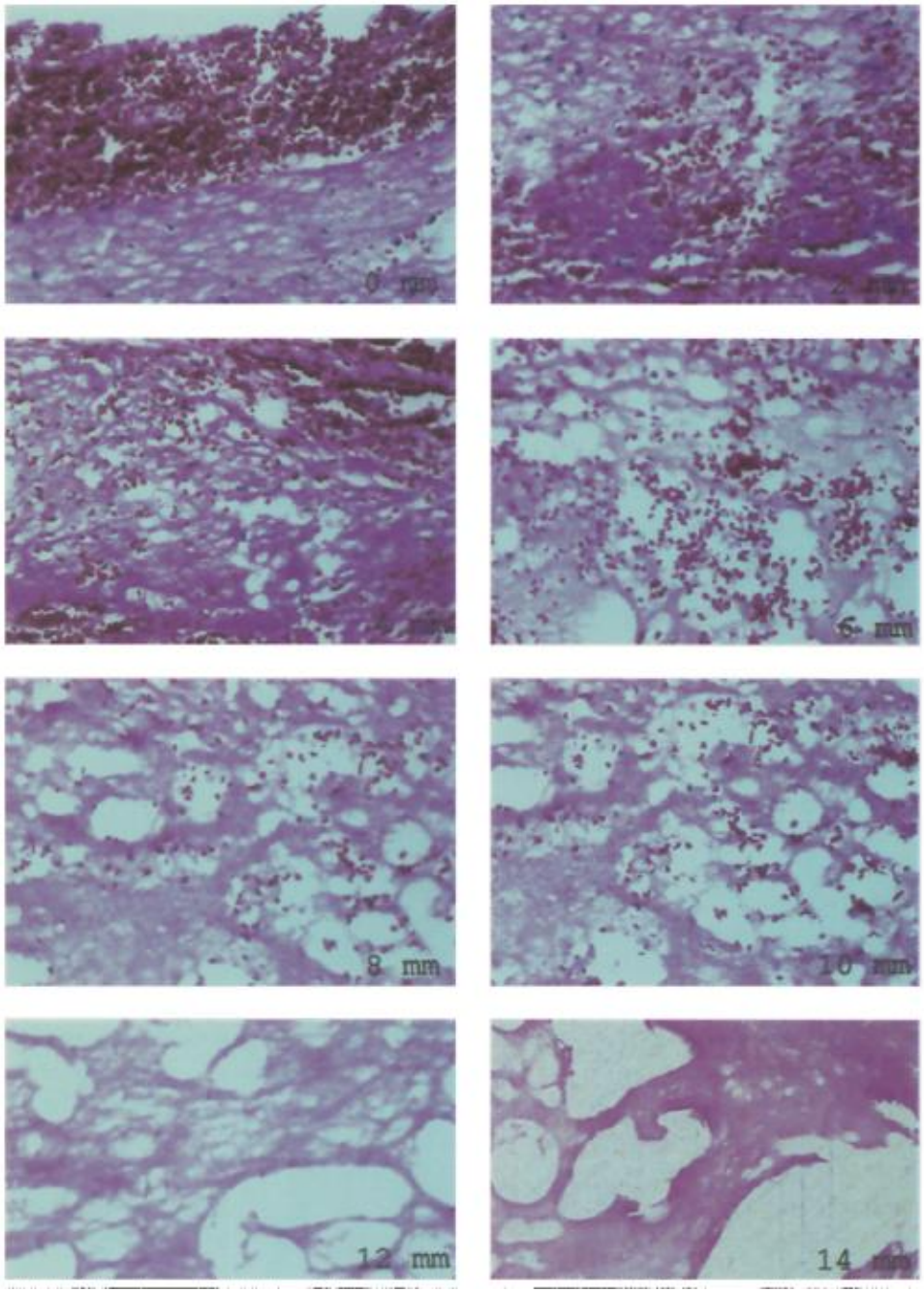

Figure 11 Structure of ILT as a function of distance from lumen. Original magnification 100x. Reprint from 17

A freshly formed ILT consists mainly of complex network of fibrin fibers[13,14] and its mechanical properties are negligible compared to the mechanical properties of the wall[14]. However, as the ILT matures, the fibrin network is gradually replaced by collagen fibers. As collagen fibers mature, they improve their mechanical properties and a matured ILT has mechanical properties comparable with those of the wall[13]. Therefore the variance in mechanical properties is great as shown in Figure 12. Gasser et al[15] performed uniaxial tests while vande Geest et al[17] performed biaxial tests of ILT. Figure 12 shows how both models describe its uniaxial tension behavior. One can immediately conclude that there is a lot to explore in this subject because the results vary by a factor of about 10.

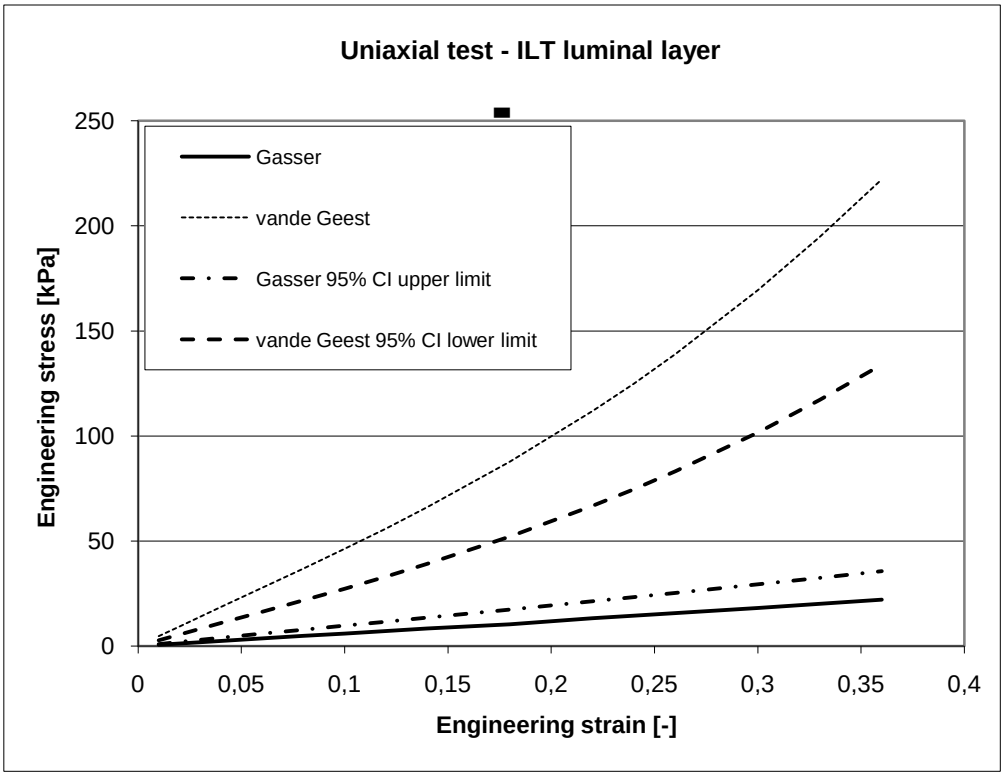

Figure 12 Comparison of available models for uniaxial test of luminal layer of ILT. Gasser et al. based their model on uniaxial experiments while vande Geest et. al on biaxial tests.

Some information about mechanical behavior of medial and abluminal layers of ILT can be found in [15]. Both layers behave nearly linearly and their Young modulus decrease from 63kPa in the luminal layer to 42kPa in the abluminal layer.

Strength of ILT layers has been evaluated from uniaxial tests as well[15]. It decreases from 150kPa in the luminal layer to some 50kPa in the abluminal layer.

Another important feature of the ILT is its porous structure[69] as shown in Figure 11. Cavities take about 80%[18] of its volume and determine its permeability which has been measured[17] to be $1.0 \pm 0.54 \cdot 10^{-12}\ Nm^4s^{-1}$. Because of the network of cavities, the blood pressure can be transmitted through the ILT to the wall. This phenomenon is described in 8.3 in greater detail.

3.3.4 Aging

Aging includes irreversible changes in the wall structure such as the diminuishing percentage of elastin in the wall, increasing percentage of collagen and calcium storage in the arterial wall called calcification. Generally, older arteries are stiffer than younger ones. The process of aging is also known to cause a progressive increase in the diameter of major arteries, estimated at 25% between the ages of 20 and 70[11,31]. The authors of [28] assume this is connected with degradation of elastin.

Calcifications are very stiff deposits in the intimal layer of the arterial wall and they exhibit linear mechanical response[12]. Their Young modulus is on the order of tens of MPa, micro

measurements estimate their Young modulus to be in order of GPa[32]. Calcifications cause also stress concentration in the surrounding tissue[34]. There is also some evidence that calcifications decrease the AAA growth rate[33].

4 AAA

AAA is a life threatening disease. Its prevalence is 3-7% in population above 65 years[19]. As defined in chapter 2, AAA is a dilatation of infrarenal abdominal aorta (see Figure 13). AAA usually ends at iliac bifurcation however it is not rare to see AAA which continues under bifurcation along iliac arteries (see Figure **13**).

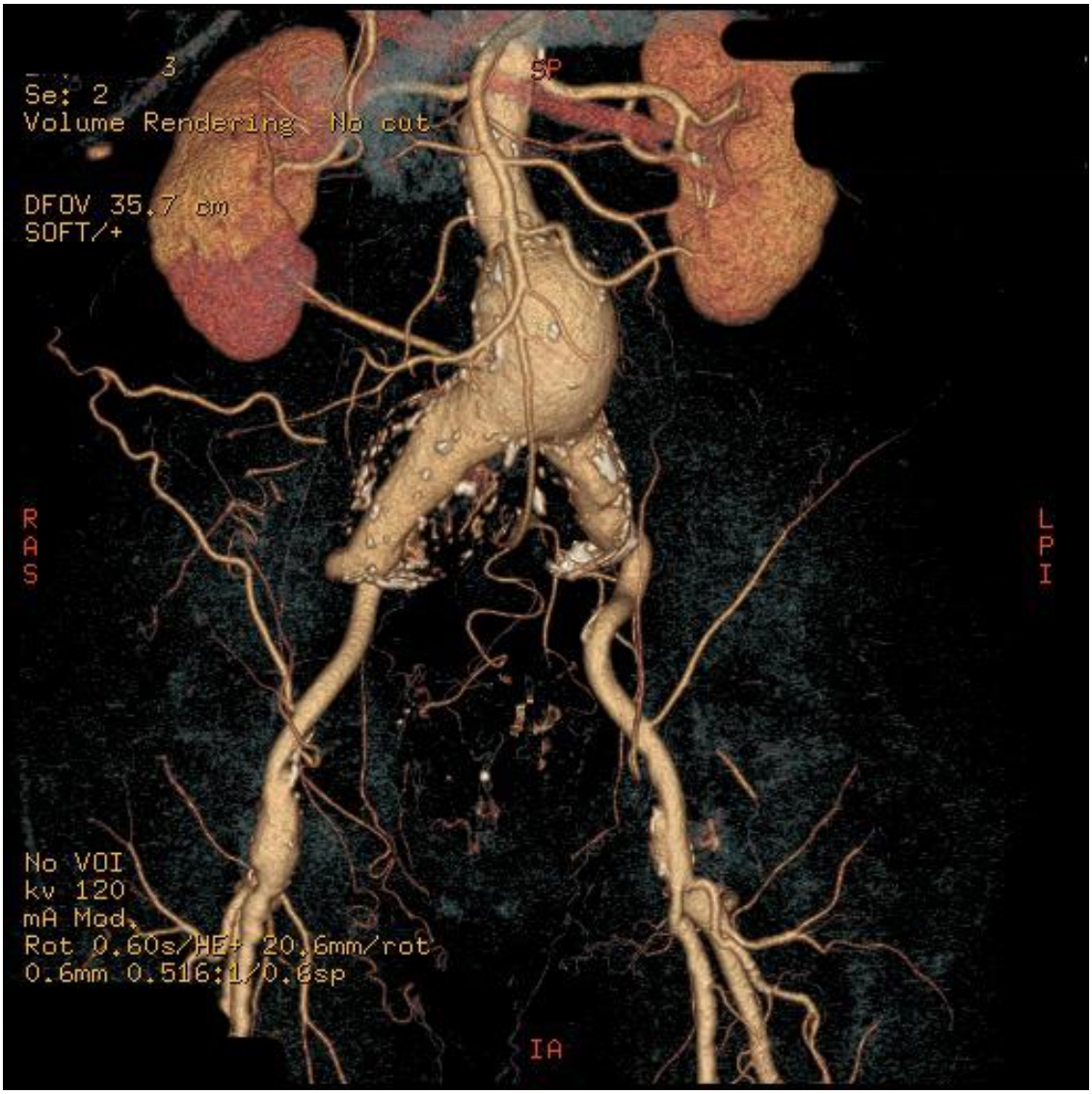

Figure 13 3D visualization of AAA from St. Anne's Hospital. You can see the aorta and other arteries (beige) and both kidneys (orange to red). AAA starts some 5cm below the renal arteries where diameter of aorta is expanding and it continues across the bifurcation, so both iliac arteries are expanded up to 5cm near the bifurcation.

Patient usually does not exhibit any symptoms. However, it brings a great risk because when an AAA ruptures, a massive internal bleeding follows and in $50 \div 70\%$ the patient dies

before help can be provided. Although the percentage of mortality is very high, one would wonder why all of patients don't die when AAA rupture occurs. For the survival rate it is crucial where the rupture occurs. 82% of AAA rupture into retroperitoneum[82] which can sustain the pressure of blood for a while which gives surgeons a precious time to safe the patient. However when the retroperitoneum ruptures as well, or the AAA ruptures directly into the abdominal cavity, then there is no other obstacle to stop the internal bleeding (except for ILT in some cases) and the patient hemorrhages to death.

From this point of view it seems to be reasonable that any diagnosed AAA should be operated. However not everyone is suitable for surgery. People above 65 can have many contraindications so only their anaesthesia might be serious risk. Operating mortality is here between 3-5%.

Another factor the surgeon must take into account is an estimation of the patient's lifetime and prediction of his quality of life. Recovering from the surgery can be rather long and hard and the quality of the patient's life is lowered during this period.

Also it is important to point out that by far not every AAA ruptures. The common maximum diameter criterion for elective surgery is based on the fact that 90÷95%[40] of AAA do rupture when their diameter exceeds 5,5cm. However, only 10%[40] of AAAs smaller than 7cm rupture during one year and there are cases when the surgery was not possible and the patient survived with an AAA of over 90mm in diameter and then he passed away by a completely unrelated disease. For more detail see chapter 6.1.

Last but also important factor to consider is the financial point of view. An elective surgery costs 15k EUR while an emergent surgery costs up to 50k EUR. So if we knew which AAAs are going to rupture we would save a great amount of money, because we could plan the surgery for the risky ones only and just monitor the rest of them.

Due to all of these reasons many researchers and clinicians have been working to find a more reliable criterion how to predict what AAA is going to rupture. However, first we need to detect the AAA, because most of them are asymptomatic. The simplest way of how to define the people with enhanced AAA risk is presented in the following chapter.

4.1 AAA risk factors

As mentioned in chapter 4, the prevalence of AAA is relatively small so that the health care system of any country cannot afford to scan all citizens above 65 to diagnose AAA. Therefore it has been much done in order to determine the risk factors. This is summarized below mostly on the basis of one study[19] only, simply because it is very recent, it contains more than 3 million individuals which is 25times more than the second largest study and its conclusions generally agree with other studies[20,21].

The identified AAA risk factors are shown in Table 1. Figure 14 shows the probability of AAA occurrence as a function of the AAA risk score, calculated as a summation of all the scores in the list. This approach allows including groups into screening which are generally omitted, like non-smoker females. Estimation of a threshold score above which people should undergo an ultrasound screening depends on possibilities of each health care system. For example if we compare groups with the score ≥42 and ≥65 we can say, that for the group ≥65 we discover only half of AAAs but we need to screen only one fifth of patients compared to ≥42 group[19].

Variable	Score	Variable	Score
Male (vs. Female)	18	Smoking, packs/day	
Age (vs <55)	11	≤10yrs	
55-59	17	<0.5	10
60-64	23	0.5-1	12
70-74	28	>1	12
75-79	31	11-20yrs	
80-84	35	<0.5	16
Race/ethnicity (vs white		0.5-1	18
Hispanic	-4	>1	19
Black	-3	21-35yrs	
Asian	-4	<0.5	21
High blood pressure	2	0.5-1	22
Coronary artery disease	6	>1	22
Family history of AAA	14	>35yrs	
High cholesterol	3	<0.5	23
Diabetes	-3	0.5-1	25
Peripheral arterial disease	5	>1	26
Carotid disease	4	Quit smoking	
Cerebrovascular history	2	<5 years ago	-1
Fruit & veg. >3times/week	-1	5-10years ago	-4
Nuts >3times/week	-1	>10years ago	-9
Exercise ≥1time/week	-2	Body mass index ≥25kg/m2	2

Table 1 Identified and quantified AAA risk factors. Data obtained from 19.

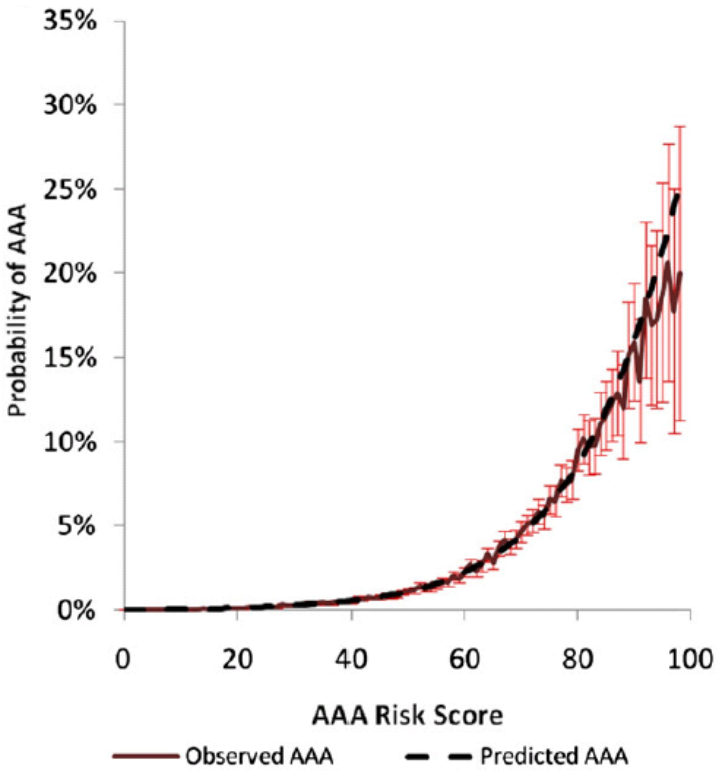

Figure 14 Probability of AAA as a function of AAA risk score. Reprint from 19

4.2 Biochemical changes in aortic wall due to presence of AAA

It has been shown that there are many changes in aortic wall when AAA is formed. This chapter summarizes the known biochemical changes in AAA with focus on the mechanically important structures. The author admits his non-specialty in the field of biochemistry so this chapter is based mainly on two review studies[27,28].

Generally, the changes in AAA are different from the changes in arteries due to atherosclerosis. Atherosclerosis affects primarily the arterial intima while the AAA formation is consequence of transmural inflammation, proteolytic fragmentation of medial elastin, loss of smooth muscle cells, and remodeling of the extracellular matrix. So AAA IS NOT caused by atherosclerosis[27].

Histological examination of aneurysms shows that media thins, medial connective tissue structure disrupts, and content of elastin decreases[58]. Destruction of the lamellar architecture is another important finding in the AAA wall, with an 80% decrease in the number of lamellas and over 80% decrease in the amount of elastic fibers per lamella. The loss of elastin is substituted by collagen, resulting in an overall decrease in the elastin to collagen ratio. This may be a result of either selective degradation of noncollagenous material or synthesis of a new collagen. It is generally believed that as the aorta dilates due to the loss of elastin and attenuation of the media, the arterial wall thickens as a result of remodeling, which involves deposition of new collagen[27].

An increased wall stress has been shown to provide a stimulus for new synthesis of connective tissue. Types 1 and 3 procollagen and tropoelastin are abundantly expressed in aortic aneurysms but remain in their soluble, unlinked form. Abdominal aortic aneurysm have been noted to have 9-fold lower levels of the mature cross-linked elastin, and a 4-to 6-fold increase in levels of tropoelastin as compared with normal aortas. These findings confirm an ongoing but ineffective elastogenesis by SMCs. This decrease of the capability of integration of new collagen and elastin fibers compromises severely the biomechanical properties of the arterial wall[27].

AAA is also formed when production of extracellular matrix (ECM) is inhibited[27].

Enzymes elastase (family of enzymes capable of degrading elastin) and collagenase (family of enzymes capable of degrading collagen) plays a key role in the degeneration of the wall in AAA. It has been shown that there is 5times more elastase in the aneurysmal wall compared to control aortas. Capacity of inhibition of elastase is also reduced which suggests that there is some disruption in the naturally occurring inhibitory mechanisms. However, this capacity returns to normal when the AAA is surgically repaired, which indicates that it could be related to either elevated wall stress or wall hypoxia due to the presence of ILT[27,28].

AAA is also associated with tissue specific elastolytic enzymes matrix metalloproteinases (MMPs). Among them MMP-2 and MMP-9 (members of both elastase and collagenase enzymes family) play the most important role by their ability to degrade both elastin (primarily the newly formed) and denatured collagen. SMCs in AAA produce 3times more MMP-2 than in the control group and its production correlates with the aneurysmal diameter, so it has been suggested that MMP-2 is responsible for the early expansion of AAA[27,28].

Infusion of Elastase itself is capable of forming AAA, but never leads to rupture; collagenase is responsible for AAA rupture[37]. It has been shown namely that infusion of collagenase leads to dilatation of artery and then to rupture[27]. It affects the damaged and non matured fibers, its effect on the matured collagen is very limited. It has been shown that breakdown products of the extracellular matrix are capable of activating collagenase MMP-1 and are not, themselves, inhibited. Therefore it has been suggested there is an unregulated feedback loop with the destruction of collagen leading to the further activation of tissue collagenase through the stimulatory effect of matrix fragments.

There is also some evidence that fibrinolysis in ILT speeds up the elastolysis in media by reducing effectivity of elastase inhibitors[27].

Destruction of the ECM components also activates inflammatory cells having a substantial potential to produce elastase MMP-12, so that it can speed up the AAA growth. It has been shown that infusion of nonspecific inflammatory agents resulted in progression in growth rate

while treatment by anti-inflammatory drugs was able to inhibit this effect[27]. Histology of AAA tissue reveals substantial infiltration of macrophages which are involved in expression of MMP-2 and MMP-9. Besides the mentioned effect on elastin and collagen, these enzymes also degrade other matrix components, including proteoglycans connecting collagen fibers (see Chapt. 3.3.1).

All these precesses require energy so it is not surprising that an elevated uptake of glucose in the aneurysmal wall has been confirmed compared to the non-aneurysmal wall[25], as well as an intensive neovascularisation which can be, to some extend, explained as a response to both need for more nutrients[24] and wall hypoxia, when the wall is covered by ILT[23].

From this chapter one can conclude that biochemical changes in arterial wall due to the presence of AAA do have its significant biomechanical consequences. Mechanical behavior of aneurysmal wall will be discussed in the next chapter.

5 Biomechanics of aneurysmal wall

From the mechanical point of view, aneurysmal wall behavior shows significant differences compared to a healthy aortic wall.

5.1 Stress-strain curves

There is always a biaxial stress state in AAA wall and due to the heterogeneous and fibrous structure of arterial wall it is more appropriate to compare its behavior obtained under biaxial testing[29]. Curves obtained from uniaxial testing include much higher extent of the fiber rotation phenomena which could lead us to wrong conclusions. It is obvious from biaxial testing of both AAA and normal aortic wall (AA) that aneurysmal wall behaves stiffer[29,85]. This can be explained by the fact that unlike the AA tissue where most of collagen remains slack under physiological conditions (see Figure 15), most of collagen in the AAA tissue is straightened and carrying the load. On the contrary, elastin is highly degenerated and it is not itself capable to carry the load [27].

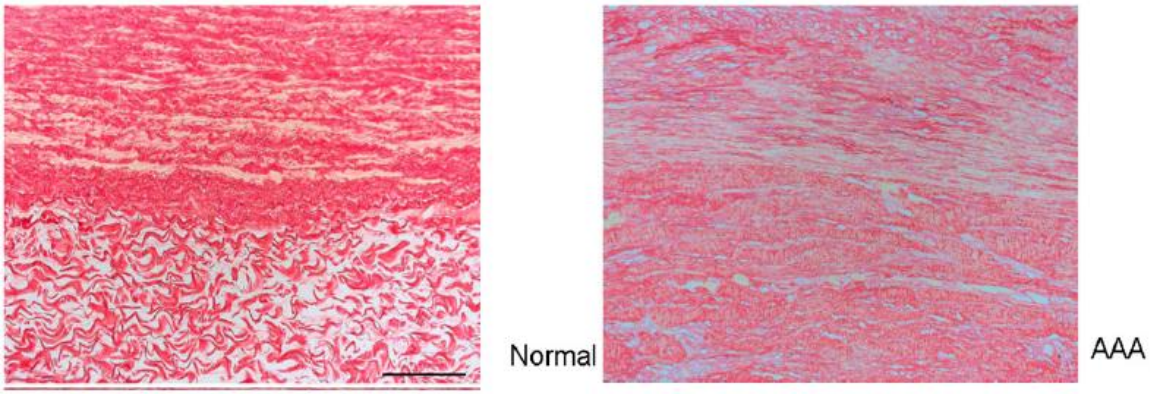

Figure 15 Collagen in normal (left) and aneurysmal arterial wall. Media is on the top. Adventitial collagen is unloaded under normal AA state. Adventitial collagen is much more stretched in case of AAA(right). Reprint from 8

Stress-strain curve of AA can be visually separated into three regions with completely different behavior as shown in Figure 16. It is basically given by mechanical behavior of elastin and collagen (see 3.3.2). At low strain rates, collagen fibers in the adventitia are just straightening from its original curly positions and all the load (under quasistatic conditions) is carried by elastin and collagen in media. Contradictory, at high strain rates most of the adventitial collagen is straightened and carrying the load (proteoglycans transmit the load between individual fibers); because collagen is several orders stiffer than elastin, all the response can be assigned to collagen. The middle region is the transient area, where collagen fibers are gradually straightened to carry the load. However, elastin layers are highly degenerated in the AAA tissue as mentioned in 4.2. Moreover SMCs are not capable of producing any stable elastin[27] to compensate its loss, so the aortic diameter grows up and the adventitial collagen is straightened to take over the load bearing capacity. This effect results

in a great reduction of the first two regions at the stress strain curve, and so the AAA tissue is much stiffer and can sustain smaller strains only.

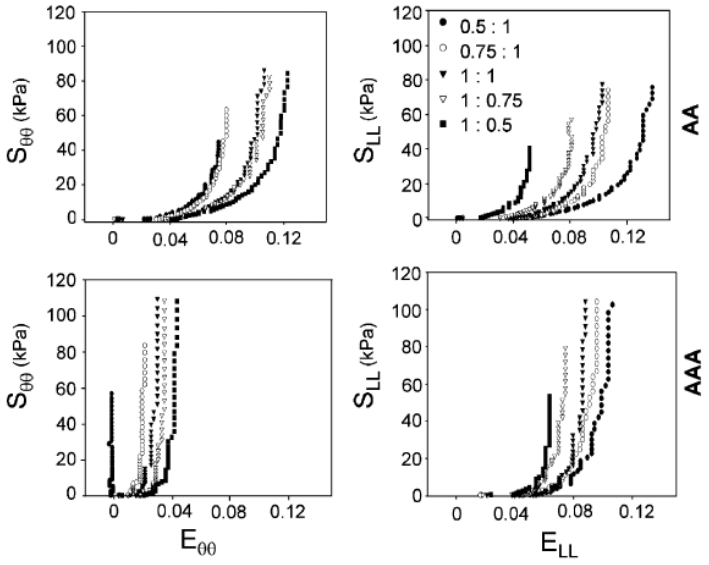

Figure 16 Comparison of biaxial behavior of normal abdominal aorta (AA) and AAA. Reprint from 29

We skipped the load bearing capacity of SMCs in the previous paragraph. It has been assumed that for the quasistatic loading SMC has enough time to relax so it is always carrying the same load. However, when loaded dynamically, its response depends on the speed of loading as mentioned in 3.3.2. However, currently there are no results of biaxial tests of living AAA tissue to quantify its dynamic load bearing capacity, so this issue remains open to further research.

Such research is now in progress in our department. Due to cooperation with 2nd Department of Surgery, St. Anne's University Hospital, we can tesi samples of a living tissue of AAA which were obtained during elective repairs of AAAs. We are able to test the samples within 3 hours after collection. Our preliminary results confirm that SMCs stiffen the wall significantly when loaded faster which is in good agreement with uniaxial tests[7]. Further information regarding our experiments with the AAA tissue will be provided in chapter 8.2.3.

5.2 Strength of AAA wall

Strength of the AAA can be measured only in uniaxial tension so far. It has been shown that the strength decreases by up to 50% in AAA compared to AA[26]. Xiong et al. reported tensile strength of AAA to be 0,93±0,25MPa[35]. This can be explained with respect to facts mentioned in 4.2 due to substantial degradation of the wall structure and by an ongoing but ineffective elastogenesis. Because engineering stress is generally expressed by the formula

$$\sigma = \frac{F}{a \cdot t} \tag{3}$$

where F is a force, a is width of the sample and t is the wall thickness (in the undeformed state), one can easily conclude that a wall with the same thickness contains less elastin and collagen fibers to carry the load, therefore the peak carried force and consequently the maximum stress before rupture (i.e. strength) is lower in AAA tissue. Presence of MMP-9 and MMP-12 also decrease the wall strength due to the degradation of elastin, collagen and proteoglycans[27,28]. Their impact on the strength depends on the time they are affecting the AAA wall which could explain why a lower strength was measured for the group of ruptured AAAs (0,540±0,06 MPa) compared to those electively repaired (0,82±0,09 MPa)[30].

Neovascularization may also decrease the strength. It has been shown that there are significantly more vasa vasorum in the area where rupture occurred[22] compared to the nonruptured AAA wall. The increased density of these arteries (induced by more intensive biological processes in the affected area[64]) lower the load bearing cross section of the AAA wall as well as increase the maximum stress through their stress concentration effect and, consequently, lower the wall strength.

Another factor which is known to influence the wall strength is thickness of the ILT covering the wall. It has been shown that the wall strength is lower when wall is covered by a thick ILT (1,38±0,19 MPa) compared to the AAA wall covered with a thin ILT (2,16±0,34 MPa) [23]. Again it can be explained by several connected issues:

1. Wall hypoxia – due to lack of oxygen, cells suffer from apoptosis so they cannot produce enough new collagen fibers to replace those having been destroyed by MMPs. This idea is supported by the observation that wall thickness is negatively correlated to the ILT thickness[23].
2. Neovascularization – as a response to hypoxia a significantly higher number of new vasa vasorum can be found in AAA wall[64] behind a thick ILT compared to the wall covered with a thin ILT[23]. Again, these arteries represent stress concentrators and their presence also decrease the loadbearing cross-section of the wall. The rupture site contains significantly more vasa vasorum than the rest of the wall[22].
3. Inflammation – macrophages infiltrate the AAA wall from the ILT and release MMP-12 which destroys immature and damaged collagen and unlinked elastin[23,27,28,36].

These processes result in decrease of the wall strength under thick ILT.

Vande Geest et al.[65] put together also other known factors which influence the strength of AAA wall, such as gender (SEX), age, smoking and family history of AAA (HIST), ILT thickness in cm (ILT) and maximum diameter of AAA normalized to the diameter of nonaneurysmal aorta (NORD) and they proposed the following formula for prediction of the strength (in N/cm^2):

$$Strength = 71.9 - 37.9\left(\sqrt{ILT} - 0{,}81\right) - 15{,}6(NORD - 2{,}46) - 21{,}3HIST + 19{,}3SEX \quad (4)$$

where HIST is 0,5 with and -0,5 without presence of AAA in the family history and SEX is 0,5 male and -0,5 female. Of note that smoking and age are not included in the eq.(4) because they were not identified as a statistically signifficant factors influencing wall strength[65] Reliability of the prediction of strength according to this formula is shown in Figure 17. The predictive capability of eq. (1) is however rather limited and this phenomenon needs further investigation. It is also important to note that no differences were found in wall strength of the ruptured and unruptured AAAs[148] which suggests that AAA ruptures rather due to the high stress level (increased even more by the elevated blood pressure during excitement) than by a slow degeneration of the wall making it too weak to sustain the blood pressure.

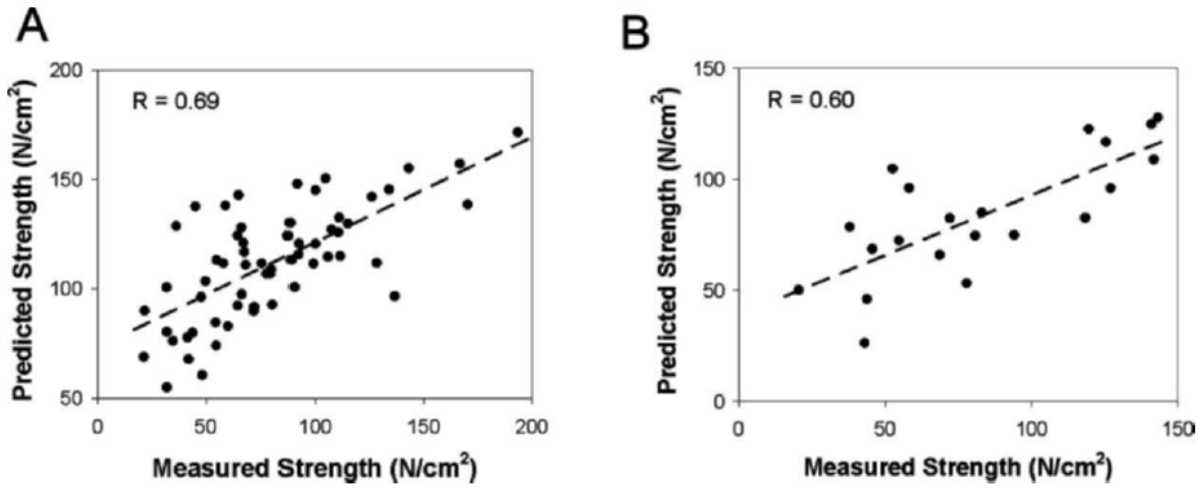

Figure 17 Measured vs. predicted strength according to eq. (1) for construction (A) and validation group (B). Reprint from 65

6 Prediction of AAA rupture

It is known that some AAA ruptures while another does not and, because of reasons mentioned in chapter 4, many researchers try to find a reliable criterion to quantify the rupture risk for a specific AAA. This Chapter is a summary of such criteria with mentioning their advantages and disadvantages.

6.1 Maximal diameter criterion

This is still a widely spread criterion. It is based on the empirical observation that bigger AAAs rupture more often than smaller ones. Some tables of mortality rates based on the diameter of AAAs are shown in Table 2.

Initial AAA diameter[cm]	Annual rupture rate [%]
4-5.5	0.6[38]-1[39]
5.5-5.9	5[41]-9.4[40]
6-6.9	7.5-10.2[40]
>7.0	27.9-34[40]

Table 2 Annual rupture rate of AAAs.

It is important to stress out that this numbers are overestimated because of the fact that most of large AAAs were not operated due to poor healthy conditions of the patients[40]. However, the difference in rupture rate is evident for AAAs greater than 5,5cm in diameter. Therefore the currently used value of this criterion is 5,5cm. Another important fact is that the 30-days post-operational mortality reaches 5-8%[38] for AAAs smaller than 5.5cm, and it can be therefore concluded that the surgery gives a worse life prediction for the AAAs smaller than 5.5cm than a surveillance only. This conclusion is shown graphically in Figure 18.

Advantages of using this criterion are:

- Simplicity. Any radiologist is capable of measuring diameter of AAA from CT scans.
- It is validated on large pool of patients by many researchers.

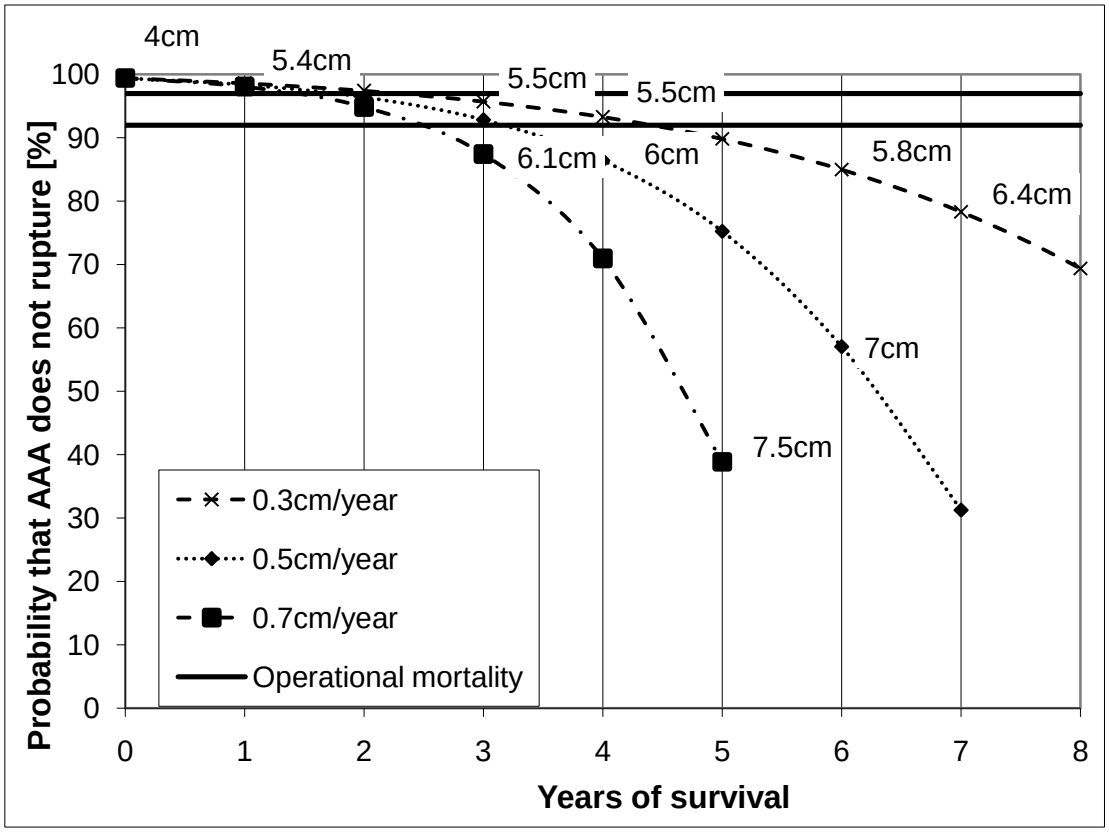

Figure 18 Life prediction for patient with 4cm AAA for different growth rates compared to the operational mortality. Curves fitted to available data as shown in Table 2

Disadvantages of using this criterion are:

- Inefficiency. Only 10 % of AAAs smaller than 7cm rupture annually as one can see from Table 2. Figure 18 respects the increasing risk of rupture during development of AAA but it also shows that only some 20% of AAAs rupture during growth from 5.5cm to 6.5cm. It means 80% of patients are operated unnecessarily during this time period and their surgery could be postponed on the basis of a more reliabble criterion.
- Consequently it is very expensive for the health care system and it also costs lost of doctors work hours which they could spend more valuably.
- It is a general criterion. It does not respect the patient's individuality although every patient has its own life and genetic history which determines mechanical properties of his arterial wall and therefore it influences his rupture risk as well.

The described disadvantages led to combine this criterion with another one.

6.2 Expansion rate

This criterion is based on the facts described in 4.2. Basically it assumes that AAA grows faster when the rupture is coming. To some extend it has been confirmed by several studies (for more detail see review by Wilson et al.[31]). Generally, radiologists suggest surgery when AAA grows more than 0,5cm in a year. However, the expansion rate is very variable and

patient specific. AAAs in diameter from 3 to 5cm can exhibit expansion rates between 0,18cm and 0,69cm in a year. It also has been pointed out that it is difficult to separate the influence of expansion rate on rupture risk from the effect of expansion rate on absolute diameter, which itself affects the rupture risk[28].
Therefore this criterion is not used alone but rather in combination with the maximal diameter criterion.

However, these criteria give currently very limited benefits to the patient. Therefore many researchers work on more reliable criteria. There were efforts to find a correlation between the rupture risk and many geometrical quantities (AAA diameter/infrarenal aorta diameter, AAA volume...)[43] but none of these criteria was proved to have a statistically significant correlation with the rupture risk. On the other hand, evaluation of the patient's rupture risk based on the wall stress in AAA is the most promising criterion so far although it still needs to be validated on large sets of patients.

7 Wall stress in AAA as a predictor of rupture

From the mechanical point of view AAA is just a pressure vessel. Stress in its wall depends on its geometry and that of the other supporting organs, pressure by which it is loaded and, because of existing large strains, on the material it is made of. Pressure vessel will rupture when the stress exceeds its strength. In principle the same approach can be applied for an AAA. Maximal diameter criterion actually reflects the wall stress approach to some extend because it is based on the Laplace law:

$$\frac{\sigma_m(z)}{r_m(z)} + \frac{\sigma_t(z)}{r_t(z)} = \frac{p(z)}{t}, \tag{5}$$

where σ_m denotes meridian stress, r_m meridian radius, σ_t tangential stress, r_t tangential radius, p pressure and t wall thickness. Early clinical works used simplified version of eq. (5) which is valid for first principal stress of an ideal cylinder only:

$$\sigma = \frac{p \cdot r}{t} \tag{6}$$

Eq. (6) says that the stress increases proportionally to the corresponding radius. Therefore larger AAAs are more endangered by rupture than smaller ones. However this approach is not very reliable, because the resulting stress depends also on the blood pressure and wall thickness even for an ideal cylinder. Moreover, this law is valid only for a cylindric vessel with approx. constant thickness, constant radius, constant wall stiffness and supports not constraining radial displacements. None of these assumptions is valid for AAA. The thickness is varying from 0,2÷4,3mm even within one AAA[43,44]. Geometry is very complex and local radii vary greatly (i.e. maximal diameter area vs. iliac bifurcation area). Wall stiffness can

change locally when calcifications are present[34]. Iliac and renal arteries constrain AAA in such a way which restricts radial deformations.

For all of these reasons it is not possible to calculate wall stress in AAA accurately by using Laplace law. Consequently also the accuracy of the maximal diameter criterion is limited as described in chapter 6.1.

On the other hand the validity of eq. (5) is more general since it describes the force equilibrium so it defines the mean membrane stresses in the wall in any geometry. However, when curvatures of geometry are changing spatially (as they do in AAAs), stresses cannot be computed analytically and some numerical approach is required. The whole problem of using eq. (5) is discussed in 8.2.1.

So to improve the criterion for the necessity of surgery, we need to calculate wall stress in AAA more accurately. Finite element method (FEM) is very suitable for this task. It has been shown that peak wall stress (PWS) correlates better with rupture (currently it is 2÷3times better than maximal diameter criterion) than any other known criterion[42]. However, the referenced study compared only the computed peak wall stresses between groups of ruptured AAAs and those electively repaired[57] which is insufficient[74] because peak wall stress generally occurs in the neck area where rupture is very rare. To establish a new criterion we need local threshold values above which the risk of rupture significantly raises.

As mentioned at the beginning of this chapter, we also need to know the strength of the wall. Then, if we calculate the ratio of local wall stress to local wall strength, we obtain a rupture risk index (RRI), the distribution of which is shown in Figure 19.

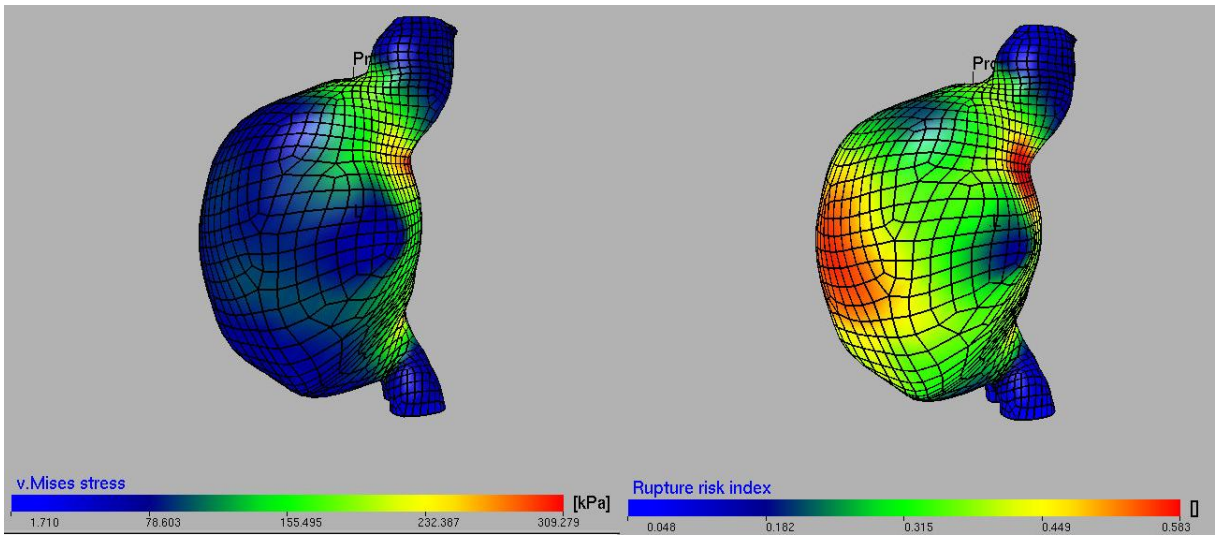

Figure 19 von Mises stress(left) and RRI distribution (right) in one AAA. Computed in A4research

Thanks to the encouraging results[86], the current effort is focused on identifying relevant entities which influence wall stress and strength in AAA to make this criterion even more

reliable. The further part of the thesis will be focused on a review of such entities which are thought to influence wall stress and strength, as well as on our achievements in the field of FEM modeling of stresses in AAAs.

8 Entities influencing wall stress in FEA of AAA

8.1 Geometry of AAA

It has been shown that idealized models of AAAs cannot predict the risk of rupture accurately. Therefore patient specific geometries of AAAs are reconstructed now. Some studies try to find statistical correlations between peak wall stress and the geometrical shape [79] but FEA of the patient specific AAA geometry can provide much more reliable results. However, there was a great deficit at our department in this field when I started my Ph.D. studies, since we were unable to reconstruct the patient-specific AAA geometries routinely. Therefore I have focused on this problem in order to manage the reconstruction of patient-specific geometries with an acceptable accuracy and time-consumption. I have passed an internship at Royal Institute of Technology, Stockholm, Sweden in a team of prof. Gasser where I have learned to use their A4research program (A4research vers.3.0, VASCOPS GmbH, Austria). This program was designed specially to reconstruct patient-specific geometries of AAAs[143] and it has been shown that the inter operator variability in PWS determination is very low[151] (in average 3.5%). As we wanted to improve the accuracy of numerical stress calculations, we have bought only the part of the program for the reconstruction of AAA geometry. The reconstruction process is as follows:

a) The set of CT images in format .DICOM (native format of Computer tomographs) is loaded (A4Research can reconstruct geometry only from the transversal sections). Then the user defines the region of interest i.e. where the AAA is located in the section. Usually it is from the iliac arteries up to renal arteries as described in chapter 4. It is noted that region of interest should start some 2cm below any arterial enlargement and ends 2cm above it due to possible artifacts at both ends of the reconstructed geometry.
b) The user defines typical intensities (in Hounsfield Units) of the lumen and ILT, so that the program can determine the gradient thresholds between the lumen and ILT, as well as between the wall and the outer space. The wall has the same range of intensities as ILT, therefore it is not possible to determine its inner boundary directly.
c) Program captures the luminal boundary in the lowest image. After this has been confirmed by the user, the whole luminal surface is captured from the bottom to the top image (against the blood flow direction). The obtained surface is then smoothed to avoid any sharp edges in it. It is noted that the program cannot capture the luminal surface correctly in case when arteries are extensively bended i.e. they go down than up and down again.
d) The outer surface of the AAA is captured next. To this end a virtual balloon expands from the luminal surface until the boundaries of the aneurysm are

detected. This expansion can be controlled by adjusting virtual parameters (viscosity, membrane and bending stiffness) of the expanding balloon.

e) The wall thickness was set in dependence on the thickness of the underlying ILT. Specifically, at sites of a thin ILT (thinner than 1.0mm) the wall thickness was 1.5mm and was reduced to 1.0mm behind a thick ILT (thicker than 25.0mm), which is in agreement with histological data[36].

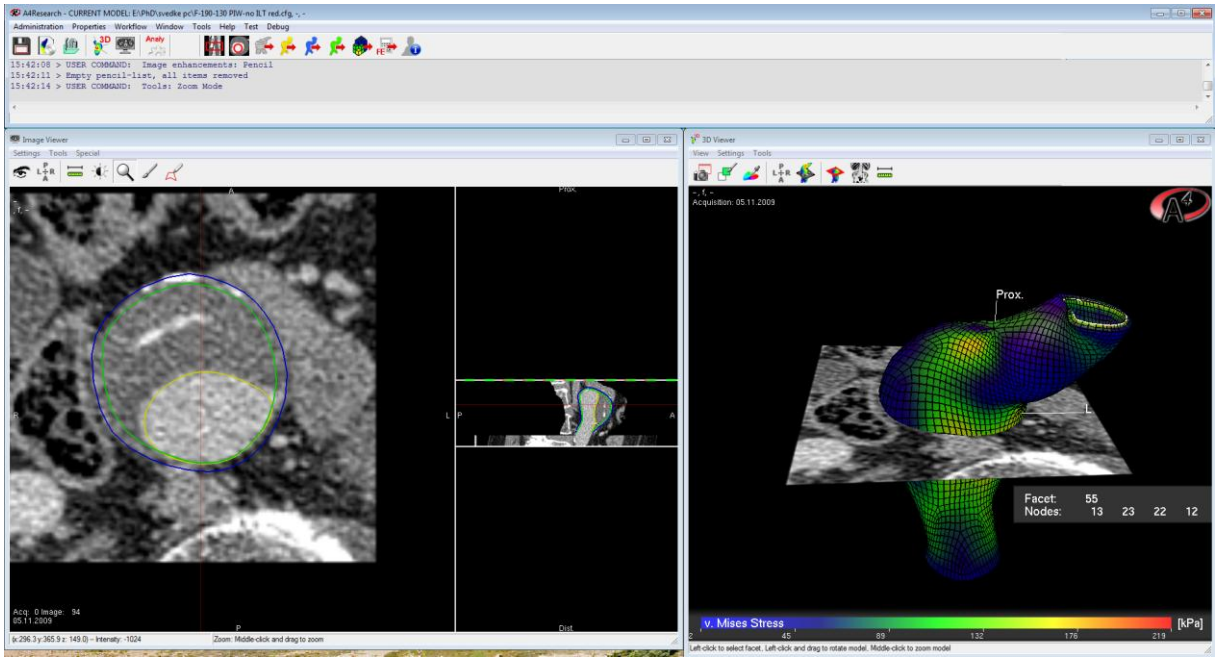

Figure 20 A4Research Interface and AAA reconstruction

The reconstructed geometry and the user interface of described program is shown in Figure 20. We are able to reconstruct a patient-specific geometry in one hour or so which greatly improved all of our studies because wall stress calculated from AAA being loaded by a mean blood pressure depends mostly on its geometry (see Appendix G)

8.1.1 Effect of the branch arteries on the wall stress in AAA.

In the aortic region where AAA exist, 6 lumbal arteries and mesenteric inferior artery (see Figure **2**) are placed; they are denoted as branch arteries below.. I see potential in examining the role of branch arteries on the wall stress because nobody considered this influence till now. It has been reported that some 80% of AAAs rupture in the lateral or posterolateral area[82,150]. Although it has been suggested that it may be caused by a structural heterogenity of aneurysmal wall[149] I believe that branch arteries may play role in it too. From the mechanical point of view it is obvious that any hole acts as a stress concentrator. On the other hand, it is possible that the wall is significantly reinforced by collagen fibers in the area of branching. One way or another, the author believes that this topic should be opened for a thorough discussion. Therefore we have investigated this topic by FEA of 5 AAAs (see Appendix G). It was confirmed that the presence of branch arteries in the model increase the wall stress as

expected. However these results need to be combined with the histological information about the collagen structure in the region of aorta with the root of the branching artery. Due to unavailability of such information in literature we have designed a study in cooperation with the team of prof. Hermanova from Department of Anatomy and Pathology and team of prof. Staffa from 2nd surgical department, both of St. Anne's University Hospital. Surgeons from the team of prof. Staffa harvested couple of aortic tissue samples containing the origin of mesenteric inferior artery. Those samples were then processed by the team of prof. Hermanova who provided stained specimens for us. The whole process was very difficult for several reasons. First we experienced that it is very hard to locate exactly the origin of the artery in vivo. Several times tissue samples were harvested which contained the branching artery but not its origin. Also it was not easy to cut 7μm thick slice from the tissue containing hole (artery). Despite this we have received so far three histological samples where the collagen orientation can be investigated as shown in Figure 21. A complicated collagen structure can be seen there which needs to be determined first. The study is now stopped until the computer program for automatic evaluation of collagen orientation from the histological sections will be finished, as described in chapter 8.2.2.1.

Figure 21 Origin of inferior mesenteric artery passing through the aortic wall. Staining van Gieson. Magnification 20x. Empty space in the middle of the image is the lumen of branching artery. Intima of branching artery contains collagen fibers oriented along the blood stream direction while media contains collagen fibers perpendicular to the plane of image. Dark purple in the image corners is the collagen in the aortic wall.

Once we finish the analysis of collagen orientation in the branching arteries we will try to assess the importance of material anisotropy in this region for both stress analysis and wall strength. Then we could improve the accuracy of the rupture risk evaluation presented in Appendix G to assess better the AAA rupture potential in this areacompare the obtained results with the calculated stresses as presented in Appendix G to determine rupture potential of this areas in AAA.

8.2 Material model

Early FEAs used linear material model[49] and there is a group of researchers who still use linear material model to obtain realistic deformations of AAA during cardiac cycle[50,61]. It is based on the observation that during cardiac cycle (between the systolic and diastolic pressures) AAA deformations are rather small and they can be described with a sufficient accuracy by a linear material model with E=5.5÷12.9MPa[62]. Such model is very simple, the stress field is obtained very quickly and within its limitations it can give acceptable results (see Appendix G).

AAA tissue however exhibits nonlinear stress-strain response as shown in Figure 16. A more precise model was proposed by Raghavan et al.[47] who fitted results of uniaxial tensile tests of the AAA tissue by Yeoh-type[87] material model:

$$\Psi = c_{10}(I_1 - 3) + c_{20}(I_1 - 3)^2 \tag{7}$$

with constants $c_{10} = 177kPa$ and $c_{20} = 1881kPa$. Currently this is by far the most widely used material model for FEA of AAAs and we also used it for some of our works. Limitation of this model is given by the fact that it has been fitted on uniaxial tensile tests while AAA is in vivo under a general 2D stress state. When Vande Geest et al. performed biaxial tensile tests of AAA tissues, they obtained a quite different stress strain response[29]. They fitted their results by an anisotropic material model proposed by Choi-Vito[88]:

$$\Psi = b_0(e^{\frac{1}{2}b_1E_{\theta\theta}^2} + e^{\frac{1}{2}b_2E_{LL}^2} + e^{b_3E_{\theta\theta}E_{LL}} - 3) \tag{8}$$

with constants: $b_0 = 0.14kPa$, $b_1 = 477$, $b_2 = 416.4$ and $b_3 = 408.3$. Both strain energy functions differ significantly as shown in Figure 22. Results presented by vande Geest et al. were recently confirmed by other study[85] and also by our results (see Appendix G), while there is no other study which would confirm the results presented by Raghavan et al.[47] It has been suggested that the difference is caused by the significant pre-tension force[29] (force used during testing to make sure that specimen remains flat) in the experiments by Raghavan et al[47].

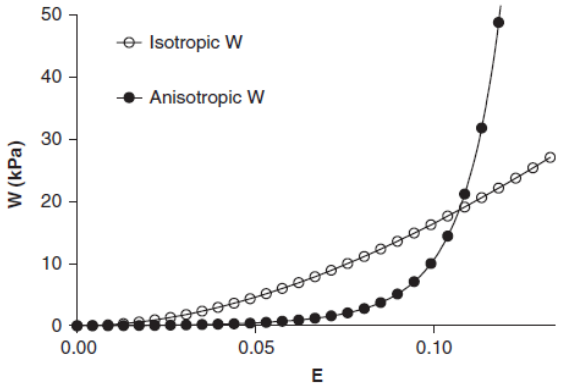

Figure 22 Strain energy function W vs. equibiaxial strain, obtained from uniaxial (isotropic) and biaxial (anisotropic) tests. Reprint from 29

The family of phenomenological material models used for modeling of aneurysmal wall is completed by model proposed by Demiray et al.[91] used in study[90] and by us as well (see appendix G):

$$\Psi = \frac{a}{b}\left(e^{\frac{b}{2}(I_1-3)} - 1\right) \tag{9}$$

The values of constants obtained in study[90] are: *a=1.04kPa* and *b=280.4.* It is noted that this is the fit to experimental data published by vande Geest et al.[29]

All models discussed above are purely phenomenological. Nevertheless there are also several models respecting more or less the histological structure of the arterial wall.

Model proposed by Holzapfel, Gasser and Ogden[89] was originally designed for a healthy arterial wall but it has been applied to aneurysmal wall[85]:

$$\Psi = \mu(I_1 - 3) + \frac{k_1}{2k_2}\left(e^{k_2\cdot[(1-\rho)(I_1-3)^2+\rho(I_4-1)^2]} - 1\right) \tag{10}$$

where the first component defines isotropic properties of the matrix which is assumed to be Neo-Hookean with μ being a stress-like parameter defining the stiffness of the matrix; k_1 and k_2 refer to the behavior of the collagen fibers and ρ describes the dispersion of the fibers around its preferred direction. The obtained values of material constants were: *μ=7kPa, k_1=97.4kPa, k_2=173.7, φ=31.9°* and *ρ=0.32* which gave a very good fit to the experimental data R^2=0.95.

Variations of this model were presented by Rodriguez et al.[90]

$$\Psi = \mu(I_1 - 3) + \frac{k_1}{2k_2}\left(e^{k_2\cdot[(1-\rho)(I_1-3)^2+\rho(I_4-I_{40})^2]} - 1\right) + \frac{k_3}{2k_4}\left(e^{k_4\cdot[(1-\rho)(I_1-3)^2+\rho(I_6-I_{60})^2]} - 1\right) \tag{11}$$

where two symmetrical families of fibers with the same properties are taken into account, and also a stretch threshold I_{40} and I_{60} is defined under which the fibers do not produce any stress response since they are not yet straightened from its original wavy position. The mentioned

study, however, uses this model to fit only one set of patient specific data and not the mean population data, therefore I do not provide the values of its constants.

Further variation of this model was performed by Baek et al.[92] who used the same model formulation as eq. (10), only with four families of fibers. Increasing numbers of families of fibers generally produce more isotropic response which can better describe the response of the aneurysmal tissue which is much less anisotropic than healthy aorta[27,29].

In fact there are two still opened questions which we tried to answer as well:

1) How important is the material model in calculation of the wall stress in AAA?
2) Is it possible to describe the aneurysmal tissue sufficiently by isotropic material models or is it necessary to use anisotropic models?

8.2.1 Effect of the material model on the wall stress in AAA

We tried to answer the first question in our study (see Appendix G) which is currently under revision in Medical Engineering & Physics journal. Briefly, we took CT scans of seven patients who underwent surgical repair of AAA and reconstructed their AAA geometries. We also obtained tissue samples from the removed AAAs and we tested them biaxially within 3 hours after surgery. Results have been fitted by isotropic Yeoh type model which served as a reference material model for each geometry. We chose other material models based on mean population data from three different studies to investigate the effect of material model on the computed wall stress in AAA. We also used prestressing (for more detail see chapter 8.5) to ensure that the deformed geometry will always be the same regardless of the material model used.

We showed that the model based on vande Geest data[29] (biaxial tests) gave practically the same results as our patient-specific models but they differ significantly from the results obtained from Raghavan data[47] (uniaxial tests) and van't Veer data[94] (linear model). This offers a simple conclusion that the calculated wall stress depends on the material model. However the whole problem is a little bit more complicated.

Problem is that LaPlace law, as described in eq. (5), is a force equilibrium equation which is valid in any geometry and it is independent on material; this is in apparent contradiction to our results. We demonstrated this problem with a simple cylindrical geometry (see Figure 7 in appendix G) where stresses on the inner and outer surfaces of the wall are plotted for different diameters of the cylinder and different material models. It is obvious that although stresses on surfaces vary significantly from model to model, their mean value satisfies always LaPlace law and is independent on material model. We concluded that highly non-linear material models produce also high stress gradients across the wall despite its relatively small thickness.

It is also important to note that high stress gradient is in contradiction to the uniform stress hypothesis[95] (for more detail see chapter 8.4). Consequently high stress gradients are most likely not physiological (at least when AAA is loaded by a mean pressure) and they should be treated as an artifact. Therefore it is meaningless to compare stresses in the individual nodes as a measure of impact of material model on the computed wall stress as many researchers do[97-101], because then you compare values influenced heavily by an error caused by the presence of a stress gradient which is not physiological.

So it is most suitable to use the stiff linear material model[94] for comparing individual aneurysms and their rupture risk potential, when they are loaded by a mean pressure; it gives an average stress across the wall close to the physiological distribution and therefore it is possible to decide which AAA is risky and which is not.

We also hypothesize that also highly nonlinear models should give the same results when residual stresses are included into the FEA of AAA, but it needs to be verified.

On the other hand, material models based on biaxial tensile tests are irreplaceable when stresses under elevated blood pressure are computed. One must keep in mind that the response of the tissue on increased pressure includes bending. Consequently stress gradients cannot be balanced by remodelation any more due to the short time period of loading by the increased pressure. Therefore it is not possible to calculate wall stresses using LaPlace law with an acceptable accuracy anymore, and a credible material model is necessary.

Based on my experience I hypothesize that an AAA rupture is result of bending of aneurysmal wall during elevated blood pressure which will increase stresses at one surface of the wall and it might damage the collagen fibers in that area which then gradually brake even under normal blood pressure up to total rupture of the arterial wall. This hypothesis needs also to be validated of course.

8.2.2 Isotropic vs. anisotropic material models

Comparison of isotropic and anisotropic models has been performed in several studies[97,99,100]. All of them provided the same conclusion that anisotropic models give higher stresses. However all of these studies compared stresses at the surfaces which are not relevant as we showed in the previous chapter. We believe that the question whether it is necessary to use anisotropic material models for an accurate prediction of wall stress in AAA (under elevated pressure) can be answered on the basis of the microstructure of aneurysmal wall.

Although collagen fiber orientation in the arterial wall has been investigated largely (see for instance studies[102,103,104]), there are very few studies investigating the collagen fibers distribution in the aneurysmal wall[93]. Another limitation is given by the method of polarized

light microscopy (PLM) used in these studies. Although this is a well established method of detection of collagen fiber orientation[105,106], it has several limitations.

First of all it is very time consuming because it requires a manual detection of each fiber by an operator. Because of that the actual process of detection has to be restricted to relatively low number of points (typically from 30 to 50)[93,102] in an area of some 15x15mm with several thousand fibers (see Figure 23). It is hard to imagine that one can accurately capture the collagen distribution from such a low number of measurements.

Second limitation is that the process is manual and consequently operator dependent. Study[93] showed that the Pearson´s correlation coefficient between two operators was 0.85 in average. It is not bad but still an unnecessary source of error. Moreover it should be emphasized that Pearson´s correlation coefficient says only how well do both curves follow the same trend but it provides no information regarding agreement in amplitudes.

Another limitation is the necessity of using only Picrosirius red staining, while different staining can provide better images. Compare Figure 23 and Figure 24.

The last limitation rises from the principle of the method. There is very low light coming into microscope due to the necessity of using a polarizer filter which significantly decreases the amount of light passing into microscope. Consequently the maximum usable magnification is some 20x to 40x. Individual collagen fibers take only few pixels under such magnification.

Because of the mentioned limitations we have decided to use some of the automatic image processing methods.

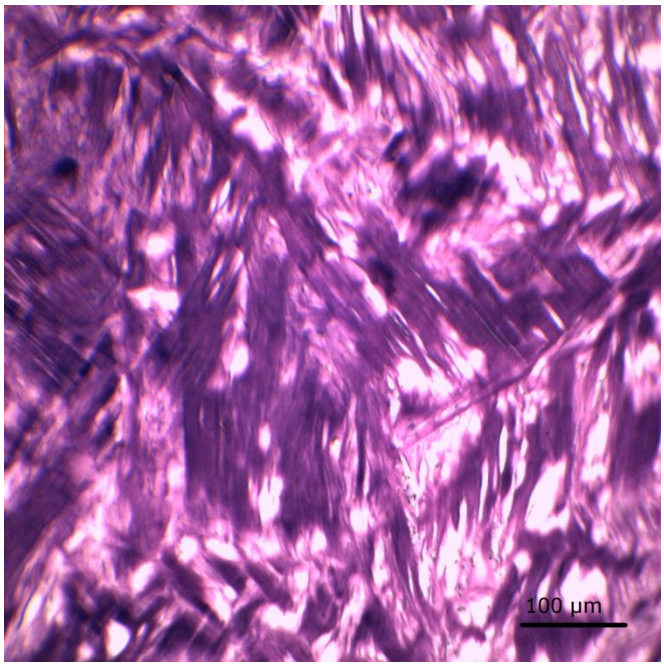

Figure 23 Collagen fibers in the aneurysmal wall. Stained by van Gieson. Magnification 20x. Note that individual collagen fibers are 2-10µm in diameter

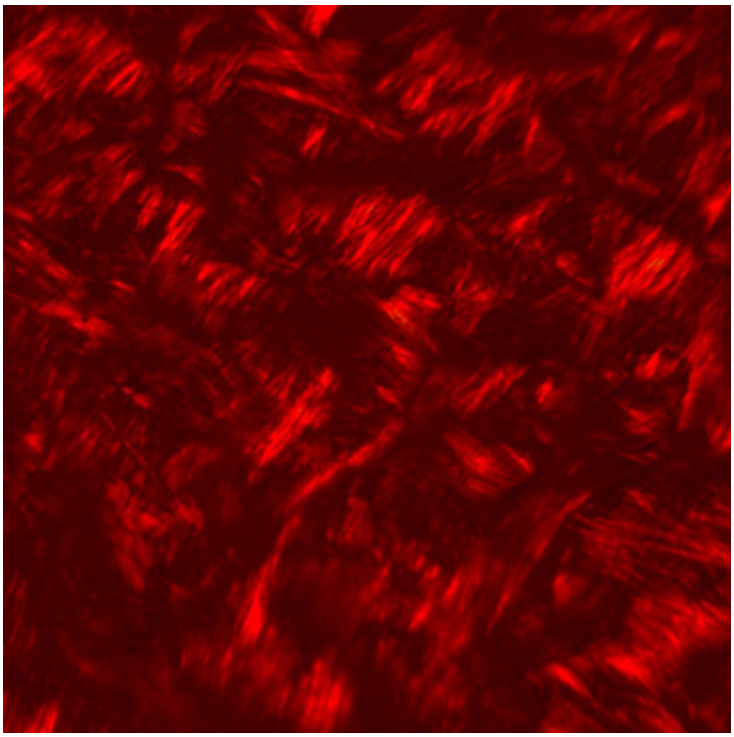

Figure 24 Collagen fibers in the aneurysmal wall. Different specimen. Staining Picrosirius red, magnification 16x

8.2.2.1 Fast Fourier transformation and image processing

I would like to stress out that this work is still in progress therefore I cannot refer to any submitted paper. Consequently this chapter will be more extensive because it is necessary to give comprehensive information.

We have based our method on the fast Fourier tranformation (FFT) of the image which was shown to be a reliable and fully automated technique when it comes to determine dominant directions in the image[107-111]. Moreover, it has been already applied in qualitative analysis of collagen orientation[108,109]. We find it more general and easier for implementation than other methods based on gradient analysis of images. These methods require the desired object to have a defined intensity to be detected, then an ellipse with the same moments of inertia is fitted to the detected object, and the longer axis of this ellipse defines the dominant orientation of the object[112,113]. Another method based on detection of valleys and ridges we found to be too complicated for programing[114].

Method description:

The proposed method is based on image analysis. The principle is adopted from the study by Ayres et. al.[109]. Programing was done in cooperation with prof. Druckmuller and Ing. Druckmullerova from the Department of Mathematics at our university. First the image is loaded and a standard filtering using dark frame and flat field images is performed. Interested readers are referred to literature on image processing regarding this operations[115,116]. In principle the proposed method can analyze only square shaped images. So if the image is not square shaped, the largest possible square is cut out for further processing.

Then the Hanning window function is defined as follows:

$$f(m,n):$$

$$\text{for } m = 1..a$$

$$\text{for } n = 1..a$$

$$\sqrt{(k-m)^2+(k-n)^2} = p$$
$$p > k \rightarrow f = 0$$
$$p < 0.8k \rightarrow f = 1$$
$$0.8k < p \leq k \rightarrow f = 0.5 + 0.5 \cdot \cos\left(\frac{5 \cdot \pi \cdot p}{k}\right), \quad (12)$$

where m,n are independent variables, a is the size of the image, $k = \frac{a}{2}$ defines the distance from the center of the image to its edge. Hanning window serves as a filter to cut off the image edges which would induce unwanted artifacts in further analysis. It filters off everything what is farrer than a half of the image size from its center and keeps everything being closer to the center of the image than 0.8k. The rest of the pixels which are between these two limits are weighted by the cosinus function, so their influence decreases with their distance from the center. This set up was found to provide a good result in filtering off the

effect of edges while affecting the smallest possible part of the image. Both the original image and the image filtered by Hanning window function are shown in Figure 25.

Next step in the analysis is performing the 2D fast Fourier transformation:

$$F(u,v) = \frac{1}{2a}\sum_{m=0}^{2a-1}\left[\frac{1}{2a}\cdot\sum_{n=0}^{2a-1} e^{\left(\frac{-2\cdot\pi\cdot i\cdot n\cdot v}{N}\right)}\cdot s(m,n)\right]\cdot e^{\left(\frac{-2\cdot\pi\cdot i\cdot m\cdot u}{M}\right)} \quad (13)$$

where $s(m,n)$ is the image processed by Hanning window function. The amplitude spectrum of F is plotted in the left part of Figure 26. The brightest point in the image center defines the lowest obtained frequency. Pixels more distant from the center represent higher frequency in the image. Low frequencies define the size of the image and its roughest components, while high frequencies represent the finest details in the image and also the noise. The bright parts in the corners and around the middle of the edges are numerical artifacts which should be filtered off. It can be seen that there are some rays going from the center in certain directions. These rays define the more frequent frequencies in the image which refers to the distinguishable directions in the analyzed image (compare Figure 25 and Figure 26).

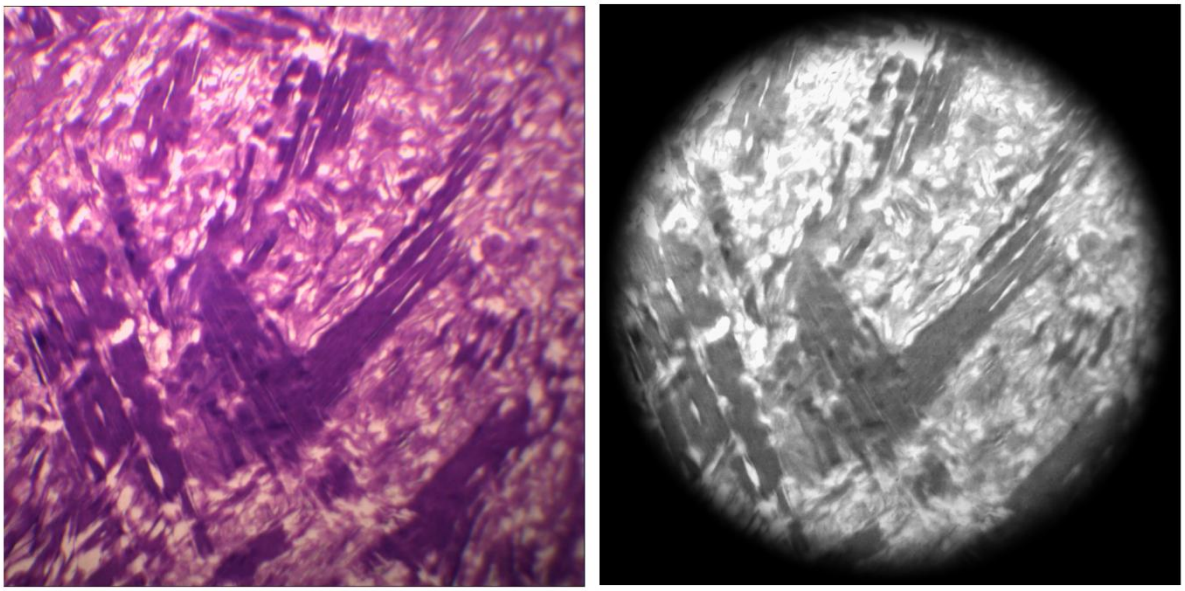

Figure 25 Original image of collagen (purple and pink) in human AAA (left) and image after filtering by Hanning window function (right). Magnification 20x, staining van Gieson.

The next part of the analysis aims at filtering off the artifacts and the noise. We use inverse Hanning window function which is defined as follows:

$$f_{INV}(m,n):$$

$$\text{for } m = 1..a$$

$$\text{for } n = 1..a$$

$$\sqrt{(k-m)^2 + (k-n)^2} = p$$

$$p \leq 0.05k \rightarrow f_{INV} = 0.5 + 0.5 \cdot \cos\left(\frac{20 \cdot \pi \cdot p}{k} - \pi\right)$$

$$0.05k < p \leq 0.5k \rightarrow f_{INV} = 1$$

$$0.5k < p \leq 0.6k \rightarrow f_{INV} = 0.5 + 0.5 \cdot \cos\left(\frac{10 \cdot \pi \cdot p}{k} - \pi\right)$$

$$p > 0.6k \rightarrow f_{INV} = 0 \quad (14)$$

Dimensions of this window were set up in order to filter out as much noise and as many artifacts as possible without affecting substantial frequencies (rays in Figure 26). The image after this filtering can be seen in the right part of Figure 26.

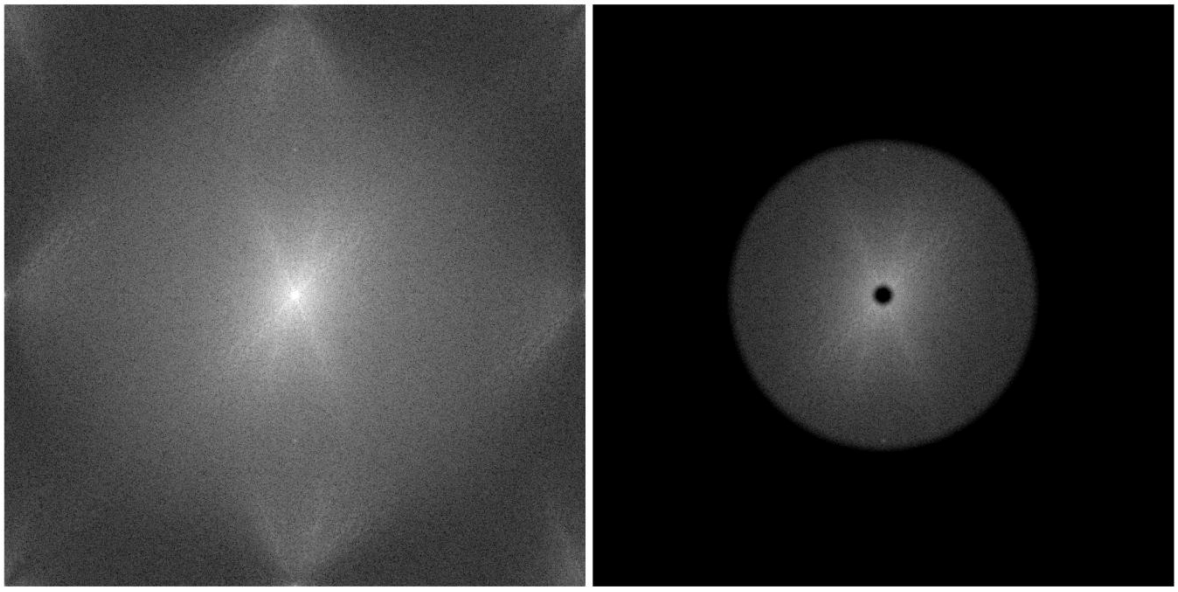

Figure 26 Amplitude spectrum of image after 2d FFT (left) and after second filtering of modified inverse Hanning window (right)

Now we need to sum the intensity of pixels in the filtered image (right part of the Figure 26) over individual directions. Therefore the image is divided into 180 sectors, each 1° wide with its corner in the center of the image and all intensities of all pixels which lay inside this sector are summarized. Finally the result is normalized, so that we obtain a distribution function of the dominant directions in the analyzed image. The final graph can be seen in Figure 27. X axis represents angles where 0 refers to the right horizontal direction while Y axis represents the probability that fiber is in the given direction.

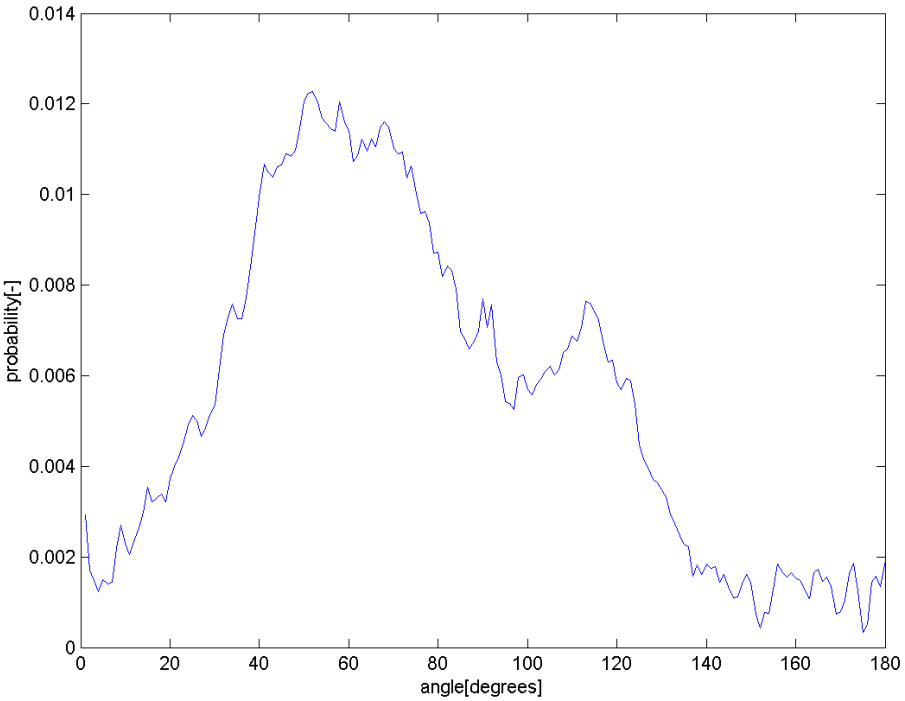

Figure 27 Distribution of collagen fibers in the analyzed image

As you can see when comparing Figure 25 with Figure 27 there is qualitative agreement in the dominant directions. What remains unclear is the quantitative comparison. It has been pointed out that there is a significant influence of background signal in FFT[117]. Although its effect is overestimated in the referred study because it is evaluated with an artificial and periodical image, it plays an important role in the analysis of real tissue images too.

Influence of a background signal:

Effect of a noise on the probability distribution is demonstrated in Figure 28. The artificial image was created with two dominant orientations of lines. First set of 56% of lines was oriented in 40° while 44% of lines were oriented in 59° and 60°. Care was taken specially to avoid periodicity (lines with the same distance between each other). Then the noise was added into this image. Both images are shown in 1st row in Figure 28.

Images were then analyzed as described above and the results are plotted in the 2nd row in Figure 28Noise decreases the importance of lines so those have a smaller probability compared to the image without noise, although the effect is underestimated here because of large dispersion (see left graph in the 2nd row in Figure 28around the peaks in case of image without noise which indicates that some unwanted periodicity is still present in the image. Consequently this fact underlines the necessity of further filtering.

As a filter we proposed a power function which is applied on the obtained FFT spectrum. :

$$F(m,n) \quad = \sum_{m=1}^{2a} \sum_{n=1}^{2a} F(m,n)^p \tag{15}$$

where *p* is an unknown power to be determined. We exploited here the property of a power that it enhances high values and suppresses low values. This effect is shown in graphs in the 3rd and 4th rows in Figure 28. These graphs were obtained by using *p=5* and *p=10,* respectively. Higher power suppressed the noise more as expected. Of course there is an upper limit for p as well. If we increased p too much it would suppress also the less dominant direction of lines which we want to capture. Therefore an optimal *p* value needs to be determined.

Determination of proper power:

It is obvious that a proper value of *p* will differ from application to application. Therefore I have determined it directly on the investigated samples of aneurysmal tissue stained by van Gieson. The first part of the process is captured in Figure 29. First I took an image of a ROI under magnification of 20x and resolution of 2592x1944 pixels (Figure 29 (a)). Then the same area was captured again but this time with magnification of 500x and resolution of 1280x960 pixels which resulted in 625 images covering the same area (example Figure 29 (b)). All images were taken by standard light optical microscope Bresser Researcher Trino II and Bresser microcam 9Mpix (Bresser GmbH, Germany).

Each of these images was then analyzed by the algorithm described above to obtain graph in Figure 29 (c)). The angle with the maximal probability of presence was then multiplied by the percentage of pixels having intensity higher than 0.1 (estimated low threshold of intensity of a collagen fiber – it must be assessed for each set of specimens) and stored. This multiplication was done in order to distinguish between an empty image with one fiber only and an image fully covered by fibers. This step also means that I assume that for magnification of 500x the fibers are distributed homogenously in the image. I am aware that it is simplifying to some extend.

The obtained histogram is then normalized (Sum over all angles equals to 1). Last step is to analyze the image captured with magnification of 20x and find the value of power *p* which results in the best mutual fit of both curves. The histogram and best fit curve are shown in Figure 30. The obtained power value was *p=8* and resulted in R^2=0.73 which is not bad but it could be improved.

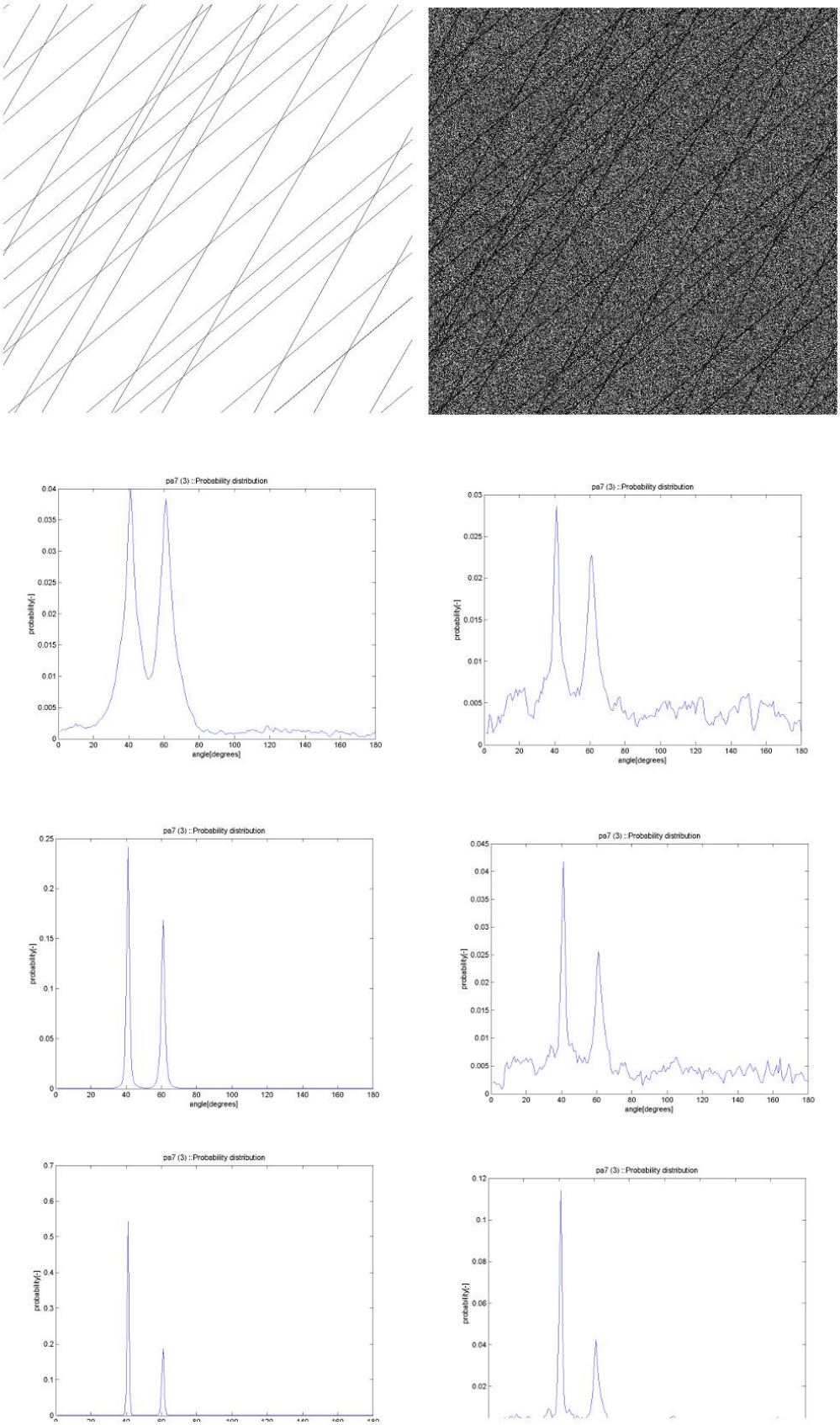

Figure 28 Effect of noise on fibers probability distribution function. Left image shows artificial image without noise, right image is the same except for the added noise. Second row contains graphs of orientations in the analyzed images. It is clear that noise induces unwanted artifacts in the graph. Effect of powering is shown on 3rd and 4th rows. Higher power (4th row) can decrease the noise and enhance the true dominant orientations better than the lower power (3rd row)

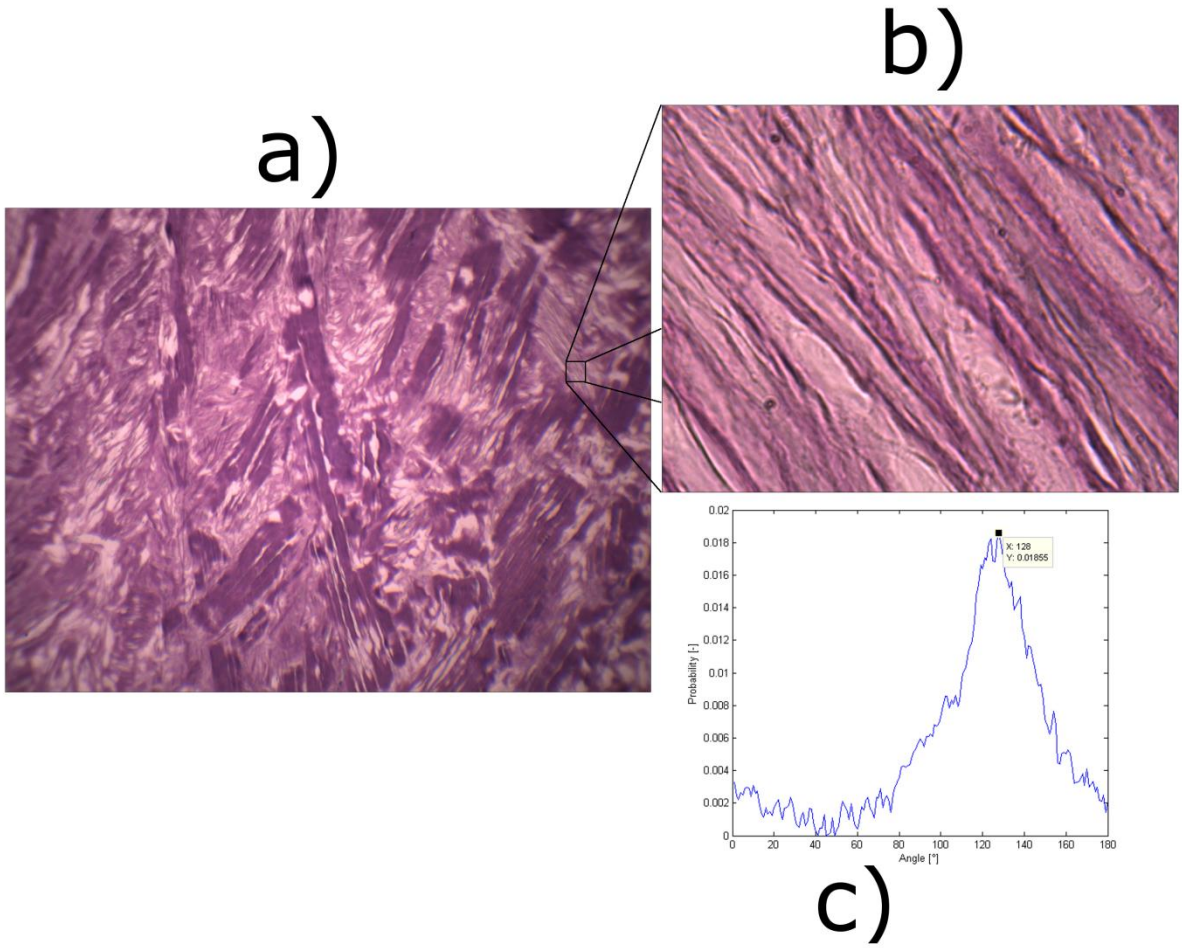

Figure 29 Image analysis process. The analyzed area is captured with magnification 20x (a). Then 500 images are captured with magnification 500x (b) which alltogether cover the same area as image (a). FFT is then performed for each image (b) and the probability distribution graph is obtained (c). Angle with maximal probability is then stored and next image is analyzed.

One way of increasing the R^2 value could be some floating averaging of the data or increasing the step size from 1° to 5° or so. It is obvious that the data obtained from analysis of 625images are not smooth which may be caused by the assumption expecting uniform orientation across the image. As I pointed out at the beginning of this chapter, this work is still in progress and a further improvement of the results can be expected.

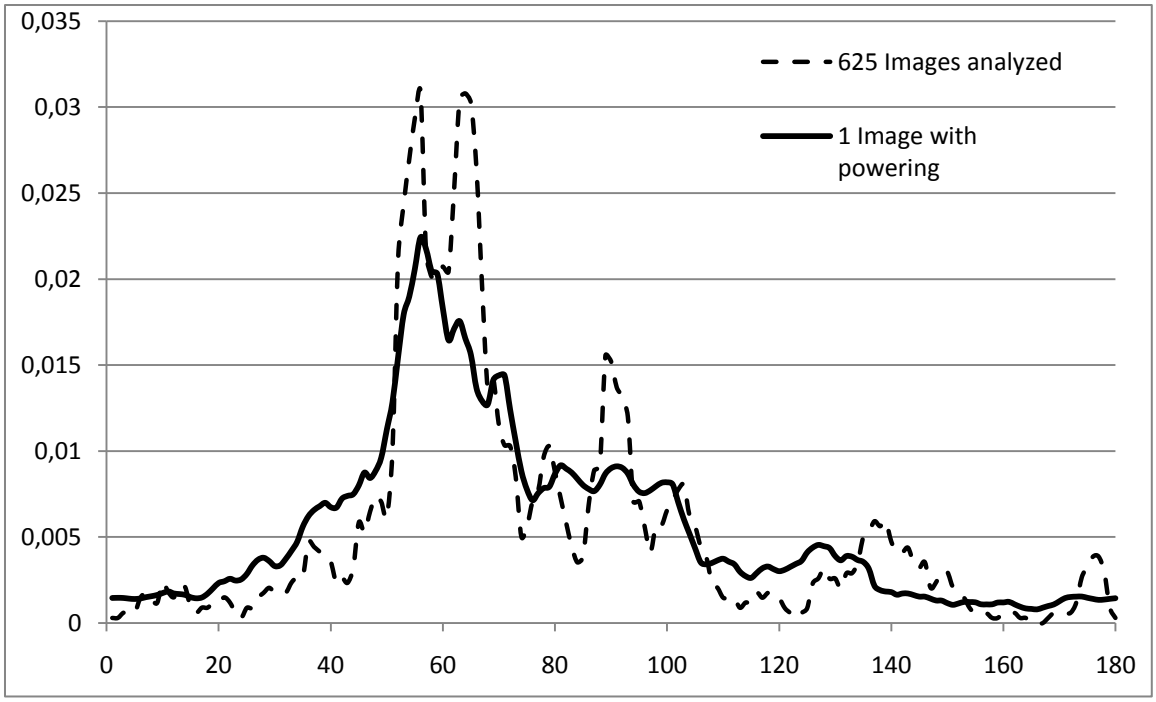

Figure 30 Best fit of distribution obtained without powering by analyzing 625images (dashed line) and by analysis of 1 image with powering (solid line)

Comparison with PLM:

To validate our algorithm we need also to compare the results with some established methos such as PLM. To do that we cooperate with prof. Gasser and Caroline Forsell at KTH Stockholm where there is a stand for PLM. They measured 5 images, in the concrete they measured collagen orientation of 5 specimens at 200points per specimen. Then the same specimen was captured and the image was analyzed by our algorithm. Results are shown in Figure 31 and Table 3 (estimated power value was $p=20$ in this case).

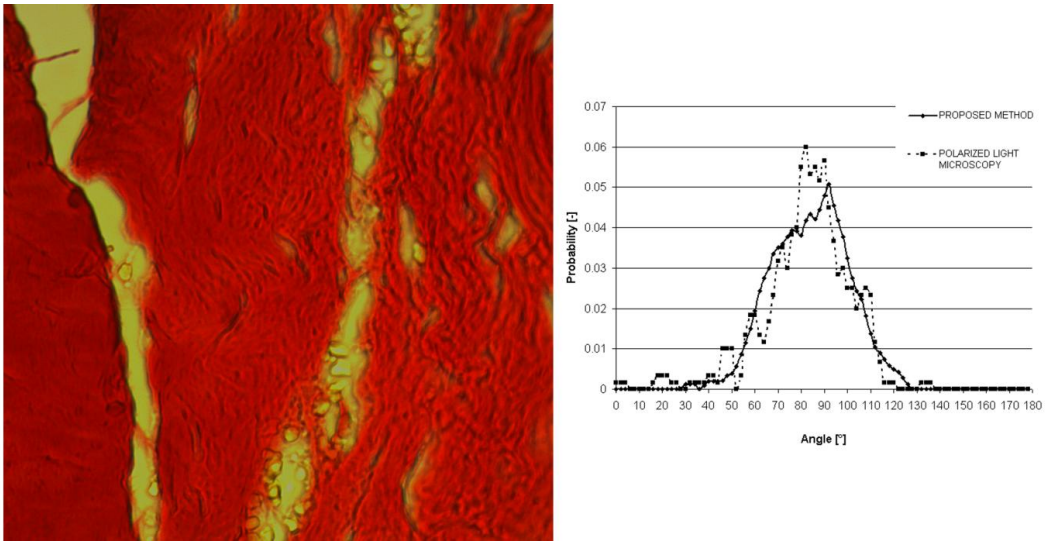

Figure 31 Comparison of distribution of fibers of image 1 (magnification 50x, staining Picrosirius red) according to the proposed method and PLM measurement

image		mode [°]	Sum of square differences	R^2
1	PLM	82		
	proposed method	92	2.69E-03	0.89
2	PLM	74		
	proposed method	78	1.34E-02	0.72
3	PLM	88		
	proposed method	88	3.46E-03	0.75
4	PLM	88		
	proposed method	92	3.10E-02	0.65
5	PLM	88		
	proposed method	90	5.00E-03	0.82

Table 3 Statistical comparison of polarized light microscopy (PLM) and the proposed method

There is qualitative as well as quantitative agreement between both methods. Differences are given by the noise on the side of our method, and by the fact that not all fibers were measured by PLM. However we can state that both methods give quantitatively matching results which means that the time consuming PLM can be replaced by our automated method based on FFT.

Study design:

As the proposed method has a potential to replace PLM, we have designed a study (in cooperation with dr. Tichy from Department of Anatomy and Pathology of St. Anne's University Hospital under supervision of prof. Hermanova) to determine a collagen fiber distribution in AAA. The team of prof. Hermanova is about to prepare histological specimens from aneurysmal wall tissue harvested during AAA elective repairs (in 2nd Department of Surgery, St. Anne's University Hospital by surgeons under supervision of prof. Staffa). These specimens (n=15) were tested biaxially first as described in 8.2.3. Then they were kept frozen in -18°C until the study was performed. Specimens 18x18mm were put for 24 hours into formaldehyde after slow thawing. Next step is to dive the specimen into wax bath to make it stiff. Each specimen was then cut as shown in Figure 32. So there are 7 samples in each direction. Theoretical sample sizes are 18x1.5mm in axial direction, 15x1.5mm in tangential direction and 15x15mm in radial direction. This sample preparation is currently in progress. In the end there will be 105 samples in each direction.

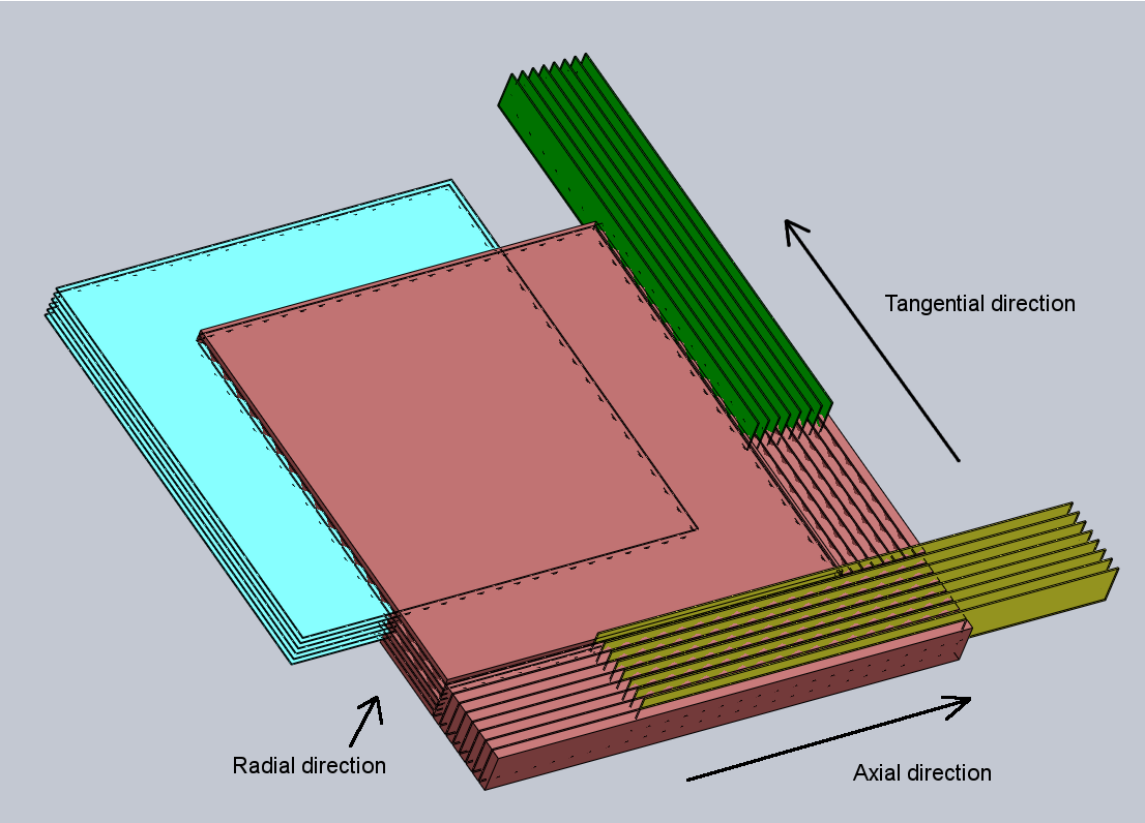

Figure 32 cutting directions in histological specimen preparation. Original tissue sample is marked pink.

Once the samples are cut they are stained by van Gieson (detailed description not mentioned here) to make collagen fibers visible. The last step will be analyses of all 315 samples using our algorithm to provide comprehensive data about dominant fiber alignment and its dispersion in 3D. This can help us to answer the question of significance of anisotropy in the aneurysmal tissue.

8.2.3 Biaxial tensile tests of AAA tissue

Biaxial tensile test is currently the best method for identifying of mechanical behavior of soft tissues[118]. However there are only two studies using biaxial tensile tests to identify the mechanical properties of aneurysmal tissue[29,85] (it was only one at the time I started my Ph.D.) Therefore we have focused also on this topic with two major goals. First one was to confirm the published results and the second was to compare capabilities of both isotropic and anisotropic material models in capturing the mechanical behavior of the aneurysmal tissue.

Experimental testing:

Our experimental device and its capabilities are extensively described elsewhere[119]. Therefore I will only briefly describe changes made since 2009. First we have changed the mounting system. Clamps are now clenched by a springs instead of screws which makes the sample

clamping process much faster (see the left image in Figure 33). More important was a change in the lever beam system which has been redesigned in order to make it possible to mount smaller samples down to 18x18mm. This was necessary due to the fact that samples harvested from elective surgery have usually similar size and it was not realistic to expect larger samples. We have also changed the strain gauges for more accurate ones from HBM (Hottinger Baldwin Messtechnik, Germany). The last change concerns the camera which was changed for a faster one Basler SCA 1300-32gm (Basler AG, Germany).

With this set up we have started our testing. Our quasi-static experiments are described in detail in Appendix G.

We have started to harvest data in February 2011 by virtue of the cooperation with the team of prof. Staffa mentioned above. This was also approved by local ethical committee of the hospital. So far we have collected data from 21 patients being generally in good agreement with the published data (see Figure 3 in Appendix G), although they appear to be shifted towards higher strains; this can be explained by different definitions of the unloaded state. Generally both referred studies used some small force (on the order of 0.05N or so) which is necessary to make the specimen flat at the beginning of the test. This small force however acts on the material with a very low initial stiffness (on the order of units of kPa), therefore it can produce strains of several %. On the other hand, we have removed the sample from the machine after preconditioning and recorded the reference image when the sample was covered only by a thin glass (see Figure 33). This was possible due to the used clamps which unlike hooks (used by the others[29,85]) do not destroy the tissue, therefore a repeated mounting and unmounting is possible. It may explain the observed differences in Figure 3 in Appendix G.

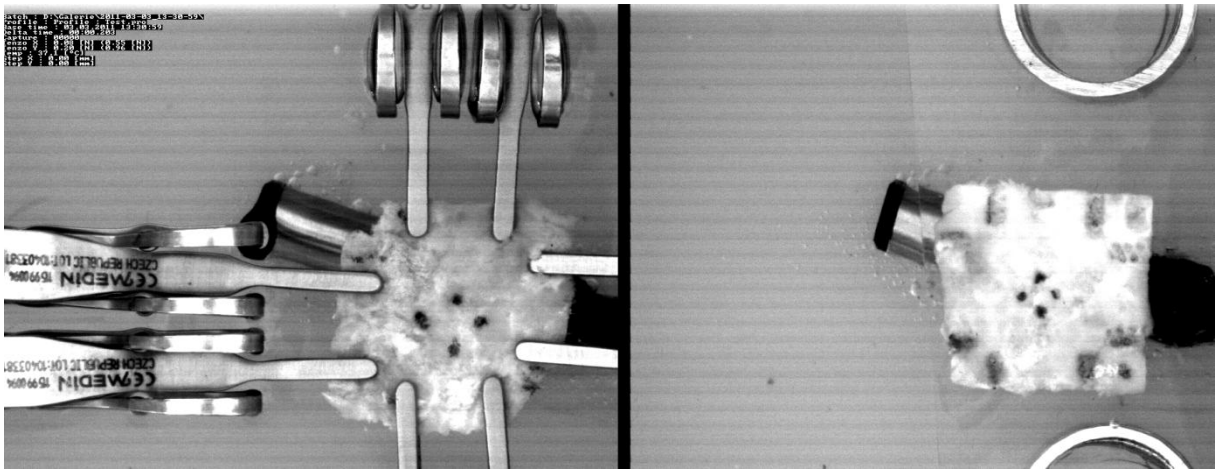

Figure 33 typical AAA sample during testing (left). Note the new clamps with springs. Unloaded sample during capturing the reference image (right).

The study will be evaluated after having harvested some 30 samples in order to provide statistically relevant data. So far the preliminary results published in Appendix G show the following facts:

- Inter-patient variability is much bigger than differences between any model and a single experiment
- Isotropic material model (Yeoh type) can fit the experimental data satisfactorily when the ratio of displacements u_x:u_y does not change more than from 2:1 to 1:2

Limitation of comparison published in Appendix G is given by the fact that only isotropic material models have been used. To further improve our results we have decided to implement anisotropic material models; it will enable usto compare wall stresses in a similar way as done in Appendix G.

8.2.4 Definition of the main directions in AAA

Key problem with using of any anisotropic model is that it requires defining principle directions in each element. This task is simple when performed on raxisymmetric geometries. Tangential, radial and axial directions are usually considered as principle material directions[10,12]. Determination of principle material directions is however difficult when it comes to patient specific geometries. Then there are basically two possibilities. First is based on the assumption that the principle material directions correlate with the directions of principle stresses or strains. This approach requires iterative loop where the directions are firstly guessed, then FEA is performed and the obtained directions of principle stresses are compared with the guessed direction. Then the principle material directions are corrected and FEA is performed again. This loop continues as long as there is a significant difference between principle stress directions and principle material directions. It implies that several FEAs are required which is very time consuming when considered that one FEA takes between 2-6 hours. Therefore we have decided to program another approach as proposed by vande Geest et al.[99]. The algorithm does the following steps:

1) The geometry is cut into 1mm thick slices according the z axis which is the axis of the body.
2) The center of mass of each slice is defined. It is assumed that radial direction of every element points toward the centre of mass in the given slice.
3) The center of mass of the slice, center of mass of the given element and the center of mass of the adjacent slice are thought to define a plane. The vector of tangential direction is defined as a normal vector of such plane.
4) The vector of axial direction is defined by vector multiplication of radial and axial vectors for each element.

The proposed algorithm was extensively tested and proved that it does not provide obviously wrong results even when applied to complicated AAAs as shown in Figure 34. One can visually confirm that radial direction is correct and axial and tangential appear to be oriented logically as well. However, it is not possible to state that this definition is correct until compared with the actual collagen orientation in the AAA, which is still investigated (study is in progress as described in 8.2.2.). Once this study is finished we will be able to validate this algorithm as well because we have the geometries of AAAs from which we have harvested the specimens for the mentioned study, and we know the place from which the tissue was taken.

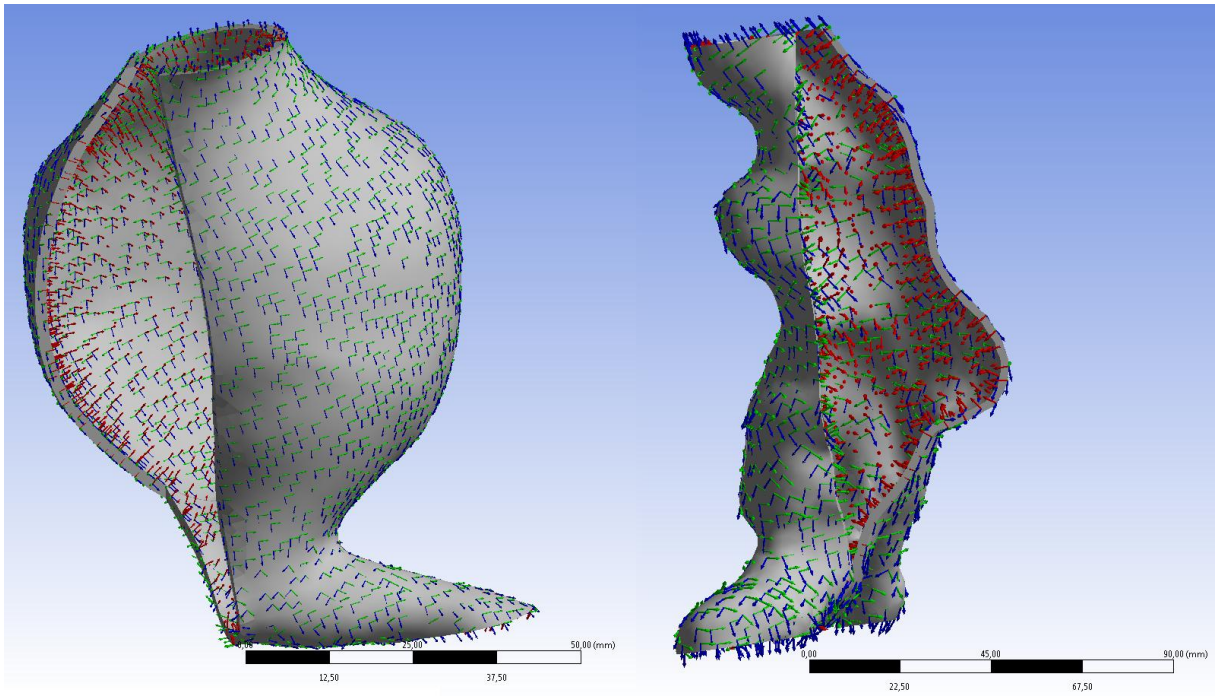

Figure 34 Two patient specific AAAs with marked principle directions. Radial directions are marked by red arrows, tangential directions by green arrows and axial directions by blue arrows. The results appear to be correct.

8.3 Intraluminal thrombus

So far we have focused on the aneurysmal wall only. However, the wall stress is also affected by the ILT (for structural description see 3.3.3), although there are still some contradictory evidences of it. Numerical studies show that the presence of ILT decreases the wall stress significantly[45,49,68],[101]. On the other hand experimental studies showed that blood pressure is almost entirely transmitted onto the wall[46,67] due to the ILT´s porous structure. Some researchers concluded therefore that ILT cannot decrease the wall stress and they do not include it in their models[50,61]. Finally, Thubrikar et al.[71] showed experimentally that the deformation of AAA increase significantly when ILT is removed (this experiment was later repeated artificially[153]) and suggest that ILT can help to carry the load because it is a net of ropes connected to the wall. Such a structure supports the wall although it does not decrease

the blood pressure. We confirmed these observations by numerical simulations where we used a poroelastic material model for ILT (see Appendix B and Appendix C). Although we used only a linear poroelastic model under finite deformations instead of a porohyperelastic formulation[123], our results were similar to those which used porohyperelastic material model[124] and demonstrated that ILT can decrease the wall stress significantly although the blood pressure is transmitted through. Such conclusion integrates nicely the results of both experimental[46,67] and numerical studies. Moreover, we have shown that the computed wall stress is the same as when a much more time efficient single phase model is used; this validated behindhand the numerical studies published so far [45,49,68],[101] and justified also the use of single phase models for ILT when AAA wall stress is computed. For more detail see Appendix B.

8.3.1 ILT rupture

Next we dealt with the question was what happens when ILT ruptures. It was observed occasionally in CT scans where crescent-like ruptures are shown[77,78]. There are some indicia that ILT rupture is somehow connected with wall rupture[34,76]. Therefore we have decided to perform FEA of patient specific AAAs to investigate how the ILT rupture influences the wall stress. We showed that although ILT rupture does not increase peak wall stress, it can even double the wall stress locally which might trigger the AAA rupture when it is located close to the wall. For more details see Appendix A.

8.3.2 Experimental testing of mechanical properties of ILT

Regarding mechanical properties of the ILT very different experimental results have been published so far[15,17,85,126], as shown in Figure 12. Those differences bring another high uncertainty into the computed wall stresses because the published mechanical properties vary by one order. Consequently we were interested in the actual mechanical properties of the ILT. From analyses of the existing papers I have noticed that their results are not very specific. It means that authors mention that they tested luminal, medial or abluminal layer of the ILT without specifying quantitatively what is the sample location with respect to the luminal surface of ILT. Without this information it is possible that the tissue in a distance let's say 10mm from the luminal surface was determined as a medial layer by one team and as abluminal layer by another team. This may partially explain the differences in mechanical properties. Therefore I believe that it is necessary to provide more precious information about the sample location and we record this in our ongoing study.

We have access to the human ILT samples thanks to cooperation with the surgeons as mentioned in 8.2.3 and we used also the biaxial testing machine described there with only

minor changes. We had to change the springs in clamps for much weaker ones, otherwise they penetrated through the whole sample with tearing it apart. We also used different position markers as shown in Figure 35. Instead of creating markers by an alcohol marker directly on the tissue we have used a white plastic platelet where black dots are created in the middle. This platelet is glued onto a thin needle (ϕ0.55mm) used to penetrate the sample. A great advantage of this approach is that the detection of the marker does not depend on the color and structure of the sample surface, which was the main problem in the AAA wall samples. Aplication of the same markers improved the results in case of the ILT as well. In addition to easier and more presious detection of the markers it also provides (due to the needles) information about average strain across the sample thickness and not only about strainon the surface recorded by the camera. Of course a disadvantage of this approach is in stress concentration caused by the needles which is hard to be quantified because we suppose that the tip of the needle will most likely just move aside the collagen fibers (dominantly reposnible for mechanical properties) in the penetrated tissue and not tear them apart. Moreover, the stress concentration factor is much lower in hyperelastic materials then in linear ones. Anyway, we will analyze this problem using FEM in the future.

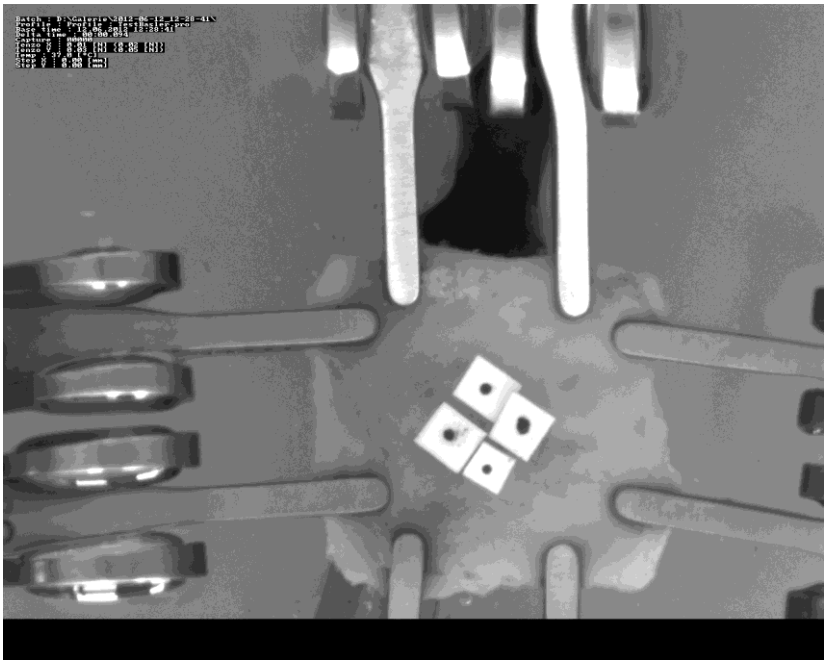

Figure 35 Biaxial testing of ILT specimen of patient 26. Note the plastic platelets as position markers.

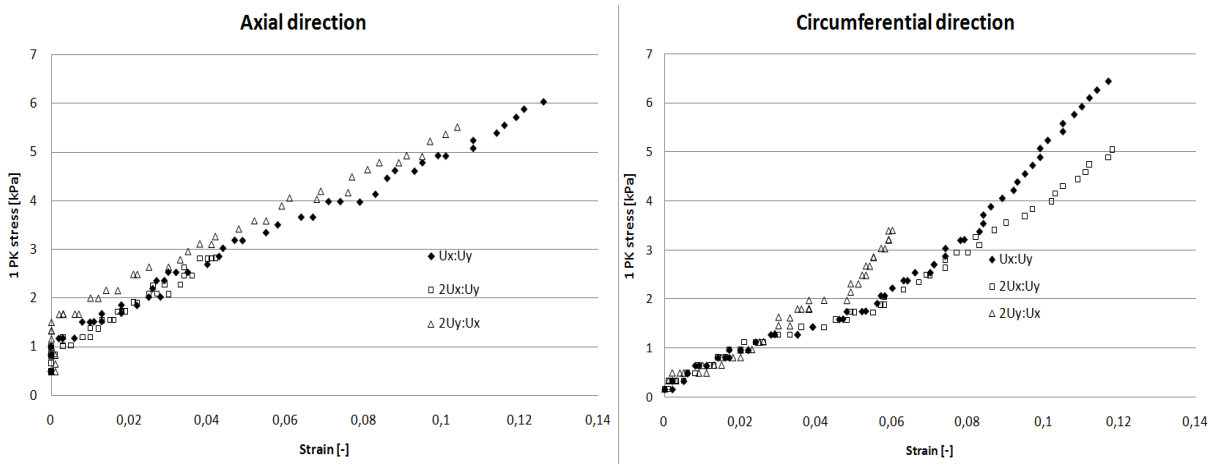

Figure 36 Experimental stress-strain curves of ILT (distance to lumen 1,7mm) of patient 26 for various tensile protocols. Stiffness of this sample is about 50kPa which agrees with the results from Gasser et al.[15].

Our preliminary results agree with the data published by Gasser et al[15] as shown in Figure 36. The observed stiffness is on the order of 50kPa and the material behaves almost isotropically and linearly which supports our results in Appendix A, where we have modeled the ILT as an isotropic linear elastic material. Of course this needs to be validated with a larger number of specimens.

8.4 Residual strains and stresses

Residual stresses (RS) are present in any artery. They can be observed when an artery is cut longitudinally, when they cause opening of the artery, which is a proof that there were some residual strains in the artery when no pressure was applied. RS are thought to be dominantly (but not exclusively – the results are not unambiguous here[144,145]) determined by elastin[144]. RS are known for more than 50 years now[127]. They are caused by vascular smooth muscle cells working actively to keep themselves under constant strain[129] or stress[128] conditions as mentioned in 3.3.2. This hypothesis states that vascular tissue remodels itself towards a preferred stress-strain state, which in turn leads to homogenization of the wall stress across the thickness. The uniform stress hypothesis is closely related to the uniform strain hypothesis[96] that assumes the strain across the wall being maintained constant during the wall remodeling. Presence of residual strains should be included in the numerical models because it influences the wall stress substantially when the artery is loaded by a blood pressure (see Appendix D and H for description in detail).

There are several major approaches how to do it. An earlier approach assumes that artery is in a strain-free state when opened by a single longitudinal cut[146]. Therefore it is assumed to induce residual strains in it by closing it back to the original position[56,130-133]. Major problem of this approach is that it cannot be used for inducing residual strains in any complex, e.g. patient specific geometry. Also it neglects the multidimensional nature of the RS, because RS were observed in both circumferential[127,134] and axial directions[135,147].

More recently there were studies which used inverse elastostatics[51] in order to induce RS in a given geometry of aneurysms[136]. Inverse elastostatics solves the problem of how to find the undeformed geometry, if we know the deformed geometry, BC's and material properties. Although it is a promising method for finding the unloaded geometry as described in 8.5, its applicability in inducing RS in patient-specific geometries is limited due to the necessity of calculating the opened geometry, which results in large displacements and high deformation of finite elements.

The latest approach uses the mixture theory and implicitly induces the RS as a part of the material models by prescribing different stress-free configurations for the different structural constituents in the wall[138-142]. Unfortunately there are no experimental data available for these models yet.

Therefore our work focused on inducing RS in patient-specific AAA geometries by using the available material models and numerical tools in commercial FE software.

8.4.1 Inducing RS by interference of two volumes

We have proposed a new approach which is based on interference of two or more layers of the wall (see Appendix D). The geometry of arterial layers is created of bulk finite elements with contact elements defined on the interface(s) of the layers; then the layers are moved against each other in order to create their interference. It induces a large penetration in the contact pairs which is then removed by compressing the inner layer and stretching the outer one as shown in Figure 37 (b). When such an artery is cut (Figure 37 (c) it opens and most (but not all) RS are released. This method should be able to induce RS in an artery very realistically when enough layers are used. It is by virtue of the nature of arterial structure which is layered as well (see chapter 3.3.1). The magnitude of interference for the two volumes needs to be defined iteratively in order to minimize the resulting stress gradient. An advantage of this approach is that RS are induced without large displacements of nodes, therefore it prevents all mesh distortion problems.

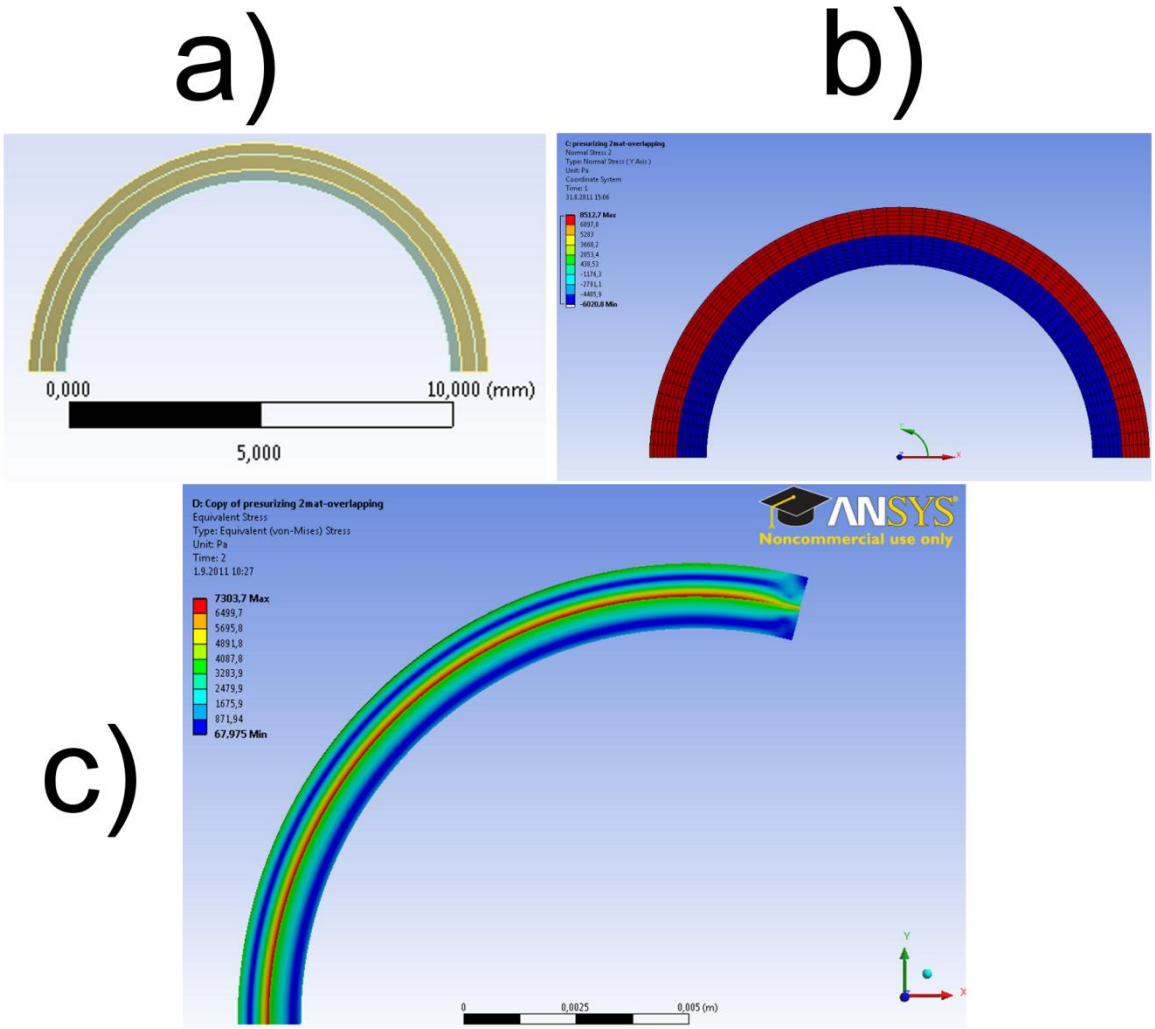

Figure 37 Inducing RS by Interference method. Original geometry with interfering layers (a). Stresses from FE solution (without any loading pressure) (b). Red color indicates tensile stresses while blue color indicates compressive stresses. Von Mises stress distribution after longitudinal cuting and RS releasing (c). It is obvious that neither the opened geometry is stress free. The highest stresses remain at the contact interface.

Applicability of this approach on patient-specific AAA geometries has been tested and it has been verified that the proposed approach reduces the wall stress gradient in those geometries significantly as shown in Figure 38. As you can see, the PWS drops by some 50%.

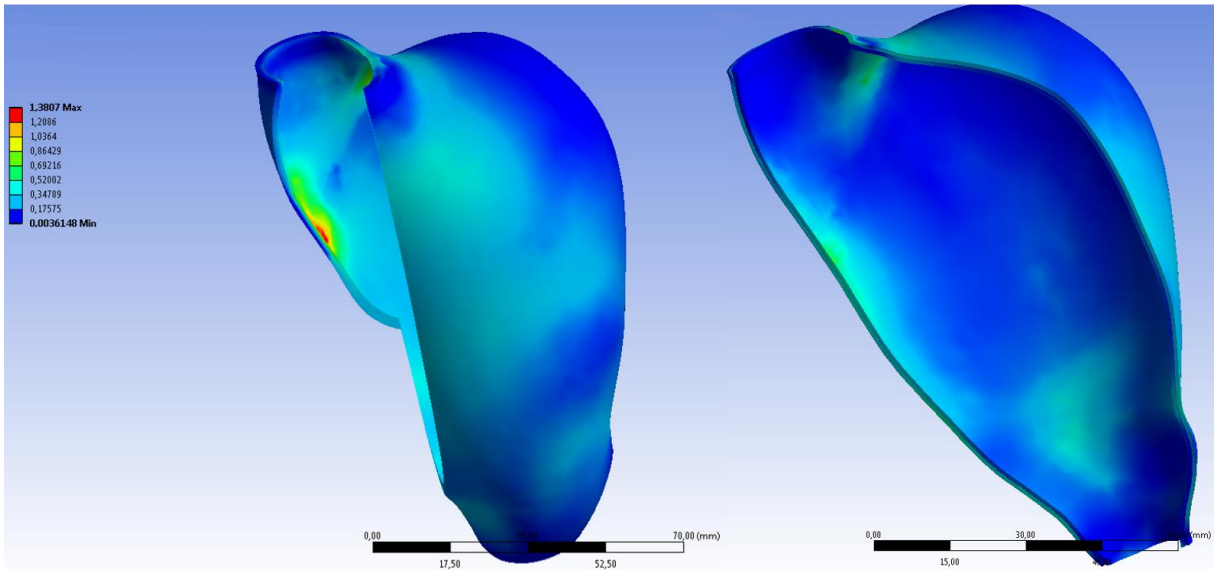

Figure 38 Effect of RS (induced by Interference method) on von Mises wall stress in a patient-specific AAA. Wall stress without RS (left) and with RS (right). PWS falls down by some 50%. Inner wall surface loaded by pressure of 26kPa and isotropic material model according to eq. (5) has been used.

Although the demonstrated method can reduce the stress gradient significantly and it can be applied to patient-specific geometries, it has still some limitations. First of all the process of creating the layered AAA geometry is very time consuming (it took me in average 1 day to prepare 1 geometry in case of two-layer models) and this operation is fully manual because it requires extensive repairs of the copied surfaces. In average one patient-specific geometry of AAA wall consists of 2000 surfaces which need to be extruded in order to create volumes. Often however, the extrusion fails due to an incorrect shape of the created volume and this volume needs to be fixed manually. For this reason it is hardly imaginable to use this approach for more than 4 layers in the model. Also this approach minimizes (circumferential) PWS only and does not care about the other stresses in the AAA.

Therefore we continued seeking for a better method and have proposed a different approach being able to remove the stress gradient much more effectively.

8.4.2 Inducing RS by decomposition of deformation gradient tensor

This approach is described in detail in Appendix H. Briefly, we have exploited the thermal-structural FEA in the Ansys software, because it uses the same principle. It is based on splitting the deformation gradient tensor into elastic and growth parts. We store the growth strain needed for removing the present stress gradient in the growth part of the deformation gradient tensor. Practically it is done by defining couples of nodes where one node at the inner surface has just one mate at the outer surface. Then the same strain is prescribed in both nodes except for sign. This ensures that only bending stress and no membrane stress is induced. RS distribution is similar to the previous approach but the RSs are changing continuously across

the wall here. Also it is easy to define a growth strain for each node separately which allows us to remove the gradient from the whole geometry. Currently it is not possible to remove stress gradients completely but we are able to decrease it to 1/10 (see Appendix H). Moreover, the mesh needed for an accurate FEA of AAA can be much coarser when RS is included as shown in Figure 39. Without RS the acceptable mesh size was 0.8mm due to high stress gradients across the wall thickness. On the other hand, the mesh could be much coarser when RS was included (up to 2.5mm in this case) and it still captured the wall stress accurately. In other words, including RS into FEA of AAA does not extend the analysis time, because the necessity of 5 to 10 FE loops is balanced by the much coarser mesh that can be used.

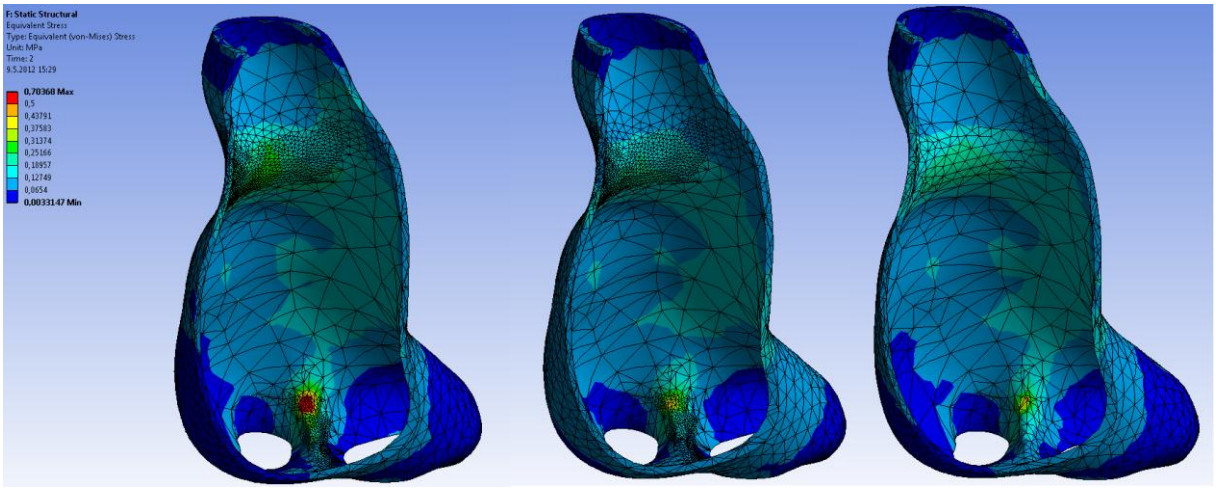

Figure 39 Comparison of the computed von Mises wall stresses with respect to RS and mesh size. AAA of patient 2 without RS with a fine mesh (left). The same AAA with including RS (middle) and with RS included and coarser mesh used (right). Practically the same results are obtained for both mesh sizes 0.8mm (middle) and 2.5mm (right).

As I mentioned in 8.2.1 and Appendix G, including of RS is a crucial when nonlinear material models are planned to be used.

8.5 Prestressing

Any CT scan shows an AAA which is already loaded by a blood pressure. So a geometry reconstructed from CT scans cannot by stress free (unloaded). However, FEA needs an unloaded geometry as an input. Up to 2006 this fact was ignored and the geometry obtained from CT scans was assumed to be unloaded. To solve this problem, two different approaches can be used in general.

The first approach is based on using inverse deformation gradient tensor[51,55,59,60,152] splitted into two parts. This approach cannot be used in commercially available software because it requires redefining of the FE code, which is hardly possible in commercial FE packages.

The second approach was proposed by Putter et al.[72,73] and called backward incremental method. Its principle is very simple. Geometry is loaded by a pressure and the obtained

displacements are then subtracted from the node position for each node of the original geometry. In case of linear material and geometric dependencies this is sufficient to obtain the unloaded geometry. In case of nonlinear material and finite deformations this approach leads to an iterative algorithm. Its advantage is applicability in a commercial FE software[73]. Its major disadvantage is non-uniqueness of the obtained solution[60].We adapted this method and proposed some minor changes to make it more resistant against divergence and destruction of the FE mesh. For more details see Appendix E. Once we have managed this approach we applied it routinely as an integral part of our FEA (see Appendix G).

8.6 Wall thickness

Wall thickness is non-uniform as mentioned in chapter 7. However, first FEAs assumed a uniform wall thickness of 1,8÷2mm because the resolution of CT scans and the contrast between wall and ILT are very low. Although the resolution of CT machines increase gradually, the contrast between ILT and the wall cannot by increased by principle. Consequently, I cannot see the possibility of determining wall thickness directly from CT scans very likely. Therefore the wall thickness has been set up according to statistics. It was shown that the wall is thinner behind the ILT, so this correlation has been already included into our numerical models.

We have measured the wall thickness in all of our tissue samples harvested for the other studies (see chapter 8.1.1 and 8.2.3). I have drawn several conclusions from these measurements and discussions with surgeons and histologists:

- All the published studies miss the information about the pressure used for wall thickness measurement although it is crucial information to determine reliability of such measurements. Higher pressure in measuring contacts (above 1kPa) increase repeatability of measurements while also increasing a systematic error by unwanted compression of the measured sample. Low pressure decrease this error but also the repeatability. It should be noted that we are talking about forces which are of the same order as the passive resistances (friction) in the measuring tools. We use a stand and drift meter as shown in Figure 40. There is no spring in the drift meter so that it is forced only by the weight of its spindle which generates a force of 0.18N. This force is distributed on the measured sample (18x18mm) trough glass plates, so that the average pressure is about 0.5kPa. This approach provides information about the average thickness which is necessary for evaluation of our planar biaxial tests described in chapter 8.2.3.
- We also observed that it is not clear where the wall ends in outwards direction. It is due to nature of adventitia as described in chapter 3.3.1. After consultation with

surgeons we cut off all the tissue that contains fat because its mechanical properties are negligible. It is not exact, but one should keep in mind that we work with the natural material here where all boundaries are kind of blurred.

In average we measured the wall thickness (n=24) to be 2.11mm (SD 0.43mm) and we did not observed wall thicker than some 2.75mm or thinner than 1.17mm. Therefore we cannot confirm the results published by others who reported that the thickness is varying from 0,2÷4,3mm even within one AAA[43,44] with median of 1.48mm. However there are several differences in our measurements. First of all, the mentioned studies published no description of their measuring device so that it is not possible to quantify the forces or pressure during measuring. Therefore we do not know how much the tissue could be compressed. However they claimed to measure wall thickness in 394 points in 4 AAAs (one ruptured) which suggests that their measuring device has a quite small active area (area being in contact with the specimen). On the other hand, we have measured the thickness across the whole 18x18mm specimen therefore our values are more averaged but of course they can be slightly overestimated. For example if there were four calcifications (which are thicker than rest of the wall) in all corners, then we would measure only their thickness.

It is also important to say that current computational models assume homogenous properties of the wall across the whole AAA which may not be true[149]. The relevant material properties of aneurysmal wall depend on collagen fibers, their density, orientation and dispersion. For instance, if there was the same amount of fibers in both thin and thick walls, the relevant stress in these fibers would be also the same under the same loading conditions (total force and elongation), despite the different wall thickness and, consequently, different wall stress. Therefore there is lot to explore in aneurysmal wall from the structural point of view.

Figure 40 Device for measuring of wall thickness. Tissue is placed between two glasses and the wall thickness is measured by a drift meter.

9 Future work

I have described all issues we have focused on in my Ph.D. with the aim to make the assessment of AAA rupture risk more reliable. However, there is still a lot of work to be done in order to reach our long term goal which is to achieve a clinically applicable tool. I have formulated the following list of possible regions of interest on the basis of my current experience in this field:

1. To finish the validation of the program for determination of collagen fibers orientation as described in chapter 8.2.2.1 and to use this program for quantitative analyses of collagen fibers distribution in the aneurysmal wall.
2. To determine the collagen distribution in the origin of branch arteries as described in chapter 8.1.1 and to include them as an integral part of FEAs of AAAs.
3. To confirm the results obtained by using poroelastic model of ILT by its application to the patient-specific geometry. Such a study should also investigate the changes of pressure under the ILT because this pressure depends on the local curvature of the wall.
4. To perform experimental measurements of mechanical properties of the ILT in dependence on the distance from the luminal layer, with the aim to avoid misinterpretations caused by using inaccurate terms such as luminal, medial and abluminal layer.
5. To perform a large cohort of FE analyses of some 150 AAAs loaded by mean and elevated pressures, with including prestressing and residual stresses, and then to try determination of the risky AAAs. This should be designed as a double blind study in order to reveal actual potential of FEA in identification of risky AAAs.

10 Summary

A summary of my three years work is presented in Table 4. The upper part compares our capabilities with the global state of art in 2009 when I started my Ph.D. As you can see, we were significantly behind other groups in both experiments and computational models, while we kept the pace in using the most advanced material models available.

During these three years we have established a cooperation with surgeons and histologists which enabled us access to samples of human aneurysmal and ILT tissues and we gained information about structure of the tested samples as well. Also this cooperation revealed me the branch arteries as a important region of interest. Further I have managed to include both prestressing and RS into patient-specific geometries of AAAs and written a macro for determination of principle material directions in soft tissues. Regarding of ILT, I have routinely managed to include it into FEA, investigated the effect of ILT fissuring on the wall

stress in the AAA and also investigated the effect of poroelasticity on the computed wall stress.

Overall I believe that my work moved the wall stress criterion closer to the clinical use.

Global state of art in 2009	**Department state of art in 2009**
Routine reconstruction of patient-specific geometry of AAA	One patient-specific geometry of AAA reconstructed
ILT included in FEA of AAA regularly	ILT omitted
Planar biaxial tests of ILT tissue	ILT not tested
Single-phase material models of ILT used	ILT omitted
Prestressing included routinely	Prestressing worked with one simple geometry
RS included in idealized models of AAA	RS omitted
Planar biaxial tests of AAA tissue	Planar biaxial tests of porcine aortic tissue
Both anisotropic and isotropic material models used for AAA wall	Both anisotropic and isotropic material models used for AAA wall
Global state of art in 2012	**Department state of art in 2012**
Routine reconstruction of patient-specific geometry of AAA	Routine reconstruction of patient-specific geometry of AAA
ILT included in FEA of AAA regularly	ILT included in FEA of AAA regularly
Planar biaxial tests of ILT tissue	Planar biaxial tests of ILT tissue
Poroelastic material models of ILT used	Poroelastic material models of ILT used
Prestressing included routinely	Prestressing included routinely
RS included in idealized models of AAA	RS included in patient-specific models of AAA
Planar biaxial tests of AAA tissue	Planar biaxial tests of AAA tissue performed within 3 hours from harvesting
Both anisotropic and isotropic material models used for AAA wall	Both anisotropic and isotropic material models used for AAA wall
Branch arteries omitted	Effect of branch arteries investigated including histological analysis
Collagen distribution in AAA determined by PLM	Collagen distribution in AAA determined more effectively by an own program
Effect of ILT fissuring omitted	Effect of ILT fissuring investigated

Table 4 Summary of my work within three years. Red lines represent topics where we were behind the others, orange lines reffer to topics which we can do with some limitations, green lines highlight the topics where our results are comparable to the others and blue lines enhance the topics where we are superior to others.

11 References

1. Gundiah NB Ratcliffe M & A Pruitt L 2007. Determination of strain energy function for arterial elastin: Experiments using histology and mechanical tests. *J Biomech,* **40,** 586-94.
2. O'Connell MKMurthy S & Phan S, Xu C, Buchanan J, Spilker R, *et al.* 2008. The three-dimensional micro-and nanostructure of the aortic medial lamellar unit measured using 3d confocal and electron microscopy imaging. *Matrix Biol,* **27,** 171-81.
3. Clark JMGlagov S 1985. Transmural organization of the arterial media. The lamellar unit revisited. *Arteriosclerosis,* **5,** 19-34.
4. Carlisle CRCoulais C & Guthold M 2010. The mechanical stress-strain properties of single electrospun collagen type I nanofibers. *Acta Biomater,* **6,** 2997-3003.
5. Roeder BAKokini K & Sturgis JE, Robinson JP, Voytik-Harbin SL 2002. Tensile mechanical properties of three-dimensional type I collagen extracellular matrices with varied microstructure. *J Biomech Eng,* **124,** 214-22.
6. Tremblay DCartier R & Mongrain R, Leask RL 2010. Regional dependency of the vascular smooth muscle cell contribution to the mechanical properties of the pig ascending aortic tissue. *J Biomech,* **43,** 2448-51.
7. Fung YC 1968. Elasticity of soft tissues in simple elongation. *Am J Physiol,* **213,** 1532-44.
8. Lindeman JHAshcroft BA & Beenakker JW, van Es M, Koekkoek NB, Prins FA, *et al.* 2010. Distinct defects in collagen microarchitecture underlie vessel-wall failure in advanced abdominal aneurysms and aneurysms in Marfan syndrome. *Proc Natl Acad Sci U S A,* **107,** 862-5.
9. Fratzl P 2008. *Collagen Structure and mechanics,* , Springer.
10. Holzapfel GASommer G & Auer M, Regitnig P, Ogden RW 2007. Layer-specific 3D residual deformations of human aortas with non-atherosclerotic intimal thickening. *Ann Biomed Eng,* **35,** 530-45.
11. Nichols,M. 2005. *McDonald´s Blood flow in arteries,* , Hodder Arnold.
12. Holzapfel GASommer G & Regitnig P 2005. Anisotropic mechanical properties of tissue components in human atherosclerotic plaques. *J Biomech Eng,* **126,** 657-65.
13. Karsaj IHumphrey JD 2010. A mathematical model of evolving mechanical properties of intraluminal thrombus. *Biorheology,* **46,** 509-27.
14. Ryan EAMockros LF & Weisel JW, Lorand L 2010. Structural origins of fibrin clot rheology. *Biophys J,* **77,** 2813-26.
15. Gasser TCGorgulu G & Folkesson M, Swedenborg J 2008. Failure properties of intraluminal thrombus in abdominal aortic aneurysm under static and pulsating mechanical loads. *J Vasc Surg,* **48,** 179-88.
16. Ashton JHVande Geest JP & Simon BR, Haskett DG 2009. Compressive mechanical properties of the intraluminal thrombus in abdominal aortic aneurysms and fibrin-based thrombus mimics. *J Biomech,* **42,** 197-201.
17. Vande Geest JPSacks MS & Vorp DA 2006. A planar biaxial constitutive relation for the luminal layer of intra-luminal thrombus in abdominal aortic aneurysms. *J Biomech,* **39,** 2347-54.
18. Adolph RVorp DA & Steed DL, Webster MW, Kameneva MV, Watkins SC 1997. Cellular content and permeability of intraluminal thrombus in abdominal aortic aneurysm. *J Vasc Surg,* **25,** 916-26.
19. Kent KCZwolak RM & Egorova NN, Riles TS, Manganaro A, Moskowitz AJ, *et al.* 2010. Analysis of risk factors for abdominal aortic aneurysm in a cohort of more than 3 million individuals. *J Vasc Surg,* **52,** 539-48.
20. Longo CUpchurch GR Jr 2005. Abdominal aortic aneurysm screening: recommendations and controversies. *Vasc Endovascular Surg,* **39,** 213-9.
21. Lederle FAJohnson GR & Wilson SE, Chute EP, Hye RJ, Makaroun MS, *et al.* 2000. The aneurysm detection and management study screening program: validation cohort and final results. Aneurysm Detection and Management Veterans Affairs Cooperative Study Investigators. *Arch Intern Med,* **160,** 1425-30.
22. Choke EThompson MM & Dawson J, Wilson WR, Sayed S, Loftus IM, *et al.* 2006. Abdominal aortic aneurysm rupture is associated with increased medial neovascularization and overexpression of proangiogenic cytokines. *Arterioscler Thromb Vasc Biol,* **26,** 2077-82.
23. Vorp DALee PC & Wang DH, Makaroun MS, Nemoto EM, Ogawa S, *et al.* 2001. Association of intraluminal thrombus in abdominal aortic aneurysm with local hypoxia and wall weakening. *J Vasc Surg,* **34,** 291-9.
24. Xu XYBorghi A & Nchimi A, Leung J, Gomez P, Cheng Z, *et al.* 2010. High levels of 18F-FDG uptake

in aortic aneurysm wall are associated with high wall stress. *Eur J Vasc Endovasc Surg,* **39,** 295-301.
25. Kotze CWMenezes LJ & Endozo R, Groves AM, Ell PJ, Yusuf SW 2009. Increased metabolic activity in abdominal aortic aneurysm detected by 18F-fluorodeoxyglucose (18F-FDG) positron emission tomography/computed tomography (PET/CT). *Eur J Vasc Endovasc Surg,* **38,** 93-9.
26. Vorp DARaghavan ML & Muluk SC, Makaroun MS, Steed DL, Shapiro R, *et al.* 1997. Wall strength and stiffness of aneurysmal and nonaneurysmal abdominal aorta. *Ann N Y Acad Sci,* **800,** 274-6.
27. Alexander JJ 2004. The pathobiology of aortic aneurysms. *J Surg Res,* **117,** 163-75.
28. Choke ECockerill G & Wilson WR, Sayed S, Dawson J, Loftus I, *et al.* 2005. A review of biological factors implicated in abdominal aortic aneurysm rupture. *Eur J Vasc Endovasc Surg,* **30,** 227-44.
29. Vande Geest JPSacks MS & Vorp DA 2006. The effects of aneurysm on the biaxial mechanical behavior of human abdominal aorta. *J Biomech,* **39,** 1324-34.
30. Di Martino ESBohra A & Vande Geest JP, Gupta N, Makaroun MS, Vorp DA 2006. Biomechanical properties of ruptured versus electively repaired abdominal aortic aneurysm wall tissue. *J Vasc Surg,* **43,** 570-6; discussion 576.
31. Wilson KAWoodburn KR & Ruckley CV, Fowkes FG 1997. Expansion rates of abdominal aortic aneurysm: current limitations in evaluation. *Eur J Vasc Endovasc Surg,* **13,** 521-6.
32. Marra SPDaghlian CP & Fillinger MF, Kennedy FE 2006. Elemental composition, morphology and mechanical properties of calcified deposits obtained from abdominal aortic aneurysms. *Acta Biomater,* **2,** 515-20.
33. Lindholt JS 2008. Aneurysmal wall calcification predicts natural history of small abdominal aortic aneurysms. *Atherosclerosis,* **197,** 673-8.
34. Li ZYU-King-Im J & Tang TY, Soh E, See TC, Gillard JH 2008. Impact of calcification and intraluminal thrombus on the computed wall stresses of abdominal aortic aneurysm. *J Vasc Surg,* **47,** 928-35.
35. Xiong JWang SM & Zhou W, Wu JG 2008. Measurement and analysis of ultimate mechanical properties, stress-strain curve fit, and elastic modulus formula of human abdominal aortic aneurysm and nonaneurysmal abdominal aorta. *J Vasc Surg,* **48,** 189-95.
36. Kazi MThyberg J & Religa P, Roy J, Eriksson P, Hedin U, *et al.* 2003. Influence of intraluminal thrombus on structural and cellular composition of abdominal aortic aneurysm wall. *J Vasc Surg,* **38,** 1283-92.
37. Dobrin PBBaker WH & Gley WC 1984. Elastolytic and collagenolytic studies of arteries. Implications for the mechanical properties of aneurysms. *Arch Surg,* **119,** 405-9.
38. **,** LANCET (1998) Mortality results for randomised controlled trial of early elective surgery of ultrasonographic surveillance for small abdominal aortic aneurysms. vol. 352:1649-16551649-55.
39. Lederle FAWilson SE & Johnson GR, Reinke DB, Littooy FN, Acher CW, *et al.* 2002. Immediate repair compared with surveillance of small abdominal aortic aneurysms. *N Engl J Med,* **346,** 1437-44.
40. Lederle FAJohnson GR & Wilson SE, Ballard DJ, Jordan WD Jr, Blebea J, *et al.* 2002. Rupture rate of large abdominal aortic aneurysms in patients refusing or unfit for elective repair. *JAMA,* **287,** 2968-72.
41. Nicholls SCGardner JB & Meissner MH, Johansen HK 1998. Rupture in small abdominal aortic aneurysms. *J Vasc Surg,* **28,** 884-8.
42. Fillinger MFRaghavan ML & Marra SP, Cronenwett JL, Kennedy FE 2002. In vivo analysis of mechanical wall stress and abdominal aortic aneurysm rupture risk. *J Vasc Surg,* **36,** 589-97.
43. Martufi GDi Martino ES & Amon CH, Muluk SC, Finol EA 2009. Three-dimensional geometrical characterization of abdominal aortic aneurysms: image-based wall thickness distribution. *J Biomech Eng,* **131,** 061015.
44. Raghavan MLKratzberg J & Castro de Tolosa EM, Hanaoka MM, Walker P, da Silva ES 2006. Regional distribution of wall thickness and failure properties of human abdominal aortic aneurysm. *J Biomech,* **39,** 3010-6.
45. Wang DHMakaroun MS & Webster MW, Vorp DA 2002. Effect of intraluminal thrombus on wall stress in patient-specific models of abdominal aortic aneurysm. *J Vasc Surg,* **36,** 598-604.
46. Schurink GWvan Baalen JM & Visser MJ, van Bockel JH 2000. Thrombus within an aortic aneurysm does not reduce pressure on the aneurysmal wall. *J Vasc Surg,* **31,** 501-6.
47. Raghavan MLVorp DA 2000. Toward a biomechanical tool to evaluate rupture potential of abdominal aortic aneurysm: identification of a finite strain constitutive model and evaluation of its applicability. *J Biomech,* **33,** 475-82.
48. Vorp DA 2007. Biomechanics of abdominal aortic aneurysm. *J Biomech,* **40,** 1887-902.
49. Mower, RM, Quifioness, WJ 1997. Effect of intraluminal thrombus on abdominal aortic aneurysm wall stress. *J Biomech,* **26,** 602-608.
50. Speelman LBosboom EM & Schurink GW, Hellenthal FA, Buth J, Breeuwer M, *et al.* 2008. Patient-specific AAA wall stress analysis: 99-percentile versus peak stress. *Eur J Vasc Endovasc Surg,* **36,** 668-

76.
51. Govindjee,S. Mihalic,P. A. 1996. Computational methods for inverse finite elastostatics *1. *Computer Methods in Applied Mechanics and Engineering,* **136,** 47;.
52. Zendehbudi GRKazemi A 2007. The accuracy of thin-shell theory in estimation of aneurysm rupture. *J Biomech,* **40,** 3230-5.
53. Vorp DAVande Geest JP 2005. Biomechanical determinants of abdominal aortic aneurysm rupture. *Arterioscler Thromb Vasc Biol,* **25,** 1558-66.
54. Raghavan MLWebster MW & Vorp DA 1997. Ex vivo biomechanical behavior of abdominal aortic aneurysm: assessment using a new mathematical model. *Ann Biomed Eng,* **24,** 573-82.
55. Lu JZhou X & Raghavan ML 2008. Inverse method of stress analysis for cerebral aneurysms. *Biomech Model Mechanobiol,* **7,** 477-86.
56. Balzani,D. Schroder,J. & Gross,D. 2007. Numerical simulation of residual stresses in arterial walls. *Computational Materials Science,* **39,** 117;.
57. Venkatasubramaniam AKFagan MJ & Mehta T, Mylankal KJ, Ray B, Kuhan G, *et al.* 2004. A comparative study of aortic wall stress using finite element analysis for ruptured and non-ruptured abdominal aortic aneurysms. *Eur J Vasc Endovasc Surg,* **28,** 168-76.
58. Hellenthal FAGeenen IL & Teijink JA, Heeneman S, Schurink GW 2009. Histological features of human abdominal aortic aneurysm are not related to clinical characteristics. *Cardiovasc Pathol,* **18,** 286-93.
59. Lu JZhou X & Raghavan ML 2007. Inverse elastostatic stress analysis in pre-deformed biological structures: Demonstration using abdominal aortic aneurysms. *J Biomech,* **40,** 693-6.
60. Gee MWReeps C & Eckstein HH, Wall WA 2009. Prestressing in finite deformation abdominal aortic aneurysm simulation. *J Biomech,* **42,** 1732-9.
61. Sander de Putter,F. G. 2005. Automatic determination of the dynamic geometry of abdominal aortic aneurysm from MR with application to wall stress simulations. *International Congress Series,* **1281,** 339-344.
62. van 't Veer MButh J & Merkx M, Tonino P, van den Bosch H, Pijls N, *et al.* 2009. Biomechanical properties of abdominal aortic aneurysms assessed by simultaneously measured pressure and volume changes in humans. *J Vasc Surg,* **48,** 1401-7.
63. Hinnen JWRixen DJ & Koning OH, van Bockel JH, Hamming JF 2006. Development of fibrinous thrombus analogue for in-vitro abdominal aortic aneurysm studies. *J Biomech,* **40,** 289-95.
64. Mayranpaa MITrosien JA & Fontaine V, Folkesson M, Kazi M, Eriksson P, *et al.* 2009. Mast cells associate with neovessels in the media and adventitia of abdominal aortic aneurysms. *J Vasc Surg,* **50,** 388-95; discussion 395-6.
65. Vande Geest JPWang DH & Wisniewski SR, Makaroun MS, Vorp DA 2006. Towards a noninvasive method for determination of patient-specific wall strength distribution in abdominal aortic aneurysms. *Ann Biomed Eng,* **34,** 1098-106.
66. Roy JLabruto F & Beckman MO, Danielson J, Johansson G, Swedenborg J 2008. Bleeding into the intraluminal thrombus in abdominal aortic aneurysms is associated with rupture. *J Vasc Surg,* **48,** 1108-13.
67. Hinnen JWKoning OH & Visser MJ, Van Bockel HJ 2005. Effect of intraluminal thrombus on pressure transmission in the abdominal aortic aneurysm. *J Vasc Surg,* **42,** 1176-82.
68. Di Martino EMantero S & Inzoli F, Melissano G, Astore D, Chiesa R, *et al.* 1998. Biomechanics of abdominal aortic aneurysm in the presence of endoluminal thrombus: experimental characterisation and structural static computational analysis. *Eur J Vasc Endovasc Surg,* **15,** 290-9.
69. Gasser TCMartufi G & Auer M, Folkesson M, Swedenborg J 2010. Micromechanical characterization of intra-luminal thrombus tissue from abdominal aortic aneurysms. *Ann Biomed Eng,* **38,** 371-9.
70. Biasetti JGasser TC & Auer M, Hedin U, Labruto F 2010. Hemodynamics of the normal aorta compared to fusiform and saccular abdominal aortic aneurysms with emphasis on a potential thrombus formation mechanism. *Ann Biomed Eng,* **38,** 380-90.
71. Thubrikar MJRobicsek F & Labrosse M, Chervenkoff V, Fowler BL 2003. Effect of thrombus on abdominal aortic aneurysm wall dilation and stress. *J Cardiovasc Surg (Torino),* **44,** 67-77.
72. de Putter SWolters BJ & Rutten MC, Breeuwer M, Gerritsen FA, van de Vosse FN 2007. Patient-specific initial wall stress in abdominal aortic aneurysms with a backward incremental method. *J Biomech,* **40,** 1081-90.
73. Merkx MAvan 't Veer M & Speelman L, Breeuwer M, Buth J, van de Vosse FN 2009. Importance of initial stress for abdominal aortic aneurysm wall motion: dynamic MRI validated finite element analysis. *J Biomech,* **42,** 2369-73.
74. Truijers MPol JA & Schultzekool LJ, van Sterkenburg SM, Fillinger MF, Blankensteijn JD 2007. Wall stress analysis in small asymptomatic, symptomatic and ruptured abdominal aortic aneurysms. *Eur J*

Vasc Endovasc Surg, **33,** 401-7.
75. Volokh KYVorp DA 2008. A model of growth and rupture of abdominal aortic aneurysm. *J Biomech*, **41,** 1015-21.
76. Meyer CAGuivier-Curien C & Moore JE Jr 2010. Trans-thrombus blood pressure effects in abdominal aortic aneurysms. *J Biomech Eng*, **132,** 071005.
77. Arita TMatsunaga N & Takano K, Nagaoka S, Nakamura H, Katayama S, *et al.* 1997. Abdominal aortic aneurysm: rupture associated with the high-attenuating crescent sign. *Radiology*, **204,** 765-8.
78. Mehard WBHeiken JP & Sicard GA 1994. High-attenuating crescent in abdominal aortic aneurysm wall at CT: a sign of acute or impending rupture. *Radiology*, **192,** 359-62.
79. Georgakarakos EIoannou CV & Kamarianakis Y, Papaharilaou Y, Kostas T, Manousaki E, *et al.* 2010. The role of geometric parameters in the prediction of abdominal aortic aneurysm wall stress. *Eur J Vasc Endovasc Surg*, **39,** 42-8.
80. Rogers WJHu YL & Coast D, Vido DA, Kramer CM, Pyeritz RE, *et al.* 2001. Age-associated changes in regional aortic pulse wave velocity. *J Am Coll Cardiol*, **38,** 1123-9.
81. Latham RD,Westerhof N & Sipkema P, Rubal BJ, Reuderink P, Murgo JP 1986. Regional wave travel and reflections along the human aorta: a study with six simultaneous micromanometric pressures. *Circulation*, **72,** 1257-69.
82. Darling RC, Messina CR, Brewster DC, Ottinger LW. 1977. Autopsy study of unoperated abdominal aortic aneurysms. The case for early resection. *Circulation*, **56,** 161-4.
83. http://visualsunlimited.photoshelter.com/image/I0000_MZ46I.PKYE
84. http://www.pages.drexel.edu/~cas95/Tissue%20Structure%20and%20Properties.html
85. Tong. J., Cohnert T., Regitnig P. and Holzapfel G.A. 2011. Effects of the age on the elastic properties of the intraluminal thrombus and the thrombus covered wall in abdominal aortic aneurysms: biaxial Exension behaviour and material modelling. Eur. *J. Vasc. Endovasc. Surg*. **xx**,1-13.
86. Gasser TC, Auer M, Labruto F, Swedenborg, Roy J. 2010. Biomechanical rupture risk assessment of abdominal aortic aneurysms: model complexity versus Predictability of finite element simulations. *Eur J Vasc Endovasc Surg* **40**:176-185
87. Yeoh, O.H.1993. Some forms of strain energy functions for rubber. *Rubber Chem. Technol*. **66**, 754–771.
88. Choi, H.S. & Vito, R.P.1990. Two-dimensional stress-strain relationship for canine pericardium. *J Biomech Eng*. **112**, 153-159.
89. Holzapfel GA, Gasser TC, Ogden RW. 2000. A new constitutive framework for arterial wall mechanics and a comparative studyof material models. *J Elasticity* 2000;**61**:1-48.
90. Rodriguez J.F., Ruiz C., Doblare M. and Holzapfel G.A. 2008. Mechanical stresses in abdominal aortic aneurysms: Influence of diameter, asymmetry and mechanical anisotropy. *J Biomech Eng*. **130**,021023-1-10.
91. Demiray, H. Large deformation analysis of some soft biological tissues. *J Biomech Eng*. 1981.**103**, 73-78.
92. Baek S., Gleason R.L., Rajagopal K.R. and Humphrey J.D. 2007. Theory of small on large: potential utility in computations of fluid-solid interactions in arteries. *Comp Meth App Mech Eng*. **196**,3070-3078.
93. Gasser T.C., Gallinetti S., Xing X., Forsell C., Swedenborg J. and Roy J. 2012. Spatial orientation of collagen fibers in the abdominal aortic aneurysm´s wall and its relation to wall mechanics. *Acta Biomater*. **8**,3091-3103.
94. van 't Veer M., Buth, J., Merkx, M., Tonino, P., van den Bosch, H., Pijls, N. & van de Vosse F.N. Biomechanical properties of abdominal aortic aneurysms assessed by simultaneously measured pressure and volume changes in humans. *J Vasc Surg*. 2009.**48**, 1401-1407.(doi: 10.1016/j.jvs.2008.06.060)
95. Fung Y. C. 1991. What are residual stresses doing in our blood vessels? *Ann. Biomed. Eng.* **19**, 237-249
96. Takamizawa K., Hayashi K. 1987. Strain energy density function and uniform strain hypothesis for arterial mechanics. J. Biomech. 20:7–17.
97. Rodriguez, J. F., Martufi, G., Doblare, M. & Finol, A. The effect of material model formulation in the stress analysis of abdominal aortic aneurysms. *Ann Biomed. Eng*. 2009.**37**, 2218-2221. (doi: 10.1007/s10439-009-9767-1)
98. Di Achille, P., Celi, S., Di Puccio, F. & Forte, P. Anisotropic AAA: computational comparison between four and two fiber family material models. *J Biomech*. 2011.**44**, 2418-2426. (doi: 10.1016/j.jbiomech.2011.06.029)
99. Vande Geest, J.P., Schmidt, D.E., Sacks, M. & Vorp, D.A. The effects f anisotropy on the wall stress analyses of Patient-specific abdominal aortic aneurysms. *Ann Biomed Eng.* 2008.**36**, 921-932. (doi: 10.1007/s10439-008-9490-3)

100. Rodriguez, J.F., Ruiz, C., Doblare, M. & Holzapfel, G.A. Mechanical stresses in abdominal aortic aneurysms: influence of diameter, asymmetry, and material anisotropy. *J Biomech Eng*. 2008.**130**, 021023, (doi: 10.1115/1.2898830)
101. Reeps, C., Gee, M., Maier, A., Gurdan, M., Eckstein, H.H. & Wall, W.A. The impact of model assumptions on results of computational mechanics in abdominal aortic aneurysm. *J Vasc Surg*. 2010.**51**, 670-688. (doi: 10.1016/j.jvs.2009.10.048)
102. Schriefl A.J., Zeindlinger G., Pierce D. M., Regitnig P. and Holzapfel G.A. 2011. Determination of the layer-specific distributed collagen fibre orientations in human thoracic and abdominal aortas and common iliac arteries. *J. R. Soc. Interface*
103. Canham P.B., Finlay H.M., Dixon J.G and Ferguson S.E. 1991. Layered collagen fabric of cerebral aneurysms quantitatively assessed by the univerzal stage and polarized light microscopy. *Anat. Rec.* **231**, 549-592
104. Finlay H.M., McCullough and Canham P.B. 1995. Three dimensional collagen organisation of human brain arteries at different transmural pressures. *J. Vasc. Res.* **32**, 301-312.
105. Jinqueria L.C., Bignolas G. and Brentani R.R.1979. Picrosirius staining plus polarization microscopy a specific method for for collagen detection in tissue sections. *Histochem. J.* **11,**447-455
106. Canham P.B., Finlay H.M., Dixon J.G., Boughner D.R. and Chen A. 1989. Measurements from light and polarised light microscopy of human coronary arteries fixed at distending pressure. *Cardiovasc. Res.* **23**, 973-982
107. Timmis L.H., Wu Q., Yeh A.T., Moore J.E. and Greenwald S.E.2010. Structural inhomogenity and fiber orientation in the inner arterial media. *Am J Physiol Heart Circ Physiol***. 298**:1537-1545.
108. Ayres CH., Bowlin G.L., Henderson S.C., Taylor L., Shultz J., Alexander J. et al. 2006. Modulation of anisotropy in electrospun tissue-engineering scaffolds: Analysis of fiber alignment by the fast Fourier tranform. *Biomater*. **27**, 5524-5534.
109. Ayres Ch.E., Jha B.S., Meredith H., Bowman J.R., Bwlin G.L., Henderson S.C. and Simpson D.G. 2008. Measuring fiber alignment in electrospun scaffolds: a user's guide to the 2D fast Fourier transform approach. *J. Biomater. Sci. Polymer Edn*. **19**:603-621.
110. Kim, K., Kim S., Minxha J and Palmore G.T.R. 2011. A novel method for analyzing images of live nerve cells. *J Neurosc Meth*. **201**:98-105.
111. Frisch K.E., Duenwald-Kuehl S.E., Kobayashi H., Chamberlein C.S., Lakes R.S. and Vanderby R. 2012. *Acta Histochem*. **144**:140-144
112. D'Amore A., Stella J.A., Wagner W.R. and Sacks M.S. 2010. Characterization of the complete fiber network topology of planar fibrous tissues and scaffolds. *Biomater*. **31**:5345-5354.
113. Krlon W.J., Covell J.W., Mcculloch A.D., Hunter J.J. and Omens J.H. 1998. Automated measurement of myofiber disarray in transgenic Mice with ventricular expression of ras. *Anatom Rec*. **252**:612-625.
114. Elbischer P.J., Bischof H., Regitnig P. and Holzapfel G.A. 2004. Automated analysis of collagen fiber orientation in the outermost layer of human arteries. *Pattern Anal Applic*. **7**:26-284.
115. http://frigg.physastro.mnsu.edu/spect_flat.html
116. http://en.wikipedia.org/wiki/Dark-frame_subtraction
117. Xu F., Beyazoglu T., Hefner E., Gurkan U.A. and Demirci U. 2011. Automated and adaptable quantification of cellular alignment from microscopic images for tissue engineering applications. *Tissue Eng part C*. **17**:641-648
118. Sacks, M.S.2000. Biaxial mechanical evaluation of planar biological materials. *J Elast*. **61**, 199-246. (doi: 10.1023/A:1010917028671)
119. Zemanek M., Ph.D. Thesis, Brno 2010
120. Basciano C.A. and Kleinstreuer C. 2009. Invariant-based anisotropic constitutive models of the healthy and aneurysmal abdominal aortic wall. *J Biomech Eng*. **131**,021009-1-11
121. Gasser T.C. and Forsell C.2011. The numerical implementation of invariant-based viscoelastic formulations at finite strains. An anisotropic model for the passive myocardium. *Comp Methods Appl. Mech. Engrg*. **200**,3637-3645
122. Hans SS, Jareunpoon O, Balasubramaniam M, Zelenock GB. Size and location of thrombus in intact and ruptured abdominal aortic aneurysms. *J Vasc Surg* 2005, **41**:584-588
123. Simon BR, Gaballa MA. Finite strain, poroelastic finite element models for large arterial cross sections. *Comput Meth Biomech Biomed Eng* 1988, **9**:325-333.
124. Ayyalasomayajula A., Vande Geest JP, Simon BR. Porohyperelastic finite element modeling of abdominal aortic aneurysms. *J Biomech Eng* 2010, **132**:104502.
125. Speelman L, Schurink GWH, Bosboom EMH, Buth J, Breeuwer M, van de Vosse FN et al. The mechanical role of thrombus on the growth rate of an abdominal aortic aneurysm. *J Vasc Surg* 2010, **51**:19-26

126. Van Dam EA, Dams SD, Peters GWM, Rutten MCM, Schurink GWH, Buth J, et al. Nonlinear viscoelastic behavior of abdominal aortic aneurysm thrombus. *Biomech model mechanobiol* 2008, **2**:127-137.
127. Bergel, D.H., 1960 The viscoelastic properties of the arterial wall. Ph.D., University of London.
128. Fung Y. C. 1991. What are residual stresses doing in our blood vessels? *Ann. Biomed. Eng.* **19**, 237-249
129. Takamizawa K., Hayashi K. 1987. Strain energy density function and uniform strain hypothesis for arterial mechanics. J. Biomech. 20:7–17.
130. Rachev A. and Hayashi K. 1999. Theoretical study of the effect of vascular smooth muscle contraction on strain and stress distribution in arteries. *Ann. Biomed. Eng.* **32**, 257-263. (doi:10.1114/1.191)
131. Raghavan M. L., Trivedi S., Nagaraj A., McPherson D. D. and Chandran K. B. 2004. Three-dimensional finite element analysis of residual stress in arteries. *Ann. Biomed. Eng.* **32**, 257-263.
132. Alastrue V., Pena E., Martinez M. A. and Doblare M. 2007 Assessing the use of the "opening angle method" to enforce residual stresses in patient specific arteries. *Ann. Biomed. Eng.* **35,** 1821-1837.
133. Humphrey J. D. 2002. Cardiovascular solid mechanics. Cells, tissues and organs. New York, NY: Springer.
134. Vaishnav R.N. and Vossoughi J. 1987 Residual stress and strain in aortic segments. *J Biomech*. **20**:235–237.
135. Vossoughi, J., 1992. Longitudinal residual strain in arteries. 11th Southern Biomedical Engineering Conference, Memphis, Tennessee, pp. 17–19
136. Zhou X. and Lu J. 2009. Estimation of vascular open configuration using finite element inverse elastostatic method. *Eng. Comp*. **25**, 49-59. (doi 10.1007/s00366-008-0104-3)
137. Zeinali-Davarani, S. & Baek. S. 2012 Medical image-based simulation of abdominal aortic aneurysm growth. *Mech. Res. Commun*. (in press).
138. Zeinali-Davarani S., Raguin L.G., Baek S. 2011 An inverse optimization approach toward testing different hypotheses of vascular homeostasis using image-based models, *Int J Struc Chan Sol*, **3**, 33-45.
139. Baek, S., Rajagopal, K. R. & Humphrey, J. D. 2006 A theoretical model of enlarging intracranial fusiform aneurysms. J. Biomech. Eng. **128**, 142–149.
140. Kroon, M. & Holzapfel, G. A. 2009 A theoretical model for fibroblast-controlled growth of saccular cerebral aneurysms. *J.Theor.Biol*. **257**,73–83.
141. Humphrey, J. D. & Rajagopal, K. R. 2002 A constrained mixture model for growth and remodeling of soft tissues. Mat. Model. Meth. App.l Sci. 12, 407–430.
142. Martufi G. & Gasser TC. 2012 Turnover of Fibrillar Collagen in Soft Biological Tissue with Application to the Expansion of Abdominal Aortic Aneurysms, , *J. R. Soc. Interface* (accepted for publication)
143. Auer, M. & Gasser, T.C.2010. Reconstruction and finite element mesh generation of abdominal aortic aneurysms from computerized tomography angiography data with minimal user interactions. *IEEE Trans. Med. Imag*. **29**, 1022-1028. (doi: 10.1109/TMI.2009.2039579)
144. Greenwald. S.E., Moore J.E., Rachev A., Kane T.P.C. and Meister J.J. 1998. Experiemntal investigation of the distribution of residual strains in the artery wall. *J. Biomech. Eng*. **119**,438-444.
145. Zeller P.J. and Skalak T.C. 1998. Contribution of individual structural components in determining the zero ztress state in small arteries. *J Vasc Res*. **35**,8-17
146. Rachev A. and Greenwald S.E. 2003. Residual strains in conduit arteries. *J Biomech.* **36**,661-670.
147. Humphrey J.D., Eberth J.F., Dye W.W. and Gleason R.L. 2009. Fundamental role of axial stress in compensatory adaptations by arteries. J Biomech. 42, 1-8.
148. Raghavan M.L., Hanaoka M.M. Kratzberg J.A. Higuchi M.L. and da Silva E.S. 2011. Biomechanical failure properties and microstructural content of ruptured and unruptured abdominal aortic aneurysms. *J Biomech*. **44**,2501-2507.
149. Hurks R., Pasterkamp G., Vink A, Hoefer, I.E., Bots M.L., van de Pavoordt H.D.W.M. et al. 2012. Circumferential heterogenity in the abdominal aortic aneurysm wall composition suggests lateral sides to be more rupture prone. *J Vasc Surg*. **55**,203-209
150. Assar A.N. and Zarins C.K. 2009. Ruptured abdominal aortic aneurysm: a surgical emergency with many clinical presentations. *Postgrad Med J* **85**:268-273.
151. Hyhlik-Durr A., Krieger T., Geisbusch, Kotelis D., Able T. and Bockler D. 2011. Reproducibility of deriving parameters of AAA rupture risk from patien-specific 3D finite element models. *J Endovasc Ther*. **18**,289-298.
152. Gee M.W. Forser Ch. and Wall W.A. 2010. A computational strategy for prestressing patient-specific biomechanical problems under finite deformation. Int. J. Numer. Meth. Biomed. Engng. **26**,52-72
153. Ene F., Gachon C., Delassus P., Caroll R., Stefanov F., O´Flynn P. and Morris L. 2011. In vitro evaluation of the effect of intraluminal thrombus on abdominal aortic anuerysm wall dynamic. *Med Eng Phys*. **33**,957-966.

12 Author's publications

12.1 Appendix A.

The impact of Intra-luminal Thrombus failure on the mechanical stress in the wall of Abdominal Aortic Aneurysms.

Stanislav Polzer[1], T.Christian Gasser[2], Jesper Swedenborg[3] and Jiri Bursa[1]

[1] Department of Solid Mechanics, Brno University of Technology, Czech Republic
[2] Department of Solid Mechanics, The Royal Institute of Technology, Stockholm, Sweden
[3] Department of Molecular Medicine and Surgery, Karolinska Institute, Stockholm, Sweden

Corresponding author: Stanislav Polzer
paper category: original article

Short title: Impact of thrombus failure on wall stress in aortic aneurysms

Published in European Journal of Vascular and Endovascular Surgery

Citation Reference: S. Polzer, T.C. Gasser, J. Swedenborg, J. Bursa. 2011. The Impact of Intraluminal Thrombus Failure on the Mechanical Stress in the Wall of Abdominal Aortic Aneurysms *Eur J Vasc Endovasc Surg*, **41:***467-473.*

Appendix A: The impact of ILT failure on the mechanical stress in AAA.

Abstract

Objectives: The role of the Intra-luminal Thrombus (ILT) in Abdominal Aortic Aneurysm (AAA) rupture is controversial and it is still not clear if an ILT increases or decreases AAA rupture risk. Specifically, signs of bleeding in the ILT are considered to increase AAA rupture risk. In order to further explore this hypothesis, intact AAAs (n=4) with clear signs of fissures in the ILT, identified by Computer Tomography Angiography (CT-A) were investigated.

Methods: Two different cases of ILT fissuring were investigated, where (i) ILT fissures were extracted directly from the CT-A data and (ii) a hypothetical fissure was introduced in the otherwise intact ILT tissue. Wall stress distributions were predicted based on detailed Finite Element (FE) models.

Results: ILT fissures extracted from CT-A data, locally increase the mechanical stress in the underlying wall by up to 30%. The largest impact on wall stress was observed if the ILT crack reaches the aneurysm wall, or if it involves large parts of the ILT. In contrast, a concentric failure in the medial ILT, which does not reach the aneurysm wall, has almost no impact on wall stress distribution. Hypothetical ILT fissures that connect the lumen with the wall causes a two fold increase of the stress in the underlying wall.

Conclusions: ILT fissures increase the stress in the underlying wall, whereas regions other than that remain unaffected. If ILT fissures reach the wall or involve large parts of the ILT, the resulting increase in wall stress could possibly cause AAA rupture.

Key words: thrombus failure, abdominal aortic aneurysm, wall stress, Finite element analysis

Appendix A: The impact of ILT failure on the mechanical stress in AAA.

Introduction

A diameter exceeding 5.5cm is the most commonly accepted criterion for elective surgical repair of abdominal aortic aneurysm (AAA) [1,2]. There is, however, a need for other predictors for rupture, since aneurysms with a diameter less than 5.5 cm can rupture[3,4] and some large aneurysms do not. An aneurysm ruptures if the mechanical stress exceeds the local wall strength, consequently Peak Wall Stress (PWS)[5, 6] and Peak Wall Rupture Risk (PWRR)[7] have been found to be more reliable parameters than diameter to assess AAA rupture risk.

Mechanical stress in the aneurysm wall is non homogeneous and PWS denotes the highest stress in the entire AAA wall. The biomechanical rupture risk approach relates stress and strength locally, which defines the stress/strength ratio shown as PWRR, which is not homogeneously distributed in the AAA wall. In vitro measurements have shown that tensile strength of the AAA wall depends on several factors: ILT, wall thickness, gender and luminal diamter[27], which to some extent is reflected by PWRR, but not by the PWS.

An Intra-luminal Thrombus (ILT) is found in most AAAs of clinically relevant size[8]. It has been suggested[10] that hypoxia in the AAA wall covered by a thick ILT is associated with neovascularization and degradation of extra cellular matrix [10]. An AAA wall segment covered by a thick ILT is also thinner and has an increased number of inflammatory cells and smooth muscle cell apoptosis[11]. Apart from these consequences, the ILT itself influences mechanical stress of the underlying vessel wall stress[12,13,14,15]. The ILT can be regarded as an elastic body[16] that redistributes stress and buffers the thin wall from mechanical stress.

Even though ILT has characteristic solid mechanical properties (stiffness, strength)[16], studies have concluded that the ILT may not reduce wall stress, based on findings of only minor or no pressure reduction under the ILT [18,26]. Finally, signs of ruptures in the ILT allowing blood to reach the weakened underlying wall are more pronounced in ruptured than intact AAAs[20].

The finite element method divides any geometry into a large number of small finite elements. All finite elements together give the FE mesh, which is used to compute stresses and strains in the whole AAA. In this study we investigate the hypothesis that ILT failure increases wall stress using Finite Element (FE) analysis of non-ruptured AAAs with intact and fissured (ruptured) ILTs.

Methods

Data acquisition

Patient with non-ruptured AAAs (two men and two women; details are given in Table 1) with signs of ILT fissures larger than 1cm in Computer Tomography-Angiography (CT-A) scans were included. GE LightSpeed16, GE MEDICAL SYSTEMS, which provides in plane and

out of plane resolutions of 1.0 mm and 0.6-:-2.0 mm, respectively was used for CT-A. Data was collected prior to elective AAA repair at Karolinska University Hospital, Stockholm, Sweden. Collection and use of data from human subjects was approved by the local ethics committee.

	Gender	Age	Pressure [mm Hg]	max.diameter [mm]	max. ILT thickness [mm]
AAA no.1	Male	81	160/90	93	43
AAA no.2	Female	71	190/130	48	24
AAA no.3	Male	90	160/90	68	25
AAA no.4	Female	71	130/80	52	23

Table 1: Clinical details about studied cases

Failure of the ILT was defined by the presence of areas with high attenuation, which were often of crescent like shape. Cases with unclear exterior aneurysm surface, often because of poor quality of the CT-A scans, were prefiltered to avoid operator dependent segmentation of the CT data. We used a pool of 63 non ruptured AAAs, from which four cases met the inclusion criteria of the present study.

Geometry reconstruction

Deformable (active) contour models provided by A4research vers.2.0 (VASCOPS GmbH, Austria) were used to reconstruct the 3D geometry of AAAs based on standard CT data. Specifically, the user defines an inflation pressure that expands a virtual balloon inside the 3D set of image, until the boundaries of the aneurysm are detected[21]. This provides smooth surfaces and excludes artifacts such as sharp edges and corners, which otherwise might cause stress artifacts of the FE simulation. The wall thickness was given values related to the thickness of the ILT. At sites with a thin ILT (less than 1mm) and a thick ILT (larger than 25 mm) a wall thickness of 1.5mm and 1.0mm respectively was used[11].

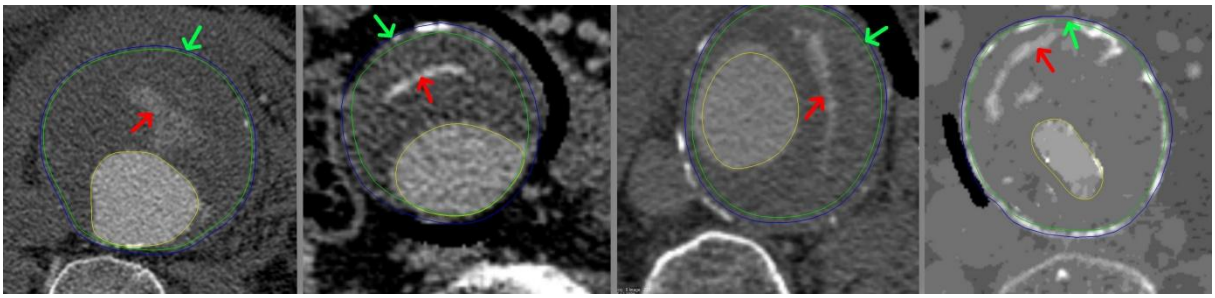

Figure 1 Reconstructed AAAs from CT-A images. The fissured ILT is indicated by red arrows. Sites, at which the highest stress increase was observed when considering ILT failure in the FE model, are marked by green arrows.

Appendix A: The impact of ILT failure on the mechanical stress in AAA.

Finite element model

A non-linear hyperelastic isotropic (uniform in all directions) constitutive model with the strain energy $\Psi=a_1(I_1-3)+a_2(I_1-3)^2$, as proposed earlier for rubber like materials, was used [30] which frequently is used for aneurysm wall. I_1 denotes a parameter measuring the strain (deformation) of the tissue. The material parameters, $a_1=174$ kPa and $a_2=1888$ kPa were both identified from in vitro testing of aneurysm tissue and reflect mean population data[23]. The stress-strain relation of the (non-linear) elastic properties of the tissue can be derived from the strain energy Ψ (mechanical energy stored in the tissue during deformation), and this constitutive model has been implemented in ANSYS vers.12.0.1 (ANSYS Inc. PA, US). The same constitutive formulation was used in A4research, where it is already integrated. ANSYS is a commercial software for the finite element simulation and A4research is a commercial software for geometrical and biomechanical analysis (FE simulations) of AAA

In contrast to the aneurysm wall, the ILT exhibits an almost linear[16] constitutive response; hence a linear elastic constitutive model was used. Likewise, the elastic modulus of the ILT decreased from the luminal to the abluminal layer to match experimental (mean population) data as reported earlier[16]. The referential Young's moduli of 63.0 kPa and 42.0 kPa were used to describe the luminal and abluminal layers of the ILT. The reconstructed geometry was considered as a load free geometry and a constant Mean Arterial Pressure (MAP) was applied at the luminal surface, to mechanically load the aneurysm wall. MAP was defined as $\frac{1}{3}$x systolic pressure $+\frac{2}{3}$x diastolic pressure, where pressures refer to the blood pressure recorded upon admission to hospital.

To investigate the impact of tissue failure in the ILT, analyses of ILT fissures were performed in two ways. In the first case, fissured ILT tissue was modeled as a soft fluid like material, and hence, predominantly carried pressure load but almost no tension stress. Fissured ILT sites were identified by high attenuation (Figure 1) and described with 5% of the stiffness of intact ILT tissue. For numerical reasons the present approach requires a non vanishing elastic stiffness (i.e. 5% of the intact ILT tissue). This modeling approximation, however, is thought to impact the FE predictions of wall stress only marginally. The analysis is subsequently denoted as `direct fissure analysis´, and has been performed entirely with A4research.

In order to investigate a worst case scenario of the fissured ILT a second type of analysis was performed, where a 2.0mm thick hypothetical crack, that reached the wall (i.e. connects the lumen with the wall), was included at the side of the thickest ILT layer (Figure 3. The fissure covered a sector of about 30 degrees with a widening of about 1cm at the abluminal site. Consequently, a piece similar to a 2mm thick slice of a pie was removed from the ILT. This analysis is subsequently denoted as "idealized fissure analysis" and was carried out in ANSYS.

The aneurysm was fixed at the renal arteries and the aortic bifurcation. For the direct fissure analysis, a hexahedral dominated finite element mesh was used. These elements provide good accuracy and efficiency in the computational time and are suitable for soft tissues, whereas the complex geometry of idealized fissure analysis was meshed with (quadratic) tetrahedral finite elements within ANSYS. These elements are necessary due to the complexity of geometry when ILT fissure is included. A mesh convergence study was used to ensure that the numerical error in PWS did not exceed 5%. To this end the mesh was refined in axial, circumferential and radial directions to accurately capture stress gradients along these directions[24].

All FE computations considered large deformations, and the stress concentration factor was calculated, i.e. the relative increase of the von Mises stress due to the insertion of the real (direct fissure analysis) or hypothetical (idealized fissure analysis) crack.

Results

Direct fissure analysis

Table 2 summarizes the impact of ILT fissuring on the wall stress. Specifically, the increase in wall stress behind (adjacent to) the fissured ILT (i.e. at the site where the fissuring in the ILT gets closest to the wall) and the increase in PWS are reported. Note that PWS can be located anywhere in the aneurysm wall and is in general not adjacent to the fissuring in the ILT.

A fissure in the ILT weakens its structural integrity and shifts stress from the ILT to the underlying wall. Consequently, a fissured ILT increases the wall stress as compared to an intact ILT. It is noted that PWS did not increase significantly (concentration coefficient: 1.06(SD 0.05)), however, there is a noticeable increase in wall stress behind a fissured ILT (concentration coefficient: 1.20(SD 0.11)).

The largest increase in wall stress behind ILT fissure was observed in AAA No. 1 and No. 4, showing stress concentration coefficients of 1.28 and 1.31, respectively. AAA No. 1 contains a fissure which affects a large volume of the luminal part of ILT and AAA No.4 shows multiple fissures in the ILT with the largest one propagating from the middle ILT all along to the aneurysm wall (see Figure 1). AAAs No.2 and No.3 show almost concentric fissures in the middle ILT, which reaches neither the lumen nor the aneurysm wall.

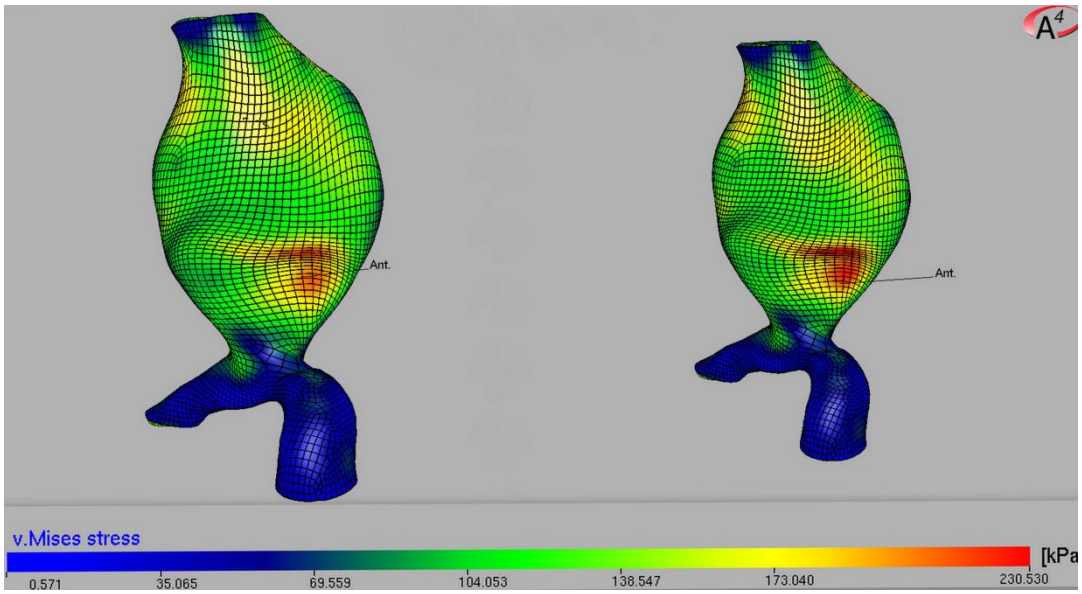

Figure 2: Wall (von Mises) stress distribution for AAA No.3. with the intact (left) and fissured (right) ILT model. ILT fissure were directly identified from CT-A images (direct fissure analysis).

Idealized fissure analysis

Table 3 summarizes the impact of the ILT fissure on the wall stress in the analyses based on the insertion of an idealized crack in the ILT. Note that due to the numerical error of the FE method PWS predictions of the intact AAAs may differ up to 10%, as it is seen by comparing the 4th column in Tables 2 and 3. However, the large differences in stress in the first column in Tables 2 and 3 are a consequence that the loci in the wall do not match.

	Stress prediction in the wall behind a fissured ILT			**PWS prediction**		
	Model with intact ILT [kPa]	Model considering ILT rupture [kPa]	Concentration coefficient [-]	Model with intact ILT [kPa]	Model considering ILT rupture [kPa]	Concentration coefficient [-]
AAA No.1	78	100	1.28	429	445	1.04
AAA No.2	64	70	1.09	197	220	1.12
AAA No.3	102	115	1.13	215	230	1.07
AAA No.4	55	72	1.31	188	189	1.01

Table 2: Wall (von Mises) stress predictions based on the FE Models using an intact and fissured ILT. Increases in stress behind the ruptured ILT and PWS were analyzed; the relative stress increase is given by the concentration coefficient. ILT fissures were directly identified from the CT-A images (direct rupture analysis).

Appendix A: The impact of ILT failure on the mechanical stress in AAA.

	stress prediction in the wall behind a fissured ILT			**PWS prediction**		
	Model with intact ILT [kPa]	Model considering idealized ILT rupture [kPa]	Concentration coefficient [-]	Model with intact ILT [kPa]	Model considering idealized ILT rupture [kPa]	Concentration coefficient [-]
AAA No.1	92	128	1.39	454	464	1.02
AAA No.2	91	164	1.80	210	215	1.02
AAA No.3	45	93	2.07	207	214	1.03
AAA No.4	112	172	1.54	173	175	1.01

Table 3 Wall stresses predictions based on FE Models using an intact and fissured ILT. Increases in (von Mises) stress behind the ruptured ILT and PWS were analyzed; relative stress increase is given by the concentration coefficient. An idealized crack (fissure) was inserted in the ILT (idealized ruptured analysis).

PWS was almost unaffected (concentration coefficient: 1.02(SD 0.01)) when inserting a crack (fissuring), however, there is a large increase in wall stress behind a fissured ILT (concentration coefficient: 1.70(SD 0.30)). Even a few centimeters away from the crack an increase of wall stress is clearly recorded, see Figure 3. The largest increase in wall stress behind the ILT fissure was observed in AAAs No. 2 and No. 3, showing stress concentration coefficients of 1.80 and 2.07, respectively. Figure 3 shows the predicted wall stresses in AAAs No. 1 and No. 2 based on the intact (left) and fissured (right) ILT model.

Appendix A: The impact of ILT failure on the mechanical stress in AAA.

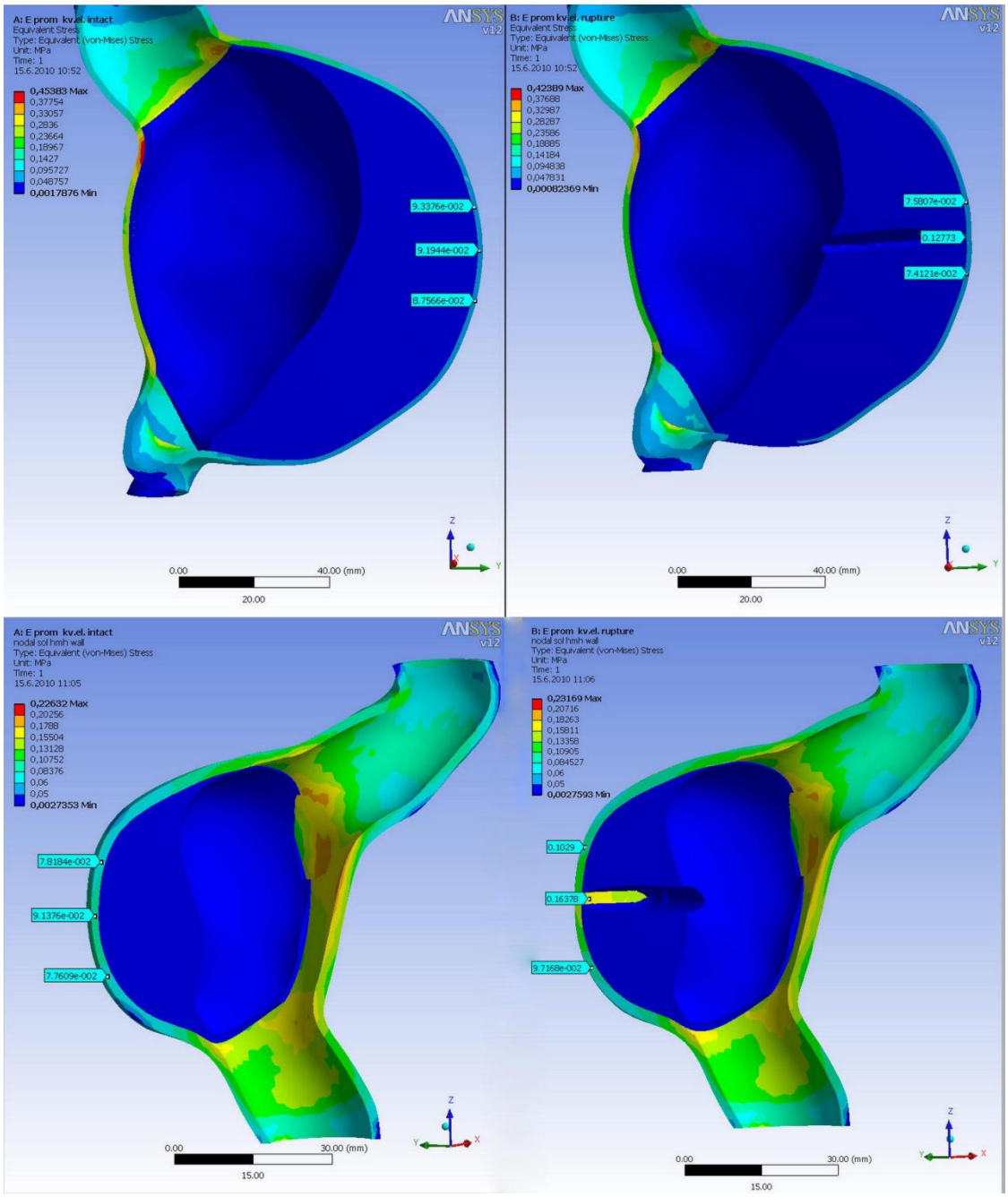

Figure 3: Wall stress distribution for AAA No.1 (top row) and No.2 (bottom row) with an intact (left column) and fissured (right column) ILT model. A hypothetical fissure (crack) all along to the aneurysm wall was included to account the ILT fissuring (hypothetical fissure analysis). Arrows indicate von Mises stress in the aneurysm wall in the vicinity of the crack tip.

Discussion

In this study, FE models were used to examine to what extent ILT fissuring increases the wall stress and, consequently, increases the AAA rupture risk. To this end ILT fissures have been directly identified from the CT-A data (direct fissure analysis), and idealized fissures (cracks) have been inserted in the ILT (idealized fissure analysis).

Appendix A: The impact of ILT failure on the mechanical stress in AAA.

The direct fissure analysis revealed that a fragmented ILT can increase the stress in the underlying wall by up to 30%. In addition, the idealized fissure analysis demonstrated that a hypothetical crack connecting the lumen with the wall could double the stress in the underlying wall. Consequently, these results underline that fissuring the ILT increases the local wall stress and in turn the risk of aneurysm rupture. This conclusion particularly holds for ILT failure that either reaches the aneurysm wall or constitutes a substantial volume of the ILT. In contrast, only a low increase in wall stress occurs for concentric fissures confined only to the medial ILT layer. Concentric fissures, which might be promoted by the onion-like structure of the ILT and do not reach the wall, cannot cause a stress concentration in the wall underneath, and hence, do not increase wall stress significantly.

The high compliance of the ILT tissue reduces the stress concentration at the crack tip, which could explain that not all cracks propagate all along to the wall. Likewise the layered (onion-like) structure of the ILT might also prevent cracks from radial propagation.

The present study used non-ruptured aneurysms, which showed signs of ILT fissuring larger than 1cm in the CT-A images, which states a restrictive inclusion criterion and enforced us to investigate a relatively small patient cohort. Visible ILT fissuring (without any size constraints) in CT-A images has been reported in 14%[20] of intact AAAs, and calculations based on data from other studies showed a prevalence of 6%[28] and 12%[29]. It is noted that a fissure in the ILT must be filled with contrast agent to become visible in CT-A images, and the low prevalence of detected ILT fissures does not imply that ILT fissuring is a relatively rare event. Alternatively ruptured aneurysm could have been used for the present study, known to have a higher prevalence for ILT fissuring (rupture) signs[20]. However, rupture alters aneurysm geometry, which makes the identification of the geometry before rupture, i.e. as it is required input for the FE model, difficult.

Naturally, FE models introduce numerous modeling assumptions and can only reflect the biomechanics of the real aneurysm to some degree of completeness. In the present study the constitution of aneurysm tissue (wall and ILT) represented mean population data and patient specific elastic properties would have increased the accuracy of the stress prediction. However, studies indicated that stress predictions in aneurysms are relatively insensitive to variable constitutive properties of the wall[22] and the ILT[32], and consequently, the geometry seems to be the most critical property of AAA FE models. ILT tissue was modeled as a homogenous single-phase material although a poroelastic model motivated by the ILT's porous microstructure of interconnected cavities[17,25] particularly under dynamic mechanical loading conditions, could be more realistic. However to our knowledge the stress field in the aneurysmal wall changes negligibly when a poroelastic model for ILT is used[31]. Likewise, calcifications and residual stresses in the load-free configuration were neglected, and considering that may have caused local differences in the wall stress. The AAA geometry, as

it was reconstructed from the CT-A data, was considered as the unloaded configuration, a simplification which is expected to increase wall stress globally. Wall stress is indirectly proportional to the wall thickness, and although the present study could not consider a patient specific wall thickness, at least the reported thinning behind a thicker ILT was implemented. Although our FE models relied on several assumptions, it clearly emphasized that the results of the present study were based on comparisons amongst FE models, and hence, it is very unlikely that more sophisticated modeling assumption would have led to different conclusions.

In conclusion, the present work demonstrates that not all cracks in the ILT are dangerous, but those reaching the aneurysm wall or constituting large volume portions of the ILT clearly increases AAA rupture risk. This is in line with earlier studies suggesting that ILT failure increases the risk of AAA rupture[20]. The study showed that inhomogenities like fissures in the ILT can have a pronounced impact on the stress in the aneurysm wall, and consequently the influence of ILT's inhomogeneous composition on the wall stress could be of interest for further investigations.

Acknowledgments

We gratefully acknowledge the support given to this work by the Young Faculty Grant No. 2006-7568 provided by the Swedish Research Council, VINNOVA and the Swedish Foundation for Strategic Research, and the EC Seventh Framework Programme, Fighting Aneurysmal Disease (FAD-200647). In addition, this work was supported by grant (GA CR No. 106/09/1732) and faculty (FSI-J-11-3) projects, and Stanislav Polzer was supported by the "Scholarship for talented Ph.D. student" provided by the city of Brno, Czech Republic.

Conflict of Interest

None

References

1. Mortality results for randomised controlled trial of early elective surgery or ultrasonographic surveillance for small abdominal aortic aneurysms. The UK Small Aneurysm Trial Participants. Lancet 1998; 352(9141):1649-55.
2. Lederle FA, Wilson SE, Johnson GR, Reinke DB, Littooy FN, Acher CW, et al.. Immediate repair compared with surveillance of small abdominal aortic aneurysms. N Engl J Med 2002;346(19):1437-44.
3. Heikkinen M, Salenius JP, Auvinen O. Ruptured abdominal aortic aneurysm in a well-defined geographic area. J Vasc Surg 2002;36(2):291-6.
4. Nicholls SC, Gardner JB, Meissner MH, Johansen HK. Rupture in small abdominal aortic aneurysms. J Vasc Surg 1998;28(5):884-8.
5. Fillinger MF, Raghavan ML, Marra SP, Cronenwett JL, Kennedy FE. In vivo analysis of mechanical wall stress and abdominal aortic aneurysm rupture risk. J Vasc Surg 2002;36(3):589-97.
6. Venkatasubramaniam AK, Fagan MJ, Mehta T, Mylankal KJ, Ray B, Kuhan G, et al.. A comparative study of aortic wall stress using finite element analysis for ruptured and non-ruptured abdominal aortic aneurysms. Eur J Vasc Endovasc Surg 2004;28(2):168-76.
7. Gasser TC, Auer M, Labruto F, Swedenborg J, Roy J. Biomechanical rupture risk assessment of abdominal aortic aneurysms: model complexity versus predictability of finite element simulations. Eur J Vasc Endovasc Surg 2010;40(2):176-85.

8. Hans SS, Jareunpoon O, Balasubramaniam M, Zelenock GB. Size and location of thrombus in intact and ruptured abdominal aortic aneurysms. J Vasc Surg 2005;41(4):584-8.
9. Alexander JJ. The pathobiology of aortic aneurysms. J Surg Res 2004;117(1):163-75.
10. Vorp DA, Lee PC, Wang DH, Makaroun MS, Nemoto EM, Ogawa S, et al.. Association of intraluminal thrombus in abdominal aortic aneurysm with local hypoxia and wall weakening. J Vasc Surg 2001;34(2):291-9.
11. Kazi M, Thyberg J, Religa P, Roy J, Eriksson P, Hedin U, et al.. Influence of intraluminal thrombus on structural and cellular composition of abdominal aortic aneurysm wall. J Vasc Surg 2003;38(6):1283-92.
12. Wang DH, Makaroun MS, Webster MW, Vorp DA. Effect of intraluminal thrombus on wall stress in patient-specific models of abdominal aortic aneurysm. J Vasc Surg 2002;36(3):598-604.
13. Mower WR, Quinones WJ, Gambhir SS. Effect of intraluminal thrombus on abdominal aortic aneurysm wall stress. J Vasc Surg 1997;26(4):602-8.
14. Li ZY, U-King-Im J, Tang TY, Soh E, See TC, Gillard JH. Impact of calcification and intraluminal thrombus on the computed wall stresses of abdominal aortic aneurysm. J Vasc Surg 2008;47(5):928-35.
15. Vorp DA, Mandarino WA, Webster MW, Gorcsan J 3rd. Potential influence of intraluminal thrombus on abdominal aortic aneurysm as assessed by a new non-invasive method. Cardiovasc Surg 1997;4(6):732-9.
16. Gasser TC, Gorgulu G, Folkesson M, Swedenborg J. Failure properties of intraluminal thrombus in abdominal aortic aneurysm under static and pulsating mechanical loads. J Vasc Surg 2008;48(1):179-88.
17. Gasser TC, Martufi G, Auer M, Folkesson M, Swedenborg J. Micromechanical characterization of intra-luminal thrombus tissue from abdominal aortic aneurysms. Ann Biomed Eng 2010;38(2):371-9.
18. Schurink GW, van Baalen JM, Visser MJ, van Bockel JH. Thrombus within an aortic aneurysm does not reduce pressure on the aneurysmal wall. J Vasc Surg 2000;31(3):501-6.
19. Choke E, Thompson MM, Dawson J, Wilson WR, Sayed S, Loftus IM, et al.. Abdominal aortic aneurysm rupture is associated with increased medial neovascularization and overexpression of proangiogenic cytokines. Arterioscler Thromb Vasc Biol 2006;26(9):2077-82.
20. Roy J, Labruto F, Beckman MO, Danielson J, Johansson G, Swedenborg J. Bleeding into the intraluminal thrombus in abdominal aortic aneurysms is associated with rupture. J Vasc Surg 2008;48(5):1108-13.
21. Auer M, Gasser TC. Reconstruction and Finite Element Mesh Generation of Abdominal Aortic Aneurysms From Computerized Tomography Angiography Data With Minimal User Interactions. IEEE Transactions on Medical Imaging,2010;29(4):1022-1028
22. Raghavan ML, Vorp DA. Toward a biomechanical tool to evaluate rupture potential of abdominal aortic aneurysm: identification of a finite strain constitutive model and evaluation of its applicability. J Biomech 2000;33(4):475-82.
23. Raghavan ML, Webster MW, Vorp DA. Ex vivo biomechanical behavior of abdominal aortic aneurysm: assessment using a new mathematical model. Ann Biomed Eng 1997;24(5):573-82.
24. Zendehbudi GR, Kazemi A. The accuracy of thin-shell theory in estimation of aneurysm rupture. J Biomech 2007;40(14):3230-5.
25. Adolph R, Vorp DA, Steed DL, Webster MW, Kameneva MV, Watkins SC. Cellular content and permeability of intraluminal thrombus in abdominal aortic aneurysm. J Vasc Surg 1997;25(5):916-26.
26. Hinnen JW, Koning OH, Visser MJ, Van Bockel HJ. Effect of intraluminal thrombus on pressure transmission in the abdominal aortic aneurysm. J Vasc Surg 2005;42(6):1176-82.
27. Vande Geest JP, Sacks MS, Vorp DA. A planar biaxial constitutive relation for the luminal layer of intra-luminal thrombus in abdominal aortic aneurysms. J Biomech 2006;39(13):2347-54.
28. Mehard WB, Heiken JP, Sicard GA. High-attenuating crescent in abdominal aortic aneurysm wall at CT: a sign of acute or impending rupture. Radiology 1994;192(2):359-62.
29. Arita T, Matsunaga N, Takano K, Nagaoka S, Nakamura H, Katayama S, et al.. Abdominal aortic aneurysm: rupture associated with the high-attenuating crescent sign. Radiology 1997;204(3):765-8.
30. Yeoh OH, Some forms of strain energy functions for rubber
Rubber Chem. Technol. 66 (1993) 754–771.
31. Polzer S, Bursa J, Poroelastic model of intraluminal thrombus in FEA of aortic aneurysm, C.T. Lim and J.C.H. Goh (Eds.): WCB 2010, IFMBE Proceedings 31, pp. 763–767, 2010
32. Di Martino ES, Vorp DA. Effect of variation in intraluminal thrombus constitutive properties on abdominal aortic wall stress. Annals of Biomedical Engineering. 2003;31::804–9.

12.2 Appendix B

Impact of poroelasticity of intraluminal thrombus on wall stress of abdominal aortic aneurysms

Stanislav Polzer[a], T.Christian Gasser[b], Bernd Markert[c] , Jiri Bursa[a] and Pavel Skacel[a]

[a]*Department of Solid Mechanics, Brno University of Technology, Czech Republic;*
[b]*Department of Solid Mechanics, The Royal Institute of Technology, Stockholm, Sweden;*
[c]*Institute of Applied Mechanics (Civil Engineering), University of Stuttgart, Germany*

Original research article. Submitted into Biomedical Engineering Online

Impact of poroelasticity of intraluminal thrombus on wall stress of abdominal aortic aneurysms

The impact of Intra-luminal Thrombus (ILT) on wall stress of abdominal aortic aneurysm (AAA) is controversially discussed in literature. To explore this phenomenon further, a poroelastic description of the ILT was integrated in Finite Element (FE) Models of the AAAs. The AAA models were loaded by a cyclic pressure wave and their transition into wall tension was investigated. To this end, ILT's permeability k^F was varied within a microstructurally motivated range of $7.5 \cdot 10^{-14} < k^F < 6.2 \cdot 10^{-8}$ $m^4N^{-1}s^{-1}$. The poroelastic model confirmed that the ILT transmits the entire arterial pressure to the wall while, at the same time, it significantly reduces the stress in the wall. The predicted stress in the AAA wall was insensitive to the permeability of the ILT and coincided with the results of AAA models using an elastic ILT description. Consequently we showed that computational efficient elastic models of the ILT can accurately predict wall stress in AAA models.

Keywords: Pore pressure; Finite element analyses; Poroelasticity; Abdominal aortic aneurysm; Intraluminal Thrombus

Background

An abdominal aortic aneurysm (AAA) ruptures when the mechanical stress exceeds the local wall strength. Commonly used criterion of maximum diameter is not reliable enough to assess AAA rupture risk. It has been shown that some aneurysms with a diameter less than 5.5cm rupture [1-4] and some large aneurysms do not. Therefore a Peak Wall Stress (PWS) [5,6] and Peak Wall Rupture Risk (PWRR) [7] have been found to be more reliable predictors of AAA rupture than the maximum diameter. However, PWS and PWRR depend on modelling assumptions; we are particularly concerned with constitutive descriptions of AAA tissues.

Intra-luminal Thrombus (ILT) is found in most AAAs of clinically relevant size [9] and its influence on wall stress remains controversial. ILT contains different types of blood [10,11] and other cells [12] as well as extracellular matrix (ECM) constituents. Specifically, new (fresh) ILT layers contain mainly fibrin fibres whereas the matured ILT, i.e. that in layers close to the vessel wall, shows a considerable amount of types I and III collagen [13]. Finally, the fibrous nano-structure is overlaid by a micro-structure of possibly interconnected cavities and pores filled by fluid [8,14,15]. The shape and dimension of these pores vary strongly with typical dimensions ranging from a few nanometres to micrometers [8]. Large pores may result from macrophages [10] and/or, especially in the abluminal layer, from micro-fissuring of the ILT. The ILT is a structural component with typical solid mechanical properties [16-20], enabling the load transition through the ILT fibrous network as mentioned by [21].

In-vivo [15] and in-vitro [22] experimental studies found that the pore pressure in the ILT is approximately equal to the blood pressure. Consequently, the ILT cannot reduce the pressure acting on the aneurysm wall and some authors [15] therefore concluded that the ILT cannot reduce wall stress either. Computational [23-25] and experimental [21] studies, with and without ILT, however demonstrate the opposite, i.e. that ILT considerably lowers stress and strain in the wall behind it. Regarding the ILT as a net of fibres that are connected to the aneurysm wall [21] could explain that the ILT lowers the wall stress even as the entire blood pressure penetrates through the pores towards the wall.

Different multi-phase and porous media theories used in modelling hydrated soft biological tissues have been proposed in literature [26-30]. Recently, even a porohyperelastic description of AAA (ILT and wall) has been proposed [31]. However, the authors investigated a rather narrow range of ILT permeabilities ($9{,}1\cdot10^{-11}\pm0{,}54\cdot10^{-11}\,\mathrm{m^4N^{-1}s^{-1}}$) that unfortunately did not include the experimentally measured value [10] of $9{,}1\cdot10^{-13}\,\mathrm{m^4N^{-1}s^{-1}}$.

The present paper aims at investigating to what extent ILT's poroelasticity influences wall stress predictions of AAA models. Specifically, the need for poroelastic modelling in the context of AAA wall stress assessment is studied, considering a wider interval of ILT permeability, as motivated by its microstructure.

Methods

Constitutive modelling of AAA tissues

Poroelastic description of the ILT

We consider the ILT as an elastic solid skeleton with a statistical distribution of interconnected pores (effective pores), which is fully saturated with a pore liquid. Consequently, the bulk volume V is given through the sum of the partial solid and fluid volumes, $V = V^S + V^F$, and the porosity (effective fluid volume fraction) is introduced as $\Phi = V^F / V$. Bounded intracellular/intrafibrillar fluids and sealed pores are considered as part of the solid phase and the ILT is modelled by Biot's theory [32,33] at quasi-static conditions.

The solid displacement vector **u** and the pore-fluid pressure p are the primary unknowns governed by the momentum balance:

$$\mathbf{0} = div\left(\boldsymbol{\sigma}_{\mathrm{E}} - \alpha p \mathbf{I}\right) + \boldsymbol{f} \tag{1}$$

and the mass balance (continuity-like equation):

$$\frac{\partial \zeta}{\partial t} + div\,\boldsymbol{q} = 0 \tag{2}$$

where $div(\bullet) = grad(\bullet)\mathbf{I}$ denotes the divergence operator with the identity tensor **I**. The effective solid Cauchy stress tensor and Biot's effective stress coefficient are denoted by $\boldsymbol{\sigma}_E$ and α, respectively, and $\boldsymbol{f}$ is the bulk body force per unit volume. Moreover, ζ describes the variation of fluid volume per reference volume and $\boldsymbol{q}$ is the flow flux vector, i. e. the fluid filter velocity. The model is completed by constitutive relations for the isotropic effective solid stress, described by the linear model

$$\boldsymbol{\sigma}_E = 2 \cdot G^S\, sym\left(grad\,\boldsymbol{u}\right) + \left(K^S - \frac{2G^S}{3}\right)\left(div\,\boldsymbol{u}\right) \cdot \mathbf{I} \tag{3}$$

as justified from macroscopic properties of the ILT [18,34]. In order to account for finite strain computations, eq.(3) is implemented through the (objective) Jaumann stress rate [35].
In addition, the variation of the specific fluid volume:

$$\zeta = \alpha\, div\,\boldsymbol{u} + \frac{1}{M}\, p \tag{4}$$

and the fluid filter velocity vector:

$$\boldsymbol{q} = -k^F \left(grad\ p - \boldsymbol{f}^F \right) \tag{5}$$

were used with M denoting the (conventional) Biot modulus.

The effective Cauchy stress in the porous solid matrix is governed by an isotropic linear elasticity law with constant elastic tangent, where G^S and K^S denote the macroscopic shear and bulk moduli of the porous solid matrix. The fluid percolation is described by an isotropic Darcy-type filter law (5) with k^F being the apparent permeability in $\mathrm{m^4N^{-1}s^{-1}}$ and $\boldsymbol{f}^F$ the volume specific fluid body force. Note that tortuosity effects as well as anisotropic and deformation-dependent permeability changes [36] are not considered, and hence the present model aims at capturing only the salient features of ILT tissue.

At physiological levels of pressure the solid and fluid constituents can be assumed as intrinsically incompressible, and the compressibility of the drained biphasic bulk material is magnitudes larger than that of its constituents. This simplifies the biphasic model, and a limit analysis gives [49] $\alpha = 1$, $M \to \infty$ and thus $\zeta \approx div\,\boldsymbol{u}$, i.e. the fluid is only influenced by the solid volumetric strain. Neglecting (gravitational) body forces ($\boldsymbol{f} = \boldsymbol{f}^F = \boldsymbol{0}$), the governing displacement–pressure ($\boldsymbol{u}$–p) formulation of the two-phase model finally yields

$$\boldsymbol{0} = div\left(\boldsymbol{\sigma}_{\mathrm{E}} - p\mathbf{I}\right) \tag{6}$$

$$div\frac{\partial \boldsymbol{u}}{\partial t} - k^F div\, grad\ p = 0 \tag{7}$$

such that the set $\{G^S, K^S, k^F\}$ of constitutive parameters defines ILT mechanical properties.

Hyperelastic description of the wall

The AAA wall is regarded as a non-linear isotropic material. We neglected its porous properties due to its low permeability [37] $\left(k^F = 7 \cdot 10^{-16}\ \mathrm{m^4N^{-1}s^{-1}}\right)$ compared to ILT. We modelled it by the strain energy function $\Psi = a_1\left(I_1 - 3\right) + a_2\left(I_1 - 3\right)^2$, which was originally proposed for rubber-like materials [38]. This model is frequently used for the AAA wall and $I_1 = tr\,\mathbf{C}$ denotes the first invariant of the right Cauchy Green deformation tensor $\mathbf{C}=\mathbf{F}^{\mathrm{T}}\mathbf{F}$, where $\mathbf{F}$ denotes the deformation gradient**.** Consequently, wall properties are characterized by the constitutive parameters $\left\{a_1, a_2\right\}$.

Parameter identification

The present study considers that ILT's shear modulus G^S gradually decreases from 21 kPa at the luminal site to 14 kPa at the abluminal site [18]. Likewise, ILT's solid skeleton under tension is modelled as an incompressible material with a Poisson's ratio of 0.4999.

Although the porosity ϕ of ILT tissue has not been measured directly, $\Phi = 0.8$ can be assumed based on the measured water content of 80% in ILT [16].

To estimate the apparent permeability $k^F = k^S / \mu$ the dynamic viscosity $\mu = 0.0044\,\mathrm{Pa\,s}$ of blood [39] is used, and the intrinsic permeability k^S in m^2 is computed according to the model

$$\frac{k^S}{a^2} = C_1 \left(\sqrt{\frac{1-\Phi_c}{1-\Phi}} - 1 \right)^{C_2} \tag{8}$$

for fibrous materials [40,41]. Here, the percolation threshold is defined by the critical porosity $\Phi_c = 0.0743$, above which permeating flow occurs; the dimensionless constants $C_1 = 0.491$ and $C_2 = 2.31$ are universal for fibre-based materials, i.e. they are independent from the actual micro-structural arrangement of the fibres. Specifically, these constants are valid for a wide range of materials like paper, wool, nylon, metal-fibre-based and collagen-fibre-based materials, when diluted by water, glycerol or air [41]. In equation (8) the characteristic length *a* defines the fibre radius of the fibrous material. ILT is regarded to be assembled by fibrin and collagen fibres, and considering radii from [14,42,43] 22 to 250nm, the equation (8) defines a range of $7.5 \cdot 10^{-14} < k^F < 9.6 \cdot 10^{-12}\ \mathrm{m^4 N^{-1} s^{-1}}$ for ILT apparent permeability.

The fibrous structure of ILT tissue is overlaid by a larger structure of pores, which, if interconnected, would define a network of large canaliculi and hence, these pores predominantly determine the ILT permeability. Considering characteristic lengths from [8] 1.0 μm to 20.0 μm for such a structure, model (8) enlarges the permeability spectrum, and consequently the present study considers a range of $7.5 \cdot 10^{-14} < k^F < 6.2 \cdot 10^{-8}\ \mathrm{m^4 N^{-1} s^{-1}}$. It is emphasized that this wide range aims at accounting for inter- and intra-patient variabilities, and that the value $k^F = 9.1 \cdot 10^{-13}\ \mathrm{m^4 N^{-1} s^{-1}}$ as measured by an in-vitro experiment [10], is included.

Finally, the AAA wall is described by material parameters a_1=174 kPa and a_2=1.89 MPa reflecting mean population data from in-vitro testing of AAA tissue [44].

Mechanical AAA model

Geometry

For simplicity and to obtain reviewable results, idealized axisymmetric AAA models were considered. Specifically, aneurysms with a length of 100 mm and maximum diameters of 60, 70 and 80 mm, subsequently denoted as AAA60, AAA70 and AAA80, were investigated. Likewise, a diameter of 20 mm describes the non-aneurysmatic infrarenal aorta, and a wall of a constant thickness of 1.8 mm was used. Bounded contact (to some extent motivated by an earlier study [21]) was selected between the ILT and the aneurysm wall. A typical investigated shape is shown in Figure 1.

The ILT was meshed by mixed tri-linear poroelastic elements, where the pore pressure is represented by an extra nodal degree of freedom, and a mixed tri-linear formulation was used for the aneurysm wall [45]. The selected finite element formulations are suitable for incompressible deformations, i.e. provide locking-free results. It is mentioned that a single element across the aneurysm wall is used, and hence, a stress state that complies with the membrane theory is predicted. This assumption enforces an almost homogeneous tangential (membrane) stress across the wall without introducing residual stresses in the load-free configuration. Finally, it is noted that when using a single solid element across the aneurysm wall, the predicted radial wall stress is meaningless.

Mesh and time step convergence has been optimised to make sure that results will not be affected by these quantities by more than 5%. Time step length which meets this condition is $t_{L\max} = 5.56 \cdot 10^{-4}\,\mathrm{s}$. The final mesh size is shown in Figure 1.

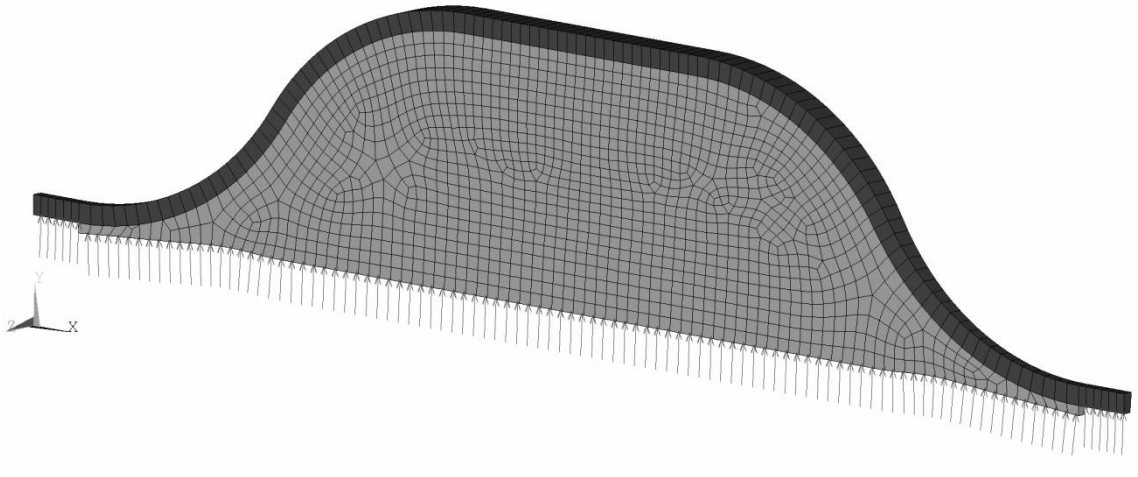

Figure 1: **Idealized AAA model to investigate the influence of the poroelastic properties of the ILT** (shown in light grey) on the stress in the aneurysm wall (shown in dark grey). The AAA model is loaded at the luminal surface by the blood pressure p_b.

Boundary conditions

Distal and proximal ends of the AAA are fixed and a blood pressure $p_b = 12\,kPa$ is applied to the luminal surface and an initial value $p_b = 12\,kPa$ of the pore pressure is prescribed within the entire ILT to reach faster convergence. Once the static solution was found, the pressure wave $p_b = (x,t)$ was prescribed at the luminal surface as shown in Figure 2. Specifically, the pressure wave propagates along the axial coordinate x of the AAA as well as in time t. Similar pressure boundary conditions are frequently applied in Computational Fluid Dynamics (CFD) [46]. Specifically, we used a wave speed of $4.7\,\mathrm{ms}^{-1}$, which reflects the lower limit of experimental data [47], therefore any possible dynamic transient processes in the stress and pore pressure fields (i.e. pressure wave reflections and interference) of AAA will become more visible.

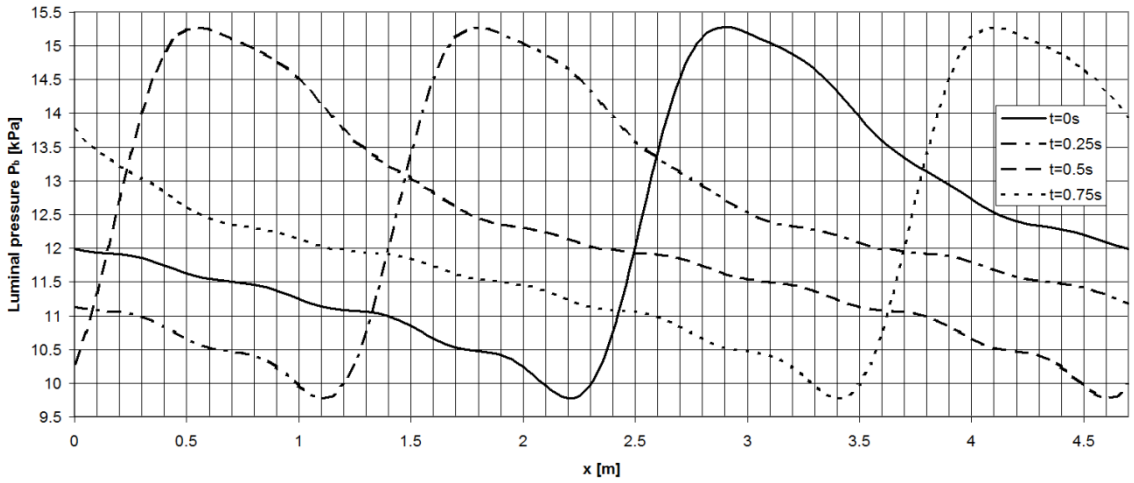

Figure 2: **Illustration of the pressure wave $p_b\,(x,t)$ applied to mimic in-vivo loading of the AAA**. The grid size of 100mm reflects the axial dimension of the investigated AAA. The mean pressure of the prescribed pressure wave is defined by $p_{MEAN} = \frac{1}{T}\int p\,dt = 12.2\,\mathrm{kPa}$, with $T = 1\mathrm{s}$ denoting the time of the cardiac cycle.

Results

Transient analyses were carried out in ANSYS 12.1., (ANSYS Inc. PA, USA), which contains the above discussed non-linear material model for the aneurysm wall as well as poroelastic elements based on the Biot's theory [32] as introduced in the Method section. Using a 4CPUs, 12GB RAM computer, the time needed for an analysis was up to 60 hours, depending on the particular model.

For permeabilities of $k^F > 10^{-13}$ $m^4N^{-1}s^{-1}$, periodic steady state solutions were reached within 15 cardiac cycles, when the computation was terminated. The convergence of the principal Cauchy stresses in the aneurysm wall and of the pore pressure in the ILT of the aneurysm model AAA70 is illustrated in Figure 3. Note that at a fixed spatial coordinate, i.e. $x = x_0$ the mean value of the steady-state pore pressure $p_{MEAN} = \frac{1}{T}\int p\,dt = 12.2\,\mathrm{kPa}$ coincides with the prescribed mean blood pressure, and that the mean value of the steady-state stresses $\sigma_{i\,MEAN} = \frac{1}{T}\int \sigma_i\,dt; i = 1,2,3$ matches the results of a traditional (single-phase) ILT description.

The pore pressure distribution during one cardiac cycle can be seen in Figure 4. It should be emphasized that the local pore pressure does not depend only on the distance from lumen but on the local geometry of AAA as well. (See neck areas in Figure 4). Finally, it is emphasized that the tensile stress in the wall during the systolic phase of the cardiac cycle is significantly reduced by the presence of the ILT, in comparison with the simulation neglecting the ILT as shown in Table 1. Table 1 shows that neither the material model of the ILT nor the prescribed BC affect resulting stresses. On the other hand, considering the ILT reduces stresses (PWS, maximum principal stress, local von Mises) significantly. The reduction is from 45% for AAA60 up to more than 60% for AAA80.

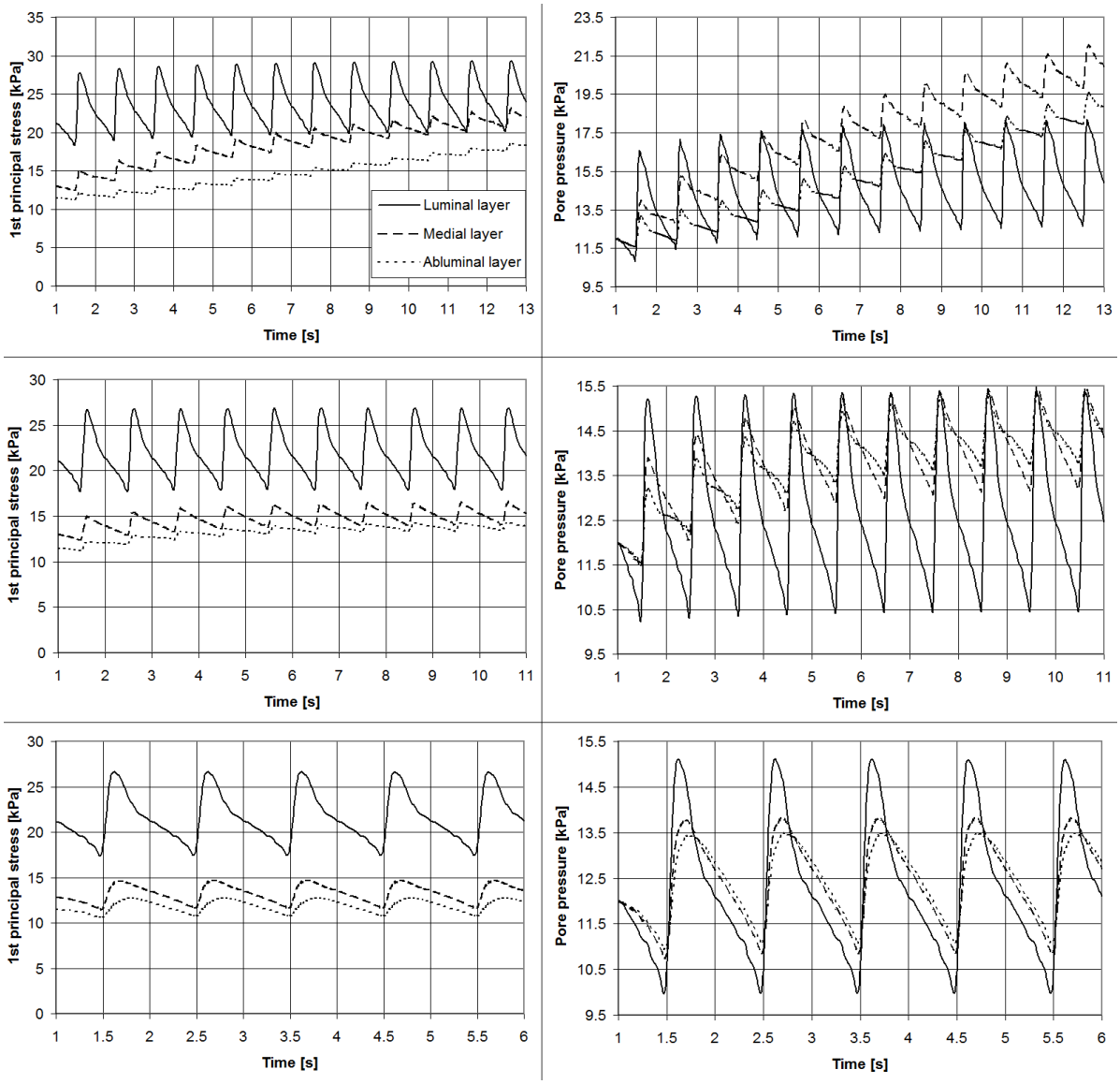

Figure 3: **Load transition processes in the AAA model AAA70 due to cycling blood pressure**. The analysis considers apparent permeabilities of $k^F = 10^{-13}\,\mathrm{m^4N^{-1}s^{-1}}$ (top row; steady-state solution not reached), $k^F = 10^{-12}\,\mathrm{m^4N^{-1}s^{-1}}$ (middle row) and $k^F = 10^{-11}\,\mathrm{m^4N^{-1}s^{-1}}$ (bottom row) of the ILT. Left column: Evolution in time of the first principal Cauchy stresses in the luminal, medial and abluminal layers of the ILT (legend is valid for all graphs). Right column: Evolution in time of the pore pressure in the luminal, medial and abluminal layers of the ILT.

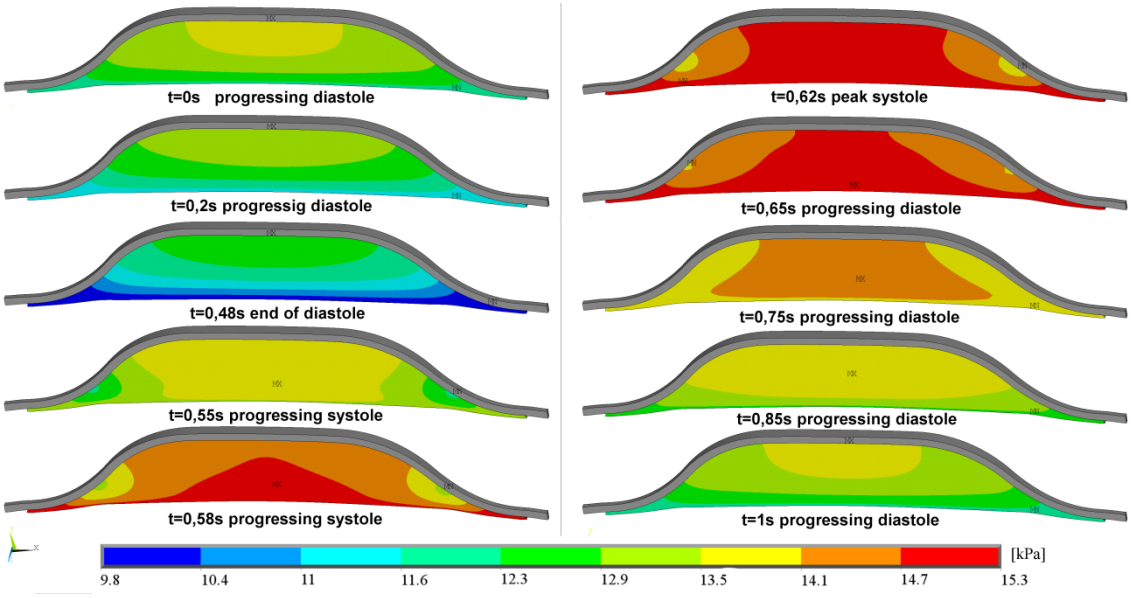

Figure 4 **Typical evolution of pore pressure during cardiac cycle; plotted for AAA60 and** $k^F = 10^{-12}\ \mathrm{m^4N^{-1}s^{-1}}$**.**

From a clinical perspective the accurate prediction of PWS (and therefore of PWRR) are most important. PWS is defined as the maximum von Mises stress in the AAA wall, as usual, i.e. $PWS = Max\left[\frac{1}{\sqrt{2}}\sqrt{(\sigma_1-\sigma_2)^2+(\sigma_1-\sigma_3)^2+(\sigma_2-\sigma_3)^2}\right]$, and its dependency on the apparent permeability was investigated in greater detail. PWS occurred at the transition from the normal to the aneurysmatic aorta and does not depend on the ILT apparent permeability, see Figure 5(right). Similarly, the von Mises wall stress (and the principal stresses) in the middle of the aneurysm, i.e. behind the thick ILT, is independent from ILT apparent permeability; see Figure 5 (left).

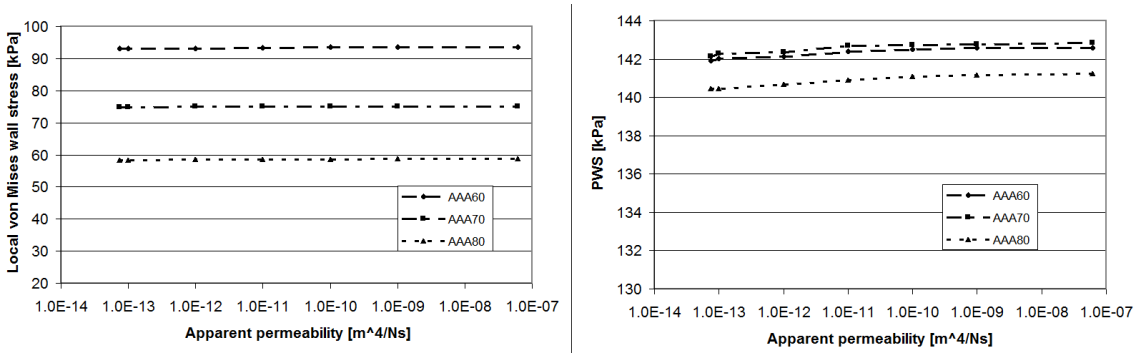

Figure 5: **Von Mises stress in the AAA wall as a function of the apparent permeability** of the ILT at the systolic phase of the last calculated cardiac cycle. Maximum wall stress in the middle of the aneurysm (left) and PWS (right).

Table 1. Influence of material model and pressure boundary condition (BC) on stress in AAA.

	Peak Wall stress (PWS) [kPa]			Peak 1st principal stress [kPa]		
Material model of ILT	Without ILT	Single-phase	Poroelastic	Without ILT	Single-phase	Poroelastic
Pressure BC	Constant	Constant	Pressure wave	Constant	Constant	Pressure wave
AAA60	259	143	142	289	153	152
AAA70	311	143	142	337	153	152
AAA80	375	141	141	400	149	149

Peak Wall Stress (PWS) (i.e. peak von Mises stress) and peak 1st principal Cauchy stress in the AAA wall predicted by different Finite Element (FE) models. FE models either neglect the ILT or consider it using a single-phase or a poroelastic description. The pressure BC considers either a constant blood pressure (constant) or a time and space-dependent blood pressure wave (Pressure wave). Inertia effects are neglected in all cases.

Table 2 Pore pressure underneath the thickest ILT [kPa]

$k^F \left[m^4 N^{-1} s^{-1} \right]$	$7.5 \cdot 10^{-14}$	10^{-13}	10^{-12}	10^{-11}	10^{-10}	10^{-9}	$6.2 \cdot 10^{-8}$
AAA60	22.4*	20.5*	14.8	13.9	15.2	15.3	15.3
AAA70	21.2*	19.6*	15.3	13.5	15.1	15.3	15.3
AAA80	18.9*	19.5*	15.8	13.9	15.0	15.3	15.3

Pore pressure underneath the thickest ILT for different AAA models and ILT permeabilities k^F . *Steady state solution not reached after 15 cycles.

Table 2 shows observed values of the pore pressure under the thickest ILT for various permeabilities. In the most extreme case, the Fluid pressure can decrease by 12% compared to the luminal pressure. Convergence was not reached for permeability values $k^F \leq 10^{-13}$ $m^4N^{-1}s^{-1}$ within 15 cardiac cycles. For these permeabilities, pore pressure grew in time and exceeded the prescribed pressure by some 5kPa in 15th cycle. It is expected, that converged pressure would be higher than 30kPa.

Discussion

Clinical relevant AAAs frequently include ILT, whose impact on the biomechanical quantities is viewed with controversy in literature. FE models can help to understand how the blood pressure transforms into the wall tension; the present study broadens conventional (single-phase) AAA models [18,20,34] with a poroelastic description of the ILT. Although a poroelastic model reflects ILT micro structure closely, this approach has not yet been fully exploited and to the author's knowledge, only a single work on this topic [31] has been reported in literature so far.

The present study found that at steady-state, stress in the AAA wall does not depend on the permeability of the ILT, and does not differ from single-phase ILT descriptions. This conclusion is of great importance, since a computationally much more efficient single-phase description can be used to predict the stress in the AAA wall reliably. Likewise, this finding validates earlier reported AAA models, which assumed ad-hoc a single-phase ILT. However, to study transport phenomena through AAA tissues, a poroelastic description can hardly be substituted.

The fact that poroelastic and single-phase descriptions of the ILT induce the same stress in the aneurysm wall may be explained by the particular nature of the structural problem. Specifically, the mobility of the pore fluid is constrained by the sealing of ILT outside (i.e. permeability magnitude of the aneurysm wall lower by 5 orders [37]) and the spatially constant blood pressure acting at the inside. These conditions lead to a pore fluid that is (almost) at rest $(\boldsymbol{q} \approx \mathbf{0})$ at the steady-state configuration, and hence, the single-phase and biphasic predictions coincide. Note that very low fluid filter velocities (10^{-7} ms^{-1}) in the ILT have also been predicted with a permeable wall description [31] although this conflicts to some extent with in-vivo-measurements [48] showing a considerable change of ILT volume over the cardiac cycle. It can be explained by the fact that it is very difficult to reconstruct AAA geometry accurately and software currently work with the error of several percent which is comparable to the reported volumetric change [48]. We assumed intrinsically incompressible skeleton and pore fluid, such that for $\boldsymbol{q} = \mathbf{0}$ a macroscopic incompressible material is used. Therefore the volumetric part of the stress, which is affected by the fluid phase according to Biot's theory [49], degenerates to a Lagrange contribution [50]. Similarly, the von Mises stress, which is independent from the hydrostatic pressure, cannot differ between poroelastic and single-phase descriptions.

Our numerical results demonstrate nicely that despite the existence of the ILT almost the entire blood pressure is transmitted to the wall. This was also confirmed by others [31]. Most interestingly we showed that the ILT remarkably reduces the stress in the wall at the same time. This is in good agreement with both experimental data [15,21,22] and published numerical analyses [23,24,25]. Consequently, it integrates conflicting views regarding the role

of the ILT in AAA biomechanics and demonstrates that the ILT helps to carry the load, in spite of the wall being exposed to the entire mean blood pressure. Specifically, for the investigated AAA models the ILT reduced wall tensile stress by a value between 46% (AAA60) and 62% (AAA80) relative to the model neglecting the ILT. It should be emphasised that this significant decrease in wall stress was obtained with a rather soft ILT [18], and using a stiffer ILT model [20,34] would reinforce the wall stress-diminishing effect [51] which explains why we obtained significantly higher wall stresses than the other study considering poroelastic description of the ILT [31]. On the other hand, it is noted that the predicted stress-diminishing effect is rather strong due to axisymmetry of the used model. For patient-specific geometries the structural impact of the ILT is lower [23,24].

Reported elastic ILT properties vary considerably [18,19,20,34] and changing them does not only influence the stress diminishing effect, but also the ILT poroelastic properties. We do not expect significant qualitative changes of our results to occur but a stiffer ILT would probably ensure that fewer loading cycles would be required to achieve a periodic solution.

Pore pressure under the ILT depended not only on the ILT permeability but also on the local geometry of the wall (see Figure 4) which may explain the differences in the reported in-vivo [15] and in-vitro [22] measurements, i.e. the measured values clearly depend on the position of pressure catheters.

Our study also found that a variation of the blood pressure along the AAA axis does not influence the stress predictions and may be neglected.

At cyclic loading the strain and pore pressure amplitudes in the abluminal ILT layer depend largely on the stiffness of the aneurysm wall. Our FE model used constitutive data for the AAA wall as reported in literature [52], where the stiffness at physiological deformation is about 2 times weaker than the more recently reported data [54]. While the predicted mean values of field variables might only be slightly affected by that discrepancy, their amplitudes could vary significantly.

For any kind of AAA model the interface conditions between wall and ILT define to a large extent the stress-diminishing effect of the ILT, and, following reported models in literature, we assumed a bounded (glued) interface. However, it is explicitly noted that opening the wall-ILT interface (cleavage formation between the ILT and the wall) allows the pore fluid to flow out, i.e. changes the exterior boundary condition for the fluid-phase at the interface.

Macroscopic ILT properties show an approximately linear First Piola Kirchhoff stretch response [8,20,34], however, the present study considers a linear response with respect to Cauchy stress, which underestimates the ILT stiffness at higher strains. As for any biological tissue, inter- and intra-patient variabilities of ILT are large, and it is not expected that this simplification could change the qualitative conclusions drawn by the present study.

We observed a significant pore pressure increase for low values of ILT permeabilities. It is noted that a comparable increase in pore pressure has not been reported from experimental studies, and the associated permeabilities may not be realistic. Moreover, the pore pressure also depends on the underlying poroelastic model and results might vary if alternative theories had been considered.

A poroelastic approach requires using mechanical properties of a solid skeleton under drained conditions, which is difficult to obtain for biological tissue. Note that mechanical properties of biological tissues literately depend on moisture environment, and consequently all published properties of ILT relate to undrained conditions.

Our study considered an almost incompressible solid skeleton although any highly porous medium (like the ILT) behaves compressibly at least under compressive stresses. The incompressibility assumption aimed at capturing the tension properties of ILT, and hence may be applicable to tension-dominated stress state in an AAA. However, this assumption should be further investigated in (in-vitro) experimental studies to gain a better understanding of ILT properties at different loading conditions.

The ILT permeability might be inhomogeneous (e.g. due to its radially changing microstructure) and strain dependent [36], similarly to other soft biological tissues like articular cartilage [53]. Due to lack of experimental data we considered a constant permeability, which is thought to capture at least the most salient features of ILT tissue. Since this study demonstrated that wall stress predictions are insensitive to the permeability, its conclusions are not expected to change when refining the permeability model of the ILT.

Acknowledgments

We gratefully acknowledge the support given to this work by the Young Faculty Grant No. 2006-7568 provided by the Swedish Research Council, VINNOVA and the Swedish Foundation for Strategic Research, and the EC Seventh Framework Programme, Fighting Aneurysmal Disease (FAD-200647). In addition, this work was supported by grant (GA CR No. 106/09/1732), by the faculty projects (FSI-J-11-14, FSI-S-11-12, FSI-S-11-11/1190), by the project Complex System for Attracting, Education and Continuing Involvement of Talented Individuals to Research Centers of AS CR and FME BUT (CZ.1.07/2.3.00/09.0228) and by the “Brno Ph.D. talent" provided by the Brno City Municipality, Czech Republic.

Competing interests

None

References

1. Lederle FA, Wilson SE, Johnson GR, Reinke DB, Littooy FN, Acher CW, et al. Immediate repair compared with surveillance of small abdominal aortic aneurysms. *N Engl J Med* 2002, **346**:1437-1444.
2. Mortality results for randomised controlled trial of early elective surgery or ultrasonographic surveillance for small abdominal aortic aneurysms. The UK Small Aneurysm Trial Participants. 1998 Lancet **352**:1649-1655.
3. Heikkinen M, Salenius JP, Auvinen O. Ruptured abdominal aortic aneurysm in a well-defined geographic area. *J Vasc Surg* 2002, **36**:291-296.
4. Nicholls SC, Gardner JB, Meissner MH, Johansen HK. Rupture in small abdominal aortic aneurysms. *J Vasc Surg* 1998, **28**:884-888.
5. Fillinger MF, Raghavan ML, Marra SP, Cronenwett JL, Kennedy FE. In vivo analysis of mechanical wall stress and abdominal aortic aneurysm rupture risk. *J Vasc Surg* 2002, **36**:589-597.
6. Venkatasubramaniam AK, Fagan MJ, Mehta T, Mylankal KJ, Ray B, Kuhan G, et al. A comparative study of aortic wall stress using finite element analysis for ruptured and non-ruptured abdominal aortic aneurysms. *Eur J Vasc Endovasc Surg* 2004, **28**:168-176.
7. Gasser TC, Auer M, Labruto F, Swedenborg J, Roy J. Biomechanical rupture risk assessment of abdominal aortic aneurysms: model complexity versus predictability of finite element simulations. *Eur J Vasc Endovasc Surg* 2010, **40**:176-185.
8. Gasser TC, Martufi G, Auer M, Folkesson M, Swedenborg J. Micromechanical characterization of intra-luminal thrombus tissue from abdominal aortic aneurysms. *Ann Biomed Eng* 2010, **38**:371-379.
9. Hans SS, Jareunpoon O, Balasubramaniam M, Zelenock GB. Size and location of thrombus in intact and ruptured abdominal aortic aneurysms. *J Vasc Surg* 2005, **41**:584-588.
10. Adolph R, Vorp DA, Steed DL, Webster MW, Kameneva MV, Watkins SC. Cellular content and permeability of intraluminal thrombus in abdominal aortic aneurysm. *J Vasc Surg*, 1997. **25**(5):916-926.
11. Kazi M, Thyberg J, Religa P, Roy J, Eriksson P, Hedin U, et al. Influence of intraluminal thrombus on structural and cellular composition of abdominal aortic aneurysm wall. *J Vasc Surg* 2003, **38**:1283-1292.
12. Folkesson M, Kazi M, Zhu C, Silveira A, Hemdahl AL, Hamsten A, Hedin U, Swedenborg J, Eriksson P. Presence of NGAL/MMP-9 complexes in human abdominal aortic aneurysms. *Thromb Haemost* 2007, **98**:427-433.
13. Karsaj I, Humhrey JD. A mathematical model of evolving mechanical properties of intraluminal thrombus. *Biorheology* 2009, **46**:509-527.
14. Collet JP. The elasticity of an individual fibrin fiber in a clot, PNAS 2005, **102**:9133-9137,
15. Schurink GW, van Baalen JM, Visser MJ, van Bockel JH. Thrombus within an aortic aneurysm does not reduce pressure on the aneurysmal wall. *J Vasc Surg* 2000, **31**:501-506.
16. Ashton JH , VandeGeest JP, Simon BR, Haskett DG. Compressive mechanical properties of the intraluminal thrombus in abdominal aortic aneurysms and fibrin-based thrombus mimics. *J Biomech*. 2009, **42**: 197-201.
17. di Martino ES, Mantero S, Inzoli F, Melissano G, Astore D, Chiesa R, et al. Biomechanics of abdominal aortic aneurysm in the presence of endoluminal thrombus: experimental characterization and structural static computational analysis. *Eur J Vasc Endovasc Surg* 1998, **15**: 290-299.
18. Gasser TC, Gorgulu G, Folkesson M, Swedenborg J. Failure properties of intraluminal thrombus in abdominal aortic aneurysm under static and pulsating mechanical loads. *J Vasc Surg* 2008, **48**:179-188.

19. Van Dam EA, Dams SD, Peters GWM, Rutten MCM, Schurink GWH, Buth J, et al. Nonlinear viscoelastic behavior of abdominal aortic aneurysm thrombus. *Biomech model mechanobiol* 2008, **2**:127-137.
20. Wang DH, Makaroun MS, Webster MW, Vorp DA. Mechanical properties and microstructure of intraluminal thrombus from abdominal aortic aneurysm. *J Biomech Eng* 2001, **123**:536-539.
21. Thubrikar MJ. Effect of thrombus on abdominal aortic aneurysm wall dilatation and stress, *J Cardiovasc Surg* 2003, **44**:67-77.
22. Hinnen JW, Koning OH, Visser MJ, Van Bockel HJ. Effect of intraluminal thrombus on pressure transmission in the abdominal aortic aneurysm. *J Vasc Surg* 2005, **42**:1176-1182.
23. Wang DH, Makaroun MS, Webster MW, Vorp DA. Effect of intraluminal thrombus on wall stress in patient-specific models of abdominal aortic aneurysm. *J Vasc Surg* 2002, **36**:598-604.
24. Li Z-Y, U-King-Im J, Tang TY, Soh E, See TC, and Gillard JH. Impact of calcification and intraluminal thrombus on the computed wall stresses of abdominal aortic aneurysm. *J Vasc Surg* 2008, **47**:928-935.
25. Mower WR, Quiñones WJ, Gambhir SS. Effect of intraluminal thrombus on abdominal aortic aneurysm wall stress. *J Vasc Surg* 1997, **33**:602–608.
26. Almeida ES, Spilker RL. Mixed and penalty finite element models for the nonlinear behavior of biphasic soft tissues in finite deformations: Part I -- Alternate formulations, *Comput Meth Biomech Biomed Eng*, 1997, **1**:25-46.
27. Ehlers W, Markert B. A linear viscoelastic biphasic model for soft tissues based on the Theory of Porous Media. *J Biomech Eng* 2001, **123**:418–424.
28. Huyghe JM, Arts T, van Campen DH and Reneman RS. Porous medium finite element model of the beating left ventricle, *Am J Physiol Heart Circ Physiol* 1992, **262**:1256-1267.
29. Lai WM, Mow VC, Zhu W. Constitutive modeling of articular cartilage and biomacromolecular solutions. *J Biomech Eng* 1993, **115**:474-480.
30. Simon BR, Gaballa MA. Finite strain, poroelastic finite element models for large arterial cross sections. *Comput Meth Biomech Biomed Eng* 1988, **9**:325-333.
31. Ayyalasomayajula A., Vande Geest JP, Simon BR. Porohyperelastic finite element modeling of abdominal aortic aneurysms. *J Biomech Eng* 2010, **132**:104502.
32. Biot MA.. General theory of three-dimensional consolidation. *J Appl Phys* 1941, **12**:155-164.
33. Biot MA.. Theory of elasticity and consolidation for a porous anisotropic solid. *J Appl Phys* 1955, **27**:459–467.
34. Vande Geest JP, Sacks MS, Vorp DA.. A planar biaxial constitutive relation for the luminal layer of intra-luminal thrombus in abdominal aortic aneurysms. *J Biomech* 2006, **39**:2347-2354.
35. Fung YC and Tong P.. Classical and computational solid mechanics (Advanced Series in Engineering Science), World Scientific, Singapore. 2001
36. Markert B. A constitutive approach to 3-d nonlinear fluid flow through finite deformable porous continua. *Transport Porous Med*. 2007, **70**:427–450.
37. Harrison RG, Massaro TA. Water flux through porcine aortic tissue due to a hydrostatic pressure gradient. *Atherosclerosis* 1976, **24**:363-367.
38. Yeoh OH. Some forms of strain energy functions for rubber *Rubber Chem Technol* 1993, **66**:754–771.
39. Shadden SC, Taylor CA.. Characterization of coherent structures in the cardiovascular system. *Ann Biomed Eng* 2008, **36**:1152–1162.
40. Gebart BR. Permeability of unidirectional reinforcements for RTM. *J Compos Mater* 1992, **26**:1100-1133.
41. Nabovati A, Llewelin E, Sousa ACM. A general model for permeability of fibrous porous media based on fluid flow simulations using the lattice Boltzmann method. *Composites: Part A* 2009, **40**:860-869.

42. Fratzl P. Collagen, structure and mechanics, Springer, 2008, 508pp.
43. Ryan AE. Structural origins of Fibrin clot rheology, *Biophys J* 1999, **77**:2813-2826.
44. Raghavan ML, Webster MW, Vorp DA. Ex vivo biomechanical behavior of abdominal aortic aneurysm: assessment using a new mathematical model. *Ann Biomed Eng* 1997, **24**:573-582.
45. ANSYS 12.1, user manual chapter 14.215
46. Biasetti J, Gasser TC, Auer M, Hedin U, Labruto F. Hemodynamics of the normal aorta compared to fusiform and sacular abdominal aortic aneurysms with emphasis on the potential thrombus formation mechanism. *Ann Biomed Eng* 2010, **2**:380-390.
47. Rogers WJ. Age-associated changes in regional aortic pulse wave velocity, *JACC* 2001, **38**:1123-1129.
48. Truijers M, Fillinger MF, Renema KW,Marra SP, Oostveen LJ, Kurvers HAJM wt al. In-Vivo Imaging of changes in abdominal aortic aneurysm thrombus volume during the cardiac cycle. *J Endovasc Ther* 2009, **16**:314-319.
49. Detournay E, Cheng, AHD. "Fundamentals of poroelasticity" Chapter 5 in Comprehensive Rock Engineering: Principles, Practice and Projects, Vol. II, Analysis and Design Method, ed. C. Fairhurst, Pergamon Press; 1993:113-171,
50. Ogden RW. Non-linear Elastic Deformations. 1997. Dover, New York.
51. Speelman L, Schurink GWH, Bosboom EMH, Buth J, Breeuwer M, van de Vosse FN et al. The mechanical role of thrombus on the growth rate of an abdominal aortic aneurysm. *J Vasc Surg* 2010, **51**:19-26
52. Raghavan ML, Vorp DA. Toward a biomechanical tool to evaluate rupture potential of abdominal aortic aneurysm: identification of a finite strain constitutive model and evaluation of its applicability. *J Biomech* 2000, **33**:475-482.
53. Lai WM, Mow VC, Roth V. Effects of nonlinear strain-dependent permeability ans rate of compression on the stress behavior of articular cartilage. *J Biom Eng* 1981, **103**:61-66.
54. Vande Geest JP, Sacks MS, Vorp DA.. The effects of aneurysm on the biaxial mechanical behavior of human abdominal aorta. *J Biomech* 2006, **39**:1324–1334

12.3 Appendix C

Poroelastic model of intraluminal thrombus in FEA of aortic aneurysm

Original research Article. Presented as an invited paper on 6th world congress of Biomechanics in Singapore 6th-9th of September 2010

Poroelastic model of intraluminal thrombus in FEA of aortic aneurysm

S. Polzer[1] and J. Bursa[1]

[1] Institute of Solid Mechanics, Mechatronics and Biomechanics, Brno University of Technology, Brno, Czech Republic

Abstract— **The influence of the intraluminal thrombus (ILT) on the biomechanics of the abdominal aortic aneurysm (AAA) has been investigated for several years both numerically and experimentally. The FE analyses published till now simplified the material of the ILT as a homogenous continuum, but there is a contradiction between experiments and FE results. Therefore we use a poroelastic constitutive model for ILT. Poroelastic behaviour of the used finite element is based on the Biot theory of consolidation, the model consists of fluid and solid parts.**

By using idealized AAA models, we showed that the pressure decrease through the ILT is small for an 18mm thick ILT. Therefore approx. 90% of the blood pressure is acting on the inner AAA wall surface. These results agree very well with all experimental results, which show either slight or no pressure reduction. The wall stresses calculated by our approach are almost the same as those obtained by using the homogenous material model for ILT.

Remarkably the model with poroelastic thrombus loaded by the blood pressure on the luminal surface of the ILT gives the same results as the model with homogeneous thrombus loaded on the inner surface of the AAA wall. These results support the theory that the stress reduction by ILT is caused by the adherent fibers, which serve as load bearing ropes stretched between different points on the arterial wall and consequently reduce the wall stress although the pressure is allowed to penetrate through without a substantial reduction.

Keywords— **Abdominal aortic aneurysm, intraluminal thrombus, poroelasticity, finite element model.**

Introduction

The role of the intra luminal thrombus (ILT) in the mechanical properties of the abdominal aortic aneurysm (AAA) has been investigated for several years and it has not been still cleared out. It has been shown that the presence of the ILT blocks the transport of the oxygen into the arterial wall which leads to AAA wall weakening, while the strength of the AAA tissue behind the ILT is reduced as well[6,7,8]. However, there is no agreement whether the presence of the ILT reduces wall stresses. Experimental study in vivo[2] showed no pressure reduction and the authors concluded therefore the wall stress is not reduced as well. Experimental study in vitro[10] showed little pressure reduction behind the ILT. Thubrikar et al.[11] confirmed this observation in their ex-vivo experimental study. Additionally, they observed the ILT reduces deformation and concluded therefore the presence of the ILT reduces wall stress as well.

On the other hand, the results of numerical simulations performed by means of the finite element method (FEM)[1] supports the hypothesis the ILT reduces the wall stress. However, these numerical studies as well as those dealing with fluid structure interaction model the ILT as a homogeneous solid, although ILT is a highly porous material; its average porosity is about 80%[3]. Every mechanical response of such tissue consists of two components: fluid phase and solid phase responses. Such a material behavior is called poroelasticity and the response can be solved by Biot's theory of consolidation[13]. We have decided to perform the FE analysis of the AAA with using the poroelastic material model for the ILT in order to be able to describe the pressure transition through the ILT as well as the mechanical stress response of the solid phase of the ILT and, consequently, the stress response in the AAA wall.

Methods

We used the FE software ANSYS 12.0.1, which contains poroelastic elements based on the Biot's theory, although only linear elastic properties of the solid phase of the poroelastic material can be included currently. However this will not decrease the accuracy of the results

in our case, because the ILT behaves almost linearly under both uniaxial[9] and biaxial states of load[4]. The large strains algorithm can be included without any problems.

The governing equations for Biot consolidation problem are:

$$\nabla \cdot (\sigma' - \alpha p I) + f = 0$$
$$\alpha \cdot \varepsilon_V^e + \frac{1}{K_m} \cdot p + \nabla \cdot q = s$$

where ∇ is divergence operator, σ' is Biot effective stress tensor, $\alpha = 1$ is Biot coefficient, p is pore pressure, I is second order identity tensor, f is body force of the porous media, ε_V^e is elastic volumetric strain of the solid skeleton, $K_m = K_f / \Phi$ is Biot modulus, $K_f = 3300$ MPa[3] is the fluid phase bulk modulus, $\Phi = 80\%$ is the porosity, q = flow flux vector, s is flow source.

The relationship between the Biot effective stress and the elastic strain of the solid skeleton is given by:

$$\sigma' = D : \varepsilon^e$$

where ε^e is the second order elastic strain tensor and D is the fourth order elasticity tensor.

The relations between the fluid flow flux and the pore pressure are described by Darcy's law:

$$q = -k \nabla p$$

where k is the second order permeability tensor (value used here $k = 10^{-12}$ m^4/Ns[7]) and ∇ is the gradient operator.

The solid phase of the ILT is modeled as linear elastic with Young's modulus E = 50000 Pa and Poisson's ratio $\mu = 0.4999$. For the AAA wall, we used a model of homogenous isotropic hyperelastic material proposed by Raghavan[5].

Idealized 2D model

To understand the principles of the poroelasticity at soft tissues, we created a simple 2D (axisymmetric with respect to Y axis) model shown in Fig 1. The deformation of the model in Y direction is constrained and there is a bonded contact between the ILT and the wall.

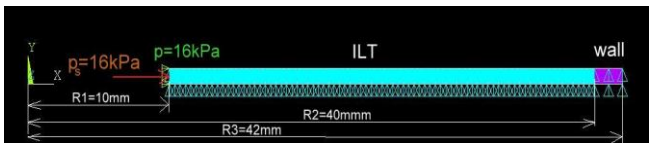

Fig. 1 Scheme of the 2D model of AAA

We simulated the blood pressure increase in the lumen by increasing both the pore pressure p and the pressure p_s on the solid phase of the ILT in the same manner. The load was linearly increasing from zero up to the peak value of 16kPa during 0.1s and then kept constant for 50s to simulate the transient process. The determination of the time necessary to achieve the equilibrium state should enlighten the importance of the transition process during a cardiac cycle.

The discretization of the model is not as important as the length of the time step. According to our experience, 80 elements across the ILT give reliable results; it was however necessary to divide the time of 0.1s

into at least 180 time steps, when there was a change in the loads. Otherwise the results were misleading due to the cumulation of numerical residuum.

Idealized 3D model of AAA

We built a 3D model of an idealized AAA as shown in Fig 2, with the maximal diameter of 60mm and the maximal thickness of the ILT of 18mm. Although axisymmetric, it approximates the AAA shape much better.

In the simulation, the load was changing as follows:

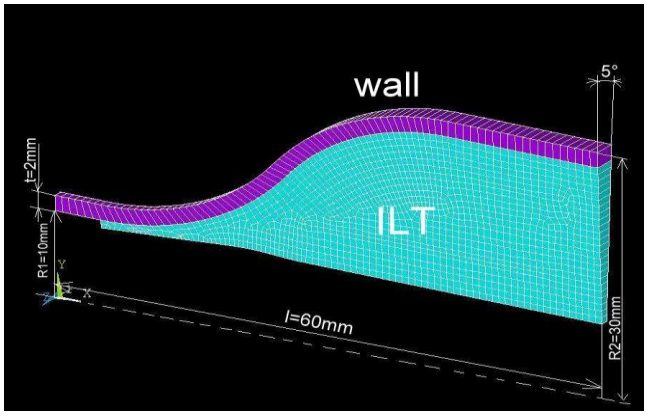

Fig. 2 Dimensions of the 3D model of AAA with max. diameter of 60mm

1. Between the times t=0 and t=1s, there is a linear increase of loads from their original zero values up to 16kPa. The pore pressure (defined as a BC) is increasing simultaneously in the whole volume of the ILT.
2. Between the times t=1s and t=1.2s, there is a linear decrease of both pore pressure and solid phase pressure down to the value of 13kPa.
3. Between the times t=1.2s and t=1.9s there is a linear decrease of both pressures down to 10kPa.
4. Between the times t=1.9s and t=2.0s there is a linear increase of both pressures up to 16kPa.
5. A loop consisting of steps 2,3 and 4 is repeated 5 times with time increasing up to the final value of 6s.

According to our experience, the dynamic balance is achieved fastest when the simulation starts from the systolic pressure; therefore we set the pore pressure to be 16kPa in the first load step. Then this BC was removed and several cardiac cycles were simulated in order to achieve the dynamic balance in the ILT.

This model was also used to compare the results obtained by using the poroelastic material model for the ILT with the analysis where the ILT is considered to be a homogenous solid. So two other FEAs with a homogenous solid ILT were performed as well, the former with the pressure applied on the luminal side of the ILT (where this exists) and the latter, in which the pressure was applied on the inner wall surface under the ILT. Comparison of these analyses will explore the necessity of including poroelastic material model to achieve correct results.

Of note we also tried to perform a FEA with the poroelastic material for a patient specific model of the AAA. However, we were not able to do that due to extreme computational demands. We used a 4 CPU computer with 12GB of RAM and hard disks set up into the RAID 0 field and

it took about 12 hours to simulate 5 cardiac cycles even for the simplified symmetric 3D model described above.

Results

Idealized 2D model

The results of this model demonstrate the transition process in the ILT. In the time t=1s, the pore pressure distribution across the ILT is decreasing from the maximum value of 16 kPa at the luminal surface to the value of approx. 9.2 kPa at the ILT-wall interface. Concerning the time dependence of these values, it takes about 20s for the pore pressure to achieve the even distribution across the 30mm thick ILT; the stress in the solid phase remains constant since the load has reached its final value, i.e. after 1 second.

Idealized 3D model

The pore pressure distribution in the systolic phase is shown in Fig 3. It has been captured in the last simulated cardiac cycle when the dynamic balance is believed to be achieved. It means the distribution of the pore pressure in the particular phase of the cardiac cycle does not change between cycles any more. We would like to point out the maximum of the pore pressure is not located at the luminal surface of the ILT but its location corresponds to the area where the ruptures of the ILT occurred[12]. The pore pressure reduction varies from 0% in the area of the maximal diameter to a maximum of 10% in the transition area.

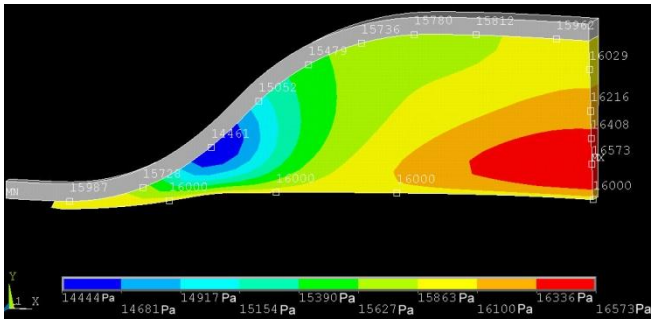

Fig. 3. Pore pressure distribution across the ILT in the systolic phase when the dynamic balance has been achieved

Stresses obtained from different FEAs are shown in Fig 5. The result A was obtained with considering homogenous solid material model for the ILT and the pressure was applied on the luminal surface of the ILT (where existing). To obtain the result B, we applied the pressure on the inner surface of the AAA wall (under the ILT). The result C was obtained by using the poroelastic material model of the ILT and the

pressure was applied in the same way as in the case A.

For all the three cases the distribution of von Mises stress as well as its peak value were virtually the same (with max. deviation of 80Pa). To demonstrate the stress reduction caused by the presence of the ILT one can compare the results in Fig 5 with the case where the ILT was not included (Fig 4). The peak stress reduction is about 55%.

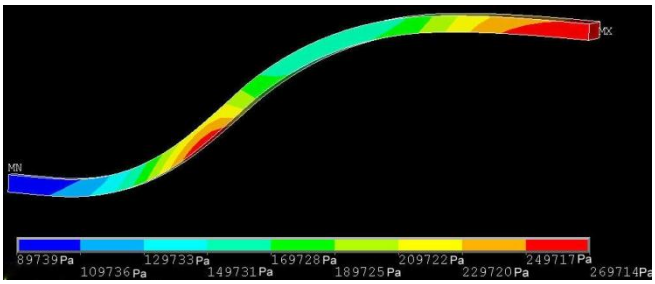

Fig. 4 Von Mises stress distribution when the ILT is not included

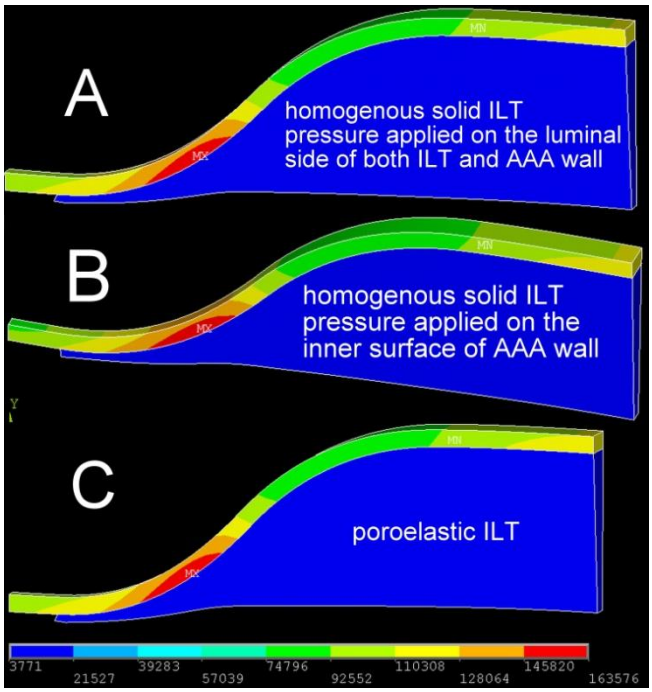

Fig. 5 Von Mises stress distribution for different material models of the ILT and different ways of the pressure application

Discussion

There are some limitations one should keep in mind when interpreting the results. We assumed Biot coefficient and the permeability to be constant because of lack of experimental results. However such a set up caused the pore pressure response to be as high as 13kPa during the diastolic phase, what is in contradiction with observations of Schurink et al.[2] and Hinnen et al.[10].

Further, we increase the load evenly in the whole AAA, while the pressure wave propagates from the proximal AAA end in fact. Then the peak pore pressure is expected to be highly localized and its value in the rest of the ILT should decrease.

We used the simple 2D model to demonstrate the length of the transition process in the ILT.

When the 30mm thick ILT is loaded by a pressure, it takes about 20s for pore pressure to reach an even distribution across the ILT. Therefore it is necessary to simulate more cardiac cycles to reach the dynamic balance. In our 3D idealized model 5 cardiac cycles were enough due to the lower ILT thickness (18mm only). Under conditions of the dynamic balance, the pore pressure was slightly reduced by the presence of the ILT. This is in good agreement with the observations made by Schurink et. al[2] who reported no pressure reduction under the ILT. Fig 3 shows very clearly that the pressure value measured under the ILT depends on the position where the measuring is performed. We also expect its dependence on the geometry of the AAA.

The FEA performed with the 3D model illustrated the wall stress is substantially reduced by comprehending the ILT in the model. However, the type of its constitutive model is not very important; the comparison in Fig 5 shows negligible differences among the individual results with poroelastic or hyperelastic models of ILT. Therefore it is not necessary to use the poroelastic material model of ILT in the analysis as long as one is not interested in the distribution of the pore pressure and cares only about the wall stress. In addition, the FEA can be performed with the pressure applied on the inner surface of the AAA wall instead on the luminal side of the ILT and the wall stress values will not be influenced as well. This can make the calculations easier and faster, because generally finite elements are more stable when loaded by tension than by compression.

Conclusions

In this study we performed the FEA of the idealized AAA model with considering the poroelasticity of the ILT. The pore pressure at the systolic phase of the cardiac cycle obtained from this analysis correlates very well with the in-vivo experiments[2]. The comparison of the wall stresses between this analysis and the analysis where ILT is excluded shows the wall stress is reduced by presence of the ILT, which is in agreement with other studies having investigated this phenomenon numerically[1].

We also showed the poroelasticity of the ILT can be neglected when the wall stress distribution is required. We achieved the same stress distribution for all the investigated cases: when the ILT is considered poroelastic and the pressure is applied on the luminal side of the AAA, or the ILT is considered a homogenous solid and the pressure is applied on the luminal surface of the AAA, as well as when the ILT is considered a homogenous solid and the pressure is applied on the inner side of the aneurysm wall below the ILT.

Acknowledgment

This work was supported by grant project of GA CR No. 106/09/1732 and by faculty project FSI-J-11-3. The author receives “scholarship for talented Ph.D. students” financed by Brno city municipality.

REFERENCES

1. Wang D H J, Makaroun S M, Webster M W, Vorp D A (2002) Effect of intraluminal thrombus on wall stress in patient-specific models of abdominal aortic aneurysm. J Vasc Surg 36: 598-604
2. Schurink G W et al. (2001) Thrombus within an aortic aneurysm does not reduce pressure on the aneurysmal wall. J Vasc Surg 21: 501-506.
3. Ashton J H, Vande Geest J P et al. (2009) Compressive mechanical properties of the intraluminal thrombus in abdominal aortic aneurysms and fibrin-based thrombus mimics. J Biomechanics 42:197-201.
4. Vande Geest J P, Sacks M S, Vorp D A (2006) A planar biaxial constitutive relation for the luminal layer of intra-luminal thrombus in abdominal aortic aneurysms, J Biomechanics 39: 2347-2354.
5. Raghavan M L, Vorp D A (2000) Toward a biomechanical tool to eva-luate rupture potential of abdominal aortic aneurysm: identification of a finite strain constitutive model and evaluation of its applicability. J Biomechanics 33: 475-482.
6. Kazi M, Thyberg J (2003) Influence of intraluminal trombus on structural and cellular composition of AAA wall. J Vasc Surg 38: 1283-1292.
7. Randall A, Vorp D A (1997) Cellular content and permeability of intraluminal trombus in abdominal aortic aneurysm. J Vasc Surg 25: 916-926.
8. Vorp D A, Lee P C, Wang D H J, Makaroun M S et al. (2001) Association of intraluminal thrombus in abdominal aortic aneurysm with local hypoxia and wall weakening. J Vasc Surg 34: 291-299.
9. Gasser T C (2008) Failure properties of intraluminal thrombus in abdominal aortic aneurysm under static and pulsating mechanical loads. J Vasc Surg 48: 179-188.
10. Hinnen W (2005) Effect of intraluminal thrombus on pressure transmission in the abdominal aortic aneurysm. J Vasc Surg 42: 1176-1182.
11. Thubrikar M J (2003) Effect of thrombus on abdominal aortic aneurysm wall dilatation and stress. J Cardiovasc Surg 44: 67-77.
12. Roy J Labruto F, Beckman M O, Danielson J et al. (2008) Bleeding into the intraluminal thrombus in abdominal aortic aneurysms is associated with rupture. J Vasc Surg 48: 1108-1113.

Detournay E, Cheng A H D (1993) Fundamentals of poroelasticity, Pergamon Press, Oxford, pp. 113

Appendix C: Poroelastic model of ILT in FEA of AAA

12.4 Appendix D

Simulation of residual stresses (strains) in arteries

Original research article presented on 5th European conference of IFMBI 14th to 18th of September 2011 in Budapest.

Simulation of residual stresses (strains) in arteries

S. Polzer[1] and J. Bursa [1]

[1] Brno University of Technology, Institute of Solid Mechanics, Mechatronics and Biomechanics, Technicka 2, Brno, Czech Republic

Abstract— **Residual stresses and strains contribute substantially to stress-strain states in arteries. They manifest themselves by opening of the artery after having been cut longitudinally and can be quantified by means of the opening angle of a ring cut out of the artery and cut longitudinally afterwards. The magnitude of the opening angle changes with species, age of the individual, artery location, etc. Although the magnitude of these stresses appears slight, they can influence the stress (and strain) distribution in the arterial wall substantially by reducing the extreme values throughout the wall. Their surprisingly high influence on the resulting stresses is given by the non-linear stress-strain characteristics of vascular wall. When applied to the blood pressure, the uniform stress and uniform strain hypotheses have been formulated to explain this phenomenon. The usual way of their modeling is based on using a model with the geometry of the opened arterial ring; the residual stresses are then induced in the model by closing it into the original approximately circular shape. This method, however, is not applicable for more complex non-symmetric arterial geometries. Because the induced strains depend on local bending stiffness. Therefore another approach is used in the paper, based on introducing an interference between two layers of aorta represented in the model. The method is demonstrated with a circular ring used typically in experimental assessment of residual strains and results of both methods are compared. In addition, the proposed interference method is numerically more stable, because of the two orders lower displacements, and it is able to induce constant strains throughout all the wall thickness by using more than two layers in the arterial wall model, .**

Keywords— **Residual stress, interference method, two-layer model, opening angle,.**

INTRODUCTION

Residual stresses are present in any artery[11] as a result of presence of smooth muscle cells (SMC´s) which work actively to preserve homeostatic conditions in its surround. It means that each SMC tries to be loaded by the same amount of strains.

Cutting an artery longitudinally is the most visible proof of presence of residual stresses and strains in it. Any artery will open after being cut in order to relax residual stresses. Much work has been done to incorporate these stresses into numerical models of arteries. There are two main approaches how to simulate residual stresses. First approach is based on decomposition of deformation gradient tensor into part related to residual stresses and part related to pressure loading[8,9]. This approach however needs to redefine FE algorithm, which is not possible in most of commercially available FE software. The second is based on the closing of the opened artery[1,7,10] when the geometry of the opened artery is assumed to be stress free and then it is closed. The inner part of artery has to compress while outer part of it is stretched which results in stress distribution as shown on Fig. 4. When such a closed artery is pressurized, residual stresses may almost remove the stress gradient across the wall thickness which follows uniform stress (strain) theory[6]. However application of this approach for a non idealized geometry is very limited because it will generate residual stresses primarily in more compliant (thinner) regions of the opened artery. This results in very nonhomogenous distribution of residual stresses along the tangential coordinate which violates the uniform strain hypothesis. Second problem is numerical. Closing of an opened artery requires moving ends of the artery by tens of millimeters which is very hard to ensure numerically and therefore this approach is not very suitable to incorporate residual stresses into patient-specific artery geometries.

Therefore we propose a new method how to incorporate residual stresses into arteries. It is based on the interference of layers existing in the arterial wall.

METHODS

The opening angle of an arterial segment (see fig. 1) was defined in [1] as a parameter to quantify the residual strains; it ranges from slightly negative values up to 160° or sometimes even more than 180°..For its given value, the residual stresses (available by calculation only) are dependent on the constitutive model used in the calculation. For a cylindrical model of the artery, the straightforward approach described above (called **opened model method** below) can be used; it is based on inducing the residual stresses (on the order of 10^0 kPa [2][5]) in the ring by its closing from the opened initial state (see fig.1), which is assumed to be stress-free.

Unfortunately, the above straightforward approach is not applicable for AAAs; it is not possible to create an opened (stress-free) patient-specific 3D geometry. Therefore we applied another approach (called **interference method** below), taking advantage of the two-layer AAA wall used in the model. The layers represent media and adventitia as the most significant layers of the wall with different constitutive parameters. This arrangement makes it possible to introduce a certain interference to the boundary between the layers.

This interference induces positive (tensile) stresses in the outer layer and negative (compressive) stresses in the inner one (see fig. 4). In this way the maximum stress at the inner wall surface is reduced, while the minimum stress at the outer surface increases; the effect is enhanced by the nonlinear material characteristics of the layers. Consequently, a stress distribution with a much lower non-uniformity (maximum to minimum circumferential stress ratio) can be obtained similarly to the classical approach.

For a known value of the opening angle, the interference between the layers was set to the value giving this opened shape when longitudinal cut is simulated (see fig. 1), If the same interference value is used in a closed (semi-circular) model, the residual stresses are induced in both layers. Then the inner pressure corresponding to mean arterial pressure (13 kPa=100 mm Hg) is applied .

Both methods have been compared for a cylindrical arterial ring with the inner diameter of 10 mm and wall thickness of 1,4 mm. The wall was created of two layers with the same thickness and different material properties, corresponding to media and adventitia. We used material model proposed by 3rd order Yeoh for both layers. Constants of this model were fit on the basis of equibiaxial tests of porcine aortas. For the media we used the following values: c_{10}=15,8kPa, c_{20}=13,5kPa, c_{30}=3,5kPa, the adventitia was best approximated by constants: c_{10}=32,2kPa, c_{20}=-18kPa, c_{30}=23,8kPa. The interference magnitude was set to obtain the lowest possible strain gradient when loaded by pressure of 13kPa =100 mm Hg.

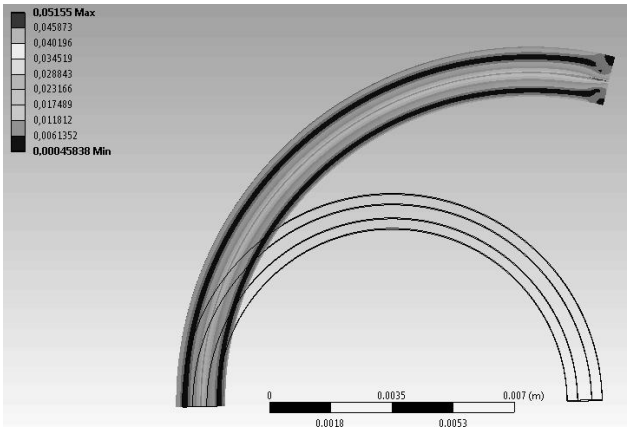

Fig. 1 Von Mises strain in the opened arterial ring (opening angle 75°) for interference method.

RESULTS

Both cases reach convergence although it took 3 times longer for model based on opened model method to converge due to numerical instabilities. Fig 1 and Fig 4 nicely demonstrate that opened state is not stress free when interference method model is used. Fig. 2 shows the circumferential Cauchy stress distribution in the model without any residual stresses, while the distribution in a model with residual stresses induced by the interference method is presented in fig. 3.

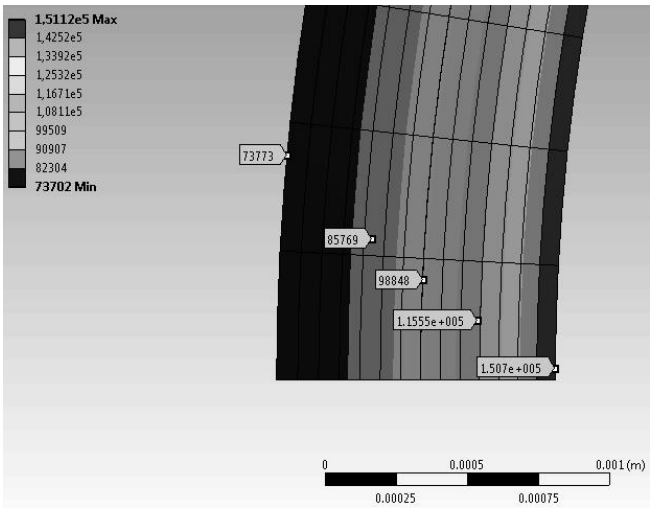

Fig. 2 Circumferential stress distribution [Pa] throughout the wall without residual stresses

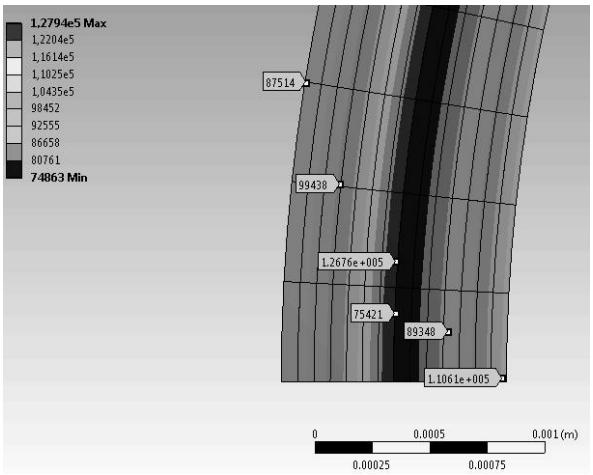

Fig. 3 Circumferential stress distribution [Pa] throughout the wall with residual stresses (interference method)

Fig. 4 presents a comparison of the residual stress distributions (in circumferential direction) calculated using different models; Curve A was obtained by the interference method for the closed artery , while curve B was calculated using the classical opened model method under the same conditions. Curve C represents residual stresses calculated by interference method in the opened state, when other approaches must give zero stresses.

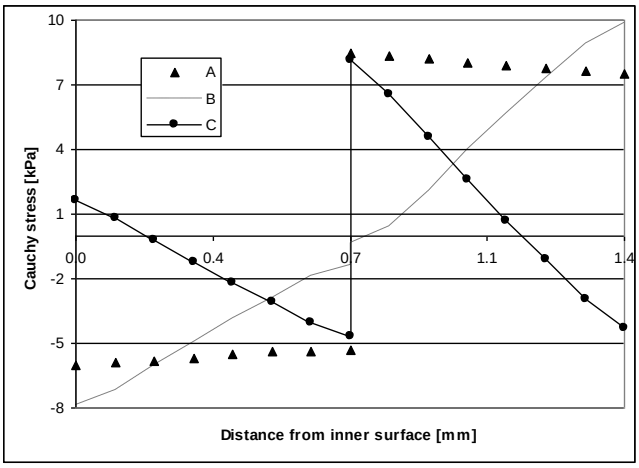

Fig. 4 Residual tangential stress [kPa] distribution in various models and distribution of tangential stress when interference model is opened (C)

If these models are loaded additionally by the inner pressure of 13 kPa (100 mm Hg), the maximum circumferential stress is reduced from 151 kPa to 107 kPa using the opened model method, while the interference method gives the value of 112kPa at the inner arterial wall and 127 kPa at the boundary of layers

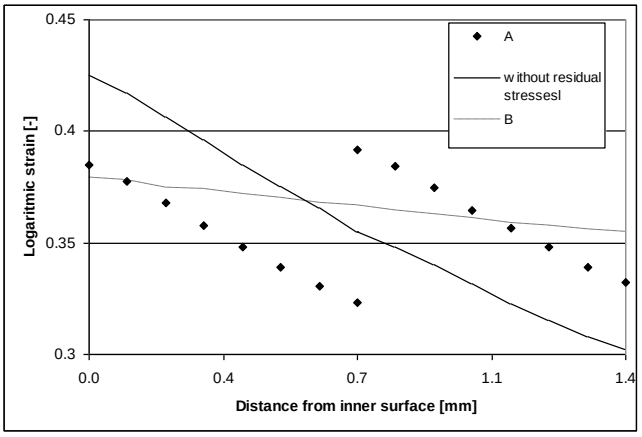

Fig. 5 Circumferential strain distribution in the wall when loaded by pressure of 13kPa

. The maximum stresses are reduced substantially by means of residual stresses and similarly the minimum stresses increase, and consequently the stress gradient in the wall is reduced substantially. Fig. 5 presents strain distribution for these models, which shows the same basic features.

. DISCUSSION

With linear elastic materials the stress gradient throughout the wall is relatively small if its relative thickness (i.e. the thickness to radius ratio) is not very high (typical range for blood vessels lies between 0,1 and 0,5). However, the nonlinear material behaviour enhances the stress gradient in the wall substantially and, consequently, the ratio of maximum and minimum of the individual stress components as well; this ratio can reach the value higher than 2 for circumferential stress component (see fig.2). Accounting for the residual stresses and strains can reduce this ratio to values close to 1, it means to make the stress (or strain) distribution throughout the wall nearly uniform. Accordingly two similar hypotheses were formulated for the role of residual stresses and strains in the arterial wall: the uniform stress hypothesis and uniform strain hypothesis [6]. They assume that the stress (strain) distribution throughout the arterial wall is approximately uniform under certain loading conditions (mean blood pressure). Biological considerations support rather the assumption of uniform strain.

The reduction of the maximum circumferential strains is substantial in both of the methods used here (see fig. 5); the stress and strain distributions calculated by both methods are much more uniform than without taking the residual stresses into account. Naturally they are some principled differences between both methods. Bending of the arterial ring from its opened geometry into the closed (circular) one in the opened model method induces residual stress distribution having its extreme values at both outer and inner surfaces (see fig. 4) and theoretically it achieves a nearly uniform strain distribution when loaded by mean pressure (see fig. 5). On the contrary, the residual stresses calculated using the interference method show a different distribution (see fig. 4) having its extreme values at the interface between both layers. This difference is given by differences in the principle of both methods. Consequently, the opened model method cannot show any residual stresses in the opened shape created as stress-free, while in the interference method the strains (and stresses as well) near the layer interface do not relax even in the opened shape (see fig. 1 and fig. 4). According to us it reflects the reality more appropriately since it has been shown that media and adventitia have different opening angles when separated so it is obvious it has to be some residual stress in opened wall when they stick together[12]. Therefore proposed interference method has a potential of better simulation of stress distribution. The quality of the stress distribution can be further improved by dividing the vessel wall into more layers than only two used in this example. The division used here was made on the basis of different material properties of media and adventitia, but in fact the arterial wall consists of many thin sublayers. The interference method enables us to divide each main layer into any number of sublayers with identical material properties and to achieve a more uniform distribution of stresses and strains in the wall by setting some partial interference value in all the interfaces between these sublayers..

Another advantage of the proposed method is that it is numerically stable due to the fact that the displacements

prescribed for the initial geometry are on the order of tenths of millimeter which is roughly two orders lower compared to the opened model method. Due to this advantage it is very suitable to apply the new method when incorporating residual strains into a general non-symmetric geometry, The method makes it possible to induce constant strains (or stresses) even in complex geometries, e.g. of bifurcations or abdominal aortic aneurysms, In this application the geometry reconstructed from CT scans can be divided into two or more layers which overlap each other to create a chosen interference in order to take the residual stresses into account.

CONCLUSIONS

The paper presents a new method of how to take residual stresses into account. Its main advantage is that it is numerically stable due to the two orders lower values of displacements prescribed in the simulation of residuals stresses compared to the opened model method. Due to this advantage it is very suitable for applications with general geometries, e.g. for abdominal aortic aneurysms. It can provide similar opening angles like classical methods and stress-strain states closer to reality, because it avoids the (generally incorrect) assumption of the stress free state in the longitudinally cut arterial ring, which is fundamental for the classical opened model method.

ACKNOWLEDGMENT

This work was supported by grant project of GA CR No. 106/09/1732. The co-author receives “scholarship for talented Ph.D. students” financed by Brno city municipality.

REFERENCES

1. Liu SQ, Fung YC (1988) Zero-Stress States of Arteries. J Biomech Eng 110:82-84
2. Vaishnav RN, Vossoughi J (1983) Estimation of residual strains in aortic segments. In Biomedical Engineering II, Recent Developments, 330-333, Pergamon Press, Oxford
3. Vaishnav RN, Vossoughi J (1987) Residual stress and strain in aortic segments. J Biomech.20:.235-239
4. Chuong CJ, Fung YC (1986) On Residual Stresses in Arteries. J Biomech Eng.108: 189-192
5. Chuong CJ, Fung YC (1986) Residual stress in arteries. In: Frontiers in Biomechanics, Springer, New York
6. Takamizawa K., Hayashi K. (1987) Strain energy density function and uniform strain hypothesis for arterial mechanics. J Biomech 20: 7-17
7. Balzani, D., Schroder J., Gross D. (2007) Numerical simulation of residual stresses in arterial walls. Comp mat science 39: 117-123
8. Bustamante R., Holzapfel G.A. (2010) Methods to compute 3D residual stress distributions in hyperelastic tubes with application to arterial walls. Int. J. Eng Science 48:1066-1082
9. Martinez M.A., Alastrue V., Doblare M. (2008) On the modeling of volumetric growth in patient-specific arteries incorporating residual stresses. J biomech 41:S1
10. Delfino A., Stergiopulos N., Moore J.E., Meister J.-J.,(1997) Residual strain effect on the stress field in a thick wall finite element model of the human carotid bifurcation. J biomech. 30 (8): 777-786
11. Matsumoto T., Goto T., Furukawa T., Sato M., (2004): Residual stress and strain in the lamellar unit of the porcine aorta: experiment and analysis. J Biomech 37: 807-815
12. Holzapfel G.A.,Sommer G., Auer M., Ogden R.W. (2007) Layer specific 3D residual deformations of human aortas with non-atherosclerotic intimal thickening. An. Biomed Eng. 35:530-545

Author: Jiri Bursa
Institute: Brno University of Technology, Institute of Solid Mechanics, Mechatronics and Biomechanics
Street: Technicka 2
City: Brno
Country: Czech Republic
Email: bursa@fme.vutbr.cz

12.5 Appendix E

FEA of prestressed abdominal aortic aneurysm

A poster presentation on Conference Human Biomechanics 2010 4th-6th of October 2010 in Sychrov

FEA of prestressed abdominal aortic aneurysm

Stanislav Polzer and Jiří Burša

Institute of Solid Mechanics, Brno University of Technology, Brno, Czech Republic, Technická 2, 61669 Brno, CZ; email: polzer@seznam.cz

Abstract

Stress distribution in the abdominal aortic aneurysm (AAA) is about to replace the criterion of the maximum AAA diameter for planning the surgery. The geometry for such FEA is obtained from CT images, where the AAA is shown when loaded by a blood pressure. However, FEA needs a load free geometry as an input. The stress distribution obtained by using the unloaded geometry is more realistic than results obtained by FEA where geometry from the CT is considered to be load free. Several different approaches of how to obtain the unloaded geometry has been published over last years. However, they require to define a new element or even to redefine the FE algorithm itself. We present a simpler algorithm but its major advantage is the use of a commercially available software; it can find the load free geometry of AAAs by using standard elements and regular FE algorithm

Keywords: aortic aneurysm; rupture risk; unloaded geometry; computer tomography

Introduction

Prestressing represents a factor with substantial impact on the wall stresses is the AAA. The patient-specific geometry is reconstructed mostly from the set of images from the CT (Maier et al 2009). However, this geometry is already loaded by a blood pressure and a FEA needs a stress free geometry as an input. We have created a new algorithm based on the backward incremental method (Putter et al 2007), which is able to work with commercially available FE software packages.

Methods

We reconstructed a patient-specific geometry of a real large AAA (max. diameter over 90mm) on the basis of its CT scans.

To reconstruct the 3D geometry of the AAA, we used the commercially available software A4research from the Vascops company. The constant wall thickness was considered 1.8mm in this study.

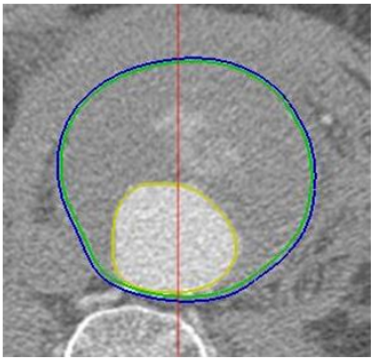

Figure 1 The CT scan of AAA with highlighted reconstructed geometry of it.

We built the FE model of the AAA in ANSYS, loaded by the blood pressure of 16kPa and using the hyperelastic isotropic material model (Raghavan 1996). Tetragonal quadratic 10 nodes elements have been used due to the complex geometry.

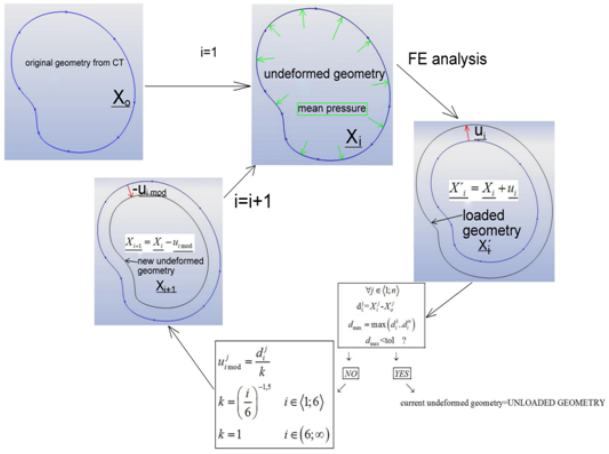

Figure 2: Scheme of the proposed algorithm

The principle of the backward incremental algorithm has been described in (Putter et al 2007). However, we used our own algorithm presented in fig. 2 and described below:

1. The original geometry (defined by the matrix of node positions) becomes the undeformed geometry. The iteration number is set to i=1.
2. The undeformed geometry is loaded by the *mean* pressure and FEA is performed and the deformation displacements of all nodes are calculated.
3. The deformed positions of nodes and the differences between the deformed and original positions of nodes are computed. If the maximal deviation between these two geometries is smaller than a chosen toleration (or starts to increase again), the algorithm is stopped and the current undeformed geometry represents the final solution of the unloaded geometry, otherwise it continues by step 4.
4. The differences between geometries are divided by certain number. This number varies according to following rule: $k = \left(\frac{i}{6}\right)^{-1,5}$ $i \in \langle 1;6 \rangle$; $k = 1$ $i \in (6;\infty)$
5. The modified differences are subtracted from the position of each node in the undeformed configuration. In this way a new undeformed geometry is obtained and the algorithm continues by step 2.

Results

The algorithm stopped in convergence in the 6th iteration. We also performed a FEA for the original CT scanned geometry of the AAA to compare the influence of the prestressing on the deformation and stress distribution in the AAA. The comparison can be seen in fig. 3, which shows different stress distributions in both cases although the magnitude of the extreme stresses is pretty much the same.

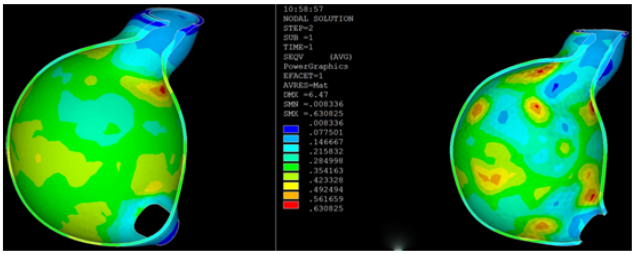

Figure 3: Von Mises stress [MPa] distribution of the AAA when loaded by the systolic pressure of 16kPa. Left: without prestressing; right: with prestressing

Discussion

The application of the prestress algorithm changed the wall stress distribution substantially, as shown in Figure 3. The stress is not distributed so regularly, many areas can be found where the stress increased significantly. More importantly, such a stress increase occurs in the areas which are under a thick ILT. Its presence decreases both the wall thickness and its strength (Vorp et al 2001). Therefore the stress increase in this area can increase the rupture risk factor substantially and the predicted danger of rupture is higher when prestressing is included, even if the maximum stress remains the same in magnitude.

Described algorithm is particularly suitable when geometry is transferred between different software (e.g. for FSI analyses) because it provides the actual unload geometry which can be loaded in any FE software in order to obtain the original CT geometry.

Acknowledgements

This work was supported by grant project of GA CR No. 106/09/1732 and faculty project FSI-J-11-3. Author is supported by "scholarship for talented Ph.D. student" by the city of Brno.

References

Fillinger MFet al. In vivo analysis of mechanical wall stress and abdominal aortic aneurysm rupture risk. J Vasc Surg (2002) 36(3) pp.589-597.

Maier A., et al. Mnichov 2009 Impact of Model Complexity on Patient Specific Wall Stress Analyses of Abdominal aortic aneurysm.

Nichols S.C., et al.. Rupture in small abdominal aortic aneurysm. J Vasc Surg (1998) 5 pp.884-888.

Putter, S, et al.. Patient-specific initial wall stress in abdominal aortic aneurysms with a backward incremental method Journal of Biomechanics (2007) 40 pp.1081–1090.

Raghavan, et al. Ex vivo biomechanical behavior of abdominal aortic aneurysm: assessment using a new mathematical model. Annals of biomedical engineering (1996) 34 pp.573-582.

Vande Geest The effects of aneurysm on the biaxial mechanical behavior of human abdominal aorta journal of biomechanics 39 (2006) 1324-1334

Vorp DA, Lee PC, Wang DH, Makaroun MS, Nemoto EM, Ogawa S, et al. Association of intraluminal thrombus in abdominal aortic aneurysm with local hypoxia and wall weakening. J Vasc Surg 2001;34:291-29

12.6 Appendix F

Branch arteries as stress concentrators in abdominal aortic aneurysms

Poster was presented on the 5th international symposium on Biomechanics in Vascular Biology and Cardiovascular Disease 14th to 16th of April 2011 in Rotterdam.

INVESTMENTS IN EDUCATION DEVELOPMENT

Branch arteries as stress concentrators in abdominal aortic aneurysms

Stanislav Polzer[1], Jiri Bursa[1], Robert Staffa[2], Robert Vlachovsky[2]

[1]Department of Solid Mechanics, Brno University of Technology, Brno, Czech Republic; [2]2nd Department of Surgery, St. Anne's University Hospital, and Faculty of Medicine, Masaryk University, Brno, Czech Republic

Introduction

Stress in an abdominal aortic aneurysm (AAA) has been shown to predict its rupture more accurately than the criterion of the maximal aortic diameter[1]. However there are still some limitations of such approach. For instance, it has been shown that a realistic AAA geometry is crucial to calculate stress accurately. Although a global patient-specific geometry of an aneurysmal sac is commonly reconstructed from computed tomography (CT) images, branch arteries such as six lumbar arteries and the inferior mesenteric artery (IMA) are generally excluded from the reconstruction. Consequences of its omitting are not discussed in literature, therefore its role in AAA rupture remains unclear.

Branch arteries (BA) could influence the stress and strength in AAA in several ways. From the mechanical point of view, any hole in the arterial wall causes a stress concentration simply by its presence. Also, if the artery is still filled by blood, a formation of intraluminal thrombus (ILT) is therefore prevented in a very small area which can behave just as ILT fissure which is another source of stress concentration[5]. On the other hand, structure of tissue in the area of origin of such artery is reinforced by collagen fibers which increases a strength of aortic wall[4].

Motivated by lack of information in literature, we have decided to investigate how much the stress would increase when branch arteries are included into the AAA geometry.

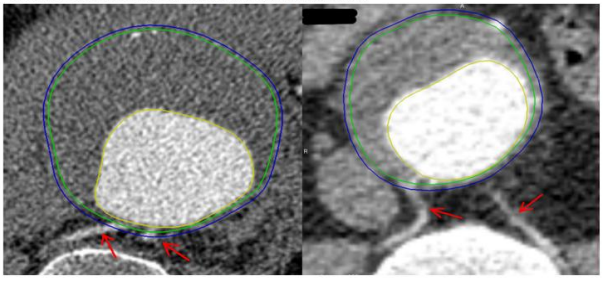

Figure 1 The CT scans of two of reconstructed AAAs in A4Research program. Red arrows indicates lumbar arteries. Outer surface is marked by blue line, wall-ILT interface by green line and lumen by yellow line.

Methods

Patient specific geometries of 5 patients were created using commercially available software A4Research (Vascops Gmbh). BA were not reconstructed in order to obtain a reference geometry (and therefore reference stress field) for each patient. Reconstruction algorithm includes wall thickness determination procedure which decreases wall thickness from its initial value of 1,8mm down up to 1mm according to the thickness of underlying ILT. Each geometry was then modified by adding branch arteries into it. Position and orientation of each artery was determined according to CT images. Lumbar arteries were modelled as tubes with diameter of 2mm, while diameter of IMA was measured from CT scans. Transition between aortic wall and branch artery was rounded by a radius of 1mm. Exact shape of transition area cannot be reconstructed from CT images due to their relatively low resolution. One AAA was reconstructed with part of aneurysmal aorta s well and BA were created there to have some referential configuration for investigation of presence of AAA on stress in the area of origin of BA.

A hyperelastic isotropic constitutive model with the strain energy $\psi=a_1(I_1-3)+a_2(I_1-3)^2$, with material parameters fitted by Raghavan et al[2]. $a_1=174$ kPa and $a_2=1881$ kPa was used for the aortic wall. A linear elastic constitutive model for an intraluminal thrombus (ILT) was used. The Young's moduli varied from 63.0 kPa in the luminal layer to 42.0 kPa in the abluminal layer of the ILT according to measurements of Gasser et al[3]. The contact between the wall and ILT was assumed bonded due to lack of information. The contact was not applied in area of origin of branch arteries to simulate the local absence of ILT. Models were fixed at distal and proximal ends.

Finite elements analyses (FEA) were performed in ANSYS 12.1. Geometries were meshed by quadratic tetrahedral elements and mesh convergence was checked to ensure that the calculated stresses depend on the mesh size by less than 5%.

Results

Two sets of patient specific geometries were investigated. One original without BA and one modified with BA. As expected, wall stress in all cases increases significantly when BA were included. Stress concentration factors were calculated as follows:

$$\alpha_{HMH} = \frac{Von\ Mises\ \ stress\ \ with\ BA}{Von\ Mises\ \ stress\ \ without\ \ BA}$$

$$\beta_n = \frac{n^{th}\ principal\ \ stress\ \ at\ BA\ origin\ in\ AAA}{n^{th}\ principal\ \ stress\ \ at\ BA\ origin\ in\ normal\ \ aorta}$$

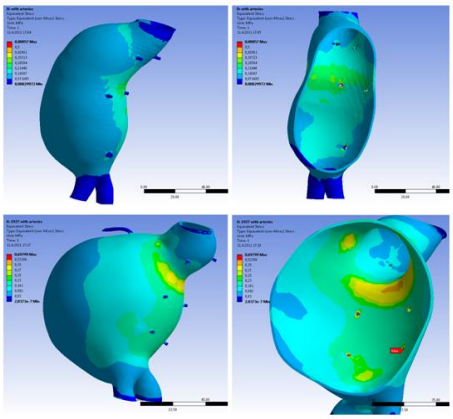

Figure 2. Von Mises stress distribution in MPa in two of reconstructed AAA. It is clearly shown that peak wall stress is located in the origin of BA

Mean value obtained from 34 measurements (5AAA=29 lumbar arteries+5IMA) was $\alpha_{HMH} = 2,95 \pm 0,72$ 1st principle stress increase was not as significant as von Mises $\beta_1 = 1,66 \pm 0,94$. We observed significant increase in 2nd principal stress compared to nonaneurysmal aorta when BA were located in the aneurysmal sac, see Figure 3. By the presence of AAA, 2nd principal stress in the region of BA origin is increased by factor of $\beta_2 = 7,96 \pm 6,88$. Limitations of values β is given by the fact, that reference values for a nonaneurysmal aorta was set on the basis of one pair of BA only.

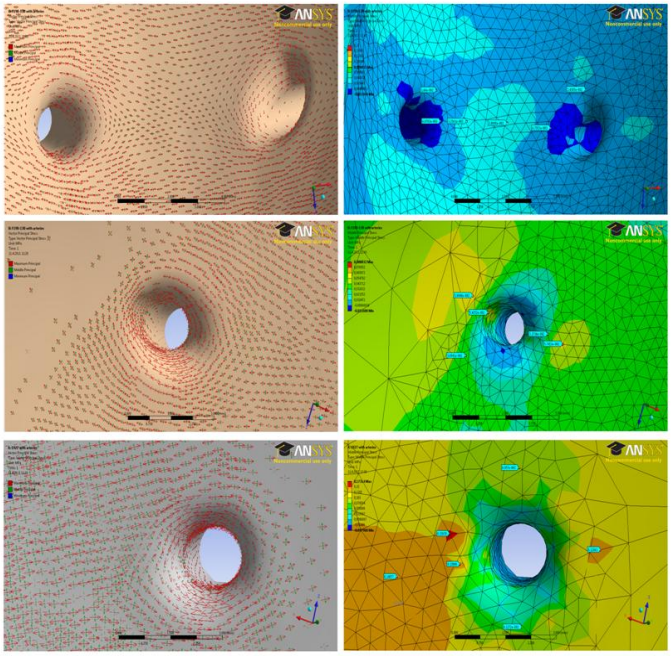

Figure 3. Top row- principal stress vector(left) and 2nd principal stress(right) in nonaneurysmal aorta. Middle and bottom row- principal stress vector(left) and 2nd principal stress (right) in the region of origin of BA in two different AAAs. Axial direction of AAA is vertical in Figure, circumferential direction in AAA is horizontal in Figure.

Discussion

Presence of BA increases von Mises stress approximately by factor of 3. Therefore BA should be always included in the patient specific geometry of AAA when stress is computed. However it is obvious that α depend not only on the geometry of AAA but on the transition radius as well. We chose R=1mm as a reasonable guess. Parametric study would of course show that smaller radius results in higher stresses. Histological analysis would be more useful in order to show what transition radii are.

Although wall stress dramatically increases when BA are included, it does not necessarily mean, that rupture risk index increases as well. It has been shown that the tissue in the apex of the bifurcation consists of dense uniformly oriented packs of collagen fibers while media is missing there[4]. The calculated directions of the 1st principal wall stresses in the region of BA origin are circumferential (with respect to the given BA) which is in agreement with described orientation of collagen fibers (see Figure 2). Also observed increase due to presence of AAA is not very high and it highly depends on the local geometry.

Results of 2nd principal stresses are more significant because if collagen fibers orientation had almost no dispersion it means consequently that the strength is very low in the direction perpendicular to fibers. In the area of BA origin this direction is equal to the direction of the 2nd principle stress. We observed that the 2nd stress in BA origin is increased by factor of 8 in BA which origin from AAA but it strongly depends on the AAA geometry as one can conclude from the huge standard deviation. On the other hand it means that for particular cases this factor can goes up to 20. Moreover, the remodeling capability of the wall in the apex region is very limited due to absence of media[4]. These two observations highlight regions of BA origin as risky areas where rupture can occur. If this hypothesis is true, than rupture should start from the region of BA origin. However this needs to be confirmed by autopsies of ruptured AAA and histological analyses of area of BA origin.

The presented analysis has of course several limitations which should be kept in mind when interpreting results. The constant transition radius was already discussed. Different material model, as well as residual stresses and prestressing would change the deformed geometry and consequently wall stresses as well, but their impact on stress concentration factors is low. Stresses in the region of BA origin in a nonaneurysmal aorta should be investigated on more samples, because it can change with diameters and mutual angle of both arteries.

Acknowledgements

This work was supported by grant project of GA CR No. 106/09/1732, by faculty project FSI-J-11-14 and by the project CZ.1.07/2.3.00/09.0228 "Complex System for Attracting, Education and Continuing Involvement of Talented Individuals to Research Centers of AS CR and FME BUT" . Author is supported by "scholarship for talented Ph.D. student" by the city of Brno.

References

1. Fillinger MF, Raghavan ML & Marra SP, Cronenwett JL, Kennedy FE 2002. In vivo analysis of mechanical wall stress and abdominal aortic aneurysm rupture risk. *J Vasc Surg*, **36,** 589-97.
2. Raghavan ML, Webster MW & Vorp DA 1997. Ex vivo biomechanical behavior of abdominal aortic aneurysm: assessment using a new mathematical model. *Ann Biomed Eng*, **24,** 573-82.
3. Gasser TC, Gorgulu G & Folkesson M, Swedenborg J 2008. Failure properties of intraluminal thrombus in abdominal aortic aneurysm under static and pulsating mechanical loads. *J Vasc Surg*, **48,** 179-88.
4. Finlay HM, Whittaker P, & Canham PB 1998. Collagen Organization in the Branching Region of Human Brain Arteries. *Stroke* , **29,** *1595-1601.*
5. Polzer S, Gasser TC, Swedenborg J, Bursa J 2011. The impact of Intra-luminal Thrombus failure on the mechanical stress in the wall of Abdominal Aortic Aneurysms. *Eur J Vasc Endovasc Surg*, **41,** 467-473.

12.7 Appendix G

Importance of Material Model in Wall Stress Prediction in Abdominal Aortic Aneurysms.

Stanislav Polzer[1], T.Christian Gasser[2], Jiri Bursa[1] , Robert Staffa[3], Robert Vlachovsky[3] , Vojtech Man[1] and Pavel Skacel[1]

[1] Institute of Solid Mechanics, Mechatronics and Biomechanics, Brno University of Technology, Czech Republic

[2] Department of Solid Mechanics, The Royal Institute of Technology, Stockholm, Sweden

[3] 2nd Department of Surgery, St. Anne's University Hospital, and Faculty of Medicine, Masaryk University, Brno, Czech Republic

Submitted for publication into Medical Engineering and Physics

Abstract

Background. Results of biomechanical simulation of the abdominal aortic aneurysm (AAA) depend on the constitutive description of the wall. Based on in-vitro and in-vivo experimental data several constitutive models for the AAA wall have been proposed in literature. Those models differ strongly from each other and their impact on the computed stress of biomechanical simulation is not clearly understood.

Methods. Finite Element (FE) models of AAAs from 7 patients who underwent elective surgical repair were used to compute wall stresses. AAA geometry was reconstructed from CT angiography (CTA) data and patient-specific constitutive descriptions of the wall were derived from planar biaxial testing of anterior wall tissue samples. In total 56 FE models were used, where the wall was described either by patient-specific or previously reported mean-population properties. This data was derived from either uniaxial or biaxial in-vitro testing. Computed wall stress fields were compared on node-by-node basis.

Results. Different constitutive models for the AAA wall cause significantly different predictions of wall stress. While mean population data from biaxial testing gives globally the same stress field as the patient-specific wall properties, the material model based on uniaxial test data overestimates the wall stress on average by 30kPa or about 67% of the mean stress. A quasi-linear description based on the in-vivo measured distensibility of the AAA wall leads to a completely altered stress field and overestimates the wall stress by about 75kPa or about 167% of the mean stress.

Conclusion. The present study demonstrated that the constitutive description of the wall as well as the reference configuration for the FE models, are crucial inputs for AAA wall stress prediction. Highly nonlinear material models should be use only when residual stresses are taken into account otherwise they produce significant stress gradient across the wall. When residual stresses are omitted the quasi-linear model seems to be most appropriate.

Key words: material model, pre-stressing, abdominal aneurysm, wall stress, FE analysis

Introduction

A diameter exceeding 5.5cm is the most commonly accepted criterion for elective surgical repair of abdominal aortic aneurysm (AAA) [1,2]. There is, however, a need for other predictors for rupture, since aneurysms with a diameter less than 5.5 cm can rupture [3,4] and 60% of larger aneurysms do not rupture [5]. According to the biomechanical rupture risk assessment an aneurysm will rupture if the mechanical stress exceeds the local strength of the wall. Consequently, it has been shown that the Peak Wall Stress (PWS) [6,7] and Peak Wall Rupture Risk (PWRR) [8,9] identify rupture-prone AAAs better than the maximal diameter criterion.

Biomechanical indices like PWS and PWRR require the computation of wall stress and typically using the Finite Element Method (FEM). The sites of PWS and PWRR may not coincide [39], and hence an accurate prediction of the whole stress field is needed for the reliable computation of PWRR. Several factors influence wall stress computations, and it has been generally accepted that the individual AAA geometry is the most important one.

While most FE models use the patient-specific AAA geometry, they rely on mean population data on tissue properties, the impact of which remains poorly understood. Using an idealized model of AAA and varying material model properties based on uniaxial tensile testing within 95% confidence interval (CI) revealed only a 5% change in PWS [16]. Other studies reported that PWS is higher [25] or lower [38] when a nonlinear material model was used instead of a linear one.

Most comprehensive data was derived from planar biaxial tensile testing [26,35] and led to an improved constitutive description of the aneurysm wall. Specifically, the nonlinearity of the AAA wall was more pronounced under biaxial than under uniaxial testing. The biomechanical consequences of that finding were investigated with the conclusion that constitutive models fitted to biaxial data exhibit higher PWS than models fitted to uniaxial data [40,43].

Although averaged results of biaxial tests show a rather small anisotropy [26,35] , the patient specific behaviour of aneurysmal tissue can be significantly anisotropic. With anisotropy taken into account, higher stresses were obtained in comparison with isotropic wall models [37,40, 43] an effect that might be difficult to distinguish from the influence of nonlinearity detailed below. However, current anisotropic models follow a purely phenomenological approach and a sound structural background is still missing to consider the distribution of e.g. collagen fibers.

Generally all studies in the literature compared single stress values (PWS or mean stress) and therefore could not provide a comprehensive picture of the impact of modeling assumptions on the wall stress distribution. In summary, more sophisticated analysis methods are required

that involve the whole stress field and allow us to draw valuable conclusions regarding the impact of FE modeling assumptions. In spite of that the present work compares wall stress predictions based on commonly used constitutive descriptions for the AAA wall with results of simulations based on patient-specific constitutive parameters. To this end solely isotropic material models are considered and the conclusions are drawn from the comparison and statistical analysis of whole stress fields. The present study involves 7 patients, which was enough to draw statistically significant conclusions.

Methods

Specimen acquisition and biaxial mechanical testing

During elective surgical AAA repair a sample of the anterior aneurysm wall was taken from male patients with asymptomatic (n=6) and symptomatic (n=1) AAAs. Within 3 hours post surgery the mechanical properties of the harvested AAA wall samples were identified through biaxial mechanical testing. To this end a test specimen (about 18x18mm) was clamped in a custom made planar biaxial tensile testing device (Camea s.r.o, Czech Republic), see Figure 1. Four markers (ink dots) were placed in the middle of the specimen (measurement area) allowing non-contact measuring of tissue strain with a CCD camera at a resolution of 0.02mm/pixel. Further details on the testing device and the methodology are reported elsewhere [28,42]. The use of human tissue for this project was approved by the local ethic committee.

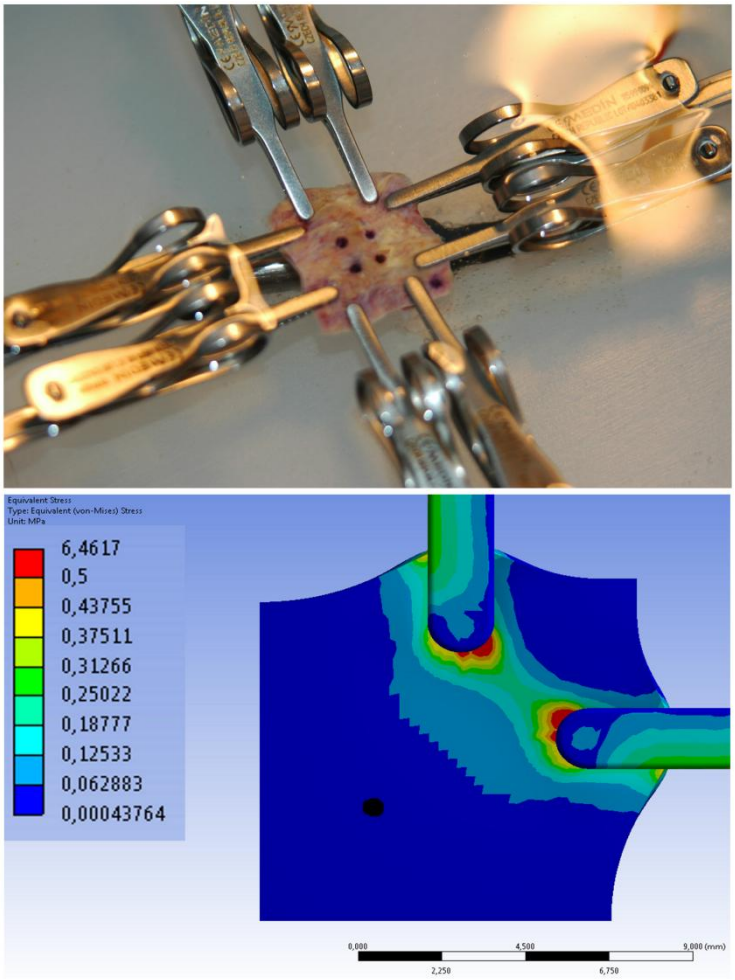

Figure1: Abdominal Aortic Aneurysm (AAA) wall specimen located in the planar biaxial testing system and immersed in physiological saline solution (upper part). Stress concentrations induced by presence of the clamps (Lowe part). Black dot represents the position of the marker.

The specimen was tested using displacement-controlled protocols, where the ratio u_x:u_y was kept constant between the clamp displacements in circumferential and axial directions, respectively. Note that a constant ratio of the clamp displacements does not imply a constant strain ratio in the testing area. In-vitro testing aims at reflecting the in-vivo loading conditions as closely as possible, and a-priori it is not clear, if a stress or strain-controlled experiment would be more appropriate. Blood pressure translates directly into wall stress, and hence a stress-based protocol would be recommended. However, in-vivo the axial expansion of the AAA is constraint, which would motivate to control the axial strain during biaxial testing.

In order to flatten the test specimen and to avoid bending during biaxial testing, it is typically slightly pre-stressed [26,35]. Although in the literature lower pre-stress is reported, all our test specimens were pre-stressed in the circumferential and axial directions by 0.2N, i.e. to ensure avoiding any bending effects during biaxial testing. Test specimens were preconditioned by four equi-displacement cycles that resulted in roughly 12% strains in the testing area [34], i.e. the preconditioning is similar to that reported earlier for biaxial testing of the AAA wall

[26,35]. Each specimen was then removed from the testing machine, placed on a glass plate and covered with another one to ensure its plainness. Then its picture was captured to define its reference configuration. After that it was placed back to the testing machine and stress and stretch data was recorded for displacement ratios of u_x:u_y=1:1, 1:2, 2:1 and at a displacement rate of 0.167mm/s, i.e. such that the test can be regarded as quasi-static.

Fixating the test specimen with clamps, like with hooks, induces stress concentrations, which must not affect the measurement area. Protocol development of our biaxial testing considered FE simulations to define the optimal clamp positions. Specifically, a sufficiently homogenous stress field in the measurement area was verified through FE simulations (see Figure 1). Finally it is noted that AAA wall tissue was kept in saline solution at 37°C from the time of surgical removal until the mechanical testing was completed. This ensured that smooth muscle cells (SMCs) contributed to the total stiffness of the specimen [36].

Constitutive modeling

Patient specific AAA wall model

The principal stretches λ_1, λ_2 of the test area in the middle of the specimen have been determined from displacements of recorded markers. In addition, the principal first Piola-Kirchhoff stresses P_1, P_2 were calculated from the recorded forces and the initial dimensions of the test specimen. Stretch and stress computations were carried out by the in-house software Tibixus.

The experimental stretch-stress data was fitted (software Hyperfit, BUT, Czech Republic) to a 5th order Yeoh model [18], described by the strain energy function:

$$\psi = \sum_{i=1}^{5} c_{i0} \left(I_1 - 3 \right)^i , \qquad (1)$$

where c_{i0} denote stress-like material constants and I_1 is a first invariant of Cauchy-Green deformation tensor. Data from test specimens was used and the estimated patient-specific material parameters are given in Table 1. Note that for non-negative material parameters the response of this model is progressively stiffening with strain, and hence well suited to model biological soft tissue. Although the AAA wall is known to be anisotropic [26,35] the isotropic constitutive law eq.(1) allowed a satisfying representation of the experimental data, as illustrated by the high R^2 values in Table 1. A representative fit (R^2=0.86) is illustrated in Figure 2 and the strain energy density for all patients is plotted in Figure 3.

Table 1 Patient-specific material constants of the Yeoh model eq.(1) fitted to biaxial tensile test data.

Patient no.	Material parameter [kPa]					R^2
	c_{10} [kPa]	c_{20} [kPa]	c_{30} [kPa]	c_{40} [kPa]	c_{50} [kPa]	
1	14.5		2259			0.81
2	20			6194	20000	0.78
3	22	1461	1000			0.82
4	6	117		35685		0.85
5	20	250		35	200000	0.86
6	12.5	367			49842	0.78
7	0.8	57	830	1479	15600	0.72

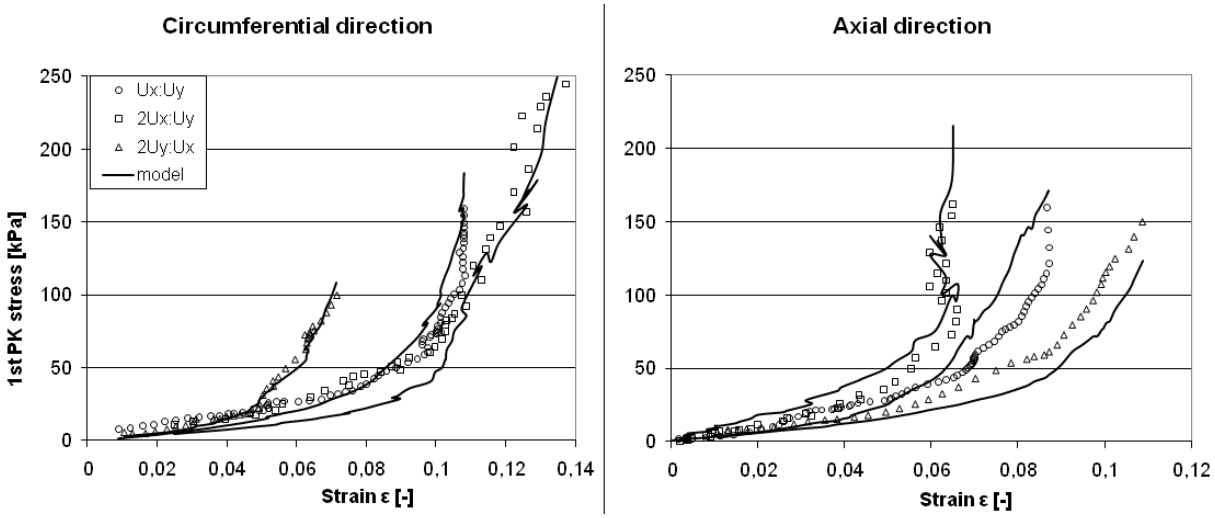

Figure2: Patient-specific mechanical properties of the Abdominal Aortic Aneurysm (AAA) wall. Dots are biaxial tensile test data and the solid lines denote best fit (R^2=0.86) using the Yeoh constitutive model. Note that the analytical solution is based on experimentally measured biaxial stretches, which causes non-smooth stress-strain curves.

Mean population models for AAA wall

Numerous constitutive descriptions of the mean-population response of the AAA wall have been reported in the literature, and some of them are considered in the present study. Specifically, it was investigated to what extend their wall stress predictions differ in comparison to computations using the patient-specific models defined above.

The best established model for AAA wall is a 2nd order Yeoh model [18] that has been fitted to circumferential and axial uniaxial tensile tests of aneurysmal tissue [16,17]. This model is subsequently denoted as RV-model and uses the parameters c_{10}=177 kPa and c_{20}=1881 kPa in eq.(1).

Another 2nd order Yeoh model [18] reflects a quasi-linear response that is based on the in-vivo deformations of AAA during a cardiac cycle [27]. This model is subsequently denoted as QL-model and uses the parameters c_{10}=1628 kPa and c_{20}=1428 kPa in eq.(1).

In addition another non-linear hyperelastic isotropic model

$$\psi = \frac{a}{b}\left(e^{\frac{b}{2}(I_1-3)} - 1 \right) \tag{2}$$

originally proposed by Demiray [31] was investigated. Here, a and b denote stress-like and dimension-less constants, respectively. This model was fitted to biaxial tensile test data of aneurysmal tissue [26]. Unfortunately the raw experimental data was not available and eq.(2) was fitted to the response of the anisotropic hyperelastic model proposed by Choi-Vito et al. [29] through the parameters reported for biaxial tensile test data of aneurysmal tissue [26]. The model eq.(2) was used since it fits biaxial data (in the range of tangential to axial stresses $S_{\Theta\Theta}$:S_{LL} from 1:2 to 2:1) of AAA wall [26] very well ($R^2 = 0.87$ for $a = 17kPa$ and $b = 88$) and it is provided through ANSYS ver.12.1 (ANSYS Inc. PA, US). This model is subsequently denoted as VG-model.

Constitutive models for intra-luminal thrombus tissue

In contrast to the aneurysm wall, the intra-luminal thrombus (ILT) exhibits a much more linear behavior, which can be captured rather accurately by a one parameter Ogden-like material model

$$\psi = c\sum_{i=1}^{3}\left(\lambda_i^4 - 1\right), \tag{3}$$

where λ_i denotes the i-th principal stretch and c is a stress-like material parameter that has been defined through in-vitro testing [15]. Specifically, ILT is stiffer at the luminal side ($c = 2.62kPa$) and gradually decreases its stiffness towards the abluminal side ($c = 1.73kPa$).

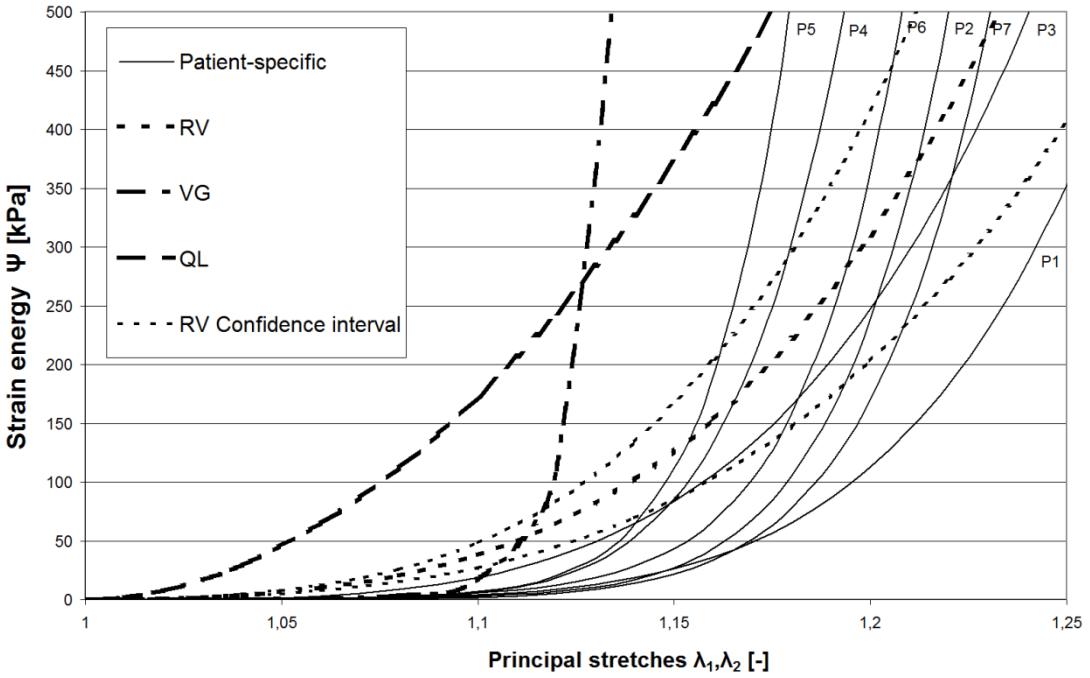

Figure3. Strain energy density at equi-biaxial stretch of the Abdominal Aortic Aneurysm (AAA) wall. Thin and thick lines represent patient-specific data and information extracted from the literature, respectively.

Geometry acquisition and reconstruction

Patients underwent CT-A of the aorta at St. Anne's University Hospital, Brno, Czech Republic at the typical image in-plane resolution of 0.5 mm and slice thickness 3 mm. Deformable (active) contour models (A4research vers.3.0, VASCOPS GmbH, Austria) were used to reconstruct the 3D geometry of AAAs from CT data [19]. To this end a virtual balloon expands until the boundaries of the aneurysm are detected. This provides smooth surfaces and excludes artifacts such as sharp edges and corners, which otherwise might cause stress concentrations in the FEM simulation. The wall thickness was set in dependence on the thickness of the underlying ILT. Specifically, at sites of a thin ILT (thinner than 1.0mm) the wall thickness was 1.5mm and reduced to 1.0mm behind a thick ILT (thicker than 25.0mm), which is in agreement with histological data [30].

Finite element models

Recently the importance of using a stress-free (unloaded) reference configuration for wall stress predictions in AAAs has been demonstrated [21,25,38].To predict the stress-free (unloaded) AAA geometry a backward incremental method as proposed earlier [24] was used. Consequently, when pressurizing the AAA at $p = 13\,kPa$ corresponding to the mean blood pressure, the stress-free configuration will map into the geometry as reconstructed from the CT data. The iterative algorithm that predicted the stress-free (unloaded) AAA geometry was

terminated at $\delta = \frac{\sum_{i=1}^{n} |X'_i - X_i|}{n} < 0.01 mm$, such that the considered pressurized ($p = 13 kPa$) and reconstructed AAA geometries were virtually identical. Here, n denotes the number of finite element nodes of the wall model and X'_i and X_i are coordinates of the *i*-th node in the reconstructed and pressurized configurations, respectively. The largest difference of 0.23mm for one individual node was obtained for the patient-specific analysis of patient 2. Prior application to real AAA geometries, the applied backward incremental method and its implementation have been validated and verified with respect to spherical and cylindrical shapes, respectively.

A rigid interface between ILT and wall was considered, i.e. separation and sliding between the ILT and the wall are constraint. The aneurysm was fixed at the renal arteries and aortic bifurcation (or at the end of AAA where it ends before the bifurcation). Mixed linear tetrahedral elements (solid 285 according to ANSYS terminology) were used to model incompressible materials, i.e. avoiding volume locking [32] through an extra degree of freedom that reflects the hydrostatic pressure at each node. In order to resolve the stress field accurately the typical element size of wall and ILT was 0.8mm and 1.5mm, respectively. Consequently, the FEM models had about 100k nodes and stress computations took about 30 hours per case at a 4CPU, 12GB RAM computer.

Data analysis

Although the ILT is included in the FEM models, ILT stress is not further investigated and we focused on the stress in the AAA wall only. Specifically, the von Mises stresses in the AAA wall according to different modeling assumptions were compared on a FE node-by-node basis as follows:

At each node the stress difference between the PS model and any other constitutive formulation was computed. This stress differences were then allocated (clustered) to 1000 classes that covered the interval from -500 kPa to +500kPa. For example, the point (42,1238) of the curve RV in Figure 4 denotes that 1238 nodes show the stress difference δ between the PS model and the RV model between $41 < \delta \leq 42$ kPa.

Finally it been verified whether obtained curves differs from each other statistically significantly. The significance was tested by comparing of their mean, median and mode

values with the Kruskal-Wallis test (MiniTab 15.1.1., Microsoft Inc, USA) and a p-value lower than 0.05 was considered to be statistically significant.

Results

A typical distribution of stress differences is shown in Figure 4, where the Ω_0 was considered by the FE computation. In this presentation, a sharp distribution around the stress difference of 0 kPa indicates predictions that are highly coherent to the patient-specific model. In contrast, a wide and flat distribution indicates a low coherence with patient-specific predictions. Figure 4 shows that the predictions based on the VG-model are closest to the patient-specific results. Likewise, the RV-model and the QL-model overestimate the PS predictions on average by some 30kPa and 75kPa, respectively.

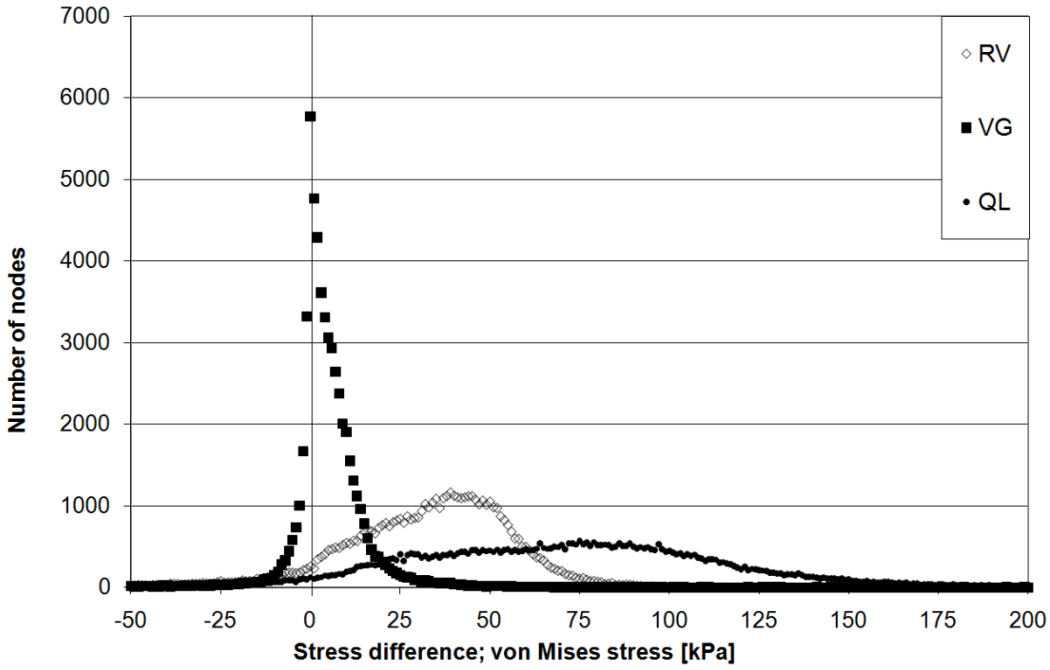

Figure4: Model-related differences of the stress in the Abdominal Aortic Aneurysm (AAA) wall of patient 1. Results from the mean-population descriptions of the AAA wall are compared to those of patient-specific modeling.

As a representative cases the results for patients 2 and 5 are illustrated in Figure 5. Again, predictions based on the VG constitutive model are most similar to the patient-specific model, while results of other models differ significantly.

Finally, the impact on PWS was investigated, and illustrates the results for all patients, for different constitutive models. Results are summarized in Figure 6.

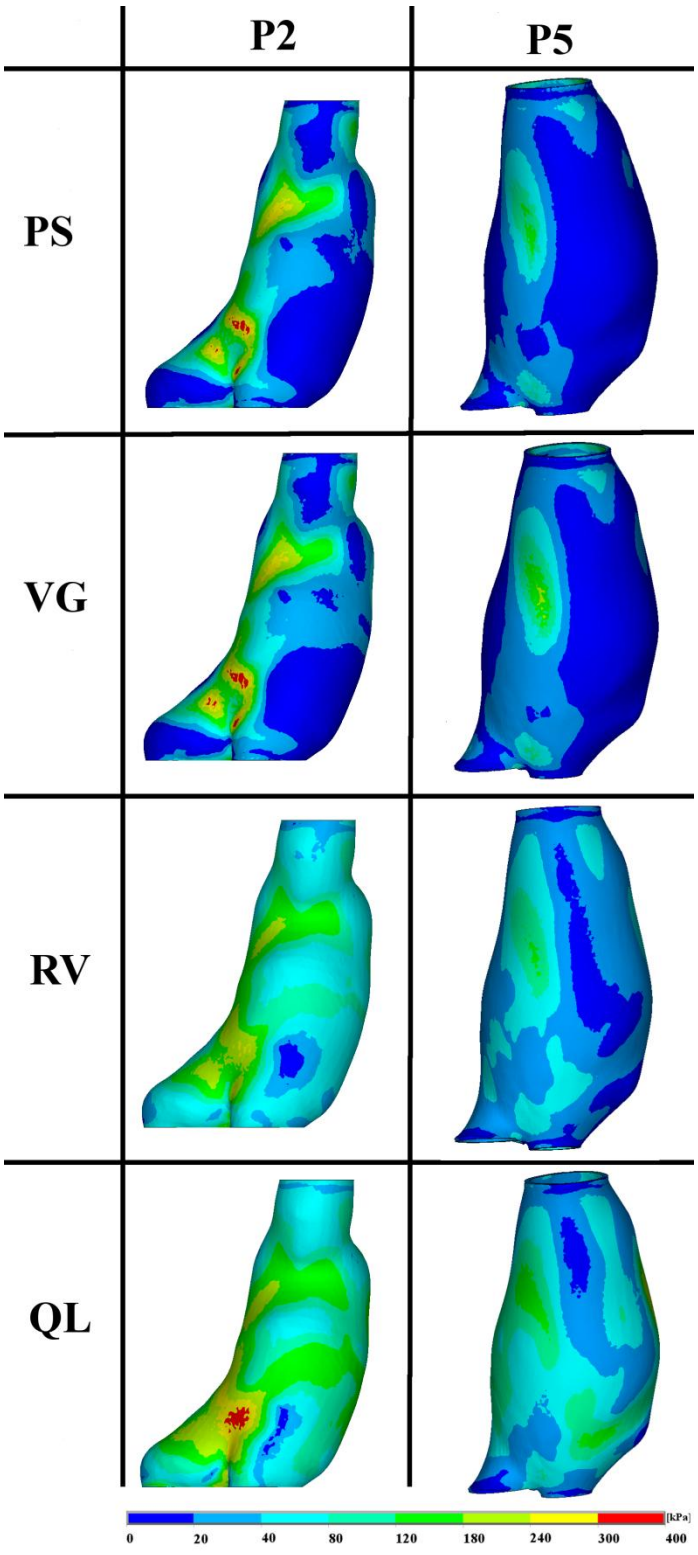

Figure5: Impact of the constitutive model and on the AAA wall stress predictions. Von Mises stress for patients 2 (left) and 5 (right] is shown.

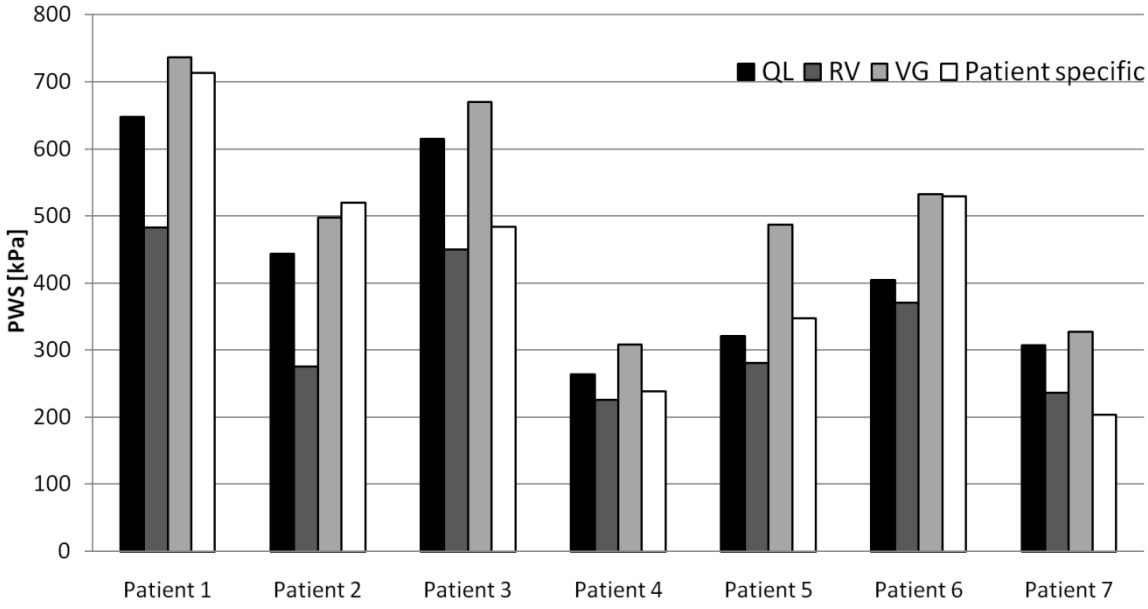

Figure6: Peak Wall Stress (PWS) predictions for each patient using different constitutive wall models.

Statistical data

Table 1 provides statistical data regarding the wall stress difference. In addition results from statistical testing are provided, where all models were investigated. These results show that a different material model provides a different wall stress field. Most significantly, although strain energy density functions of the VG and patient-specific models differ from each other significantly (see Figure 3), they lead to practically the same stress fields in the wall.

Table 1 Wall stress differences according to variation of the material model. Statistical data and Results from hypothesis testing.

Wall stress difference with respect to the patient-specific constitutive wall model				
Constitutive AAA wall model	Mean [kPa]	Median [kPa]	Mode [kPa]	Standard deviation [kPa]
RV-model	29.4	30.3	29	22.4
VG-model	2.7	0.6	0.3	11
QL-model	71.7	78.1	83.9	52.3

(I) Null hypothesis: The difference between the patient specific model and the other models (QL,VG, RV) is the same.	
Mean	p<0.001
Median	p<0.001
Mode	p=0.001

Discussion

The alteration of wall stress as a consequence of different modeling assumptions was studied. To this end AAAs were reconstructed from CT-A data and equipped with either patient-specific or mean-population wall properties. The results presented in this study were not limited to PWS or mean stress as reported earlier [16,25,33,38,40,41,43], but they compared the whole wall stress field. The statistical significance of wall stress differences was verified by sufficiently low p-values so that increasing the number of patients would not change the conclusions drawn in the present study.

This study showed that different material models lead to significantly altered wall stress. Although the patient-specific wall models differed significantly from the VG-model (in terms of the transition point from soft to stiff properties, as well as in high-strain stiffnesses, see Figure 3) they gave practically the same results. In contrast, the RV-model, which is used most frequently in the literature and relies on data from uniaxial testing, overestimates wall stresses on average by 20kPa. Finally, the QL-model gives completely different results, and overestimations are comparable with the magnitude of the average wall stress ($45 \pm 17\, kPa$).

Although not mentioned specifically, the above discussed observation is consistent with data published in the literature, see Figure 5 in ref. [40]. This clearly illustrates that the stress field that was computed by the constitutive model based on biaxial data (referred to as ‘aniso’ in ref. [40]) showed significantly larger area of very low stresses compared to the model fitted to uniaxial data (referred to as ‘iso’ in ref. [40]). The same result is illustrated in Figure 5 when comparing the VG and RV models. Since our results were obtained with isotropic models, we believe that this difference is not a specific consequence of ‘isotropic versus anisotropic’ wall models as suggested in [40] and explanation needs to be found elsewhere.

For better understanding we analyzed the impact of the material model on the circular cylinder of different inner diameters. Specifically, the deformed inner diameter changed between 40 and 60 mm, the deformed thickness was set to 1.5mm and a prestress pressure of 10kPa was used. The FEA applied to the circular cylindrical geometries was the same than for the AAAs, and the results are shown in the Figure 7. When comparing the stress at the inner and outer surface of the wall, this figure clearly shows that the VG model leads a non-negligible stress gradient across the wall. In contrast the RV gives a much lower gradient and the QL model produces almost no stress gradient across the wall. For completeness, also the stress according to the law of LaPlace was added in the figure.

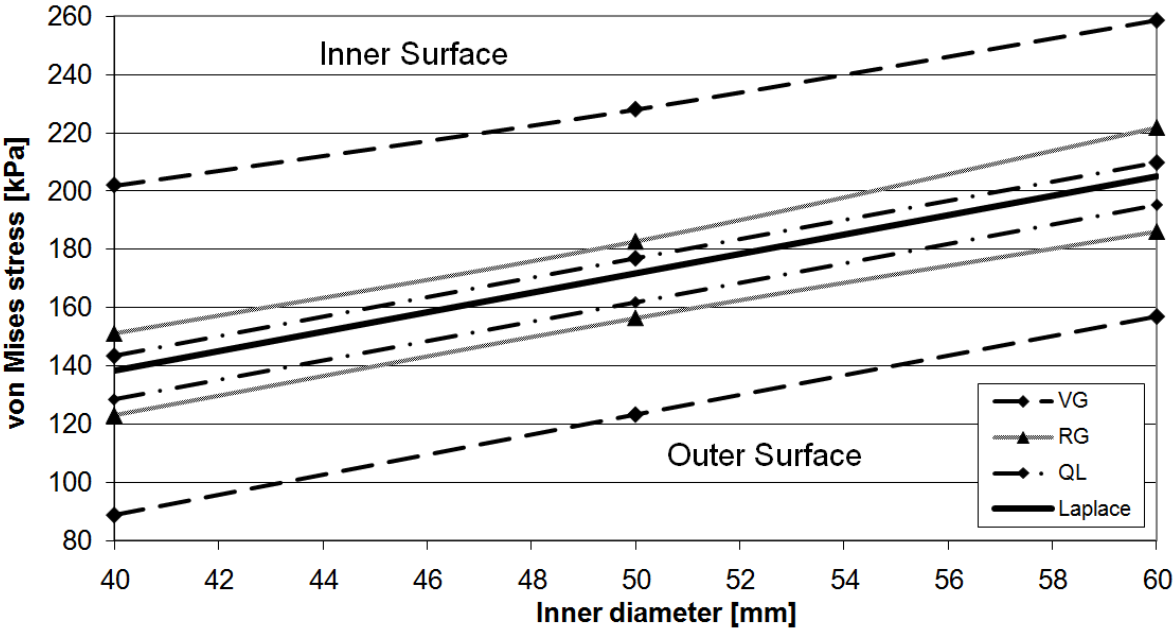

Figure 7 Impact of material model on the wall stress of the circular cylinder. All curves above the LaPlace curve (black solid line) refer to the inner surface, while curves below the LaPlace curve refer to wall stresses computed at the outer surface of the cylinder. Note that different constitutive models produce different stress gradient across the wall.

From Figure 7 it gets clear that, even for the circular cylindrical geometry, different constitutive models predict highly different PWS values while the average stress complies with the law of LaPlace, i.e. as it is required to satisfy the momentum equations. Specifically, the highly non-linear stress strain curves that have been identified through biaxial testing lead to strong stress gradients across the wall. Of note that there is also bending during deformation of patient-specific AAAs therefore no simple analogy with example is possible and stresses had to be compared on the node-by node basis.

High stress gradient is in contradiction with the uniform stress theory [44] and also caused by neglecting residual stresses in the load-free configuration. Including residual stresses into patient-specific AAA models would most likely remove the stress gradients. However, for complex geometries such as AAAs, residual stresses are unknown, and hence not considered in current biomechanical studies [16,25,33,38,40,41,43]. Consequently, PWS values are biased by a non-physiological stress gradient. Finally, due to its linear character and the thin AAA wall, the QL model predicts a quite homogenous stresses across the wall, which would be in good agreement with uniform stress hypothesis.

The predicted high stress gradients across the wall for highly non-linear stress strain curves could also explain the apparent conflict with the study [16]. This study reported that varying material constants within the 95% confidence interval changed PWS by only 5%. Note that neither residual stresses nor prestressing were used in [16], and the shape of the strain energy

density function was not altered. In contrast, the present study investigated three completely different strain energy density functions (see Figure 3), and the AAA models were pre-stressed, which in turn provided a more comprehensive picture of the wall stress.

Although the isotropic constitutive models used in the present study cannot capture the uniaxial data reported in [16], they are align with more recently reported biaxial data [26,35]. It is likely that the strain energy density function obtained in [16] was affected by the significant pretension of the test specimens, as also suggested earlier [26].

Our biaxial testing results are different from the data reported in the literature [26,35]. Most interestingly, our data showed the transition point from compliant to stiff mechanical properties at higher strains (see Figure 3), which indicates different definitions of the reference configuration for the biaxial testing. The tissue samples of the present study were tested within 3 hours and kept always in saline solution at 37 degrees. Consequently, more SMCs might have been contributing to the tissue behavior in our experiments than in the reference study [26]. Despite that explanation, the observed differences in strain energy density functions might also be caused by different deformation rate in both experiments. We used the deformation rate of 0.167mm s^{-1}, while the study [35] used (1^{st} Piola Kirchhoff) stress rate of 50kPa s^{-1}. Although these values are not directly comparable because of different controlled quantities, the study [35] used indeed a much higher speed of loading than our study.

Numerous limitations of the present study should be kept in mind when interpreting results. For simplicity and due to a lack of histological data the present study used isotropic wall models. Specifically, anisotropic constitutive data of the AAA wall that has been reported in the literature [26] was approximated through an isotropic wall model. While isotropy seems to be an inappropriate simplification for the normal aorta, it is widely applied for the AAA wall. The AAA wall of those subjects investigated in the present study responded almost isotropically in a range of strains that is expected in-vivo.

In summary, we demonstrated that the constitutive description of the AAA model is a crucial factor for stress predictions, where specifically the degree of model nonlinearity needs to be assessed. Models that are based on planar biaxial experiments (e.g. VG-model) led to the most significant stress gradient across the wall, and therefore they should only be use when residual stresses in the aneurysm's load-free configuration are considered. On the other hand they describe true elastic properties of the arterial wall and they are irreplaceable when response of AAA to increased pressure is calculated. Models based on uniaxial tests or on clinical observation (QL) produce significantly different stress fields which are in better agreement with uniform stress theory [44]. Which makes them most suitable to calculate the stress response to the mean pressure. Their disadvantage is that they will not be capable of

describing AAA response to immediately raised pressure. We also demonstrated that the stress should be averaged across the wall, when comparing PWS predictions for example, to adjust for possible non-physiological stress gradients.

Acknowledgments

We gratefully acknowledge the support given to this work by the Young Faculty Grant No. 2006-7568 provided by the Swedish Research Council, VINNOVA and the Swedish Foundation for Strategic Research, and the EC Seventh Framework Programme, Fighting Aneurysmal Disease (FAD-200647). In addition, this work was supported by Czech Science Foundation (GA 106/09/1732) and BUT (FSI-J-11-3) projects, and Stanislav Polzer was supported by the "Brno Ph.D. talent" provided by the city of Brno, Czech Republic.

Competing interest: None

Funding: Young Faculty Grant No. 2006-7568 provided by the Swedish Research Council, VINNOVA and the Swedish Foundation for Strategic Research, and the EC Seventh Framework Programme, Fighting Aneurysmal Disease (FAD-200647). In addition, this work was supported by Czech Science Foundation project (GA 106/09/1732) and Brno University of Technology project (FSI-J-11-3).

Ethical approval: Ethical committee at St. Anne's University Hospital, Chairman Vladimir Soska MD, PhD. Reference number: 49V/2010

References

1. Mortality results for randomised controlled trial of early elective surgery or ultrasonographic surveillance for small abdominal aortic aneurysms. The UK Small Aneurysm Trial Participants. Lancet 1998; **352**(9141):1649-55.
2. Lederle, F.A , Wilson, S.E. , Johnson, G.R. , Reinke, D.B. , Littooy, F.N., Acher, C.W. , Ballard, D.J. , Messina, L.M. , Gordon, I.L. , Chute, E.P., *et al.*. Immediate repair compared with surveillance of small abdominal aortic aneurysms. *N Engl J Med*. 2002 **346**, 1437-1444. (doi: 10.1056/NEJMoa012573)
3. Heikkinen, M., Salenius, J.P. & Auvinen, O. Ruptured abdominal aortic aneurysm in a well-defined geographic area. *J Vasc Surg*. 2002.**36**, 291-296. (doi: 10.1067/mva.2002.125479)
4. Nicholls, S.C., Gardner, J.B., Meissner, M.H. & Johansen, H.K. Rupture in small abdominal aortic aneurysms. *J Vasc Surg*. 1998. **28**, 884-888.
5. Darling, R.C., Messina, C.R., Brewster, D.C. & Ottinger, L.W. Autopsy study of unoperated abdominal aortic aneurysms. The case for early resection. *Circulation.*1977. **56**, II161-4.
6. Fillinger, M.F., Raghavan, M.L., Marra, S.P., Cronenwett, J.L. & Kennedy, F.E. In vivo analysis of mechanical wall stress and abdominal aortic aneurysm rupture risk. *J Vasc Surg*. 2002.**36**, 589-597. (doi: 10.1067/mva.2002.125478)

7. Venkatasubramaniam, A.K., Fagan, M.J., Mehta, T., Mylankal, K.J., Ray, B., Kuhan, G., Chetter, I.C. & McCollum, P.T. A comparative study of aortic wall stress using finite element analysis for ruptured and non-ruptured abdominal aortic aneurysms. *Eur J Vasc Endovasc Surg*. 2004.**28**, 168-176. (doi: 10.1016/j.ejvs.2004.03.029)
8. Gasser, T.C., Auer, M., Labruto, F., Swedenborg, J. & Roy, J. Biomechanical rupture risk assessment of abdominal aortic aneurysms: model complexity versus predictability of finite element simulations. *Eur J Vasc Endovasc Surg*. 2010.**40**, 176-185. (doi: 10.1016/j.ejvs.2010.04.003)
9. Maier, A, Gee, MW, Reeps C, Pongratz J, Eckstein HH, Wall WA. A Comparison of diameter, wall stress, and rupture potential index for abdominal aortic aneurysm rupture risk prediction. *Ann Biomed Eng*. 2010.**38**, 3124-3134,
10. Hans, S.S., Jareunpoon, O., Balasubramaniam, M. & Zelenock, G.B. Size and location of thrombus in intact and ruptured abdominal aortic aneurysms. *J Vasc Surg*. 2005.**41**, 584-588. (doi: 10.1016/j.jvs.2005.01.004)
11. Alexander, J.J. The pathobiology of aortic aneurysms. *J Surg Res*. 2004.**117**, 163-175. (doi: 10.1016/j.jss.2003.11.011)
12. Vorp, D.A., Lee, P.C., Wang, D.H., Makaroun, M.S., Nemoto, E.M., Ogawa, S. & Webster, M.W. Association of intraluminal thrombus in abdominal aortic aneurysm with local hypoxia and wall weakening. *J Vasc Surg*. 2001.**34**, 291-299. (doi: 10.1067/mva.2001.1148139)
13. Kazi, M., Thyberg, J., Religa, P., Roy, J., Eriksson, P., Hedin, U. & Swedenborg, J. Influence of intraluminal thrombus on structural and cellular composition of abdominal aortic aneurysm wall. *J Vasc Surg*. 2003.**38**, 1283-92. (doi: 10.1016/S0741)
14. Wang, D.H., Makaroun, M.S., Webster, M.W. & Vorp, D.A. Effect of intraluminal thrombus on wall stress in patient-specific models of abdominal aortic aneurysm. *J Vasc Surg*. 2002.**36**, 598-604. (doi: 10.1067/mwa.2002.126087)
15. Gasser, T.C., Gorgulu, G., Folkesson, M. & Swedenborg, J. Failure properties of intraluminal thrombus in abdominal aortic aneurysm under static and pulsating mechanical loads. *J Vasc Surg.* 2008.**48**, 179-188. (doi: 10.1016/j.jvs.2008.01.036)
16. Raghavan, M.L. & Vorp, D.A. Toward a biomechanical tool to evaluate rupture potential of abdominal aortic aneurysm: identification of a finite strain constitutive model and evaluation of its applicability. *J Biomech*. 2000.**33**, 475-482. (doi: 10.1016/S0021-9290(99)00201-8)
17. Raghavan, M.L., Marshall, W. Webster, M.W. & Vorp, D.A. Ex vivo biomechanical behavior of abdominal aortic aneurysm: assessment using a new mathematical model. *Ann Biomed Eng*. 1997.**24**, 573-582. (doi: 10.1007/BF02684226)
18. Yeoh, O.H. Some forms of strain energy functions for rubber. *Rubber Chem. Technol*. 1993.**66**, 754–771.
19. Auer, M. & Gasser, T.C. Reconstruction and finite element mesh generation of abdominal aortic aneurysms from computerized tomography angiography data with minimal user interactions. *IEEE Trans. Med. Imag*. 2010.**29**, 1022-1028. (doi: 10.1109/TMI.2009.2039579)
20. Merkx, M.A., van 't Veer, M., Speelman, L., Breeuwer, M., Buth, J. & van de Vosse, F.N. Importance of initial stress for abdominal aortic aneurysm wall motion: dynamic MRI validated finite element analysis. *J Biomech*. 2009.**42**, 2369-2373. (doi: 10.1016/j.jbiomech.2009.06.053)
21. Gee, M.W., Reeps, C., Eckstein, H.H. & Wall, W.A. Prestressing in finite deformation abdominal aortic aneurysm simulation. *J Biomech*. 2009.**42**, 1732-1739. (doi: 10.1016/j.biomech.2009.04.016)
22. Raghavan, M.L., Ma, B. & Fillinger, M.F. Non-invasive determination of zero-pressure geometry of arterial aneurysms. *Ann Biomed Eng*. 2006. **34**, 1414-1419. (doi: 10.1007/s10439-006-9115-7)
23. Lu, J., Zhou, X. & Raghavan, M.L. Inverse elastostatic stress analysis in pre-deformed biological structures: Demonstration using abdominal aortic aneurysms. *J Biomech*. 2007.**40**, 693-696. (doi: 10.1016/j.jbiomech.2006.01.015)

24. de Putter, S., Wolters, B.J., Rutten, M.C., Breeuwer, M., Gerritsen, F.A. & van de Vosse, F.N. Patient-specific initial wall stress in abdominal aortic aneurysms with a backward incremental method. *J Biomech*. 2007.**40**, 1081-1090. (doi: 10.1016/j.jbiomech.2006.04.019).
25. Speelman, L., Bosboom, E.M., Schurink, G.W., Buth, J., Breeuwer, M., Jacobs, M.J. & van de Vosse, F.N. Initial stress and nonlinear material behavior in patient-specific AAA wall stress analysis. *J Biomech*. 2009.**42**, 1713-1719. (doi: 10.1016/j.jbiomech.2009.04.020).
26. Vande Geest, J.P., Sacks, M.S. & Vorp, D.A. The effects of aneurysm on the biaxial mechanical behavior of human abdominal aorta. *J Biomech*. 2006.**39**, 1324-1334. (doi: 10.1016/j.jbiomech.2005.03.003)
27. van 't Veer M., Buth, J., Merkx, M., Tonino, P., van den Bosch, H., Pijls, N. & van de Vosse F.N. Biomechanical properties of abdominal aortic aneurysms assessed by simultaneously measured pressure and volume changes in humans. *J Vasc Surg*. 2009.**48**, 1401-1407.(doi: 10.1016/j.jvs.2008.06.060)
28. Sacks, M.S. Biaxial mechanical evaluation of planar biological materials. *J Elast*. 2000.**61**, 199-246. (doi: 10.1023/A:1010917028671)
29. Choi, H.S. & Vito, R.P. Two-dimensional stress-strain relationship for canine pericardium. *J Biomech Eng*. 1990.**112**, 153-159.
30. Kazi M, Thyberg J, Religa P, Roy J, Eriksson P, Hedin U, et al. Influence of intraluminal thrombus on structural and cellular composition of abdominal aortic aneurysm wall. *J Vasc Surg*. 2003.**38**, 1283-1292.
31. Demiray, H. Large deformation analysis of some soft biological tissues. *J Biomech Eng*. 1981.**103**, 73-78.
32. Onate, E., Rojek, J., Taylor, R.L. & Zienkiewicz, O.C. Finite calculus formulation for incompressible solids using linear triangles and tetrahedra. *Int J Num Meth Eng*. 2004.**59**, 1473-1500. (doi: 10.1002/nme.922)
33. Di Martino, E.S. & Vorp, D.A. Effect of variation in intraluminal thrombus constitutive properties on abdominal aortic aneurysm wall stress. *Ann Biomed Eng*. 2003.**31**, 804-809. (doi: 10.1114/1.1581880)
34. Zemanek, M., Bursa, J. & Detak, M. Biaxial tension tests with soft tissues of arterial wall. *Engineering Mechanics.* **16**, 3-12. 2009.
35. Tong, J., Cohnert, T., Regitnig, P. & Holzapfel, G.A. Effects of age on the elastic properties of the intraluminal thrombus and the thrombus-covered wall in abdominal aortic aneurysms: biaxial extension behaviour and material modelling. *Eur J Vasc Endovasc Surg*. 2011.**42**, 207-219. (doi: 10.1016/j.ejvs.2011.02.017)
36. Nichols, M.2005. *McDonald´s Blood flow in arteries*. Hodder Arnold.
37. Rodriguez, J.F., Ruiz, C., Doblare, M. & Holzapfel, G.A. Mechanical stresses in abdominal aortic aneurysms: influence of diameter, asymmetry, and material anisotropy. *J Biomech Eng*. 2008.**130**, 021023, (doi: 10.1115/1.2898830)
38. Reeps, C., Gee, M., Maier, A., Gurdan, M., Eckstein, H.H. & Wall, W.A. The impact of model assumptions on results of computational mechanics in abdominal aortic aneurysm. *J Vasc Surg*. 2010.**51**, 670-688. (doi: 10.1016/j.jvs.2009.10.048)
39. Georgakarakos, E., Ioannou, C.V., Papaharilaou, Y., Kostas, T., Tsetis, D. & Katsamouris, A.N. Peak wall stress does not necessarily predict the location of rupture in abdominal aortic aneurysms. *Eur J Vasc Endovasc Surg*. 2010.**39**, 302-304. (doi: 10.1016/j.ejvs.2009.11.021)
40. Vande Geest, J.P., Schmidt, D.E., Sacks, M. & Vorp, D.A. The effects f anisotropy on the wall stress analyses of Patient-specific abdominal aortic aneurysms. *Ann Biomed Eng.* 2008.**36**, 921-932. (doi: 10.1007/s10439-008-9490-3)
41. Di Achille, P., Celi, S., Di Puccio, F. & Forte, P. Anisotropic AAA: computational comparison between four and two fiber family material models. *J Biomech*. 2011.**44**, 2418-2426. (doi: 10.1016/j.jbiomech.2011.06.029)

42. Burša J., Zemánek M.: Evaluation of Biaxial Tension Tests of Soft Tissues. Studies in health technology and informatics, IOS Press, Vol. 133, 2008, pp. 45-55, ISBN 978-1-58603-828-1.
43. Rodriguez, J. F., Martufi, G., Doblare, M. & Finol, A. The effect of material model formulation in the stress analysis of abdominal aortic aneurysms. *Ann Biomed. Eng*. 2009.**37**, 2218-2221. (doi: 10.1007/s10439-009-9767-1).
44. Fung Y. C. What are residual stresses doing in our blood vessels? *Ann. Biomed. Eng.* 1991.**19**, 237-249

12.8 Appendix H

A numerical implementation to predict residual strains from the homogeneous stress hypothesis with application to abdominal aortic aneurysms

Stanislav Polzer[1], Jiri Bursa[1] , T.Christian Gasser[2], Robert Staffa[3] and Robert Vlachovsky[3]

[1] Institute of Solid Mechanics, Mechatronics and Biomechanics, Brno University of Technology, Czech Republic

[2] Department of Solid Mechanics, The Royal Institute of Technology, Stockholm, Sweden

[3] 2nd Department of Surgery, St. Anne's University Hospital, and Faculty of Medicine, Masaryk University, Brno, Czech Republic

Submitted for publication into Annals of Biomedical Engineering

Abstract

Background. Wall stress analysis of abdominal aortic aneurysm (AAA) is a promising method of identifying AAAs at high risk of rupture. However, neglecting residual strains (RS) in the load-free configuration of patient-specific finite element analysis (FEA) models is a sever limitation that strongly affects the computed wall stresses. Although several methods for including RS have been proposed, they cannot be directly applied to patient-specific AAA simulations.

Methods. RS in the AAA wall are predicted through volumetric growth that aims at satisfying the homogeneous stress hypothesis at mean arterial pressure loading. Tissue growth is interpolated linearly across the wall thickness and aneurysm tissues are described by isotropic constitutive formulations . The total deformation is multiplicatively split into elastic and growth contributions, and a staggered schema is used to solve the field variables. The algorithm is qualitatively validated at a cylindrical artery model and then applied to patient-specific AAAs (n=5).

Results. The induced RS state is fully three-dimensional and in qualitative agreement with experimental observations, i.e. wall strips that were excised from the load-free wall showed stress-releasing-deformations that are typically seen in laboratory experiments. Compared to RS-free simulations, the proposed algorithm reduced the von Mises stress gradient across the wall by a 10-fold. Accounting for RS leads to homogenized wall stresses, which apart from reducing the peak wall stress (PWS) also shifted its location in some cases.

Conclusion. The present study demonstrated that the homogeneous stress hypothesis can be effectively used to predict RS in the load-free configuration of the vascular wall. The proposed algorithm leads to a fast and robust prediction of RS, which is fully capable for a patient-specific AAA rupture risk assessment. Not accounting for RS lead to a non-realistic wall stress that severely overestimates the PWS. Prescribing only bending-like growth deformation was not able to fully release the stress gradients in patient-specific AAA models. Membrane growth deformation would in addition be required, such that the AAA could grow into shapes that support a pure membrane stress state in the wall.

Introduction

A diameter exceeding 5.5cm is the most commonly accepted criterion for elective surgical repair of abdominal aortic aneurysm (AAA) [1,2]. There is, however, a need for other predictors for rupture, since aneurysms with a diameter less than 5.5 cm can rupture [3,4] and 60% of larger aneurysms do not rupture [5]. According to biomechanical rupture risk assessment an aneurysm will rupture if the mechanical stress exceeds the local strength of the wall. Consequently, indices like Peak Wall Stress (PWS) [6,7] and Peak Wall Rupture Risk (PWRR) [8,9] identify rupture-prone AAAs better than the maximal diameter criterion.

Biomechanical indices like PWS and PWRR are based on wall stresses predictions that typically use the concept of Finite Element Analysis (FEA). Especially with non-linear constitutive models, realistic stress state predictions should account for residual strains (RS) in the load-free configuration, which for complex geometries like AAAs are unfortunately unknown. Neglecting RS in the load-free configuration typically leads to significant stress gradients across the wall thickness that is in contradiction to the uniform stress hypothesis [10]. This hypothesis states that vascular tissue (cells and extra cellular matrix) remodels towards a preferred stress-strain state, which in turn leads to homogenization of the wall stress across the thickness. The uniform stress hypothesis is closely related to the uniform strain hypothesis [11] that assumes that the strain across the wall is maintained constant during wall remodeling.

RS in the arteries are known for at least half a century [40] and their biomechanical consequence is well discussed in the literature [10,38,41,45]. It´s reported that both circumferential [38,41] as well as longitudinal strips [39] that were excised from a load-free arterial tube change their curvature. Consequently, RS in the vascular wall is clearly multi-dimensional. However, early works were based on the assumption that a wall segment that develops when cut-open a load-free arterial ring, opened-up ring configuration say, releases their stresses fully, i.e. deforms into a stress-free configuration [12-16]. Consequently, many vascular simulations assumed the opened-up ring configuration as their stress-free reference configuration [13,14,37] and hence clearly missed at the axial component of the RS state. Although cutting a vascular body into many (hopefully) unstressed pieces has been suggest for general geometries [27], it remains unclear where to cut in order to maintain a (fully) unstressed body. Consequently, such an approach seems only be applicable for idealized vascular geometries and can hardly be used for complex 3D patient-specific geometry such as the AAA. Same limitation applies to approaches based on inverse elastostatics [25] due to necessity of calculating opened geometry.

Remodeling of the wall takes place in its current (loaded) configuration and simultaneously develops RS in its (hypothetical) load-free configuration. It is very unlikely that the stress-free configuration is compatible, i.e. the stress can only be completely released by splitting the body into an infinite number of stress-free material points. This is to some extend indicated by a laboratory experiment [42] that releases continuously RS when continuously removing tissue layers.

Initialized by the constraint mixture approach [32] different growth models for vascular tissues have been proposed that used different stress-free configurations for the different structural constituents in the wall [28,29,30,31,33,34]. These approaches also implicitly develop RS, but require time-consuming computations. Likewise, such constitutive models are under continuous development and currently not available in commercial software packages.

In present work we propose a new algorithm that iteratively generates RS for a patient-specific AAAs by using a staggered two-field solution approach. Specifically, the proposed algorithm is based on the concept of isotropic growth [17], where the amount of growth is set such that the stress gradient across the wall is minimized. The method is validated on an idealized tubular geometry and then applied to patient-specific AAA models.

Methods

Continuum mechanical description of growth

With reference to the load-free configuration, the proposed method aims at inducing compressive stress at the inner surface of the arterial wall and tensile stresses at its outer surface. Following the finite growth kinematics concept [17], we apply multiplicative decomposition of the deformation gradient tensor

$$\mathbf{F} = \mathbf{F}_e\mathbf{F}_g\,, \tag{1}$$

where $\mathbf{F}_e$ and $\mathbf{F}_g$ represent elastic and growth deformation gradients, respectively. We limit ourselves to volumetric growth, such that the growth deformation gradient is spherical and reads

$$\mathbf{F}_g = (1 + c)\mathbf{I}, \tag{2}$$

where c is an engineering-like growth strain. Consequently, the elastic deformation gradient is related to the total deformation gradient $\mathbf{F}$ according to

$$\mathbf{F}_{\mathrm{e}} = \mathbf{F}\mathbf{F}_{\mathrm{g}}^{-1} . \tag{3}$$

Finally, using standard arguments [43] the Cauchy stress tensor $\boldsymbol{\sigma}$ for a hyperelastic and mechanically incompressible materials reads [17].

$$\boldsymbol{\sigma} = 2\mathbf{F}_{\mathbf{e}} \frac{\partial \Psi}{\partial \mathbf{C}_{\mathrm{e}}} \mathbf{F}_{\mathrm{e}}^{\mathrm{T}} - p\mathbf{I} \ , \tag{4}$$

where $\mathbf{C_e} = \mathbf{F}_{\mathrm{e}}^{\mathrm{T}}\mathbf{F}_{\mathrm{e}}$ is the elastic right Cauchy-Green deformation tensor, Ψ is the strain energy density function and p is the hydrostatic stress.

Constitutive models for AAA tissues

Regardless the fact that the AAA wall shows a mild anisotropy [19] we used the isotropic strain energy function

$$\psi = \frac{a}{b}\left(e^{\frac{b}{2}(I_1-3)} - 1 \right) \tag{5}$$

originally proposed by Demiray [18], where a and b denote stress-like and dimensionless material constants, respectively. Specifically, values of $a = 17\ kPa$ and $b = 88$ has been used to accurately (R^2=0.87) [35] fit published biaxial data of the human aneurysm wall [19].

Most clinical relevant AAAs contain an intra-luminal thrombus (ILT) [23] which influences the wall stress [24,44] and therefore were included it in our FEA models. In contrast to the aneurysm wall, the ILT exhibits an almost linear behavior, which can be captured by a one parameter Ogden-like material model [20]

$$\psi = \alpha \sum_{i=1}^{3} \left(\lambda_i^4 - 1 \right), \tag{6}$$

where λ_i denotes the i-th principal stretch and α is a stress-like material parameter. Specifically, ILT is stiffer at the luminal site ($\alpha = 2.62kPa$) and gradually decreases its stiffness towards the abluminal site ($\alpha = 1.73kPa$) [20]. No RS in the ILT were considered.

Possible 3d generalizations of the homogeneous stress hypothesis

The homogeneous stress hypothesis was originally formulated for the circumferential stress component [10] and a generalization to 3D is naturally not unique. In this study, we investigated two different generalizations, where the gradient of the von Mises stress

(approach (a)) and the gradient of the hydrostatic stress (approach (b)) were minimized across the wall thickness. The von Mises stress is a widely used scalar representation of the stress state, while the hydrostatic stress is work-conjugate to the volumetric growth. No consensus regarding the biomechanical quantity that actually drives wall growth has been achieved, and the two proposed stress quantities can be regarded as the simplest trial. Specifically, their evaluation does not require directional information, such that they are easily accessible for arbitrary 3D geometries.

Numerical realization

The governing equations (1)-(4) render a coupled two field problem, that is fully determined by the elastic displacements $\mathbf{u}_e$ and the growth variable c. The system is coupled through the multiplicative kinematics relation (1), which, for small elastic and/or small growth deformations fully uncouples. Consequently, for deformations of relevance for our applications the system is only weakly coupled, and hence, can be effectively solved through a staggered solution schema. Here, the elastic displacements $\mathbf{u}_e$ are kept frozen when solving for the growth variable c and vice versa.

In order to induce a growth deformation with compression at the inner wall surface and tension at the outer wall surface a linear interpolation across the thickness h according to

$$c = -2c_0 Z/H \,, \tag{7}$$

was introduced. Here, Z denotes the thickness coordinate with $Z = -H/2$ and $Z = H/2$ at the inner and outer surface, respectively. Consequently, c_0 represents the maximum growth at the surfaces of the vascular wall, and eq.(7) ensures that the $c=0$ at $Z = 0$, i.e. in the middle of the wall, such that no membrane strain is induced through growing. In addition according to eq.(7) the net growth across the wall is zero, such that the wall thickness remains constant regardless the amount of growing. To avoid self-penetration the condition $\det\mathbf{F}_g > 0$ has to be satisfied, which immediately leads to the constraint $c_0 < 1$.

Finally, it is noted that the linear interpolation (7) was sufficiently accurate to minimize the stress gradient across the relatively thin wall of AAAs and for thicker walls other interpolations could be more effective.

Growing step

In order to predict the volumetric growth, an incremental approach was used. At each iteration i the elastic displacements $\mathbf{u}_e$ were frozen and the stress difference Δ_{ik} between the inner and the outer surface of the wall was computed. Specifically, for approach (a) the von Mises stress difference and for approach (b) the hydrostatic stress difference was computed. The index $k = 1, \dots, n_{\text{nodes}}$ denotes an individual surface node with n_{nodes} being the total number of inner surface nodes. For each node at the inner wall surface the closest node at the outer wall surface has been found. From stress difference Δ_{ik} the increment of growth deformation at the k-th node was estimated according to $\Delta c_0 = 0.15 \cdot \Delta_{ik}$ where the factor 0.15 was based on numerical experience with the algorithm. Specifically, it reflects the highest value that still ensured monotonic convergence of the method for all investigated AAAs.

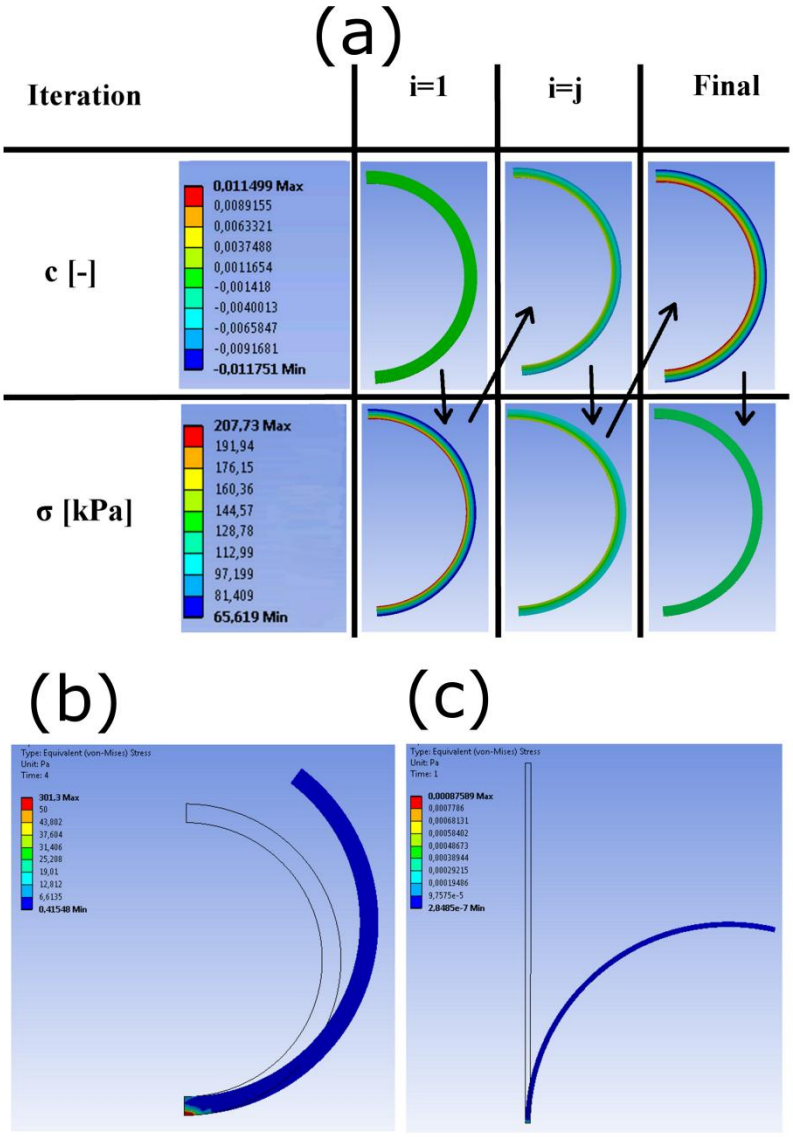

Figure 1: Application of the proposed algorithm to a cylindrical artery. (a) Staggered solution schema to solve for the amount of volumetric growth, i.e. residual strain (RS) that is required to homogenize the von Mises stress

across the wall. Upper row shows the predicted field of the growth variable $\boldsymbol{c}$. The lower row shows the von Mises stress distribution at 13kPa inflation. Note the high stress gradient at *i=1*, i.e. without RS, which in turn decreases virtually to zero at the end of the iteration. (b) Deformation of a circumferential strip to release RS, i.e. when arterial ring is cut axially. (c) Deformation of a longitudinal strip to release RS, i.e. when an axial strip is cut from the artery. The luminal side of the artery is on the left.

Elastic deformation step

At each iteration i the RS state was frozen, i.e. the growth deformation $\mathbf{F}_g$ was fixed, such that the elastic deformation $\mathbf{F}_e$ could be expressed through eq.(3). Then the stress in the wall and the ILT of the loaded artery was calculated according to eq. (5) and (6), respectively. Consequently, the stress difference Δ_{ik} across the wall could be computed and the algorithm continued with the next growing step, see above.

The iterative algorithm was terminated as soon as the maximal stress difference was lower than 1kPa ($\max(\Delta_{ik}) < 1\text{kPa}$) or increased with respect to the previous iteration ($\Delta_{ik} > \Delta_{ik}$). A thermo-mechanical analysis within ANSYS 14.0 (ANSYS Inc. PA, USA) was used, where the temperature field was used to store the growth variable c at each FE mesh node.

Figure 1 illustrates the iterative development of the growth deformation for approach (a), i.e. until the von Mises stress gradient across the wall thickness vanishes. The underlying algorithm is shown in the Figure 2, and used a staggered solution approach, where the inflation of the artery was fixed at 13kPa.

Benchmark example

A cylindrical artery (diameter of 25mm, wall thickness of 1.5mm) at 13 kPa inflation was used to illustrate the basic features of the proposed algorithm, see Figure 1. This example aims at illustrating firstly, that the stress gradient in the inflated structure vanished and, secondly, that the predicted RS state is in qualitative agreement with experimental observation. Specifically, the RS-releasing deformation of hypothetically excised circumferential and longitudinal wall strips was investigated. The cylindrical artery model used 6 quadratic elements across the wall thickness and the boundary conditions were set, such that no axial load acts at the artery.

Patient-specific AAA analysis

The present study used five AAA patients that underwent Computer Tomography-Angiography (CT-A) at St. Anne's University Hospital, Brno, Czech Republic, at an in-plane resolution of 0.5 mm and a slice thickness of 3 mm. Deformable (active) contour models (A4research vers.4.0, VASCOPS GmbH, Austria) were used to reconstruct the 3D geometry

of AAAs from CT data [21]. To this end a virtual balloon expands inside the 3D set of image data until the boundaries of the aneurysm are detected. This provides smooth surfaces and excludes artifacts such as sharp edges and corners, which otherwise might cause stress concentrations in the FEA simulation. The wall thickness was related to the thickness of the underlying ILT. Specifically, at sites of a thin ILT (thinner than 1.0mm) the wall thickness was 1.5mm and reduced to 1.0mm behind a thick ILT (thicker than 25.0mm), which is in agreement with histological data [22]. Although at CT-A the patient's aorta is pressurized, for simplicity we considered the reconstructed geometry as load-free for the present study.

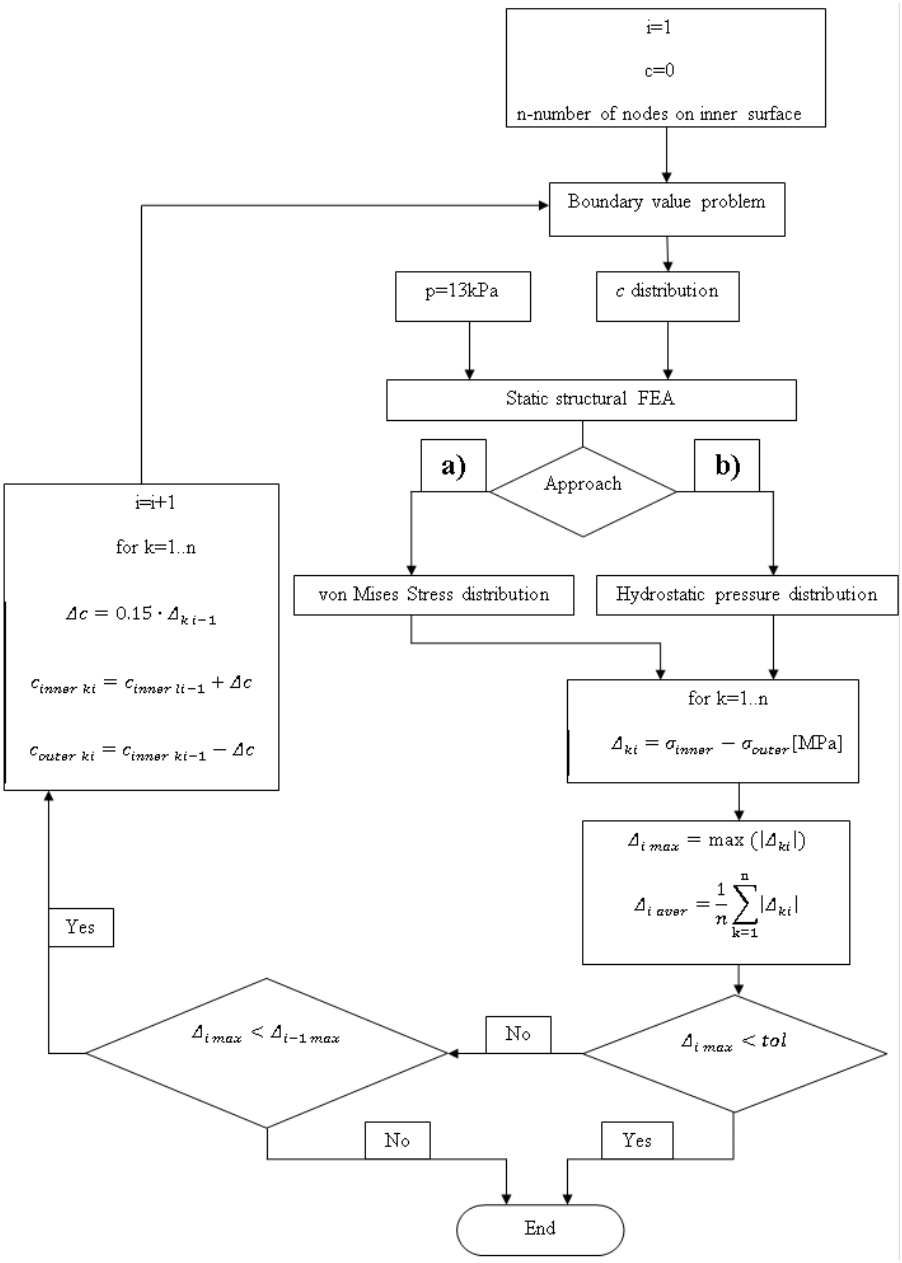

Figure 2: Description of the staggered solution schema to compute the elastic and growing deformation of the arterial wall. The gradients of the von Mises stress (approach (a)) or of the hydrostatic stress (approach (b)) across the wall are minimized.

The AAA wall was discretized by two meshes with coinciding nodes reflecting the elastic and growing deformations, respectively. Specifically, mixed quadratic tetrahedral elements (ANSYS solid 187) captured the incompressible elastic deformations, and quadratic thermal elements (ANSYS solid 87) stored the growing deformation. A mesh convergence study verified a numerical error of less than 5%. At least two quadratic elements across the wall thickness were used in the high stress regions to ensure that potential stress gradients are captured accurately. Typically the mesh consists of 80k nodes. A rigid interface between ILT and wall was considered, i.e. separation and sliding between the ILT and the wall were constrained. The aneurysm was fixed at the renal arteries and aortic bifurcation.

Results

Benchmark example

By neglecting RS in the vascular wall the stress difference between the inner and outer wall was remarkable: von Mises stress of 141kPa for approach (a) and hydrostatic stress of 40kPa for approach (b). The proposed algorithm converged continuously within $i = 5$ iterations and effectively reduced this stress difference to 1kPa for approach (a) as well as approach (b), see Figure 1(a).

When considering the predicted RS state, the wall stress matched the result from the LaPlace equation, i.e. the circumferential stress $\sigma = \frac{p \cdot r}{t} = \frac{13 \cdot 14.37}{1.43} \cong 130 kPa$, where r and t are the deformed radius and wall thickness, respectively.

The deformation of the vascular wall due to releasing RS is shown in Figure 1(b) and (c). Here, circumferential and axial strips were hypothetically excised from the load-free artery and cut in order to release the RS. Note that the results are in qualitative agreement with experimental observations [38, 39, 41].

Patient-specific AAA analysis

The typical convergence of the algorithm (approach (a) and approach (b)) is shown in Figure 3, which also illustrates an about 10-fold decrease of the von Mises stress difference and the hydrostatic stress difference across the wall, respectively. It is noted that, contrast to the benchmark example shown above, the difference of these stress properties did not vanish completely for the patient-specific AAA examples. Results from all five patients are summarized in Table 1 which demonstrates that, apart from the stress gradient, also the maximum von Mises stress, i.e. the PWS value was naturally strongly affected by RS. In average the maximum von Mises stress (PWS) decreased from 957(SD379)kPa to

311(SD140)kPa and to 390(SD213)kPa for approach (a) and approach (b), respectively. Finally, it is noted that the maximal stress difference does in general not coincided with the stress difference at the site of the maximum von Mises stress (PWS).

Table 1: Effect of residual stain (RS) on the von Mises stress and hydrostatic stress in the wall of patient-specific Abdominal Aortic Aneurysms (AAAs). Differences are taken between the inner and outer surface of the wall. Mean properties are averaged over all surface nodes of the Finite Element (FE) model. Approach (a) and approach (b) denote different assumption for the prediction of the RS state in the load-free configuration.

AAA No.	Residual Strain (RS) in the load-free configuration	Maximum von Mises stress (kPa)	Maximum hydrostatic stress (kPa)	Maximum von Mises stress difference (kPa)	Maximum hydrostatic stress difference (kPa)	Mean von Mises stress difference (kPa)	Mean hydrostatic stress difference (kPa)
1	none	422	136	283	118	66	23
	approach (a)	140	78	19	33	4	16
	approach (b)	163	74	130	10	1	9
2	none	606	292	459	204	51	19
	approach (a)	428	195	73	62	5	11
	approach (b)	471	177	302	27	19	2
3	none	1001	339	852	275	72	21
	approach (a)	421	259	57	60	6	19
	approach (b)	647	200	394	26	26	2
4	none	486	259	411	207	71	33
	approach (a)	253	169	60	99	2	13
	approach (b)	280	125	160	18	14	2
5	none	1312	602	1213	539	81	35
	approach (a)	313	165	21	76	3	10
	approach (b)	394	134	270	23	19	1

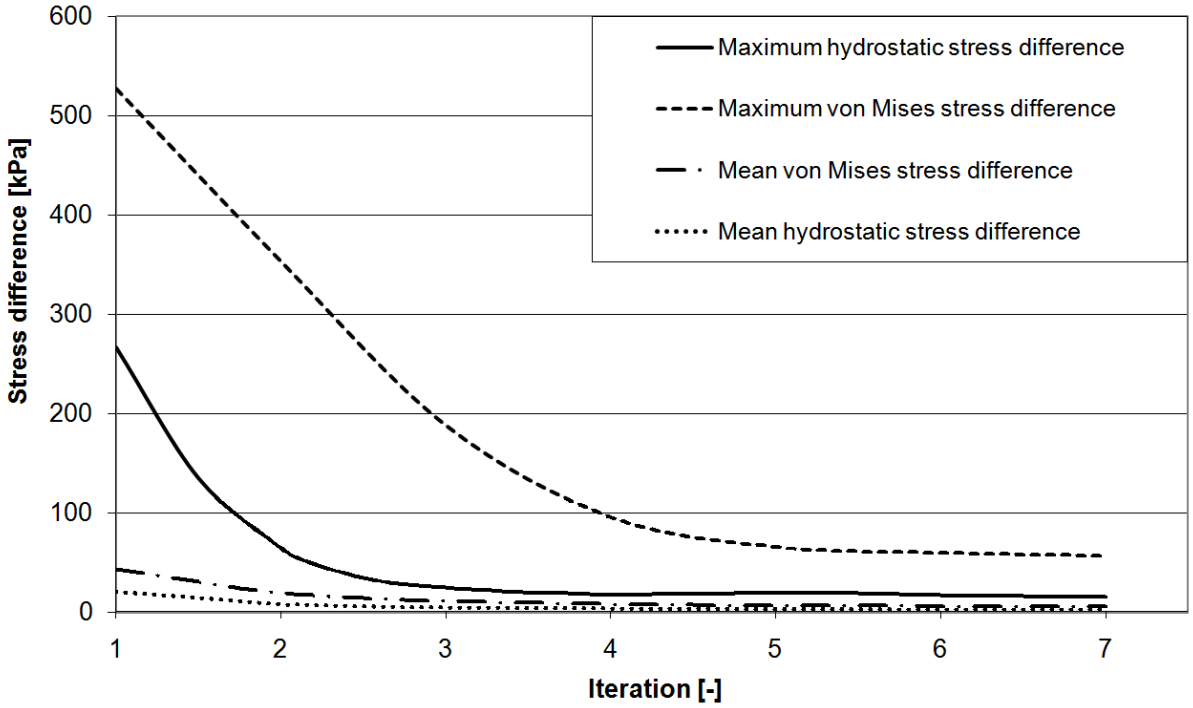

Figure 3: Decrease of the difference of the von Mises stress (approach (a), solid lines) and the difference of the hydrostatic stress (approach (b), dashed lines) between inner and outer surface of the wall. Abdominal Aortic Aneurysm (AAA) case 3 is illustrated, and the evolution is shown with respect to the number of algorithmic iterations.

The strains for AAA no. 2 that arose from growth deformation and from elastic deformation are shown in the left and right images of Figure 4, respectively. The growth deformation is highest at the bifurcation and neck regions, i.e. where the RS-free model would predict the highest stress gradients.

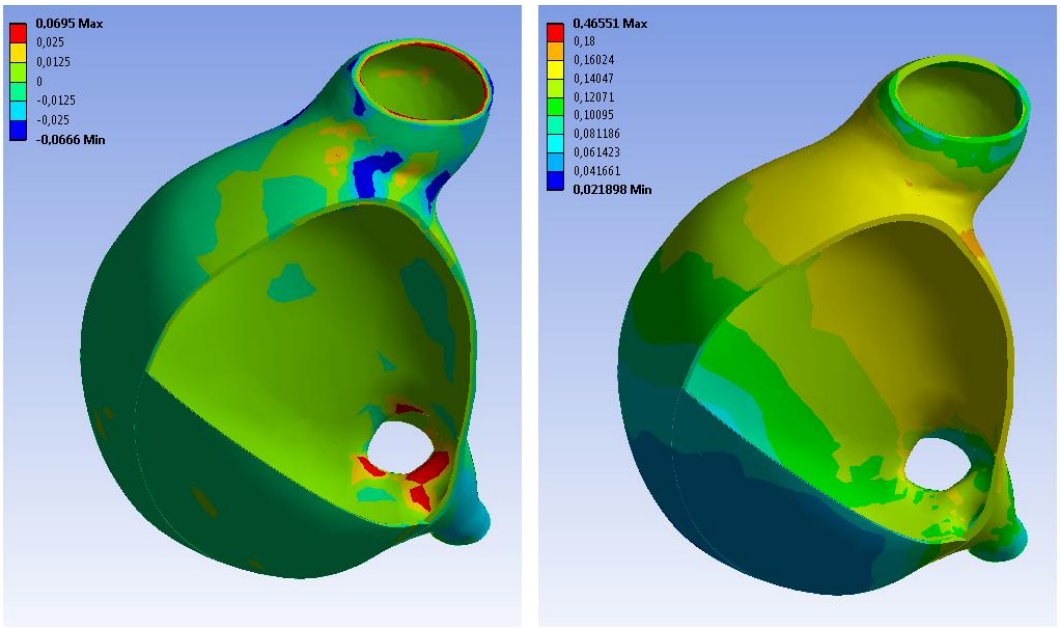

Figure 4: Logarithmic engineering strain due to volumetric tissue growth (left) and due to elastic deformation (right). Abdominal Aortic Aneurysm (AAA) case 2 is shown and Residual strain (RS) prediction in the load-free configuration was based on approach (a).

Accounting for RS in the load-free configuration with either approach (a) or approach (b) lead to a homogenized wall stress. Considering RS did not only reduce the maximum von Mises stress (PWS) but shifted also its location in some cases, see Figure 5. Due to the homogenization effect of RS a much coarser FE meshes could be used as compared to a RS-free analysis. Mesh sizes up to 3mm gave still an acceptable wall stress results for the investigated AAA cases.

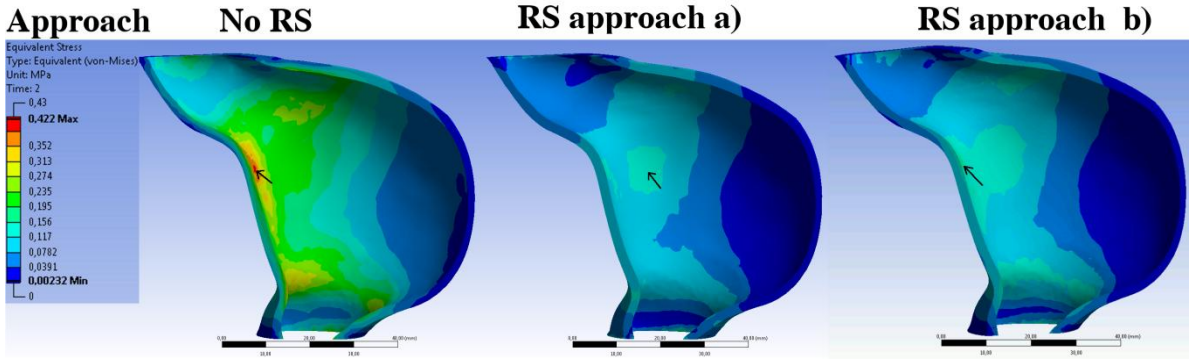

Figure 5 Effect of residual strain (RS) in the load-free configuration on the wall stress of Abdominal Aortic Aneurysm (AAA) case 1. Von Mises stress prediction without RS (left), and with RS predicted according to approach (a) (middle) and approach (b) (right). Note that the maximum von Mises stress (peak wall stress; PWS) decreased for the models that accounted for RS, and changed from the posteral neck area to postero-latereal part for approach (a). The location of the maximum von Mises stress is indicated by the arrows.

Discussion and Conclusion

Accounting for tissue growth can significantly improve the predictions of biomechanical simulations, and the objective of the present study was to develop a fast and generally applicable numerical concept that allows a more accurate prediction of AAA wall stress. We used local volumetric growth and two possible 3D generalizations of the homogeneous stress hypothesis [10] to predict RS in the vascular bodies' load-free configurations. The growth deformation was multiplicatively considered on top of the elastic deformation, where a weak coupling between these two fields allowed the application of a staggered solution schema. The proposed method converged quickly, does not require knowledge of the stress-free geometry, and relies entirely on a conventional constitutive description of the AAA wall.

The developed multi-dimensional RS state was in qualitative agreement with experimental observation, i.e. an arterial ring opens [38, 41] and an axial arterial strip bended outwards [39]. Qualitative validation of our results was not possible since no RS data from the AAA wall is available in the literature. RS data of the AAA wall might differ significantly from the normal aorta due to the much lower elastin content [36], which is mainly responsible for the RS-releasing deformations [1,42].

The proposed method has been verified through five patient-specific AAA models to demonstrate its application to complex 3D geometries. In all cases the stress gradient across

the wall could be reduced by about a 10-fold when compared to results that neglect the RS state. In general, accounting for RS in the load-free configuration homogenized the wall stress distribution, which besides lowering the PWS was even able to shift its location.

The stress gradient across the wall in the cylindrical artery model could be completely removed, which shows that a bending-like growing deformation, i.e. that was prescribed through eq.(7), was sufficient. In contrast, for the more general geometries of patient-specific models, eq.(7) could not fully remove the stress gradient, neither with approach (a) nor with approach (b). There are two reasons for that. Firstly, we had to use mesh due to complex geometry. Therefore it is only ensured that each node at the inner node was coupled with the closest node at the outer surface but not vice versa. Consequently there might be several cases when one node at the outer surface is coupled to several nodes at the inner surface. Naturally it is possible to prescribe only one growth strain at this outer surface node which is an average value required by nodes at the inner surface. This happens at the bifurcation area where there is a big change in the curvature. However our approach is still able to reduce stress gradient by a 10-fold which we consider satisfying.

Second reason is related to a fact that in order to allow a solution with zero stress difference (von Mises stress or hydrostatic stress), i.e. a membrane stress state, the local wall curvature must allow for that. For example, a flat plate under pressure loading will always develop bending stress in order to satisfy the equilibrium conditions. Consequently, for the general geometries investigated in this study, it is unlikely that the equilibrium conditions would permit a pure membrane wall stress state. Consequently, on top of the bending-like growth also a membrane-like growth contribution would be required, such that the wall could expand locally. Hence, the wall could potentially grow into a shape that could carry the pressure loading through a pure membrane stress state. However, our current growth model can only prescribe bending-like deformation and the results of the proposed algorithm can be seen as an optimization under this constraint.

Remodeling of vascular tissue is rather quick and vascular collagen has a half-life time of about 60 days [1]. Although we did not explicitly introduce a time scale in our model, this scale would also apply to our model.

It is noted that although at mean arterial pressure the stress gradients across the wall might be small, a significant stress gradient might be characteristic for systolic blood pressure. A fact that might be considered in a AAA rupture risk analysis. Despite accounting for the RS state that was defined through mean arterial pressure, at a prescribed systolic pressure of 18kPa, the investigated five AAA models showed maximum and mean von Mises stress differences across the wall of 119(SD42) kPa and 13(SD4) kPa for approach (a) and 145kPa(SD58) and 23(SD7) for approach (b), respectively.

We assumed isotropic tissue growth while the anisotropic structure of the vascular wall might motivate an anisotropic growth. Likewise, a linear interpolation of tissue growth across the wall thickness was used without any experimental evidence.

We used a RS-free ILT, and due to the almost linear and rather soft ILT [20], we do not expect a significant impact on the wall stress due to this simplification. Similarly, for simplicity and to focus exclusively on RS we assumed that the geometry reconstructed from CT is load-free, which however is not the case.

References

1. Mortality results for randomised controlled trial of early elective surgery or ultrasonographic surveillance for small abdominal aortic aneurysms. The UK Small Aneurysm Trial Participants. Lancet 1998; **352**(9141):1649-55.
2. Lederle, F.A , Wilson, S.E. , Johnson, G.R. , Reinke, D.B. , Littooy, F.N., Acher, C.W. , Ballard, D.J. , Messina, L.M. , Gordon, I.L. , Chute, E.P., *et al.* 2002. Immediate repair compared with surveillance of small abdominal aortic aneurysms. *N Engl J Med*. **346**, 1437-1444. (doi: 10.1056/NEJMoa012573)
3. Heikkinen, M., Salenius, J.P. & Auvinen, O. 2002. Ruptured abdominal aortic aneurysm in a well-defined geographic area. *J Vasc Surg*. **36**, 291-296. (doi: 10.1067/mva.2002.125479)
4. Nicholls, S.C., Gardner, J.B., Meissner, M.H. & Johansen, H.K. 1998. Rupture in small abdominal aortic aneurysms. *J Vasc Surg*. **28**, 884-888.
5. Darling, R.C., Messina, C.R., Brewster, D.C. & Ottinger, L.W. 1977. Autopsy study of unoperated abdominal aortic aneurysms. The case for early resection. *Circulation*. **56**, II161-4.
6. Fillinger, M.F., Raghavan, M.L., Marra, S.P., Cronenwett, J.L. & Kennedy, F.E.2002. In vivo analysis of mechanical wall stress and abdominal aortic aneurysm rupture risk. *J Vasc Surg*. **36**, 589-597. (doi: 10.1067/mva.2002.125478)
7. Venkatasubramaniam, A.K., Fagan, M.J., Mehta, T., Mylankal, K.J., Ray, B., Kuhan, G., Chetter, I.C. & McCollum, P.T.2004. A comparative study of aortic wall stress using finite element analysis for ruptured and non-ruptured abdominal aortic aneurysms. *Eur J Vasc Endovasc Surg*. **28**, 168-176. (doi: 10.1016/j.ejvs.2004.03.029)
8. Gasser, T.C., Auer, M., Labruto, F., Swedenborg, J. & Roy, J.2010. Biomechanical rupture risk assessment of abdominal aortic aneurysms: model complexity versus predictability of finite element simulations. *Eur J Vasc Endovasc Surg*. **40**, 176-185. (doi: 10.1016/j.ejvs.2010.04.003)
9. Maier, A, Gee, MW, Reeps C, Pongratz J, Eckstein HH, Wall WA. 2010. A Comparison of diameter, wall stress, and rupture potential index for abdominal aortic aneurysm rupture risk prediction. *Ann Biomed Eng*. **38**, 3124-3134.
10. Fung Y. C. 1991. What are residual stresses doing in our blood vessels? *Ann. Biomed. Eng.* **19**, 237-249
11. Takamizawa K., Hayashi K. 1987. Strain energy density function and uniform strain hypothesis for arterial mechanics. J. Biomech. 20:7–17.
12. Rachev A. and Hayashi K. 1999. Theoretical study of the effect of vascular smooth muscle contraction on strain and stress distribution in arteries. *Ann. Biomed. Eng.* **32**, 257-263. (doi:10.1114/1.191)
13. Raghavan M. L., Trivedi S., Nagaraj A., McPherson D. D. and Chandran K. B. 2004. Three-dimensional finite element analysis of residual stress in arteries. *Ann. Biomed. Eng.* **32**, 257-263.
14. Balzani D., Schroder J. and Gross D. 2007. Numerical simulation of residual stress in arterial walls. *Comp. Mat. Sci.* **39**, 117-123.
15. Alastrue V., Pena E., Martinez M. A. and Doblare M. 2007 Assessing the use of the "opening angle method" to enforce residual stresses in patient specific arteries. *Ann. Biomed. Eng.* **35,** 1821-1837.
16. Humphrey J. D. 2002. Cardiovascular solid mechanics. Cells, tissues and organs. New York, NY: Springer.
17. Rodriguez E.K., Hoger A. and McCulloch A.D.1994. Stress-dependent finite element growth in soft elastic tissues. *J Biomech*. **27**, 455-467
18. Demiray, H.1981. Large deformation analysis of some soft biological tissues. *J Biomech Eng*. **103**, 73-78.

19. Vande Geest, J.P., Sacks, M.S. & Vorp, D.A.2006. The effects of aneurysm on the biaxial mechanical behavior of human abdominal aorta. *J Biomech*. **39**, 1324-1334. (doi: 10.1016/j.jbiomech.2005.03.003)
20. Gasser, T.C., Gorgulu, G., Folkesson, M. & Swedenborg, J.2008. Failure properties of intraluminal thrombus in abdominal aortic aneurysm under static and pulsating mechanical loads. *J Vasc Surg*. **48**, 179-188. (doi: 10.1016/j.jvs.2008.01.036)
21. Auer, M. & Gasser, T.C.2010. Reconstruction and finite element mesh generation of abdominal aortic aneurysms from computerized tomography angiography data with minimal user interactions. *IEEE Trans. Med. Imag*. **29**, 1022-1028. (doi: 10.1109/TMI.2009.2039579)
22. Kazi M, Thyberg J, Religa P, Roy J, Eriksson P, Hedin U, et al. 2003. Influence of intraluminal thrombus on structural and cellular composition of abdominal aortic aneurysm wall. *J Vasc Surg*. **38**, 1283-1292.
23. Hans S.S., Jareunpoon O., Balasubramaniam M. and Zelenock G.B.2005. Size and location of thrombus in intact and ruptured abdominal aortic aneurysms. *J Vasc. Surg.* **39,** 584-8.
24. Wang D.H., Makaroun M.S., Webster M.W. and Vorp D.A. 2002. Effect of intraluminal thrombus on wall stress in patient-specific models of abdominal aortic aneurysm. *J. Vasc. Surg*. **36,** 598-604.
25. Zhou X. and Lu J. 2009. Estimation of vascular open configuration using finite element inverse elastostatic method. *Eng. Comp*. **25**, 49-59. (doi 10.1007/s00366-008-0104-3)
26. Ambrosi D., Guillou A. and diMartino E.S. 2008. Stress-modulated remodeling of a non-homogenous body. *Biomechan. Model. Mechanobiol.* **7**, 63-76
27. Alastrue V., Martinez M.A. and Doblare M. 2008. Modelling adaptative volumetric finite growth in patient-specific residually stresses arteries. *J Biomech*. **41**, 1773-1781.
28. Zeinali-Davarani, S. & Baek. S. 2012 Medical image-based simulation of abdominal aortic aneurysm growth. *Mech. Res. Commun*. (in press).
29. Zeinali-Davarani S., Raguin L.G., Baek S. 2011 An inverse optimization approach toward testing different hypotheses of vascular homeostasis using image-based models, *Int J Struc Chan Sol*, **3**, 33-45.
30. Baek, S., Rajagopal, K. R. & Humphrey, J. D. 2006 A theoretical model of enlarging intracranial fusiform aneurysms. J. Biomech. Eng. **128**, 142–149.
31. Kroon, M. & Holzapfel, G. A. 2009 A theoretical model for fibroblast-controlled growth of saccular cerebral aneurysms. *J.Theor.Biol*. **257**,73–83.
32. Humphrey, J. D. & Rajagopal, K. R. 2002 A constrained mixture model for growth and remodeling of soft tissues. Mat. Model. Meth. App.l Sci. 12, 407–430.
33. Wilson J.S., Baek S. & Humphrey J.D. 2012 Importance of initial aortic properties on the evolving regional anisotropy, stiffness and wall thickness of human abdominal aortic aneurysms, *J. R. Soc. Interface*, doi: 10.1098/rsif.2012.0097
34. Martufi G. & Gasser TC. 2012 Turnover of Fibrillar Collagen in Soft Biological Tissue with Application to the Expansion of Abdominal Aortic Aneurysms, , *J. R. Soc. Interface* (accepted for publication)
35. Polzer S, Gasser TC, Bursa J , Staffa R, Vlachovsky R , Man V and Skacel P . Importance of Material Model in Wall Stress Prediction in Abdominal Aortic Aneurysms. (submitted for publication)
36. Rizzo R.J., McCarthy W.J., Dixit S.N., Lilly M.P., Shively V.P., Flinn W.R.,& Yao J.S.T. 2011 Collagen types and matrix protein content in human abdominal aortic aneurysms. *J. Vasc. Surg*., **10**, 365–373.
37. T.C. Gasser, C. Schulze Bauer, and G.A. Holzapfel.2001. A three-dimensional finite element model for arterial clamping. *ASME J. Biomech. Eng*., **124**, 355-363.
38. R. N. Vaishnav and J. Vossoughi. 1987 Residual stress and strain in aortic segments. *J Biomech*. **20**:235–237.
39. Vossoughi, J., 1992. Longitudinal residual strain in arteries. 11th Southern Biomedical Engineering Conference, Memphis, Tennessee, pp. 17–19.
40. Bergel, D.H., 1960 The viscoelastic properties of the arterial wall. Ph.D., University of London.
41. Chuong, C.J., Fung, Y.C., 1986. On residual stresses in arteries. *J Biomech Eng* **108**, 189–192.
42. Greenwald SE, Moore JE Jr, Rachev A, Kane TP, Meister JJ.1997. Experimental investigation of the distribution of residual strains in the artery wall. *J Biomech Eng*.;**119**(4):438-44.
43. R. W. Ogden.1997 Non-linear Elastic Deformations. Dover, New York.
44. Polzer S, Gasser TC, Swedenborg J, Bursa J. 2011. The Impact of Intraluminal Thrombus Failure on the Mechanical Stress in the Wall of Abdominal Aortic Aneurysms. *Eur J Vasc Endovascr Surg*., **41**:467-473
45. A. Rachev, S.E. Greenwald. 2003. Residual strains in conduit arteries, *J Biomech* **36,** 661–670.